Electronic Supplementary Material (ESI) for Chemical Communications.

Tuning the photophysical properties of luminescent lanthanide complexes through regioselective antenna fluorination

Daniel Kocsi, Andreas Orthaber, and K. Eszter Borbas*

Department of Chemistry, Ångström Laboratory, Box 523, Uppsala University, 75120, Uppsala, Sweden.

eszter.borbas@kemi.uu.se

Table of contents

General experimental procedures

^{1}H NMR (400 MHz), ^{13}C NMR (100 MHz) and ^{19}F NMR (376 MHz) spectra were recorded on a JEOL 400 MHz instrument. Chemical shifts were referenced to residual solvent peaks and are given as follows: chemical shift (δ, ppm), multiplicity (s, singlet; br, broad; d, doublet, t, triplet; q, quartet; m, multiplet), coupling constant (Hz), integration. HR-ESI-MS analyses were performed at the Organisch Chemisches Institut WWU Münster, Germany or at the Stenhagen Analyslab AB, Mölndal. All compounds displayed the expected isotope distribution pattern. Anhydrous solvents were obtained from an Inert Puresolv solvent purification system.

Compounds **3**,[1] **S1**,[2] and **S2**[3] were synthesized following literature methods. All other chemicals were from commercial sources and used as received.

Paramagnetic ^{1}H NMR. ^{1}H NMR spectra of Eu-complexes were recorded at ambient temperature (21 °C) at 400 MHz in methanol-d_4 (~2 mM) using the following parameters: relaxation delay: 1 s; number of scans: 32; number of points: 262144; range: –30 to +50 ppm. ^{19}F NMR spectra of Eu-complexes were recorded at ambient temperature (21 °C) at 376 MHz in methanol-d_4 using the following parameters: relaxation delay: 1 s; number of scans: 32; number of points: 262144; range: –300 to +100 ppm. In all cases chemical shifts were referenced to methanol-d_4 (3.31 ppm), phase correction and exponential decay as apodization function 3 and 10 Hz has been applied for ^{1}H and ^{19}F spectra, respectively.

Chromatography. Preparative chromatography was carried out on silica gel [Normasil 60 chromatographic silica media (40–63 micron)] and aluminium oxide [activated, neutral, Brockmann Activity I, Sigma-Aldrich]. Thin layer chromatography was performed on silica-coated (60G F254) aluminium plates from Merck and aluminium oxide coated with 254 nm fluorescent indicator aluminium plates from Sigma-Aldrich. Samples were visualized by UV-light (254 and 365 nm).

HPLC-MS analysis using an Agilent 1290 Infinity II HPLC system equipped with a 1290 Infinity II High Speed pump and a 1260 II Infinity DAD HS UV-vis detector, using an InfinityLab POROSHELL 120 EC-C18 column with dimensions of 50 mm×2.1 mm and 1.9 μm particle size was performed. The

HPLC is coupled to an InfinityLab LC/MSD G6125B equipped with an ESI source as ionization. LC separation was performed using water (A, 0.1 % formic acid) and acetonitrile (B) eluent system using the method: 0 → 1 min 10% B; 1 → 10 min 10 → 90% B; 10 → 11 min 90% B; 11 → 12 min 10% B. Flow rate: 0.8 ml/min.

Photochemical reactions. Photochemical reactions were carried out in an RPR-100 Rayonet Photochemical Chamber Reactor equipped with a set of 16 UV-lamps 2537 Å (254 nm) and power of 35 W (RPR-2537A), all purchased from Southern New England Ultraviolet Company and a cooling fan. Reactions were performed in quartz cylinders with a 185 mL volume capacity (RQV-118: Rayonet; Ø 20 mm), 8.5 cm far from the light sources and approximately at 30 °C.

Electrochemistry. Cyclic voltammograms (CV) were obtained in an argon atmosphere at room temperature (~20 °C) using an AUTOLAB PGSTAT 100 potentiostat, or an AUTOLAB PGSTAT 204N potentiostat, equipped with a 3 mm glassy carbon (GC) working electrode, a Pt wire auxiliary electrode, and an $Ag/AgCl/KCl_{(sat)}$ as a reference. The solution was allowed to equilibrate for 10 s at the start potential before starting the measurements. A step potential of –0.9 mV was used for 100 mV/s scan rate. Measurements were carried out in dry DMF in the presence of $TBAPF_6$ (0.1 M) as the supporting electrolyte.

General procedure for CV measurements: the electrolyte solution was added to the electrochemical cell, and the sample was purged with a stream of Ar for 10 min prior to each measurement. The working electrode was polished with 0.05 μm alumina on a polishing pad, washed with water and ethanol, and dried with air. The three electrodes (GC working electrode, Pt wire auxiliary electrode, and $Ag/AgCl/KCl_{(sat)}$ reference electrode) were inserted into the cell setup and a background scan was recorded with a scan rate of 100 mV/s, and four sweeps. The appropriate compound (2 mM) was added and the resulting solution was purged with argon for 10 min. Scans were recorded at 100 mV/s rate with four sweeps for each measurement.

Calculations of the free energy change of the electron transfer (ΔGE_T). The driving force for PeT from the antenna to Eu(III) was calculated to be thermodynamically feasible according to Eq. S1:

$$\Delta G_{ET} = (E_{ox} - E_{red}) - E_s - \frac{e_0^2}{\varepsilon} \qquad \text{Eq. S1}$$

E_{ox} is the electron donor oxidation potential, determined to be +1.81, +1.77, +1.86, and +1.73 V (vs NHE) by cyclic voltammetric analysis of the model compounds **AcCS**, **AcCS^{6F}**, **AcCS^{5F}** and **AcCS^{3F}**, respectively. E_{red} of Eu(III) was approximated with the cathodic potential of the overall uncharged 4-CF-substituted do3a-based complex with a value of –0.89 V (vs NHE).[4] E_s is the excited state energy of the antenna, determined from the first vibronic band of the **GdL^{F}** spectra at 77 K as 3.56, 3.48, 3.58, and 3.61 eV for **GdL^{H}**, **GdL^{6F}**, **GdL^{5F}** and **GdL^{3F}**, respectively. The last term for Coulombic stabilization of the charge-separated system was taken as ~0.15 eV.[5] The calculated ΔG values for Eu(III) reduction were –1.01, –0.97, –0.98, and –1.14 eV for **EuL^{H}**, **EuL^{6F}**, **EuL^{5F}** and **EuL^{3F}** complexes, respectively.

Fluorescent lifetime decays. The fluorescence lifetime decays in the nanosecond range were measured on a Spectrofluorometer FS5 system from Edinburgh Instruments. The system was equipped with picosecond pulsed light emitting diode EPLED-340 with excitation wavelength at 341.5 nm. The data were acquired in the 50 ns measurement range with peak pre-set at 10^4 counts in 1024 channels. The repetition rate of the excitation source was 10 MHz, and the synchronization delay was 80 ns. The scatter light profile (prompt signal, blue in the decay figures, Figures S49–76) was recorded for each experiment individually in the same quartz cuvette using diluted Ludox® (Sigma Aldrich) solution in HPLC water at 341.5 nm emission wavelength with similar parameters as were used for the measured sample (red in the decay figures, Figures S49–76). All measurements were done at r.t. with such concentration of the sample that A ~ 0.1 at 341.5 nm and maximum optical power of the excitation source. All compounds were measured at an identical emission wavelength (see Table S5). The solvents were MeCN and PIPES buffered HPLC-grade water (pH ~ 6.5) for carbostyrils and **LnL**, respectively. The obtained data were fitted using the DecayFit software (black trace in the decay figures, Figures S43–64) using either mono- (Eq. S2) or biexponential (Eq. S3) reconvolution fit model, where τ_1 and τ_2 are the lifetimes, t is time represented in ns, a_1 and a_2 are the populations of τ_1 and τ_2, respectively.

$$R(t) = a_1 * \exp(-t/\tau_1) \qquad \text{Eq. S2}$$

$$\boldsymbol{R(t) = a_1 * \exp\left(-\frac{t}{\tau_1}\right) + a_2 * \exp\left(-\frac{t}{\tau_2}\right)} \qquad \text{Eq. S3}$$

UV-Vis absorption and emission spectroscopy. All measurements were performed in PIPES-buffered distilled water or D_2O at pH 6.5 or pD 6.5. [**LnL**] was nominally 10 µM, however, small quantities of Ln salts may diminish this. Glycerol was of 99.9+% purity. Quartz cells with 1 cm optical pathlengths were used for the room temperature measurements. The absorbance spectra were measured by a Varian Cary 100 Bio UV-Visible spectrophotometer. The emission and excitation spectra, lifetimes, time-resolved spectra and quantum yields were recorded on a Horiba FluoroMax-4P. All emissions were corrected by the wavelength sensitivity (correction function) of the spectrometer. All measurements were performed at room temperature unless stated otherwise.

Quantum yields were measured at room temperature, using quinine sulfate (QS) in H_2SO_4 0.05 M (Φ_{ref} = 0.59) as reference[6] in Equation S4. Quantum yields were calculated according to Eq. S4, with Φ_s the quantum yield of the sample, Φ_{ref} the quantum yield of the reference, I the integrated corrected emission intensity of the sample (*s*) and of the reference (*ref*), f_A the absorption factor of the sample (*s*) and of the reference *(ref*) at the excitation wavelength and *n* the refractive indexes of the sample (*s*) and of the reference (*ref*). The concentration of the complexes was adjusted to obtain an absorbance around the maxima of the antennae matching that of the QS fluorescence standard. The excitation wavelength where the absorption factors of the samples and of the reference were the same was chosen (*i.e.* where the absorptions are identical). The corrected emission spectra of the sample and reference standard were then measured under the same conditions over the 315–800 nm spectral range as well as blank samples containing only the solvent. The appropriate blanks were subtracted from their respective spectra, and the antenna fluorescence and Ln(III) luminescence were separated by fitting the section of the antenna emission overlapping the Ln(III) emission with an exponential decay or with a scaled emission spectrum from the corresponding Gd(III) complexes. The quantum yields were then calculated according to Eq. S4. The given relative error on the quantum yields ($\delta\Phi = \Delta\Phi/\Phi$, where $\Delta\Phi$ is the absolute error) take into account the accuracy of the spectrometer and of the integration procedure [$\delta(I_s/I_{ref}) < 2\%$], an error of 0.59 ±0.01 on the quantum yield of the reference QS [$\delta(\Phi_{ref}) < 2\%$], an error on the ratio of the absorption factors [$\delta(f_{Aref}/f_{As}) < 5\%$, relative to the fixed absorption factor of the reference QS] and an

error on the ratio of the squared refractive indexes [$\delta(n_s^2/n_{ref}^2) < 1\%$, < 0.25% around 1.333 for H_2O, 1.328 for D_2O,[7] and 1.344 for MeCN[8] on each individual refractive index], which sums to a total estimated relative error that should be $\delta\Phi_s < 10\%$. A limit value of 10% is thus chosen.

$$\Phi = \frac{I_s}{I_{ref}} \cdot \frac{f_{Aref}}{f_{As}} \cdot \frac{(n_s)^2}{(n_{ref})^2} \cdot \Phi_{ref} \qquad \text{Eq. S4}$$

Low temperature measurements were done in quartz capillaries (0.2 cm optical pathlength) at 77 K by immersion in a liquid N_2-filled quartz Dewar and with addition of glycerol (1 drop) to the solutions (9 drops) measured at room temperature.

Lifetimes were recorded 0.05 ms after pulsed excitation at the excitation maxima (λ_{ex}) by measuring the decay of the lanthanide main emission peak (Eu 615 nm and Tb 545 nm). The increments after the initial delay were adjusted between 0.2–20 μs depending on the lifetime in order to have a good sampling of the decay. The obtained data were fitted by single and double exponential decay models in OriginPro 9, and the most reliable value was chosen according to the adjusted R^2 value and the shape of the residuals. A relative error of 10% is typically found among a series of measurements on the same sample.

Hydration numbers (q) were obtained by measuring the lifetimes of the same quantity of complex in a PIPES buffered solution in H_2O and in D_2O and fitting the difference according to the model of Horrocks *et al.*[9] and Beeby *et al.*[10]

X-ray crystallography. Crystals were obtained by the slow evaporation of the solvent from concentrated solutions in acetonitrile (**CS^{5F}**) and MeOH (**CS^{3F}**, **CS^{6F}**). All SC-XRD measurements are performed using graphite-monochromatized Mo Kα radiation using a Bruker D8 APEX-II equipped with a CCD camera. Data reduction was performed with SAINT. Absorption corrections for the area detector were performed using SADABS. The structure was solved by direct methods and refined by full-matrix least-squares techniques against F2 using all data (SHELXT, SHELXS). All non-hydrogen atoms were refined with anisotropic displacement parameters if not stated otherwise. Hydrogen atoms constrained in geometric positions to their parent atoms using OLEX2. The hydrogen atoms of the NH_2 group are refined without geometric constraints. Further details of the structure solutions can be found below and are deposited at the CCDC. 2155036–2155038 contain the supplementary crystallographic data for this paper. These data can be obtained free of charge via www.ccdc.cam.ac.uk/data_request/cif, or by emailing data_request@ccdc.cam.ac.uk, or by contacting The Cambridge Crystallographic Data Centre, 12, Union Road, Cambridge CB2 1EZ, UK; fax: +44 1223 336033.

Table S1. Crystal data and structure refinement for CS^{3F}.

Identification code CCDC no.	2155036
Empirical formula	$C_9H_7FN_2O$
Formula weight	178.17
Temperature/K	180
Crystal system	monoclinic
Space group	$P2_1/c$
a/Å	5.2349(8)
b/Å	8.1302(13)
c/Å	18.418(3)
α/°	90
β/°	91.160(3)
γ/°	90
Volume/Å^3	783.7(2)
Z	4
ρ_{calc}g/cm^3	1.510
μ/mm^{-1}	0.118
F(000)	368.0
Crystal size/mm^3	0.12 × 0.12 × 0.1
Radiation	MoK_α (λ = 0.71073)
2Θ range for data collection/°	4.424 to 57.834
Index ranges	$-7 \leq h \leq 7$, $-11 \leq k \leq 11$, $-25 \leq l \leq 24$
Reflections collected	13765
Independent reflections	2051 [R_{int} = 0.0264, R_{sigma} = 0.0171]
Data/restraints/parameters	2051/0/125
Goodness-of-fit on F^2	1.066
Final R indexes [I>=2σ (I)]	R_1 = 0.0444, wR_2 = 0.1270
Final R indexes [all data]	R_1 = 0.0606, wR_2 = 0.1385
Largest diff. peak/hole / e Å^{-3}	0.32/–0.21

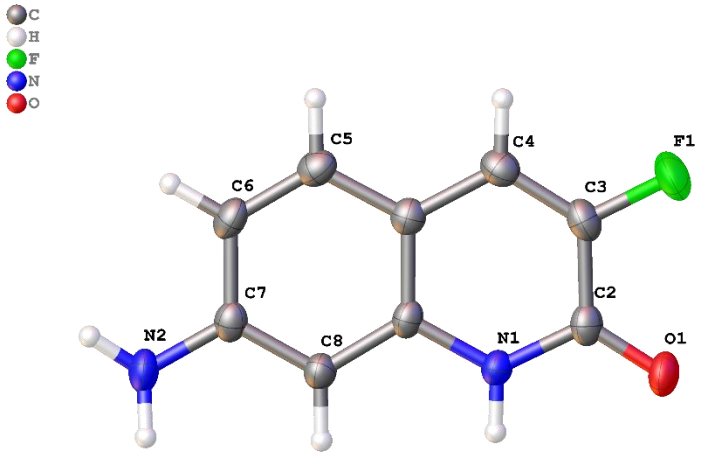

Figure S1. Solid state-structure of **CS^{3F}**; ORTEP-style with thermal ellipsoids at 50% probability level.

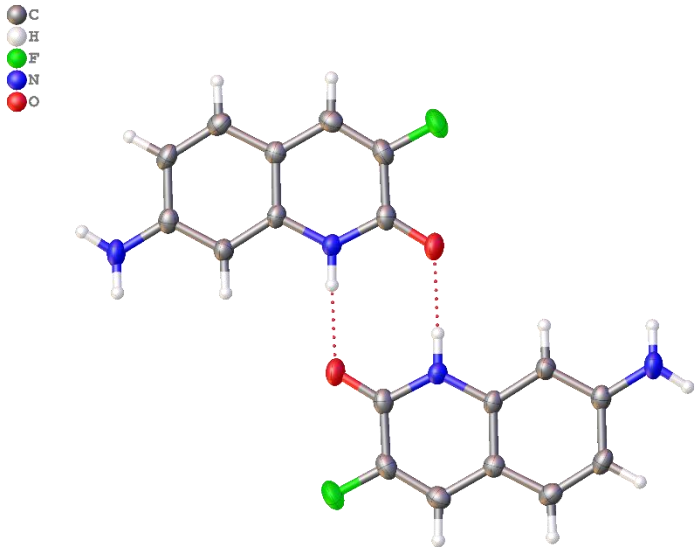

Figure S2 Hydrogen bonded dimer of **CS^{3F}**. Selected distances [Å] and angles [°]: N1-H1 0.88; O1···H1 1.95, N1···O1 1 2.8223(18), N1-H1···O1 172.3.

Table S2. Crystal data and structure refinement for CS^{6F}.

Identification code CCDC no.	2155037
Empirical formula	$C_9H_7FN_2O$
Formula weight	178.17
Temperature/K	180
Crystal system	monoclinic
Space group	$P2_1/c$
a/Å	7.481(2)
b/Å	6.777(2)
c/Å	15.561(5)
α/°	90
β/°	100.970(6)
γ/°	90
Volume/Å^3	774.5(4)
Z	4
ρ_{calc}g/cm^3	1.528
μ/mm^{-1}	0.119
F(000)	368.0
Crystal size/mm^3	0.16 × 0.15 × 0.09
Radiation	MoK_α (λ = 0.71073)
2Θ range for data collection/°	5.334 to 57.872
Index ranges	$-10 \leq h \leq 10$, $-9 \leq k \leq 9$, $-21 \leq l \leq 20$
Reflections collected	14239
Independent reflections	2041 [R_{int} = 0.0550, R_{sigma} = 0.0360]
Data/restraints/parameters	2041/0/125
Goodness-of-fit on F^2	1.062
Final R indexes [I>=2σ (I)]	R_1 = 0.0516, wR_2 = 0.1104
Final R indexes [all data]	R_1 = 0.0936, wR_2 = 0.1304
Largest diff. peak/hole / e Å^{-3}	0.24/–0.25

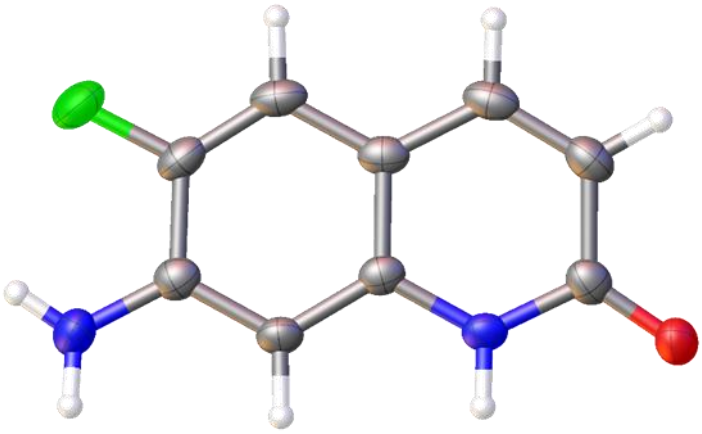

Figure S3 Solid state-structure of **CS^{6F}**; ORTEP-style with thermal ellipsoids at 50% probability level.

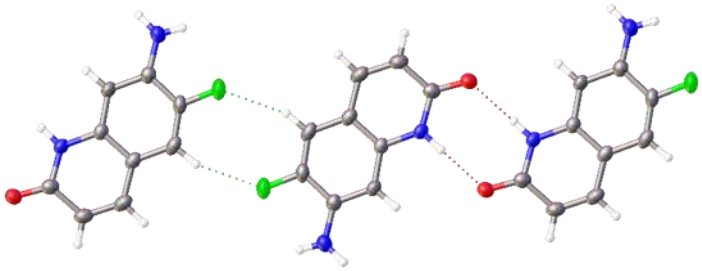

Figure S4 Hydrogen bonded network of the solid structure of **CS^{6F}**.
Selected distances [Å] and angles [°]: N1-H1 0.88; O1···H1 1.99, N1···O1, 2.861(2), N1-H1···O1 170.5, C5-H5 0.95, F1···H5 2.42, C5···F1 3.310(2), C5-H5···F1 155.3.

Table S3. Crystal data and structure refinement for CS^{5F}.

Identification code CCDC no.	2155038
Empirical formula	$C_9H_7FN_2O$
Formula weight	178.17
Temperature/K	180
Crystal system	monoclinic
Space group	$P2_1/c$
a/Å	7.6379(14)
b/Å	6.7755(12)
c/Å	15.015(3)
α/°	90
β/°	104.312(4)
γ/°	90
Volume/Å^3	752.9(2)
Z	4
ρ_{calc}g/cm^3	1.572
μ/mm^{-1}	0.123
F(000)	368.0
Crystal size/mm^3	0.13 × 0.12 × 0.12
Radiation	MoK_α (λ = 0.71073)
2Θ range for data collection/°	5.504 to 57.032
Index ranges	$-10 \leq h \leq 10$, $-9 \leq k \leq 8$, $-20 \leq l \leq 19$
Reflections collected	10754
Independent reflections	1798 [R_{int} = 0.0433, R_{sigma} = 0.0328]
Data/restraints/parameters	1798/0/125
Goodness-of-fit on F^2	1.067
Final R indexes [I>=2σ (I)]	R_1 = 0.0484, wR_2 = 0.1239
Final R indexes [all data]	R_1 = 0.0719, wR_2 = 0.1399
Largest diff. peak/hole / e Å^{-3}	0.47/–0.18

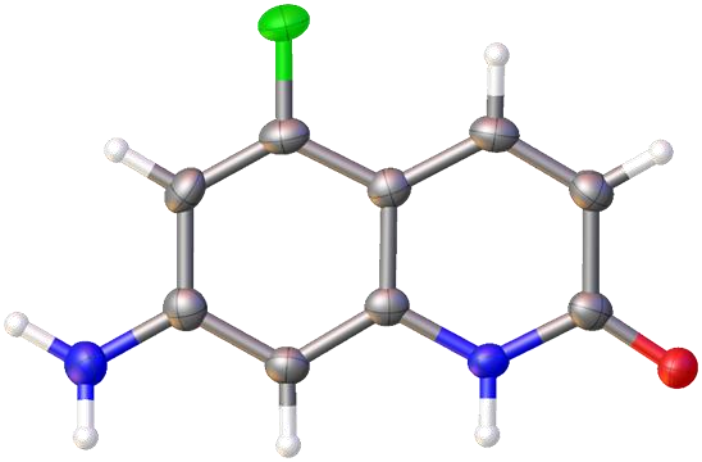

Figure S5 Solid state-structure of **CS^{5F}**; ORTEP-style with thermal ellipsoids at 50% probability level.

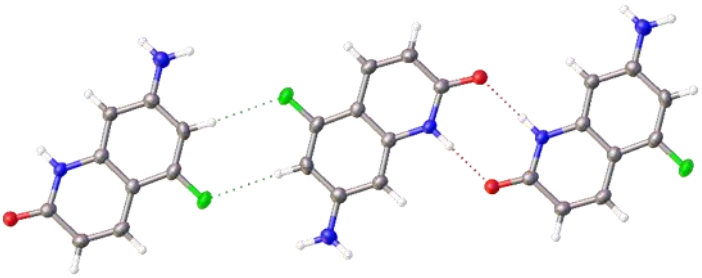

Figure S6 Hydrogen bonded network of the solid structure of **CS^{5F}**.
Selected distances [Å] and angles [°]: N1-H1 0.88; O1···H1 1.92, N1···O1, 2.7924(19), N1-H1···O1 171.8, C6-H6 0.95, F1···H6 2.57, C5···F1 3.498(2), C6-H6···F1 165.6.

Additional synthetic procedures and characterisation data

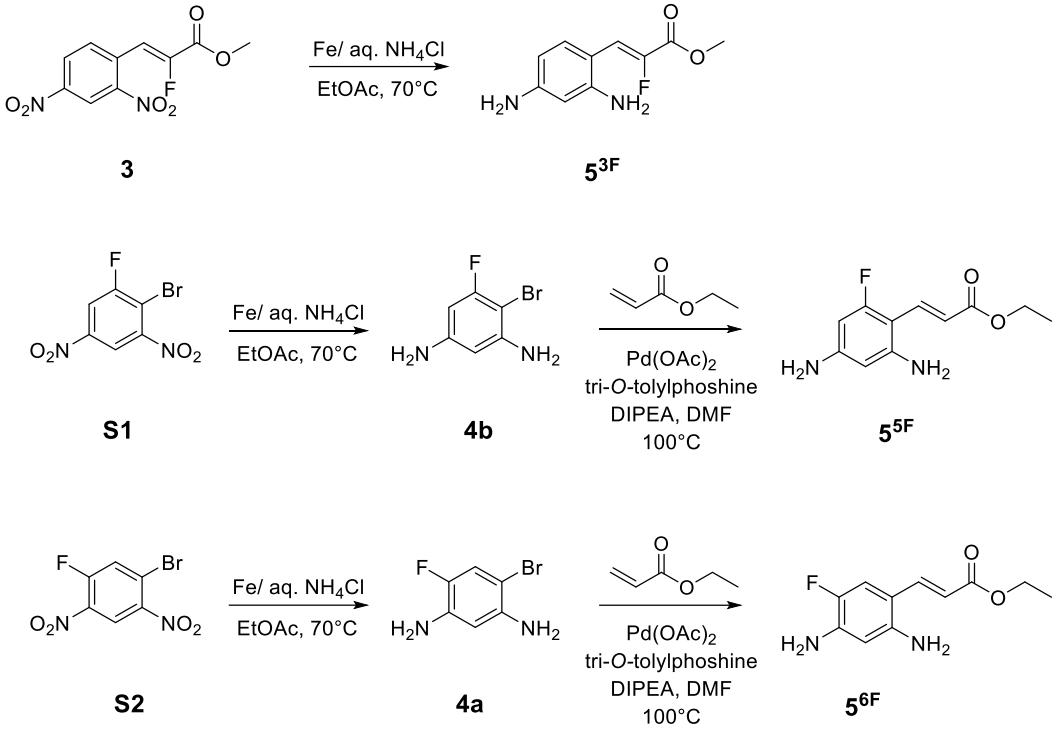

Scheme S1.

General procedure of the reduction

Dinitro compound **3**, **S1**, or **S2** (1.0 mmol, 1.0 equiv) was dissolved in a mixture of EtOAc and water 1:1 (0.1 M). NH_4Cl (8.0 equiv) and iron powder (6.0 equiv) were added to the mixture. The mixture was heated to 75 °C and stirred for 1 h. After TLC analysis showed full conversion of the starting material, the reaction mixture was allowed to cool down to r.t., filtered through a celite pad, and the filter cake was washed with water and EtOAc. The phases of the filtrate were separated. The aqueous phase was extracted twice with EtOAc, dried over Na_2SO_4, filtered, and the filtrate was evaporated to dryness. The crude product was purified by column chromatography on silica gel (0→50 % EtOAc in *n*-Heptane) yielding **1**^{3F}, **S3** or **S5**.

5^{3F}. (533 mg, 71%, orange solid): ^{1}H NMR (400 MHz, DMSO-d_6) δ = 7.32 (d, J = 8.5 Hz, 1H), 7.04 (d, J = 38.0 Hz, 1H), 5.90 (dd, J_1 = 8.5 Hz, J_2 = 2.5 Hz, 1H), 5.86 (d, J = 2.0 Hz, 1H), 5.47 (s, 2H), 5.35 (s, 2H), 3.75 (s, 2H). ^{13}C NMR (101 MHz, DMSO-d_6) δ = 162.0 (d, J = 39 Hz), 151.8, 150.1, 142.3 (d, J = 252 Hz), 131.7 (d, J = 14 Hz), 114.4 (d, J = 3 Hz), 105.2, 103.5 (d, J = 5 Hz), 99.0, 51.9. ^{19}F NMR (376 MHz, DMSO-d_6) δ −136.5 (d, J = 38.1 Hz, 1F). HR-ESI-MS obsd 211.0883, calcd 211.0877 [(M + H)$^+$, M = $C_{10}H_{11}FN_2O_2$].

4b. (1.67 g, 77%, beige solid): ^{1}H NMR (400 MHz, DMSO-d_6) δ 5.83 (dd, J_1 = 2.5 Hz, J_2 = 1.0 Hz, 1H), 5.75 (dd, J_1 = 11.5, J_2 = 2.5 Hz, 1H), 5.27–5.12 (m, 4H). ^{13}C NMR (101 MHz, DMSO-d_6) δ 159.7 (d, J = 236 Hz), 149.4 (d, J = 14 Hz), 147.4 (d, J = 6 Hz), 95.4, 90.6 (d, J = 25 Hz), 80.2 (d, J = 23 Hz). ^{19}F NMR (376 MHz, DMSO-D_6) δ –109.1 (d, J = 11.4 Hz, 1F). HR-ESI-MS obsd 204.9777 and 206.9756, calcd 204.9772 and 206.9751 [(M + H)$^+$, M = $C_6H_7BrN_2$].

4a. (1.58 g, 75%, beige solid): ^{1}H NMR (400 MHz, DMSO-d_6) δ 6.98 (d, J = 10.5 Hz, 1H), 6.20 (d, J = 9.0 Hz, 1H), 5.02 (s, 2H), 4.80 (s, 2H). ^{13}C NMR (101 MHz, DMSO-d_6) δ 143.4 (d, J = 230 Hz), 142.3, 136.5 (d, J = 13 Hz), 117.5 (d, J = 22 Hz), 101.7 (d, J = 4 Hz), 91.5 (d, J = 10 Hz). ^{19}F NMR (376 MHz, DMSO-d_6) δ –146.9 (dd, J_1 = 10.8, J_2 = 8.7 Hz, 1F). HR-ESI-MS obsd 204.9771 and 206.9750, calcd 204.9772 and 206.9751 [(M + H)$^+$, M = $C_6H_6BrFN_2$].

General procedure of Heck-coupling

Under an argon atmosphere the diamino intermediate **4a** or **4b** (1.0 mmol, 1.0 equiv), $Pd(OAc)_2$ (0.05 equiv) and tri-*o*-tolyl phosphate (0.4 equiv) were dissolved in dry DMF (0.25 M). DIPEA (2.0 equiv) and ethyl acrylate (1.5 equiv) were added, and the mixture was stirred at 100 °C for 1 h. After TLC analysis showed full conversion of the starting material, the reaction mixture was allowed to cool down to r.t. Water and EtOAc were added, and the aqueous phase was extracted twice with EtOAc. The combined organic phase was washed with brine, dried over Na_2SO_4, filtered, and concentrated. The crude product was purified by column chromatography on silica gel (0→50 % EtOAc in *n*-Heptane) yielding $\mathbf{1}^{\mathbf{5F}}$ and $\mathbf{1}^{\mathbf{6F}}$.

$\mathbf{5}^{\mathbf{5F}}$. (420 mg, 43 %, yellow solid): ^{1}H NMR (400 MHz, DMSO-d_6) δ 7.60 (d, J = 16.0 Hz, 1H), 6.07 (dd, J_1 = 16.0 Hz, J_2 = 1.5 Hz, 1H), 5.74–5.67 (m, 4H), 5.55 (s, 2H), 4.12 (q, J = 7.0 Hz, 2H), 1.22 (t, J = 7.0 Hz, 3H). ^{13}C NMR (101 MHz, DMSO-d_6) δ 167.7, 164.3 (d, J = 246 Hz), 152.4 (d, J = 16 Hz), 151.3 (d, J = 9 Hz), 135.6, 111.9 (d, J = 13 Hz), 96.6 (d, J = 14 Hz), 94.9, 90.9 (d, J = 26 Hz), 59.2, 14.4. ^{19}F NMR (376 MHz, DMSO-d_6) δ –111.6 (d, J = 14.0 Hz, 1F). HR-ESI-MS obsd 247.0853, calcd 247.0859 [(M + Na)$^+$, M = $C_{11}H_{13}FN_2O_2$].

$\mathbf{5}^{\mathbf{6F}}$. (1.35 g, 80%, orange solid): ^{1}H NMR (400 MHz, DMSO-d_6) δ 7.72 (dd, J_1 = 15.5 Hz, J_1 = 2.0 Hz, 1H), 7.14 (d, J = 13.0 Hz, 1H), 6.03 (d, J = 15.5 Hz, 1H), 5.99 (d, J = 8.5 Hz, 1H), 5.53 (s, 2H),

5.26 (s, 2H), 4.11 (q, J = 7.0 Hz, 2H), 1.22 (t, J = 7.0 Hz, 3H). ^{13}C NMR (101 MHz, DMSO-d_6) δ 167.3, 146.5, 144.4 (d, J = 229 Hz), 140.5, 140.4, 112.1 (d, J = 18 Hz), 109.4, 105.9 (d, J = 6 Hz), 101.0 (d, J = 3 Hz), 59.2, 14.4. ^{19}F NMR (376 MHz, DMSO-d_6) δ −147.3 (ddd, J_1 = 13.0 Hz, J_2 = 8.7 Hz, J_3 = 2.3 Hz, 1F). HR-ESI-MS obsd 223.0888, calcd 223.0888 [$(M - H)^-$, M = $C_{11}H_{13}FN_2O_2$].

General procedure of ring closure

The appropriate olefin was dissolved in alcohol (**5^{3F}** in MeOH, **5^{5F}** and **5^{6F}** in EtOH; 0.1 M). The solution was split into 10 mL fractions and transferred into quartz reaction vessels. The reaction mixtures were irradiated ($h\nu$ = 254 nm) in a photoreactor. After TLC analysis showed full conversion (typically ~5 h) of the starting material, the initially split reaction mixtures were combined and concentrated under reduced pressure. The residual solid was washed with DCM, filtered, and the filter cake was dried under high vacuum.

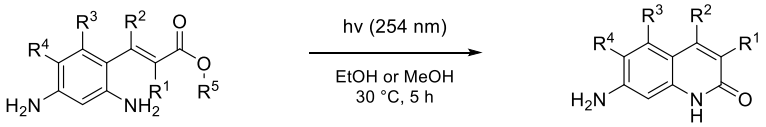

5^{3F} R^1 = F, R^2 = R^3 = R^4 = H, R^5 = Me
5^{5F} R^3 = F, R^1 = R^1 = R^4 = H, R^5 = Et
5^{6F} R^4 = F, R^1 = R^2 = R^3 = H, R^5 = Et

CS^{3F} R^1 = F, R^2 = R^3 = R^4 = H
CS^{5F} R^3 = F, R^1 = R^1 = R^4 = H
CS^{6F} R^4 = F, R^1 = R^2 = R^3 = H

Scheme S2.

CS^{3F}. (335 mg, 96%, beige powder): ^{1}H NMR (400 MHz, DMSO-d_6) δ 11.83 (d, J = 5.5 Hz, 1H), 7.58 (d, J = 11.5 Hz, 1H), 7.25 (d, J = 8.5 Hz, 1H), 6.49 (dd, J_1 = 8.5 Hz, J_2 = 2.0 Hz, 1H), 6.41 (d, J = 2.0 Hz, 1H), 5.75 (s, 2H). ^{13}C NMR (101 MHz, DMSO-d_6) δ 156.1 (d, J = 27 Hz), 150.6, 147.0 (d, J = 242 Hz), 138.0, 128.4 (d, J = 5 Hz), 120.1 (d, J = 16 Hz), 111.6, 107.9 (d, J = 7 Hz), 96.7. ^{19}F NMR (376 MHz, DMSO-d_6) δ −141.4 (dd, J_1 = 11.5 Hz, J_2 = 5.5 Hz, 1F). HR-ESI-MS obsd 179.0621, calcd 179.0615 [$(M + H)^+$, M = $C_9H_7FN_2O$].

CS^{5F}. (133 mg, 48%, beige powder): ^{1}H NMR (400 MHz, DMSO-d_6) δ 11.45 (s, 1H), 7.67 (d, J = 9.5 Hz, 1H), 6.22 (dd, J_1 = 12.5 Hz, J_2 = 1.9 Hz, 1H), 6.19 (s, 1H), 6.08 (s, 2H), 6.06 (d, J = 9.5 Hz, 1H). ^{13}C NMR (101 MHz, DMSO-d_6) δ 162.5, 159.3 (d, J = 246 Hz), 152.2 (d, J = 13 Hz), 142.0 (d, J = 9 Hz), 132.5 (d, J = 4 Hz), 115.1, 99.3 (d, J = 20 Hz), 95.3 (d, J = 22 Hz), 92.7. ^{19}F NMR (376 MHz,

DMSO-d_6) δ −122.8 (d, J = 12.5 Hz, 1F). HR-ESI-MS obsd 179.0615, calcd 179.0615 [(M + H)$^+$, M = $C_9H_7FN_2O$].

CS^{6F}. (466 mg, 86%, brown powder): ^{1}H NMR (400 MHz, DMSO-d_6) δ 11.42 (s, 1H), 7.61 (d, J = 9.5 Hz, 1H), 7.26 (d, J = 11.5 Hz, 1H), 6.57 (d, J = 8.0 Hz, 1H), 6.12 (d, J = 9.5 Hz, 1H), 5.91 (s, 2H). ^{13}C NMR (101 MHz, DMSO-d_6) δ 162.4, 147.0 (d, J = 235 Hz), 140.1 (d, J = 15 Hz), 139.7 (d, J = 3 Hz), 137.4, 116.4, 112.1 (d, J = 20 Hz), 108.9 (d, J = 8 Hz), 98.7 (d, J = 4 Hz). ^{19}F NMR (376 MHz, DMSO-d_6) δ −140.5 (dd, J_1 = 11.6 Hz, J_2 = 8.0 Hz, 1F). HR-ESI-MS obsd 179.0615, calcd 179.0615 [(M + H)$^+$, M = $C_9H_7FN_2O$].

Summary of attempted syntheses of CS^{4F}

According to the literature the formation of *β*-fluoro olefins is challenging, further complicated by the need to have amino or nitro groups in fixed positions. Synthetic pathways to photochemical olefin cyclization substrate **S14** were designed from cheap starting materials **S10**, **S11** or **S12** (**Scheme S3**). **S14** was proposed to form via silver-assisted regioselective fluorine addition to the triple bond of **S13**.[11] However, despite extensive experimentation **S13** could not be obtained via Sonogashira coupling.

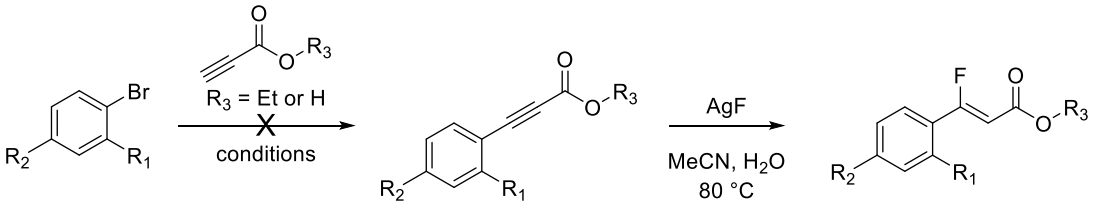

S10 R_1 = NO_2, R_2 = NO_2
S11 R_1 = NH_2, R_2 = NO_2
S12 R_1 = NO_2, R_2 = NH_2

S13 **S14**

Scheme S3.

Based on other methodologies Sonogashira coupling with trimethylsilylacetylene followed by desilylation was envisioned to yield the desired terminal acetylene.[12] This sequence starting from **S11** using established conditions yielded **S17**. Lithiation in the presence of an unprotected NH_2-group was expected to be difficult, and to avoid such a situation the synthesis was

modified. **S16** was readily obtained starting from 1-bromo-2,4-dinitrobenzene **S10**, but the deprotection reaction yielded immediate degradation of the acetylene **S18**.

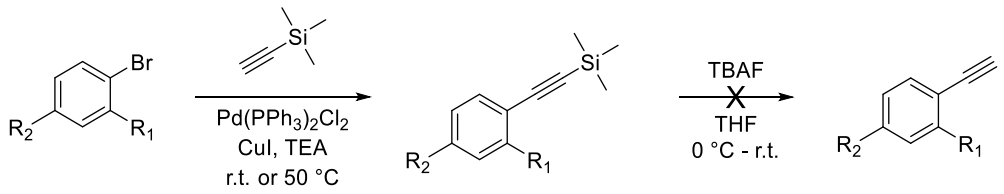

S11 $R_1 = NH_2$, $R_2 = NO_2$
S10 $R_1 = NO_2$, $R_2 = NO_2$

S15 $R_1 = NH_2$, $R_2 = NO_2$
S16 $R_1 = NO_2$, $R_2 = NO_2$

S17 $R_1 = NH_2$, $R_2 = NO_2$
S18 $R_1 = NO_2$, $R_2 = NO_2$

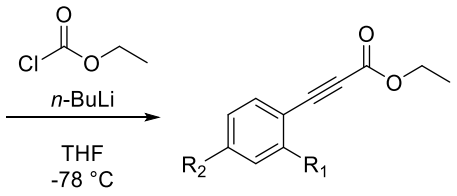

S19 $R_1 = NH_2$, $R_2 = NO_2$
S20 $R_1 = NO_2$, $R_2 = NO_2$

Scheme S4.

At this point an alternative route was devised. The key intermediate **S8** was obtained according to modified literature procedures (Scheme S5).[13-15] Several different conditions were tested for chloride to fluoride exchange.[16-17] Despite extensive efforts the desired **S9** intermediate was not possible to isolate. In order to optimize the reaction conditions various solvents (DMSO, DMF, NMP) and conditions (microwave irradiation) along with varied temperature and reaction time were tested. KF and CsF ware chosen as fluoride source. Pre-treatment of these compounds is crucial and was performed according to literature procedures. HPLC-MS and ^{19}F NMR analysis of the reaction mixtures revealed several undesired side reactions. According to ^{19}F NMR multiple fluorine containing species formed through the reaction. Even though none of the side products were isolated nor characterised, we believe that **S9** might undergo degradation upon reaction conditions. Bearing these considerations in mind, this transformation is not reproducible, lacking of robustness and low yielding.

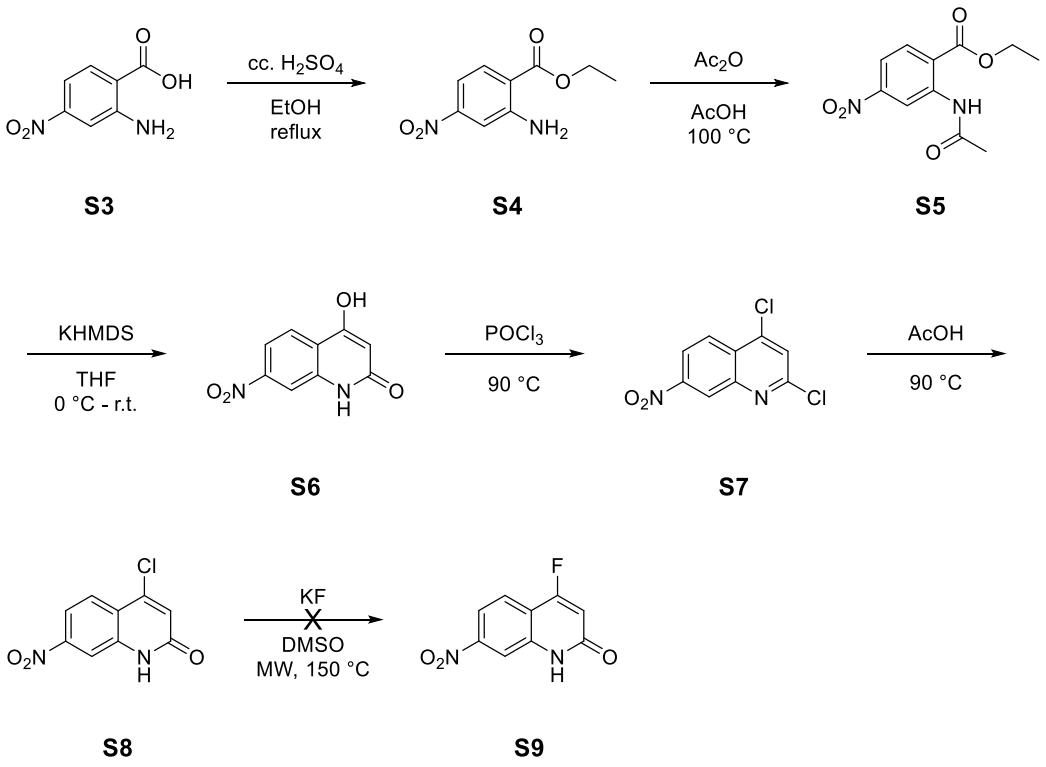

Scheme S5.

2-Amino-4-nitrobenzoic acid **S3** (4.0 g, 21.9 mmol, 1.0 equiv.) was dissolved in EtOH (200 mL). H_2SO_4 (cc., 4 mL) was added, and the reaction mixture was heated at reflux for 3 days. Then the solvent was evaporated, the residue was dissolved in AcOH (20 mL), and Ac_2O (20 mL, 219 mmol, 10.0 equiv) was added to the solution. The reaction mixture was heated at 100 °C with stirring for 1 h. After TLC analysis showed full conversion of **S4**, the reaction mixture was allowed to cool down to r.t., was poured onto ice, and the mixture was extracted three times with EtOAc. The combined organic layer was dried over Na_2SO_4, filtered, and the filtrate was concentrated under reduced pressure. The crude product was purified by column chromatography on silica gel (0→30 % EtOAc in *n*-Heptane) yielding **S5**.

S5. (2.5 g, 45%, yellow solid): ^{1}H NMR (400 MHz, DMSO-d_6) δ 10.64 (s, 1H), 8.97 (d, J = 2.5 Hz, 1H), 8.09 (d, J = 8.5 Hz, 1H), 7.98 (dd, J_1 = 8.5 Hz, J_2 = 2.5 Hz, 1H), 4.35 (q, J = 7.0 Hz, 2H), 2.16 (s, 3H), 1.34 (t, J = 7.0 Hz, 3H). ^{13}C NMR (101 MHz, DMSO-d_6) δ 169.1, 165.7, 149.9, 139.8, 131.9, 124.0, 117.5, 115.7, 61.9, 24.4, 13.9. HR-ESI-MS obsd 275.0637, calcd 275.0638 [$(M + Na)^+$, M = $C_{11}H_{12}N_2O_5$].

Under an Ar atmosphere **S5** (2.4 g, 9.5 mmol, 1.0 equiv.) was dissolved in dry THF (20 mL), and the solution was cooled down to 0 °C. KHMDS (1 M in THF, 45 mL, 45 mmol, 4.7 equiv.) was added

dropwise while the temperature was kept below 5 °C. The reaction mixture was allowed to warm up to r.t. and was stirred for 2 h. Then 6 M HCl was added to the reaction mixture, the temperature was carefully kept under 15 °C. When the pH of the mixture reached pH = 1 the mixture was extracted three times with EtOAc. The combined organic layer was dried over Na_2SO_4, filtered, and the filtrate was concentrated under reduced pressure. The residue was suspended in DCM and the solid was collected by centrifugation. The solid was washed five times with DCM, and then dried over high vacuum yielding **S6**.

S6. (752 mg, 38%, brown solid): ^{1}H NMR (400 MHz, DMSO-d_6) δ 11.81 (s, 1H), 11.61 (s, 1H), 8.09 (d, J = 2.0 Hz, 1H), 7.98 (d, J = 9.0 Hz, 1H), 7.91 (dd, J_1 = 9.0, J_2 = 2.0 Hz, 1H), 5.88 (s, 1H). ^{13}C NMR (101 MHz, DMSO-d_6) δ 163.4, 161.3, 148.4, 139.2, 124.6, 119.6, 115.2, 110.2, 101.1. HR-ESI-MS obsd 205.0254, calcd 205.0255 [$(M - H)^-$, M = $C_9H_6N_2O_4$].

Starting material **S6** (745 mg, 3.61 mmol, 1.0 equiv.) was dissolved in $POCl_3$ (12 mL) and the mixture was stirred at 90 °C for 2 h. After TLC analysis showed full conversion of the starting material, the reaction mixture was allowed to cool down to r.t., was poured onto ice, and its pH was adjusted to 10 by the addition of aqueous ammonia (25 %). The resulting solid was separated by centrifugation yielding **S7**. Intermediate **S7** was dissolved in AcOH (20 mL) and the solution heated at 100 °C with stirring for 24 h. After TLC analysis showed full conversion of the starting material, the reaction mixture was allowed to cool down to r.t. and was poured onto ice. The solid was separated by centrifugation and was washed twice with water. The crude product was suspended in EtOH, the solvent was evaporated at reduced pressure, and the product was dried under vacuum yielding **S8**.

S8. (520 mg, 64%, brown solid): ^{1}H NMR (400 MHz, DMSO-d_6) δ 12.39 (s, 1H), 8.18 (d, J = 2.0 Hz, 1H), 8.10–8.02 (m, 2H), 7.08 (s, 1H). ^{13}C NMR (101 MHz, DMSO-d_6) δ 160.3, 148.8, 143.0, 138.7, 126.7, 124.8, 121.5, 116.5, 110.9. HR-ESI-MS obsd 222.9915, calcd 222.9916 [$(M - H)^-$, M = $C_9H_5ClN_2O_3$].

General procedure of carbostyril acetylation

The appropriate 7-aminocarbostyril (0.15 mmol) was dissolved in 6:1 mixture of AcOH and Ac_2O (0.3 M), and the mixture was stirred at 100 °C for 1 h. After TLC analysis showed full conversion of

the starting material, water was added, the resulting precipitate was collected by centrifugation. The solid was washed twice with water. The crude product was suspended in EtOH, and the solvent was evaporated under reduced pressure. The solid was finally washed with diethyl ether, and was dried under vacuum.

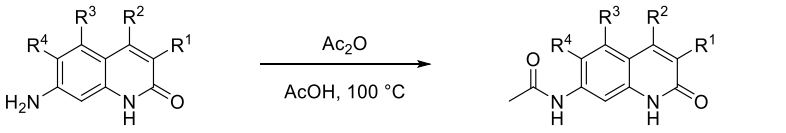

CS $R^1 = R^2 = R^3 = R^4 = H$
CS^{3F} $R^1 = F$, $R^2 = R^3 = R^4 = H$
CS^{5F} $R^3 = F$, $R^1 = R^1 = R^4 = H$
CS^{6F} $R^4 = F$, $R^1 = R^2 = R^3 = H$

AcCS $R^1 = R^2 = R^3 = R^4 = H$
AcCS^{3F} $R^1 = F$, $R^2 = R^3 = R^4 = H$
AcCS^{5F} $R^3 = F$, $R^1 = R^1 = R^4 = H$
AcCS^{6F} $R^4 = F$, $R^1 = R^2 = R^3 = H$

Scheme S6.

AcCS. (25 mg, 79%, beige solid): ^{1}H NMR (400 MHz, DMSO-d_6) δ 11.67 (s, 1H), 10.20 (s, 1H), 7.80–7.75 (m, 2H), 7.54 (d, J = 8.5 Hz, 1H), 7.26 (dd, J_1 = 8.5, J_2 = 2.0 Hz, 1H), 6.33 (d, J = 9.5 Hz, 1H), 2.07 (s, 3H). ^{13}C NMR (101 MHz, DMSO-d_6) δ 168.8, 162.3, 141.1, 139.9, 139.8, 128.3, 119.7, 115.0, 113.6, 104.1, 24.2. HR-ESI-MS obsd 225.0634, calcd 225.0635 [(M + Na)$^+$, M = $C_{11}H_{10}N_2O_2$].

AcCS^{3F}. (22 mg, 71%, beige solid): ^{1}H NMR (400 MHz, DMSO-d_6) δ 12.22 (d, J = 5.5 Hz, 1H), 10.21 (s, 1H), 7.86 (d, J = 2.0 Hz, 1H), 7.77 (d, J = 11.0 Hz, 1H), 7.54 (d, J = 8.5 Hz, 1H), 7.31 (dd, J_1 = 8.5 Hz, J_2 = 2.0 Hz, 1H), 2.07 (s, 3H). ^{13}C NMR (101 MHz, DMSO-d_6) δ 168.8, 155.9 (d, J = 27 Hz), 149.5 (d, J = 245 Hz), 140.3 (d, J = 3 Hz), 136.6, 128.0 (d, J = 6 Hz), 119.2 (d, J = 17 Hz), 114.4, 113.5 (d, J = 7 Hz), 104.2, 24.1. ^{19}F NMR (376 MHz, DMSO-d_6) δ −134.7 (dd, J_1 = 11.0 Hz, J_2 = 5.5 Hz, 1F). HR-ESI-MS obsd 243.0539, calcd 243.0540 [(M + Na)$^+$, M = $C_{11}H_9FN_2O_2$].

AcCS^{5F}. (22 mg, 71%, beige solid): ^{1}H NMR (400 MHz, DMSO-d_6) δ 11.90 (s, 1H), 10.36 (s, 1H), 7.85 (d, J = 9.5 Hz, 1H), 7.46 (s, 1H), 7.27 (dd, J_1 = 12.5 Hz, J_2 = 2.0 Hz, 1H), 6.39 (d, J = 9.5 Hz, 1H), 2.07 (s, 3H). ^{13}C NMR (101 MHz, DMSO-d_6) δ 169.1, 162.1, 158.2 (d, J = 247 Hz), 141.8 (d, J = 13 Hz), 140.9 (d, J = 8 Hz), 132.0 (d, J = 4 Hz), 120.2, 104.2 (d, J = 20 Hz), 100.0 (d, J = 3 Hz), 99.0 (d, J = 25 Hz), 24.2. ^{19}F NMR (376 MHz, DMSO-d_6) δ −120.8 (d, J = 12.4 Hz, 1F). HR-ESI-MS obsd 243.0539, calcd 243.0540 [(M + Na)$^+$, M = $C_{11}H_9FN_2O_2$].

AcCS^{6F}. (24 mg, 78%, beige solid): ^{1}H NMR (400 MHz, DMSO-d_6) δ 11.71 (s, 1H), 8.14 (d, J = 7.0 Hz, 1H), 7.78 (d, J = 9.5 Hz, 1H), 7.56 (d, J = 11.5 Hz, 1H), 6.43 (d, J = 9.5 Hz, 1H), 2.14 (s, 3H). ^{13}C NMR (101 MHz, DMSO-d_6) δ 169.2, 161.9, 148.2 (d, J = 240 Hz), 139.1 (d, J = 3 Hz), 135.9, 129.0 (d, J = 14 Hz), 121.4, 114.7 (d, J = 9 Hz), 112.6 (d, J = 21 Hz), 108.1, 23.8. ^{19}F NMR (376 MHz, DMSO-D_6) δ −133.2 (dd, J_1 = 11.4 Hz, J_2 = 7.0 Hz, 1F). HR-ESI-MS obsd 243.0539, calcd 243.0540 [(M + Na)$^+$, M = $C_{11}H_9FN_2O_2$].

General procedure for the chloroacetylation of 7-aminocarbostyrils:

A sample of the 7-aminocarbostyril (**CS**, **CS^{3F}**, **CS^{5F}**, **CS^{6F}**, 1.0 mmol, 1.0 equiv.) was dissolved in DMF (3 mL). To this solution DIPEA (2.0 mmol, 2.0 equiv.) was added followed by chloroacetyl chloride (1.5 mmol, 1.5 equiv.). After stirring at r.t. for 2 h and additional 0.5 equiv. chloroacetyl chloride was added, and the reaction mixture was stirred at r.t. for 2 h. At this stage TLC analysis showed full conversion of the starting material. The mixture was poured onto ice, and stirring was continued for 1 h. The resulting solid was collected by centrifugation, and was washed twice with water. The crude product was suspended in EtOH, and the solvent was evaporated under reduced pressure. The solid was finally washed with diethyl ether, and dried under vacuum.

6^{H}. (174 mg, 95 %, green solid): ^{1}H NMR (400 MHz, DMSO-d_6) δ 11.74 (s, 1H), 10.58 (s, 1H), 7.81 (d, J = 9.5 Hz, 1H), 7.76 (d, J = 2.0 Hz, 1H), 7.59 (d, J = 8.5 Hz, 1H), 7.30 (dd, J_1 = 8.6 Hz, J_2 = 2.0 Hz, 1H), 6.37 (dd, J_1 = 9.5, J_2 = 1.5 Hz, 1H), 4.29 (s, 2H). ^{13}C NMR (101 MHz, DMSO-d_6) δ 165.0, 162.2, 140.3, 139.9, 139.7, 128.6, 120.2, 115.5, 113.8, 104.6, 43.6. HR-ESI-MS obsd 259.0243, calcd 259.0244 [(M + Na)$^+$, M = $C_{11}H_9ClN_2O_2$].

6^{3F}. (273 mg, quant., green solid): ^{1}H NMR (400 MHz, DMSO-d_6) δ 12.30 (d, J = 5.5 Hz, 1H), 10.61 (s, 1H), 7.83 (s, 1H), 7.80 (d, J = 11.0 Hz, 1H), 7.59 (d, J = 8.5 Hz, 1H), 7.35 (d, J = 8.5 Hz, 1H), 4.29 (s, 2H). ^{13}C NMR (101 MHz, DMSO-d_6) δ 165.1, 155.9 (d, J = 27 Hz), 149.8 (d, J = 249 Hz), 139.5 (d, J = 3 Hz), 136.6, 128.3 (d, J = 6 Hz), 119.2 (d, J = 17 Hz), 114.6, 114.2 (d, J = 7 Hz), 104.7, 43.6. ^{19}F NMR (376 MHz, DMSO-d_6) δ −134.0 (dd, J_1 = 11.0 Hz, J_2 = 5.5 Hz, 1F). HR-ESI-MS obsd 277.0151, calcd 277.0151 [(M + Na)$^+$, M = $C_{11}H_8ClFN_2O_2$].

6^{5F} (157 mg, 83 %, brown solid): ^{1}H NMR (400 MHz, DMSO-d_6) δ 11.97 (s, 1H), 10.74 (s, 1H), 7.88 (d, J = 9.5 Hz, 1H), 7.46 (d, J = 2.0 Hz, 1H), 7.28 (dd, J_1 = 12.0 Hz, J_2 = 2.0 Hz, 1H), 6.43 (dd, J_1 = 9.5

Hz, J_2 = 1.3 Hz, 1H), 4.29 (s, 2H). ^{13}C NMR (101 MHz, DMSO-d_6) δ 165.3, 162.0, 158.2 (d, J = 247 Hz), 140.9 (d, J = 8 Hz), 140.8 (d, J = 3 Hz), 132.0 (d, J = 4 Hz), 120.8, 104.8 (d, J = 19 Hz), 100.6 (d, J = 3 Hz), 99.3 (d, J = 25 Hz), 43.6. ^{19}F NMR (376 MHz, DMSO-d_6) δ −120.2 (d, J = 12.2 Hz, 1F). HR-ESI-MS obsd 277.0152, calcd 277.0151 [(M + Na)$^+$, M = $C_{11}H_8ClFN_2O_2$].

6^{6F} (214 mg, 84%, brown solid): ^{1}H NMR (400 MHz, DMSO-d_6) δ 11.78 (s, 1H), 10.30 (s, 1H), 8.13 (d, J = 6.5 Hz, 1H), 7.81 (dd, J_1 = 9.5 Hz, J_2 = 1.5 Hz, 1H), 7.61 (dd, J_1 = 11.5 Hz, J_2 = 1.5 Hz, 1H), 6.47 (d, J = 9.5 Hz, 1H), 4.42 (s, 2H). ^{13}C NMR (101 MHz, DMSO-d_6) δ 165.5, 161.9, 148.3 (d, J = 241 Hz), 139.1 (d, J = 3 Hz), 135.9, 128.2 (d, J = 14 Hz), 121.8, 115.4 (d, J = 9 Hz), 112.9 (d, J = 21 Hz), 108.4, 43.3. ^{19}F NMR (376 MHz, DMSO-d_6) δ −133.0 (dd, J_1 = 11.2 Hz, J_2 = 6.9 Hz, 1F). HR-ESI-MS obsd 277.0151, calcd 277.0151 [(M + Na)$^+$, M = $C_{11}H_8ClFN_2O_2$].

General procedure for the *t*Bu-ester protected ligand synthesis:

Tris tert-butyl ester-protected DO3A (1.0 mmol, 1.0 equiv.), the appropriate chloroacetylated antenna (1.1 mmol, 1.1 equiv.) and K_2CO_3 (1.5 mmol, 1.5 equiv.) were placed in a vial. MeCN (10 mL, 0.1 M) was added, and the reaction mixture was stirred at 70 °C for 16 h, at which point TLC analysis showed full conversion of the starting material. The solids were removed by filtration, the filter cake was washed with MeCN, and the filtrate was concentrated under reduced pressure. The crude product was purified by column chromatography packed with neutral alumina. Elution with CH_2Cl_2:MeOH (100:0 → 90:10) yielded the title compounds as beige solids.

8^{H}. (278 mg, 55 %, beige slolid): ^{1}H NMR (400 MHz, DMSO-d_6) δ 11.77 (s, 1H), 10.65 (s, 1H), 7.87 (dd, J_1 = 8.5 Hz, J_2 = 2.0 Hz, 1H), 7.82 (d, J = 9.5 Hz, 1H), 7.47 (d, J = 8.5 Hz, 1H), 7.10 (d, J = 2.0 Hz, 1H), 6.35 (dd, J_1 = 9.5, J_2 = 2.0 Hz, 1H), 3.63–1.81 (m, 24H, overlap with DMSO and H_2O), 1.52–1.27 (s, 27H). ^{13}C NMR (101 MHz, DMSO-d_6) δ 172.6, 171.3, 140.8, 139.9, 139.5, 127.9, 120.0, 115.4, 114.5, 104.5, 81.2 (d, J = 3.4 Hz), 56.5, 56.0, 55.3, 52.4, 48.1, 27.6. HR-ESI-MS obsd 737.4207, calcd 737.4208 [(M + Na)$^+$, M = $C_{37}H_{58}N_6O_8$].

8^{3F}. (390 mg, 67 %): ^{1}H NMR (400 MHz, DMSO-d_6) δ 12.33 (d, J = 5.5 Hz, 1H), 10.48 (s, 1H), 7.92 (dd, J_1 = 8.5 Hz, J_2 = 2.0 Hz, 1H), 7.81 (d, J = 11.0 Hz, 1H), 7.49 (d, J = 8.7 Hz, 1H), 7.10 (d, J = 2.0 Hz, 1H), 3.64–1.86 (m, 24H, overlap with DMSO and H_2O) 1.48–1.28 (m, 27H). ^{13}C NMR (101 MHz,

DMSO-d_6) δ 172.6, 171.3, 155.9 (d, J = 28 Hz), 149.6 (d, J = 248 Hz), 139.9, 136.3, 127.7 (d, J = 5 Hz), 119.2 (d, J = 17 Hz), 115.3, 114.0 (d, J = 7 Hz), 104.5, 81.2, 56.4, 55.3, 52.3, 48.0, 27.6. ^{19}F NMR (376 MHz, DMSO-d_6) δ −134.2 (dd, J_1 = 10.9 Hz, J_2 = 5.3 Hz, 1F). HR-ESI-MS obsd 755.4113, calcd 755.4114 [(M + Na)$^+$, M = $C_{37}H_{57}FN_6O_8$].

8^{5F} (147 mg, 34 %): ^{1}H NMR (400 MHz, DMSO-d_6) δ 12.01 (s, 1H), 10.87 (s, 1H), 7.86 (d, J = 9.5 Hz, 1H), 7.80 (dd, J_1 = 13.0 Hz, J_2 = 2.0 Hz, 1H), 6.90 (d, J = 2.0 Hz, 1H), 6.40 (dd, J_1 = 9.5 Hz, J_2 = 2.0 Hz, 1H), 3.68–1.85 (m, 24H, overlap with DMSO and H_2O), 1.65–1.16 (m, 27H). ^{13}C NMR (101 MHz, DMSO-d_6) δ 172.6, 171.9, 165.6, 162.0, 161.1, 158.1 (d, J = 246 Hz), 141.5 (d, J = 14 Hz), 140.4 (d, J = 8 Hz), 132.1, 120.5, 104.4 (d, J = 19 Hz), 100.1 (d, J = 10 Hz), 81.2, 56.4, 56.0, 55.3, 52.5, 47.9, 27.5. ^{19}F NMR (376 MHz, DMSO-d_6) δ −121.0 (d, J = 12.8 Hz, 1F). HR-ESI-MS obsd 755.4105, calcd 755.4114 [(M + Na)$^+$, M = $C_{37}H_{57}FN_6O_8$].

8^{6F}. (290 mg, 54 %): ^{1}H NMR (400 MHz, DMSO-d_6) δ 11.84 (s, 1H), 10.47 (s, 1H), 7.85 (d, J = 10.0 Hz, 1H), 7.57 (d, J = 10.5 Hz, 1H), 7.33 (d, J = 6.5 Hz, 1H), 6.49 (d, J = 10.0 Hz, 1H), 3.56–1.85 (m, 24H, overlap with DMSO and H_2O) 1.46–1.20 (m, 27H). ^{13}C NMR (101 MHz, DMSO-d_6) δ 172.3, 170.8, 161.7, 150.9 (d, J = 244 Hz), 139.1, 135.5, 127.7 (d, J = 15 Hz), 122.2, 116.9 (d, J = 8 Hz), 113.2 (d, J = 22 Hz), 112.0, 81.1, 56.1, 55.3, 52.1, 48.5, 27.6. ^{19}F NMR (376 MHz, DMSO-d_6) δ −127.4 (s, 1F). HR-ESI-MS obsd 755.4115, calcd 755.4114 [(M + Na)$^+$, M = $C_{37}H_{57}FN_6O_8$].

General procedure for free ligand preparation:

A sample of the *t*Bu-ester protected ligand (0.38 mmol, 1.0 equiv.) was dissolved in a 1:1 mixture of DCM and TFA (6.0 mL, ~60 mM). The reaction mixture was stirred for 24 h at room temperature. When TLC and HPLC-MS analyses showed full conversion, the volatile components were removed at reduced pressure. The crude product was dissolved in a minimal amount of MeOH, diethyl ether was added, the precipitate was filtered. The filter cake was washed three times with DEE:MeOH 9:1, and was dried under vacuum. This procedure yielded **L^{6F}** and **L^{3F}** analytically pure as theirs TFA salts. **L^{5F}** was purified by column chromatography on silica gel. Elution with a mixture of MeCN:NH_4OH (25% aq.) (90:10 → 80:20 → 70:30) yielded analytically pure ligand **L^{5F}**. **L^{H}** was further purified by reverse phase

chromatography on a TELOS C18 12g flash column. Elution with H_2O:MeCN (5% isocratic) yielded analytically pure ligand $\mathbf{L^H}$.

$\mathbf{L^H}$. (138 mg, 73 %, pale yellow solid): ^{1}H NMR (400 MHz, D_2O) δ 7.86 (dd, J = 9.0 Hz, 1H), 7.60 (d, J = 2.0 Hz, 1H), 7.58 (d, J = 8.5 Hz, 1H), 7.19 (dd, J_1 = 8.5, J_2 = 2.0 Hz, 1H), 6.52 (d, J = 9.0 Hz, 1H), 3.45–3.33 (m, 2H), 3.13–2.89 (m, 6H), 2.63–2.20 (m, 16H). ^{13}C NMR (101 MHz, D_2O) δ 172.4, 167.4, 164.0, 142.2, 140.8, 139.1, 128.7, 118.3, 118.0, 116.0, 109.3, 59.0, 58.6, 57.5, 50.9, 50.6. HR-ESI-MS obsd 569.2329, calcd 569.2330 [$(M + Na)^+$, M = $C_{25}H_{34}N_6O_8Na$].

$\mathbf{L^{3F}}$. (66 mg, quant., off-white powder): ^{1}H NMR (400 MHz, D_2O) δ 7.31-7.19 (m, 2H), 7.05 (d, J = 8.6 Hz, 1H), 6.77 (d, J = 7.0 Hz, 1H), 4.03-2.93 (m, 24H). ^{13}C NMR (101 MHz, D_2O) δ 173.7, 170.3, 157.2 (d, J = 27 Hz), 148.7 (d, J = 246 Hz), 138.8, 134.5, 128.0, 120.8 (d, J = 17 Hz), 115.4, 114.7, 104.6, 55.8, 54.8, 53.1, 51.0, 48.3. HR-ESI-MS obsd 563.2257, calcd 563.2271 [$(M – H)^–$, M = $C_{25}H_{33}FN_6O_8$].

$\mathbf{L^{5F}}$. (47 mg, 76%, beige solid): ^{1}H NMR (400 MHz, D_2O) δ 7.79 (d, J = 9.6 Hz, 1H), 7.08 (s, 1H), 6.73 (d, J = 11.2 Hz, 1H), 6.38 (d, J = 9.6 Hz, 1H), 3.89 (s, 4H), 3.71 (s,2H), 3.64 (s, 2H), 3.59-3.39 (m, 8H), 3.24-3.00 (m, 8H). ^{13}C NMR (101 MHz, D_2O) δ 174.3, 170.1, 164.5, 158.0 (d, J = 249 Hz), 140.4 (d, J = 13 Hz), 138.7 (d, J = 7 Hz), 134.3, 117.9, 106.2 (d, J = 20 Hz), 101.1, 100.8, 56.5, 55.0, 53.3, 51.3, 51.2, 48.2, 48.0. ^{19}F NMR (376 MHz, D_2O) δ -120.3 (d, J = 11.5 Hz). HR-ESI-MS obsd 563.2256, calcd 563.2271 [$(M – H)^–$, M = $C_{25}H_{33}FN_6O_8$].

$\mathbf{L^{6F}}$. (218 mg, quant., off-white powder): ^{1}H NMR (400 MHz, D_2O) δ 7.62 (d, J = 6.5 Hz, 1H), 7.44 (d, J = 9.5 Hz, 1H), 6.90 (d, J = 11.0 Hz, 1H), 6.34 (d, J = 9.5 Hz, 1H), 4.13–2.91 (m, 24H, overlap with residual MeOH). ^{13}C NMR (101 MHz, D_2O) δ 174.1, 170.2, 163.9, 148.2 (d, J = 243 Hz), 141.1, 133.7, 128.5, 118.4, 117.8, 115.6, 112.3 (d, J = 21 Hz), 107.0, 55.8, 54.8, 51.2, 48.3. ^{19}F NMR (376 MHz, D_2O) δ –132.5 (s, 1F). HR-ESI-MS obsd 563.2258, calcd 563.2271 [$(M – H)^-$, M = $C_{25}H_{33}FN_6O_8$].

General procedure for lanthanide complex formation:

The ligand (1.0 equiv.) and anhydrous $LnCl_3$ (1.05 equiv.) were placed in a vial. A stirring bar was added, followed by a mixture of H_2O and EtOH (1:1, 0.05 M). 3.0 equiv. of NaOH (1 M aqueous solution) was added, the vial was sealed and the reaction mixture was heated at 45 °C. After 2–3 hours

the pH was adjusted to 8 by the addition of NaOH (1 M aqueous solution) and stirring was continued for 16 h. When TLC analysis showed full conversion of the starting material the mixture was loaded directly onto a silica gel chromatography column. Elution with ACN:H_2O (100:0 → 90:10 → 80:20 → 70:30 → 60:40) yielded the complexes as white solids.

GdL^{H}. (15 mg, 58%); HR-ESI-MS obsd 724.1335, calcd 724.1342 [$(M + Na)^+$, M = $C_{25}H_{31}GdN_6O_8Na$].

TbL^{H}. (11 mg, 43%); HR-ESI-MS obsd 725.1353, calcd 725.1349 [$(M + Na)^+$, M = $C_{25}H_{31}TbN_6O_8Na$].

EuL^{H}. (14 mg, 55%); HR-ESI-MS obsd 719.1311, calcd 719.1310 [$(M + Na)^+$, M = $C_{25}H_{31}EuN_6O_8Na$].

GdL^{3F}. (4 mg, 32%); HR-ESI-MS obsd 718.12647, calcd 718.12774 [$(M – H)^–$, M = $C_{25}H_{30}FGdN_6O_8$].

TbL^{3F}. (7 mg, 55%); HR-ESI-MS obsd 719.12845, calcd 719.12898 [$(M – H)^–$, M = $C_{25}H_{30}FTbN_6O_8$].

EuL^{3F}. (9 mg, 71%); HR-ESI-MS obsd 713.12269, calcd 713.12486 [$(M – H)^–$, M = $C_{25}H_{30}FEuN_6O_8$].

GdL^{5F}. (11 mg, 87%); HR-ESI-MS obsd 718.12704, calcd 718.12774 [$(M – H)^–$, M = $C_{25}H_{30}FGdN_6O_8$].

TbL^{5F}. (9 mg, 71%); HR-ESI-MS obsd 719.12709, calcd 719.12898 [$(M – H)^–$, M = $C_{25}H_{30}FTbN_6O_8$].

EuL^{5F}. (10 mg, 78%); HR-ESI-MS obsd 713.12365, calcd 713.12486 [$(M – H)^–$, M = $C_{25}H_{30}FEuN_6O_8$].

GdL^{6F}. (4 mg, quant.); HR-ESI-MS obsd 718.12727, calcd 718.12774 [$(M – H)^–$, M = $C_{25}H_{30}FGdN_6O_8$].

TbL^{6F}. (7 mg, 37%); HR-ESI-MS obsd 719.12869, calcd 719.12898 [$(M – H)^–$, M = $C_{25}H_{30}FTbN_6O_8$].

EuL^{6F}. (9 mg, 87%); HR-ESI-MS obsd 713.12340, calcd 713.12486 [$(M – H)^–$, M = $C_{25}H_{30}FEuN_6O_8$].

EuL^{6F}. (65 mg, 77%); HR-ESI-MS obsd 737.12134, calcd 737.12157 [$(M + Na)^+$, M = $C_{25}H_{30}FEuN_6O_8Na$].

Paramagnetic ^{1}H and ^{19}F NMR spectroscopy

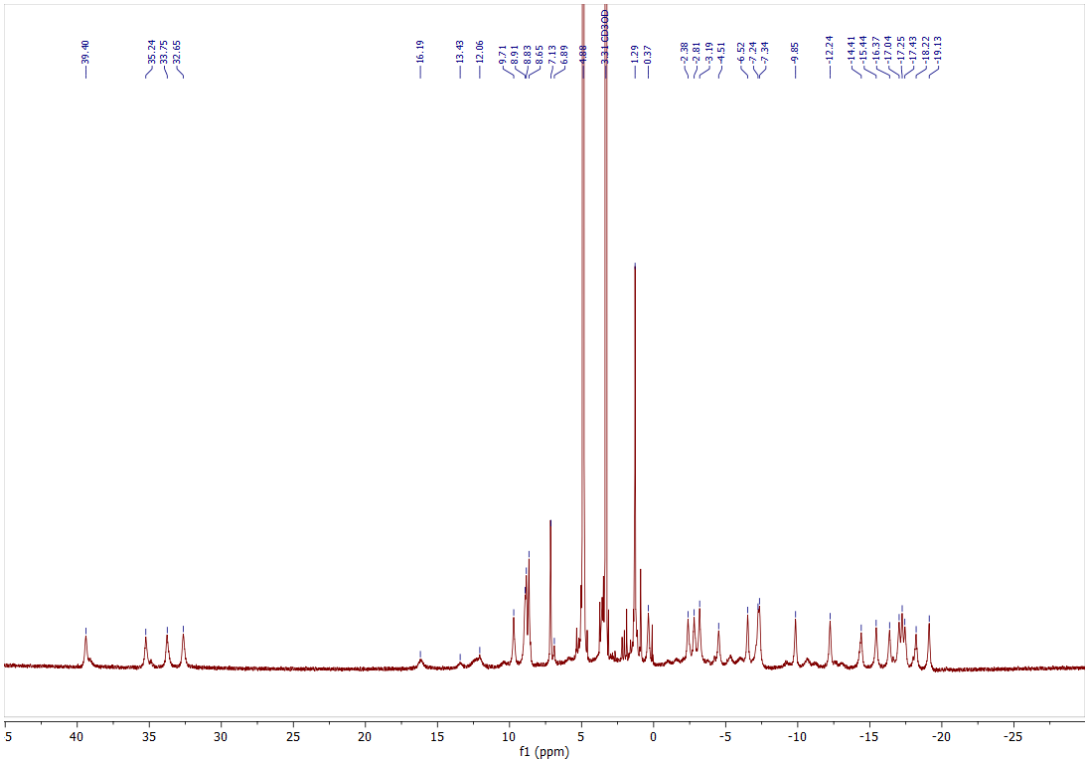

Figure S7 ^{1}H NMR spectrum of **EuL^{H}** at 294 K. Chemical shifts were referenced to methanol-d_4.

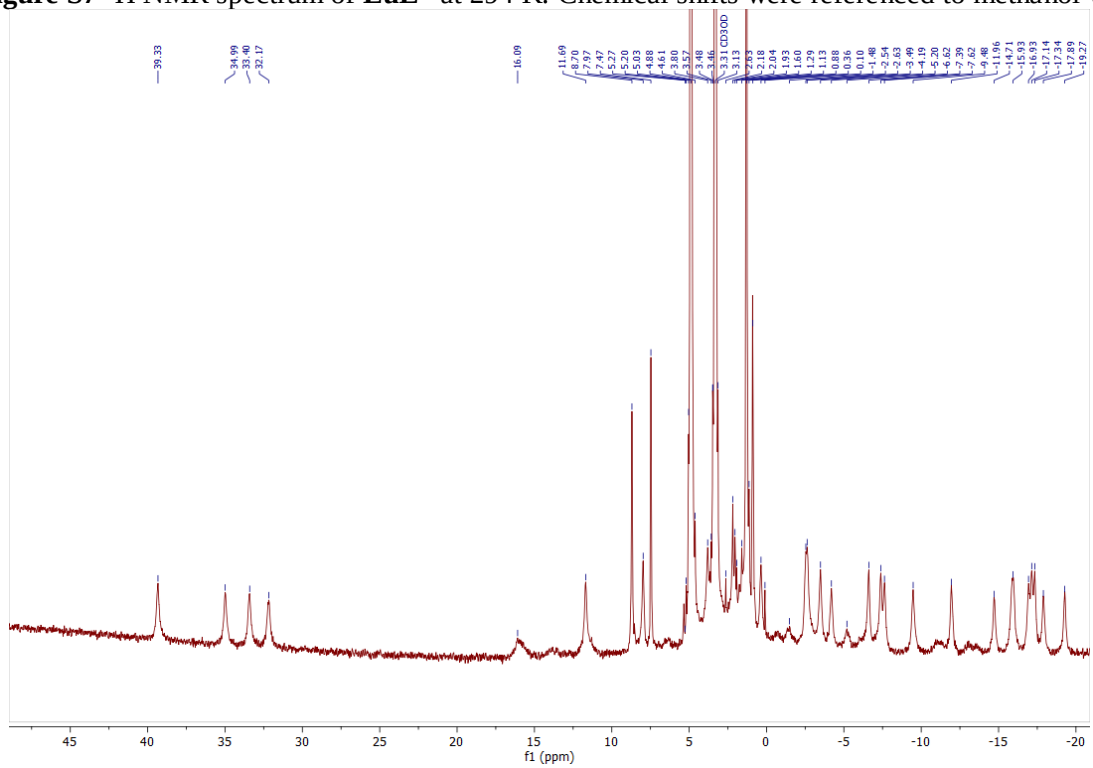

Figure S8 ^{1}H NMR spectrum of **EuL^{6F}** at 294 K. Chemical shifts were referenced to methanol-d_4.

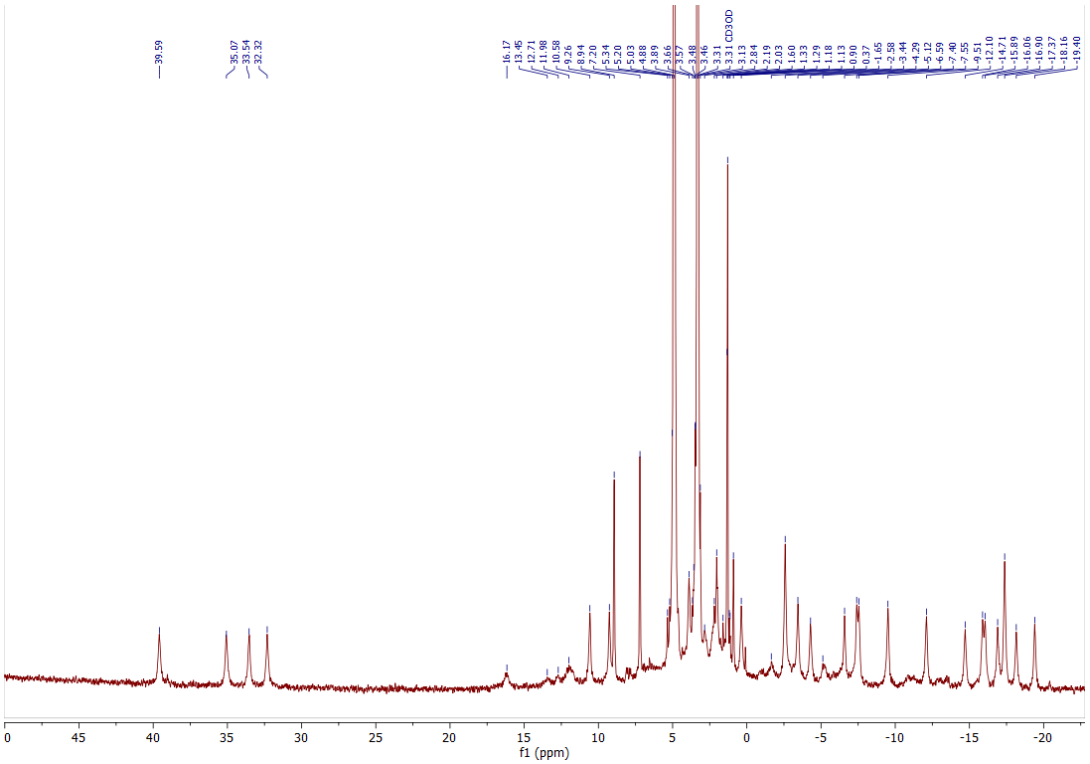

Figure S9 ^{1}H NMR spectrum of **EuL^{5F}** recorded at 294 K. Chemical shifts were referenced to methanol-*d*$_4$.

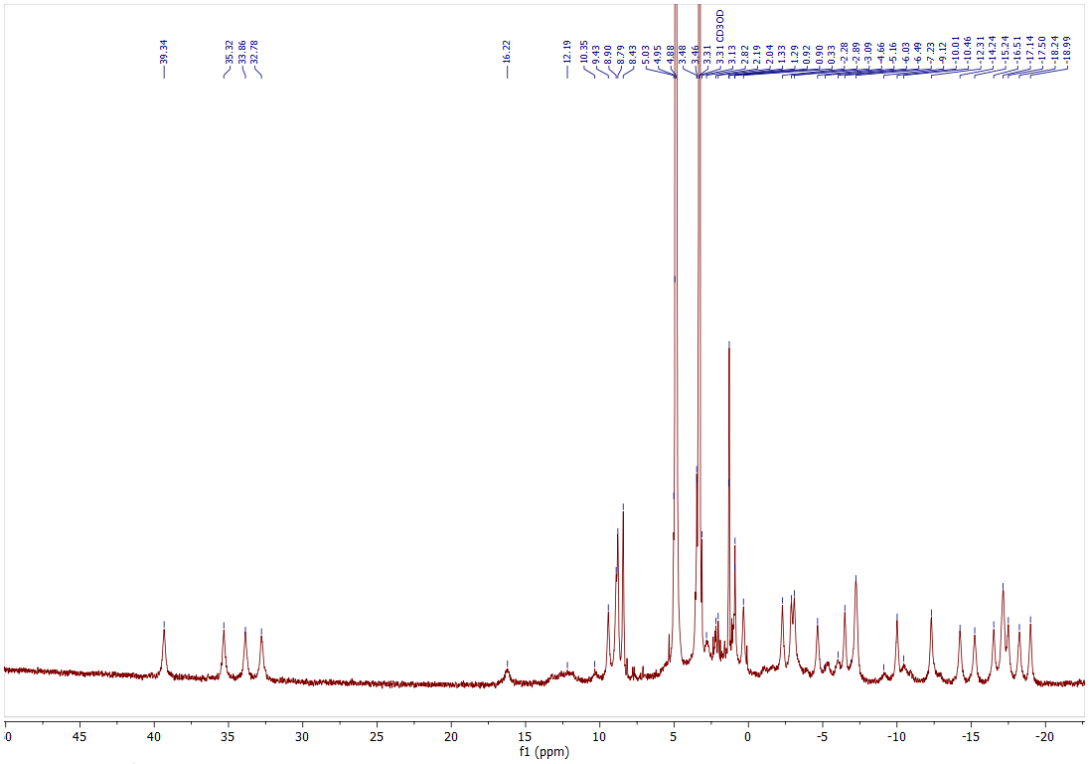

Figure S10 ^{1}H NMR spectrum of **EuL^{3F}** recorded at 294 K. Chemical shifts were referenced to methanol-*d*$_4$.

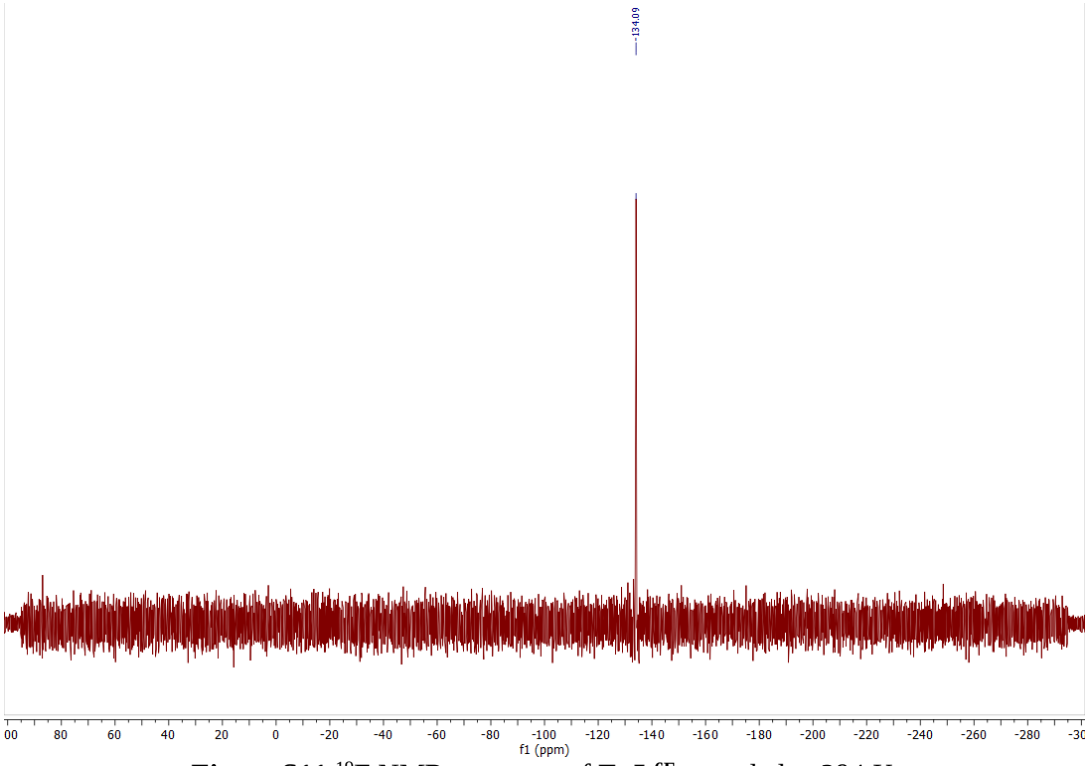

Figure S11 ^{19}F NMR spectrum of **EuL^{6F}** recorded at 294 K.

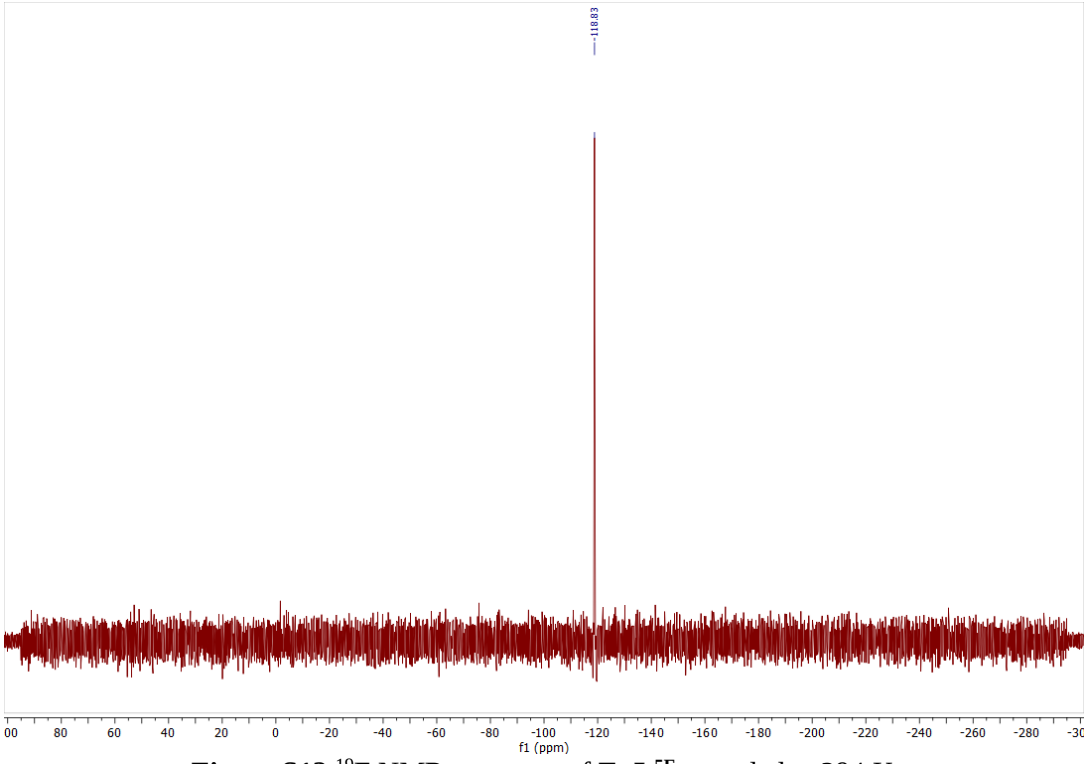

Figure S12 ^{19}F NMR spectrum of **EuL^{5F}** recorded at 294 K.

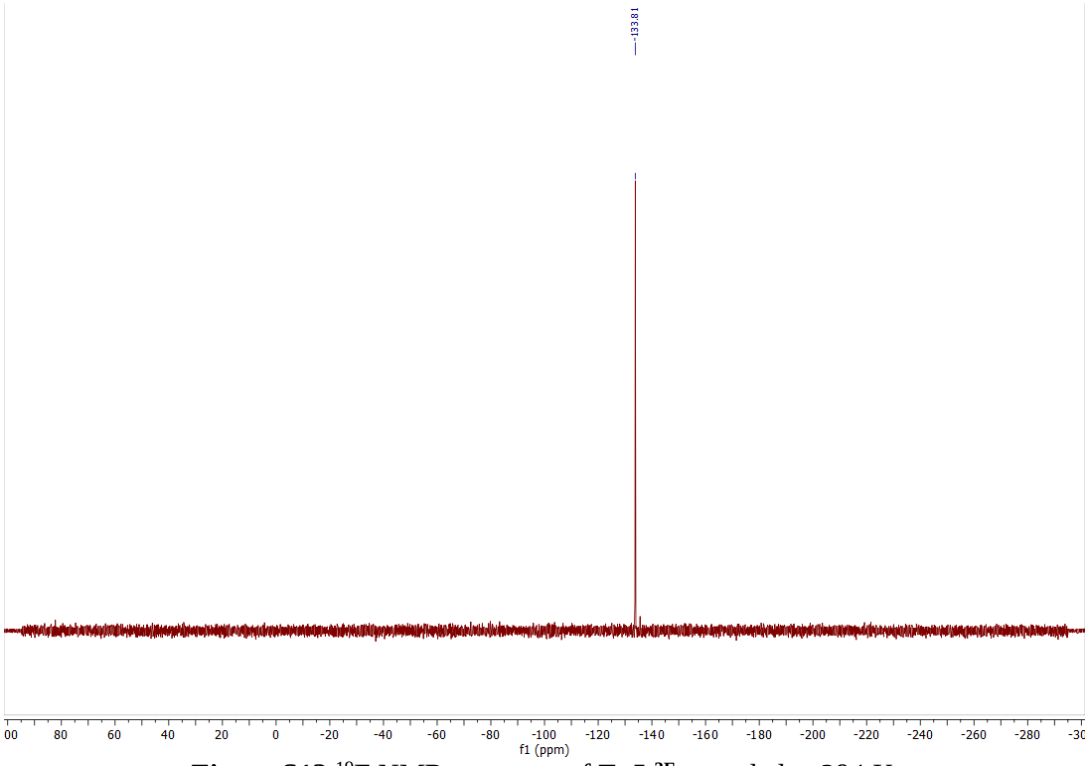

Figure S13 ^{19}F NMR spectrum of **EuL^{3F}** recorded at 294 K.

Electrochemical characterization

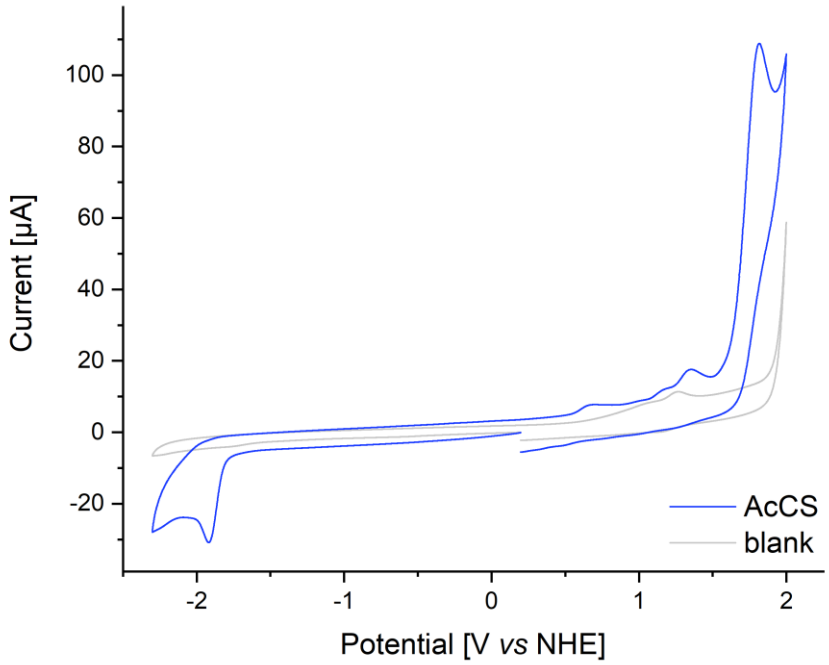

Figure 14 Cyclic voltammogram of **AcCS** (2 mM) in DMF under Ar using a glassy carbon working electrode with $TBAPF_6$ (100 mM) as supporting electrolyte.

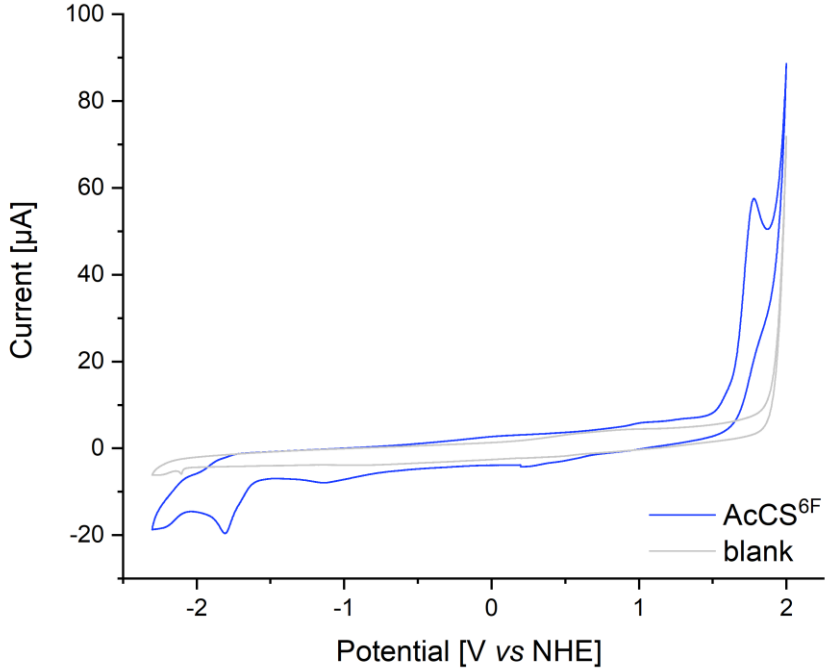

Figure S15 Cyclic voltammogram of **AcCS^{6F}** (2 mM) in DMF under Ar using a glassy carbon working electrode with $TBAPF_6$ (100 mM) as supporting electrolyte.

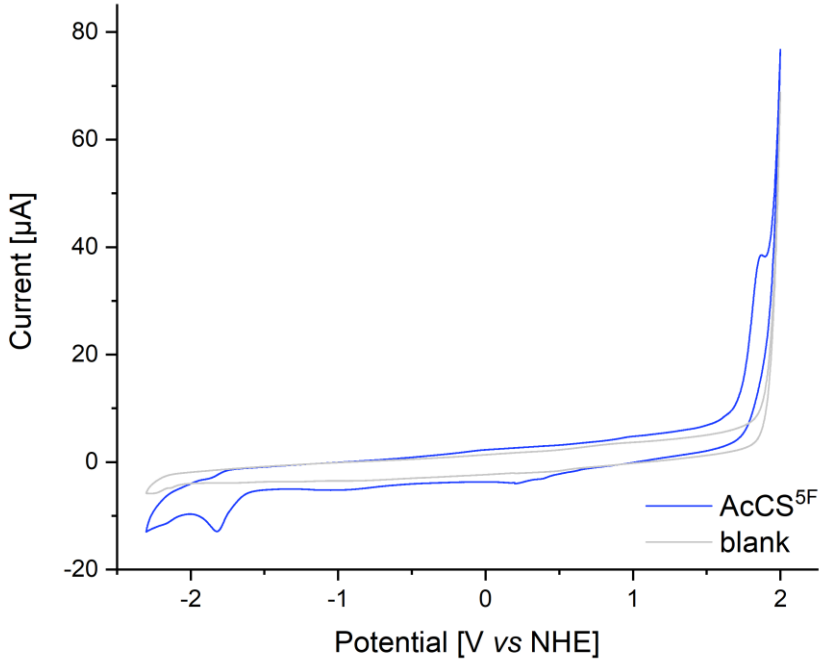

Figure S16 Cyclic voltammogram of **AcCS^{5F}** in DMF under Ar (2 mM) using a glassy carbon working electrode with $TBAPF_6$ (100 mM) as supporting electrolyte.

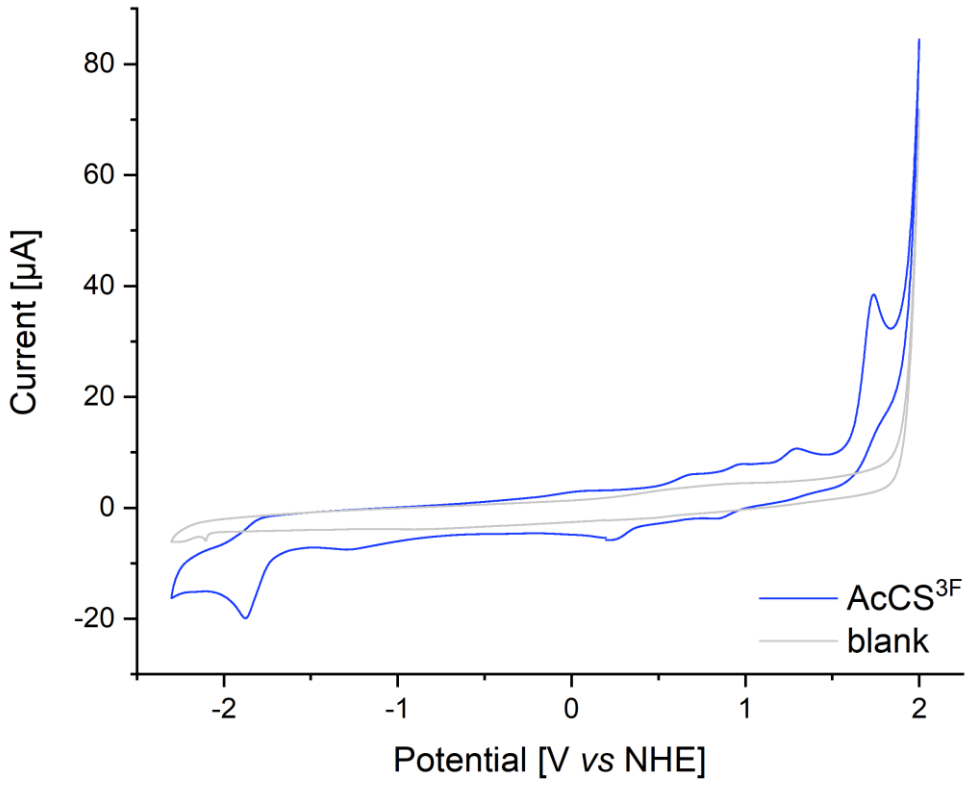

Figure S17 Cyclic voltammogram of **AcCS^{3F}** (2 mM) in DMF under Ar using a glassy carbon working electrode with $TBAPF_6$ (100 mM) as supporting electrolyte.

Photophysical characterization

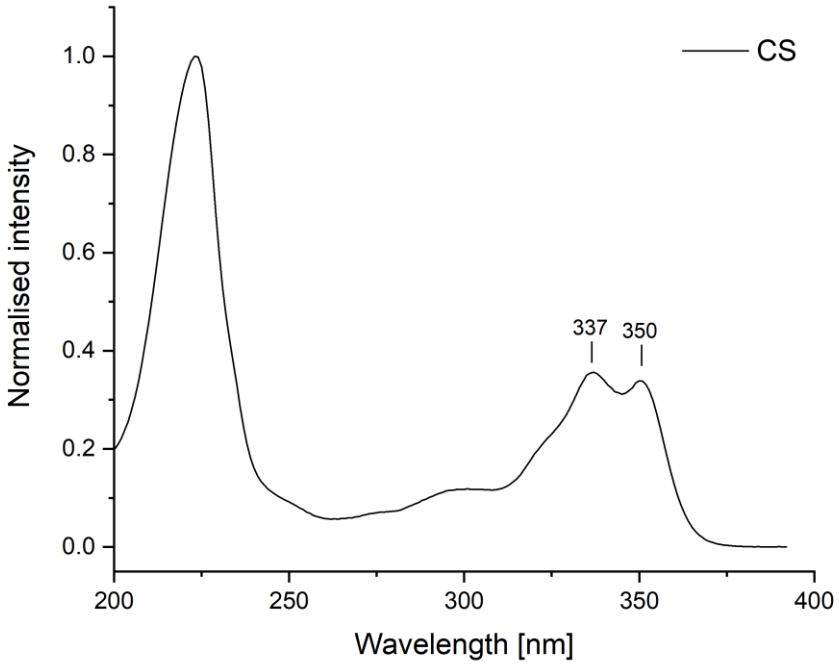

Figure S18 Normalized absorption spectrum of **CS** in MeCN.

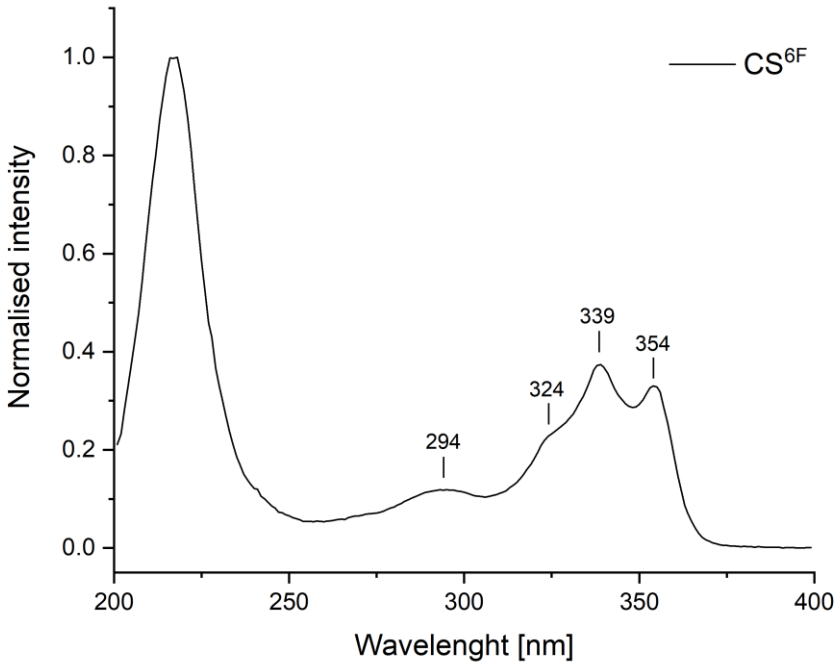

Figure S19 Normalized absorption spectrum of **CS^{6F}** in MeCN.

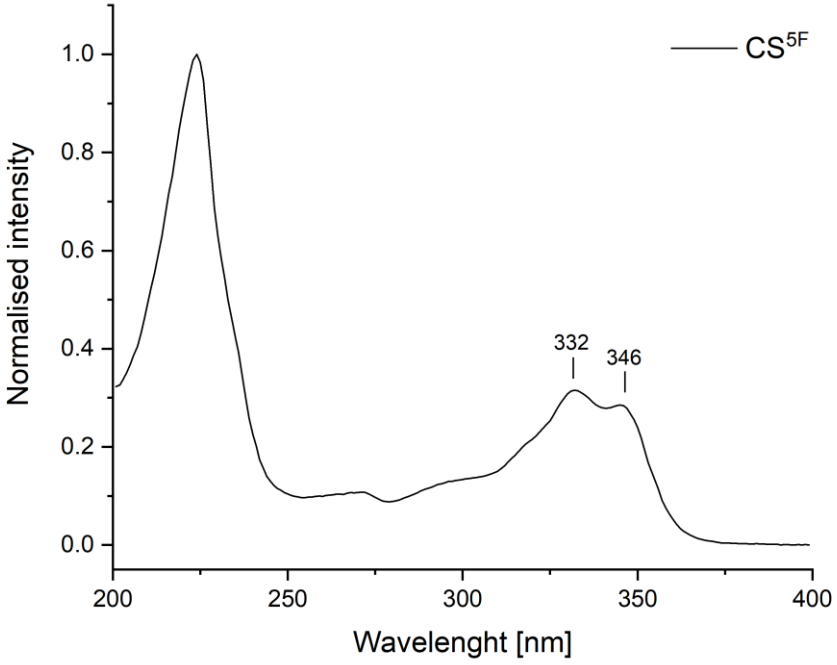

Figure S20 Normalized absorption spectrum of **CS^{5F}** in MeCN.

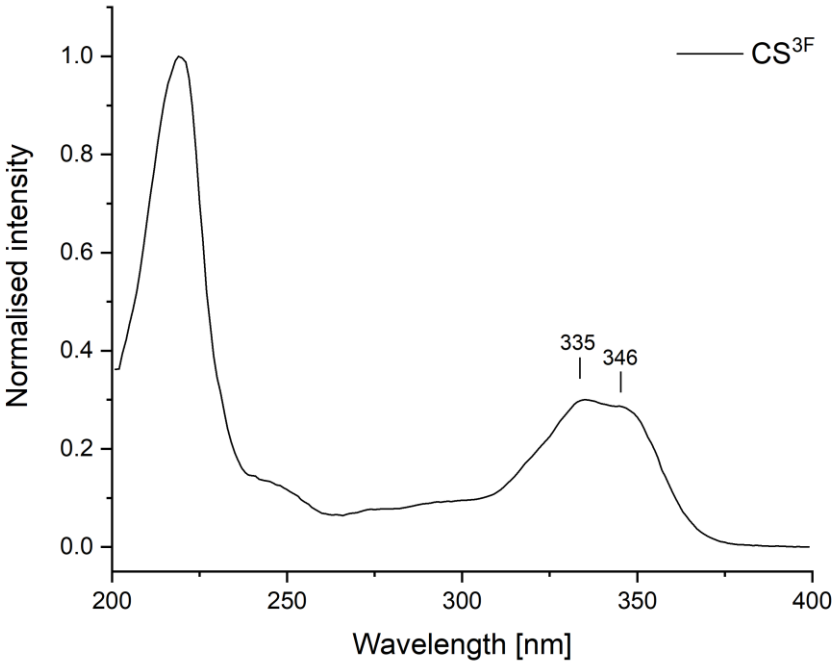

Figure S21 Normalized absorption spectrum of **CS^{3F}** in MeCN.

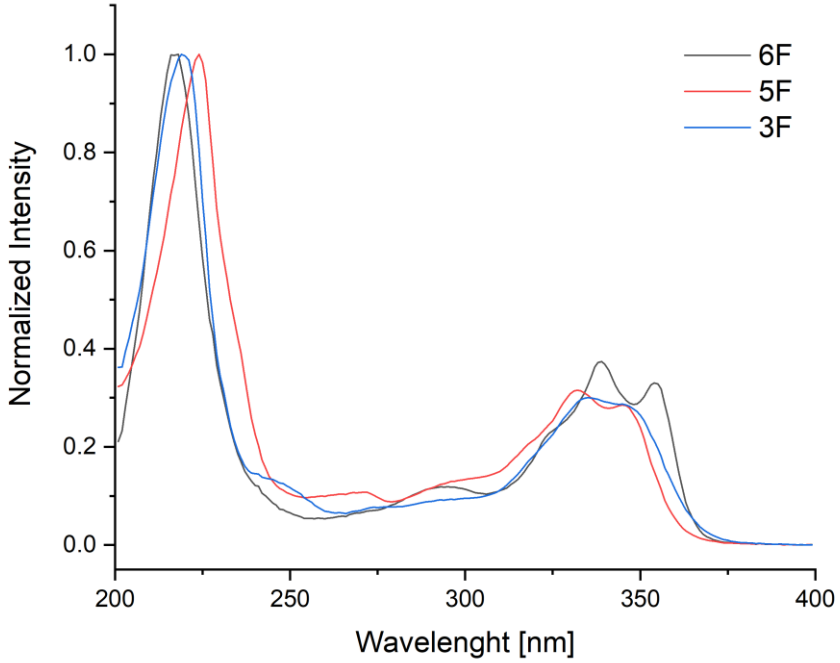

Figure S22 Superimposed absorption spectra of **CS**^{6F} (black), **CS**^{5F} (red) and **CS**^{3F} (blue) in MeCN.

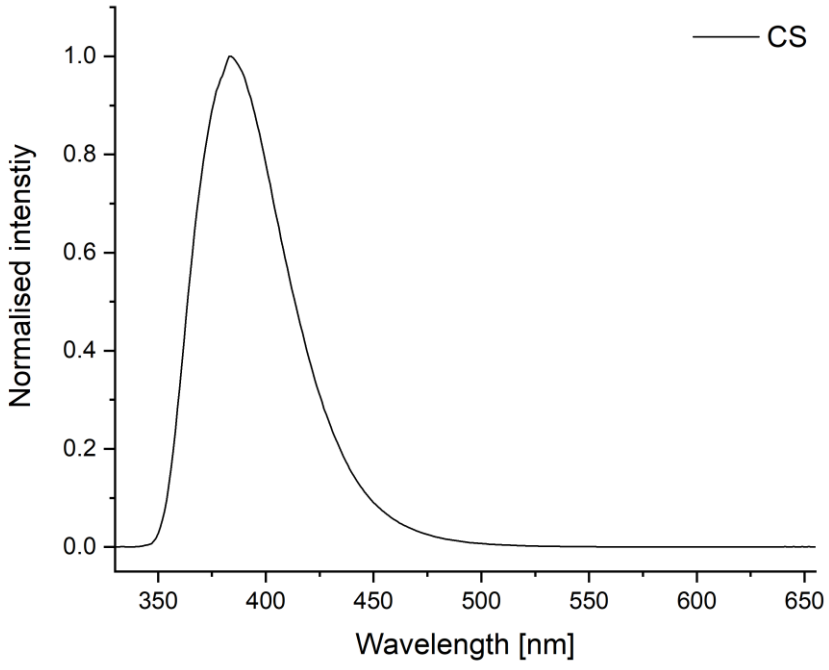

Figure S23 Steady-state emission spectrum of **CS** at 298 K in MeCN, λ_{ex} = 335 nm, [**CS**^{6F}] = 10 μM.

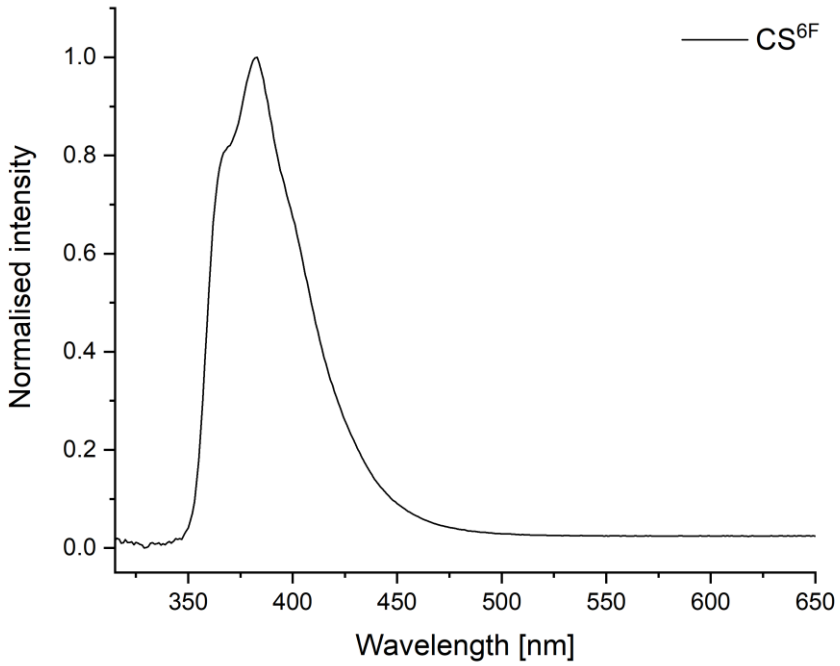

Figure S24 Steady-state emission spectrum of **CS^{6F}** at 298 K in MeCN, λ_{ex} = 338 nm, [**CS^{6F}**] = 10 μM.

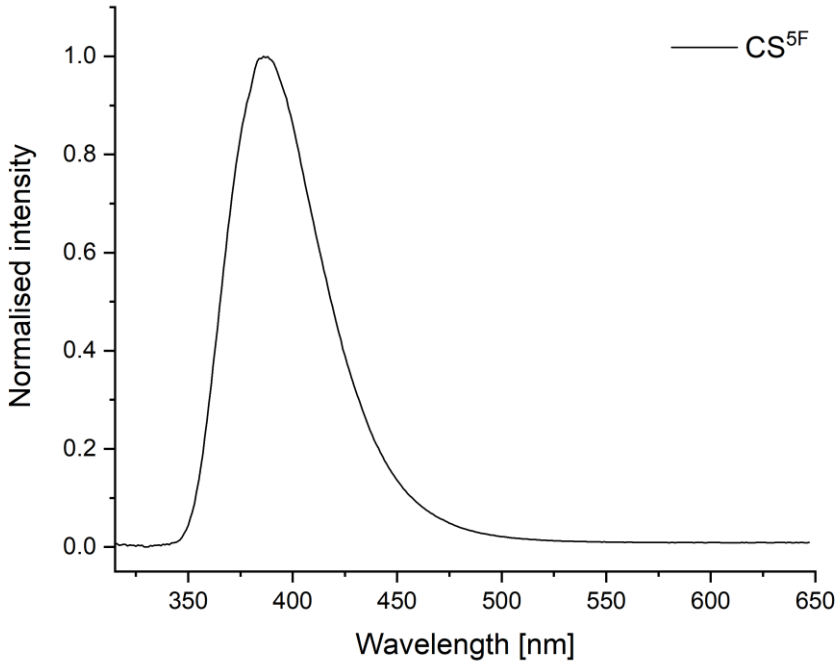

Figure S25 Steady-state emission spectrum of **CS^{5F}** at 298 K in MeCN, λ_{ex} = 331 nm, [**CS^{5F}**] = 10 μM.

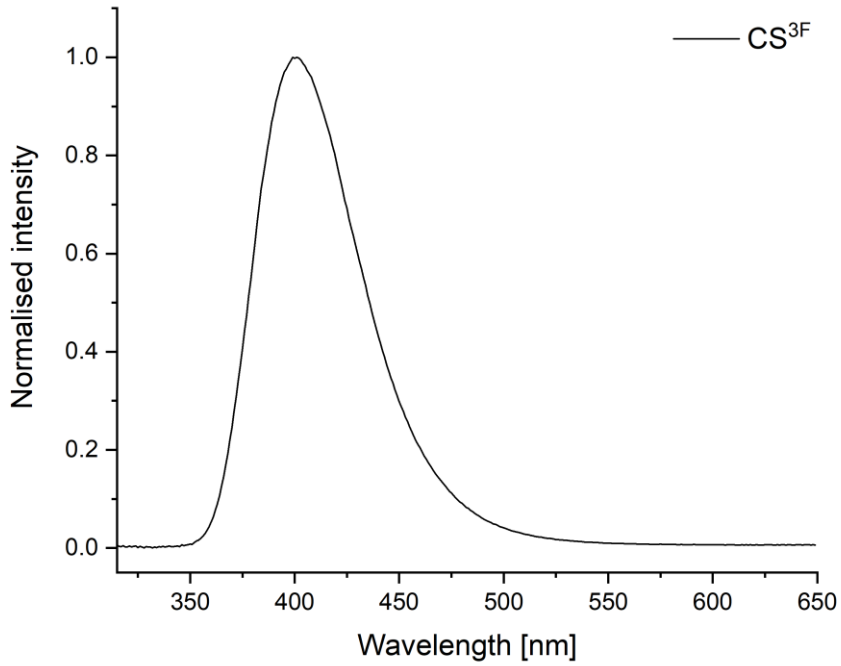

Figure S26 Steady-state emission spectrum of **CS^{3F}** at 298 K in MeCN, λ_{ex} = 332 nm, [**CS^{3F}**] = 10 μM.

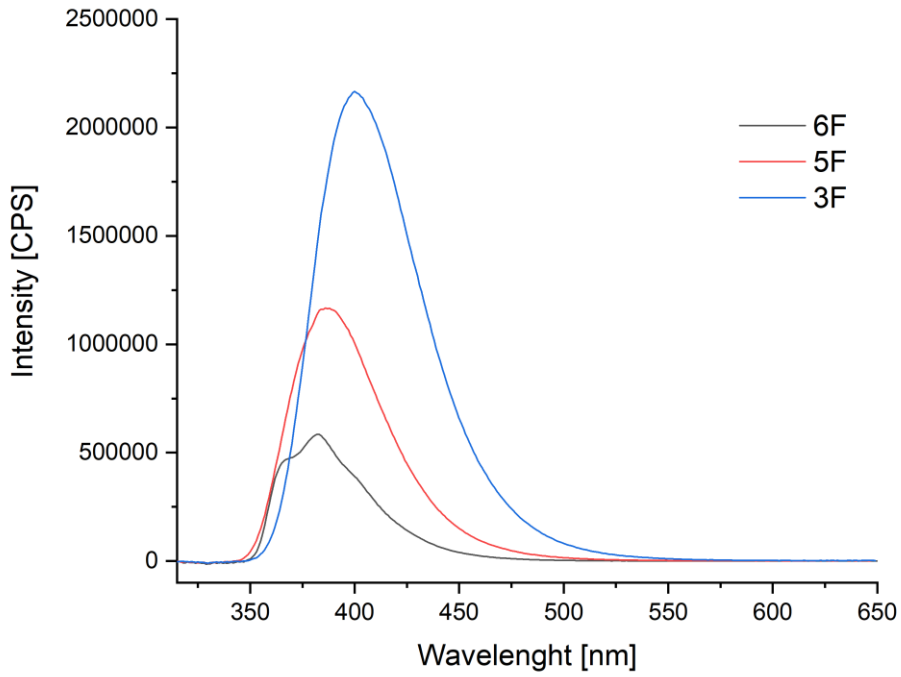

Figure S27 Superimposed steady-state emission spectra of **CS^{6F}** (black, λ_{ex} = 338 nm), **CS^{5F}** (red, λ_{ex} = 331 nm) and **CS^{3F}** (blue, λ_{ex} = 332 nm) at 298 K in MeCN, [**CS^{F}**] = 10 μM.

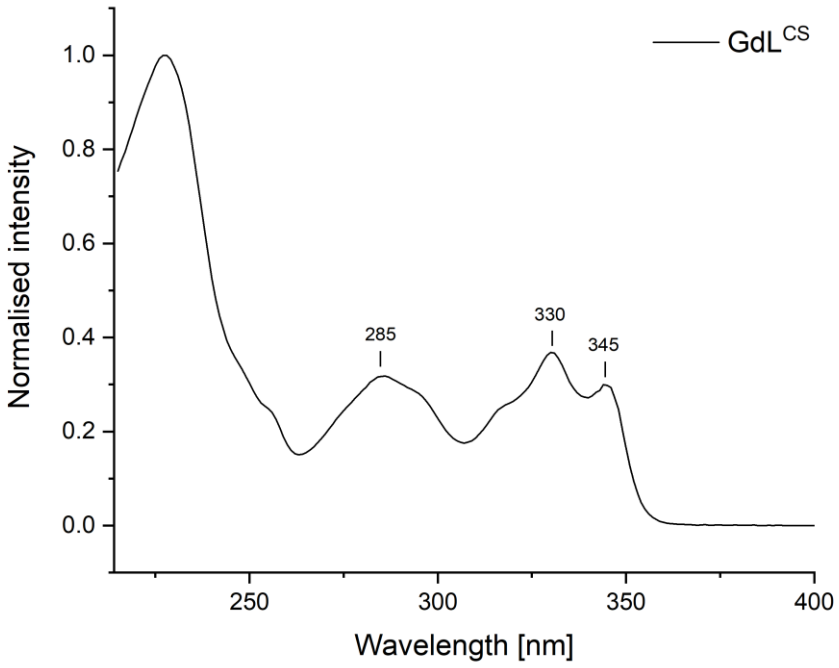

Figure S28 Normalized absorption spectrum of **GdL^{H}** in 0.01 M PIPES-buffered aqueous solution, pH 6.5. Black numbers show local maxima of the spectra.

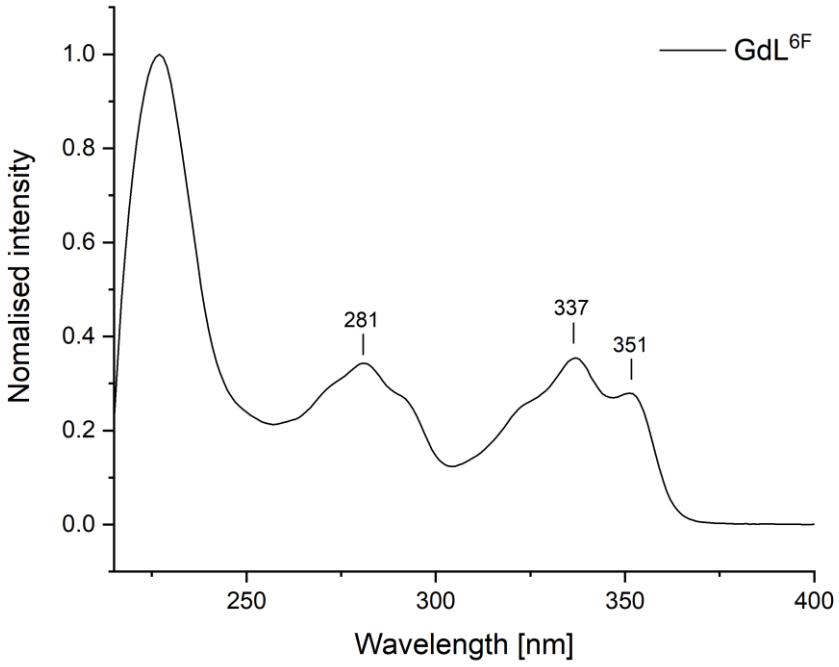

Figure S29 Normalized absorption spectrum of **GdL^{6F}** in 0.01 M PIPES-buffered aqueous solution, pH 6.5. Black numbers show local maxima of the spectra.

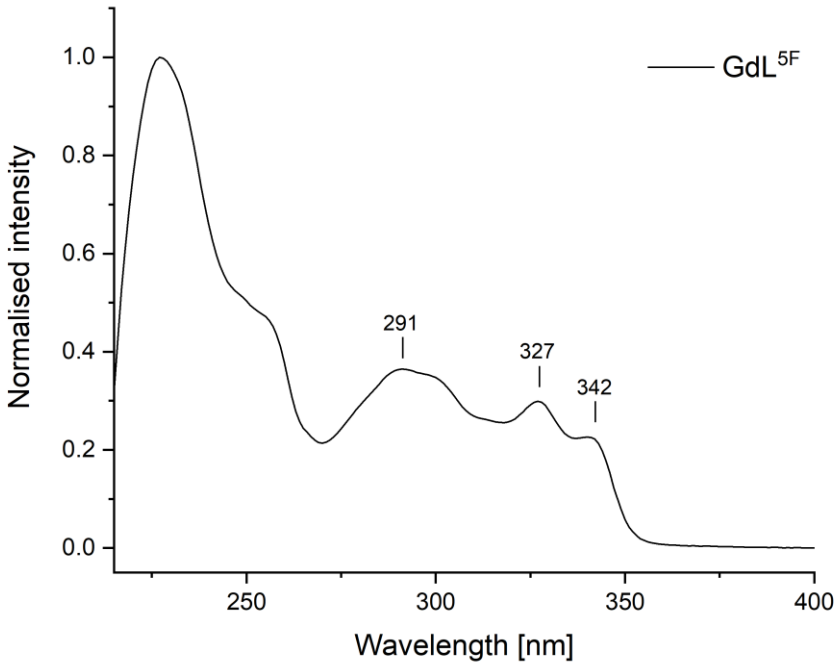

Figure S30 Normalized absorption spectrum of **GdL^{5F}** in 0.01 M PIPES-buffered aqueous solution, pH 6.5. Black numbers show local maxima of the spectra.

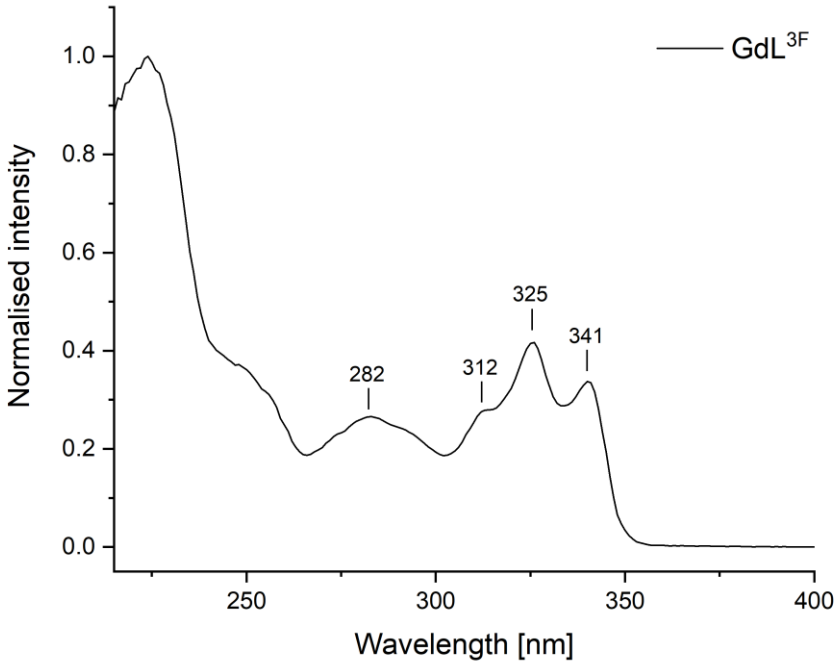

Figure S31 Normalized absorption spectrum of **GdL^{3F}** in 0.01 M PIPES-buffered aqueous solution, pH 6.5. Black numbers show local maxima of the spectra.

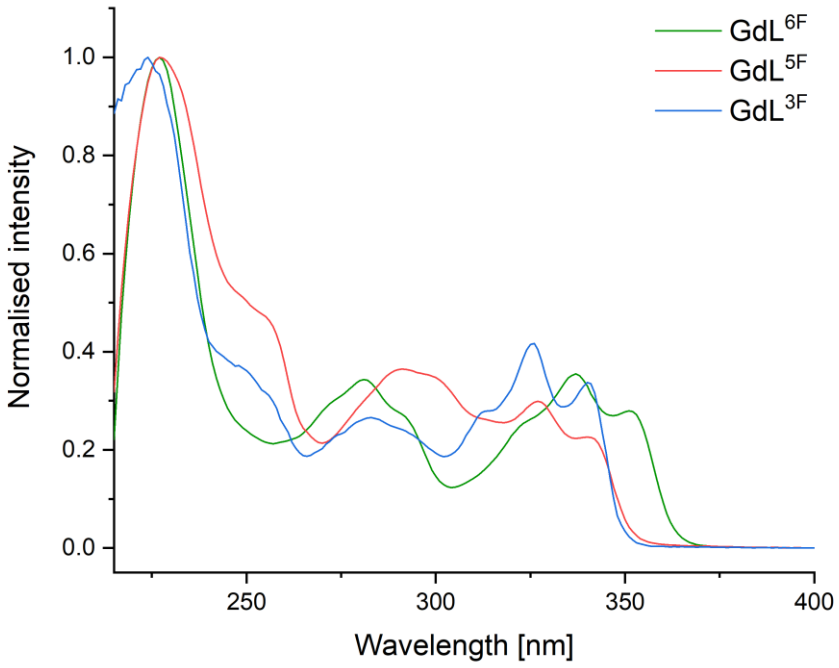

Figure S32 Superimposed absorption spectrum of **GdL^{6F}** (green), **GdL^{5F}** (red) and **GdL^{3F}** (blue) in 0.01 M PIPES-buffered aqueous solution, pH 6.5.

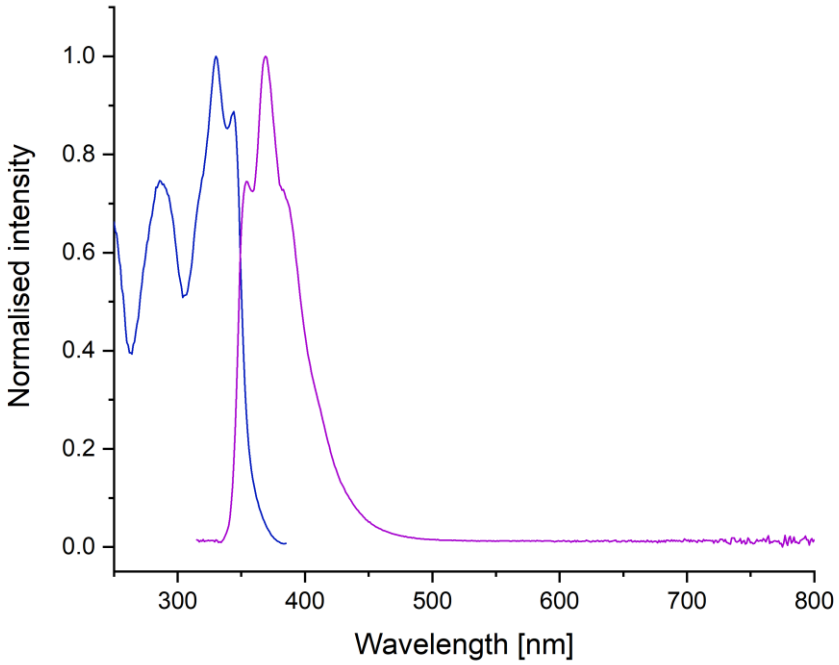

Figure S33 Excitation (blue) and steady-state emission (purple) spectra of **GdL^{H}** at 298 K in 0.01 M PIPES-buffered aqueous solution, pH = 6.5, λ_{em} = 369 nm, λ_{ex} = 330 nm, [**GdL^{H}**] = 10 μM.

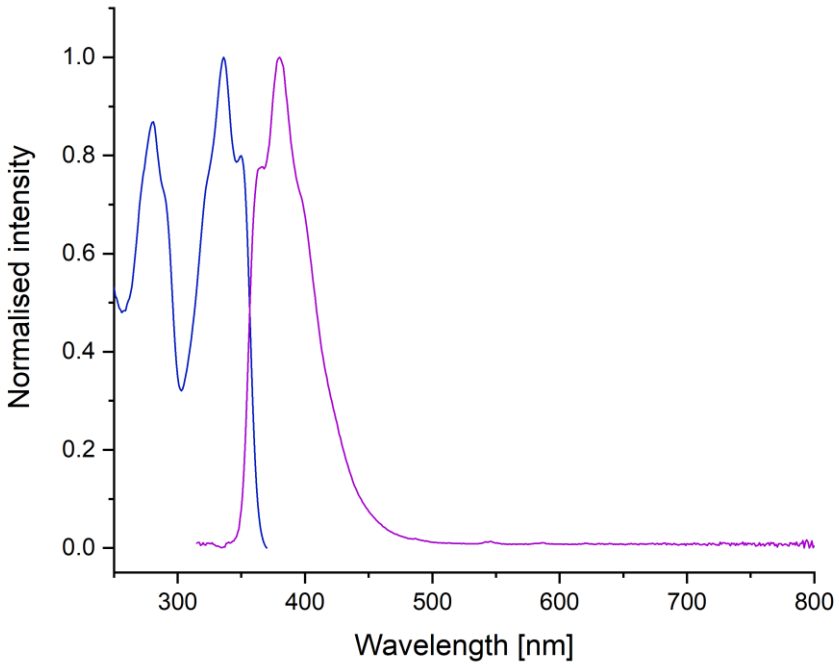

Figure S34 Excitation (blue) and steady-state emission (purple) spectra of **GdL^{6F}** at 298 K in 0.01 M PIPES-buffered aqueous solution, pH = 6.5, λ_{em} = 380 nm, λ_{ex} = 335 nm, [**GdL^{6F}**] = 10 μM.

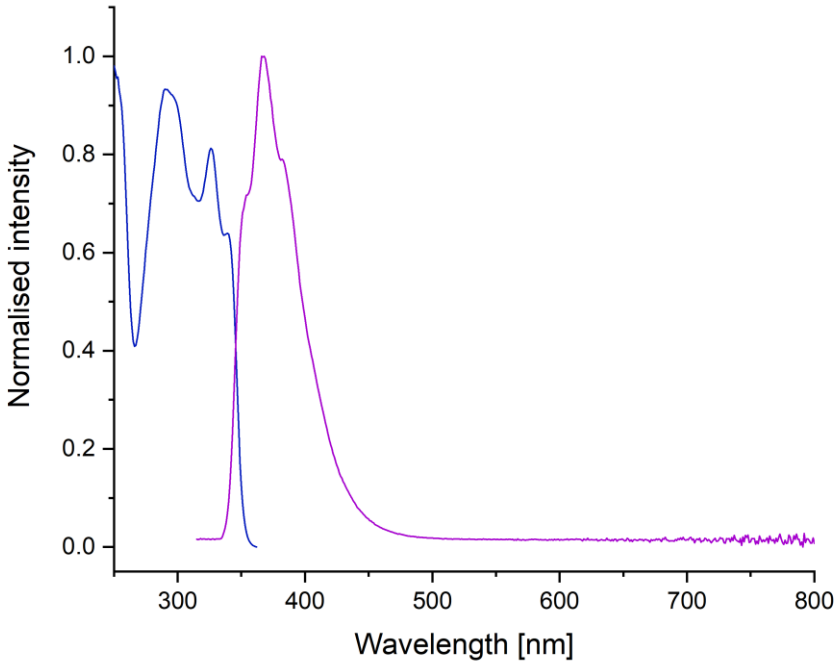

Figure S35 Excitation (blue) and steady-state emission (purple) spectra of **GdL^{5F}** at 298 K in 0.01 M PIPES-buffered aqueous solution, pH = 6.5, λ_{em} = 368 nm, λ_{ex} = 327 nm, [**GdL^{5F}**] = 10 μM.

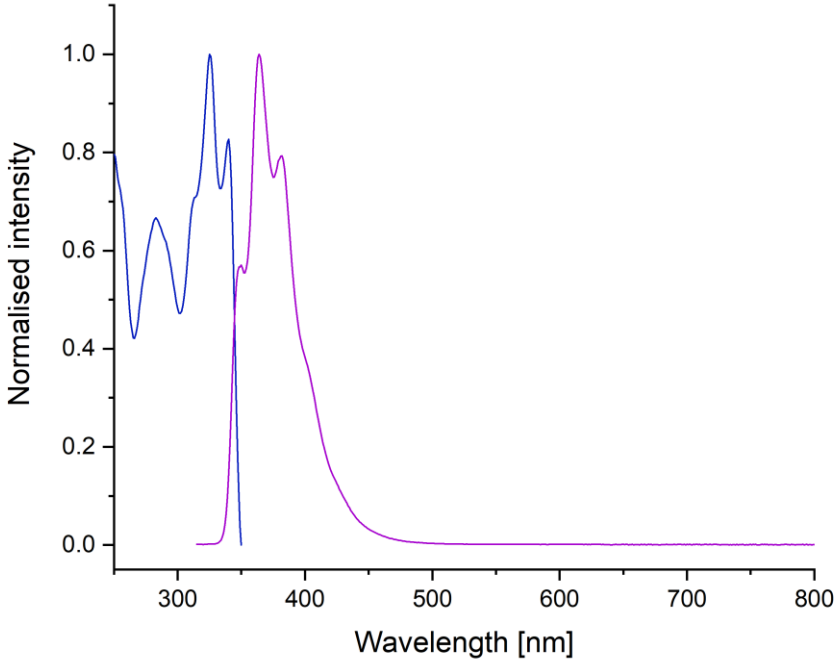

Figure S36 Excitation (blue) and steady-state emission (purple) spectra of **GdL^{3F}** at 298 K in 0.01 M PIPES-buffered aqueous solution, pH = 6.5, λ_{em} = 364 nm, λ_{ex} = 325 nm, [**GdL^{3F}**] = 10 μM.

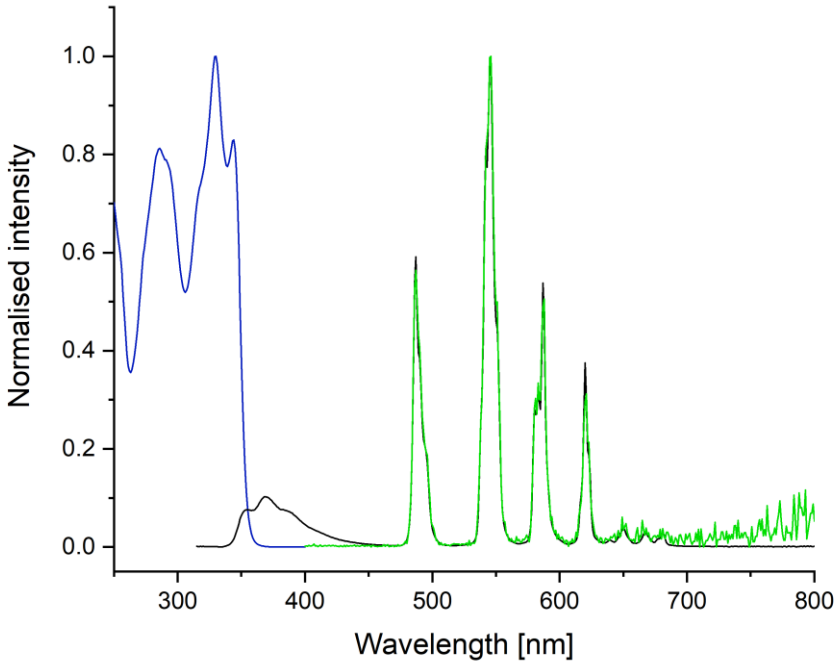

Figure S37 Excitation (blue) and steady-state emission (black) and time-resolved emission (green) spectra of **TbL^{H}** at 298 K in 0.01 M PIPES-buffered aqueous solution, pH = 6.5, λ_{em} = 546 nm, λ_{ex} = 330 nm, [**TbL^{H}**] = 10 μM.

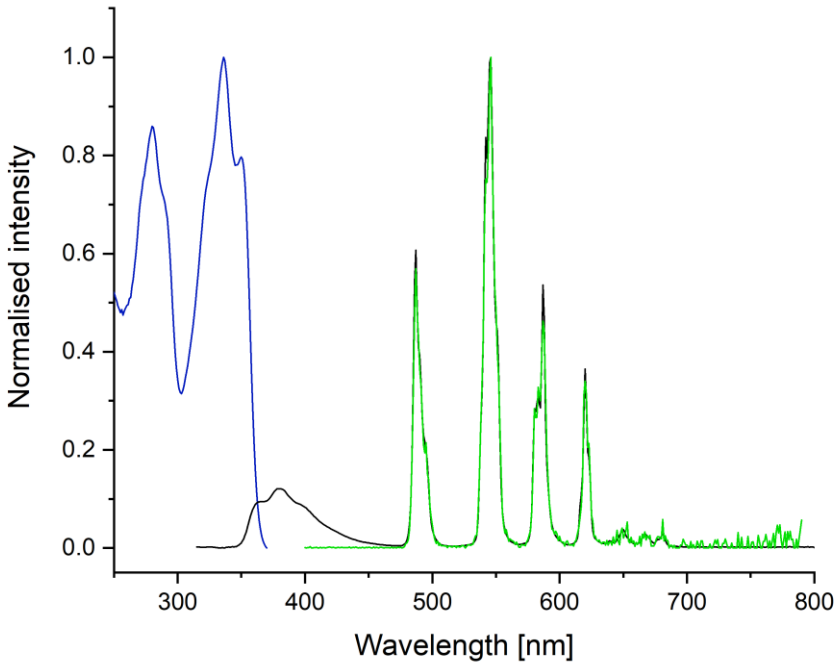

Figure S38 Excitation (blue) and steady-state emission (black) and time-resolved emission (green) spectra of **TbL^{6F}** at 298 K in 0.01 M PIPES-buffered aqueous solution, pH = 6.5, λ_{em} = 546 nm, λ_{ex} = 335 nm, [**TbL^{6F}**] = 10 μM.

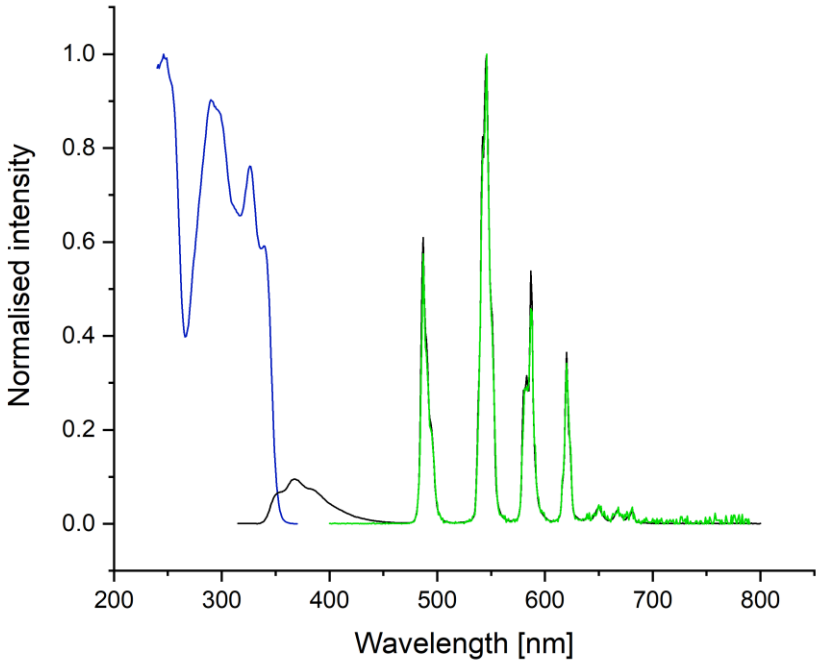

Figure S39 Excitation (blue) and steady-state emission (black) and time-resolved emission (green) spectra of **TbL^{5F}** at 298 K in 0.01 M PIPES-buffered aqueous solution, pH = 6.5, λ_{em} = 546 nm, λ_{ex} = 327 nm, [**TbL^{5F}**] = 10 μM.

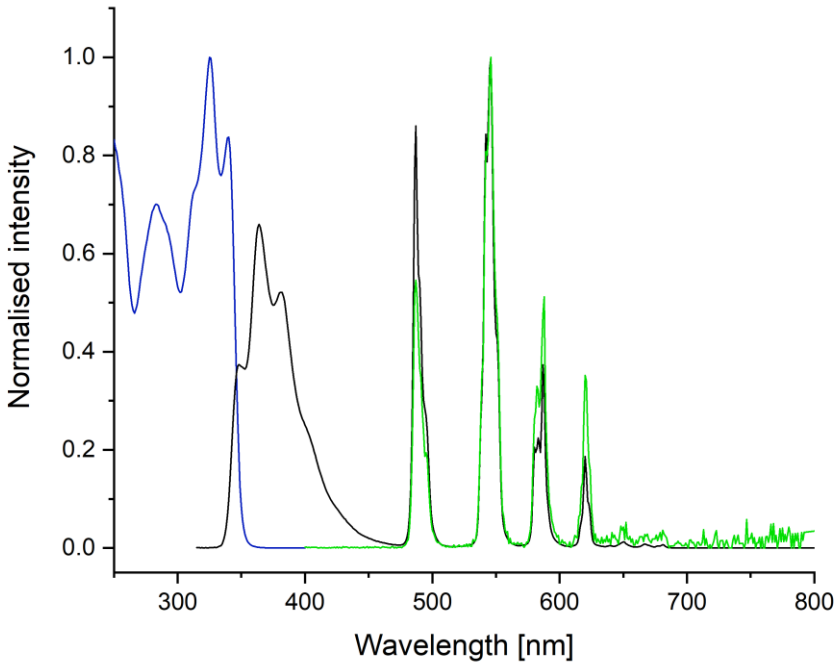

Figure S40 Excitation (blue) and steady-state emission (black) and time-resolved emission (green) spectra of **TbL^{3F}** at 298 K in 0.01 M PIPES-buffered aqueous solution, pH = 6.5, λ_{em} = 546 nm, λ_{ex} = 325 nm, [**TbL^{3F}**] = 10 μM.

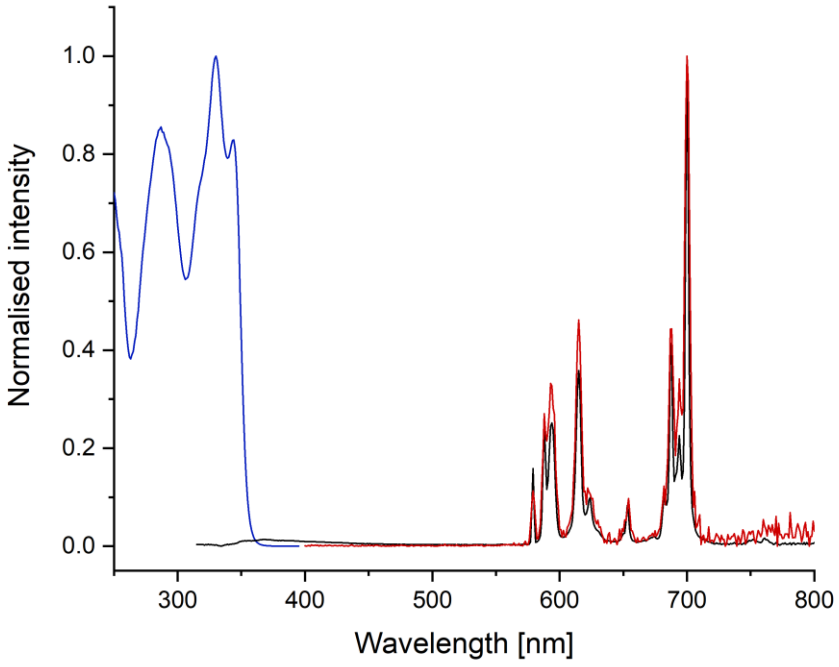

Figure S41 Excitation (blue) and steady-state emission (black) and time-resolved emission (green) spectra of **EuL^{H}** at 298 K in 0.01 M PIPES-buffered aqueous solution, pH = 6.5, λ_{em} = 615 nm, λ_{ex} = 330 nm, [**EuL^{H}**] = 10 μM.

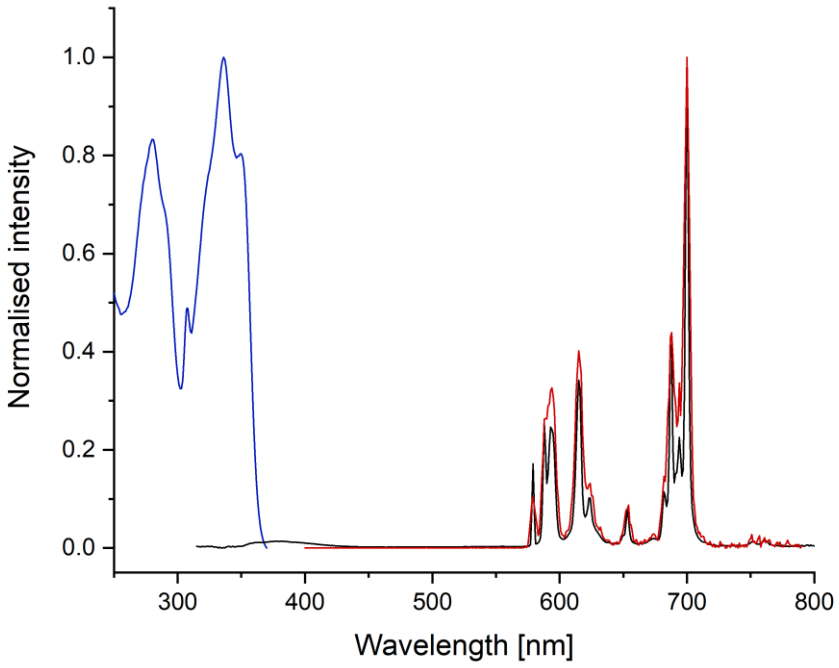

Figure S42 Excitation (blue) and steady-state emission (black) and time-resolved emission (green) spectra of **EuL^{6F}** at 298 K in 0.01 M PIPES-buffered aqueous solution, pH = 6.5, λ_{em} = 615 nm, λ_{ex} = 335 nm, [**EuL^{6F}**] = 10 μM.

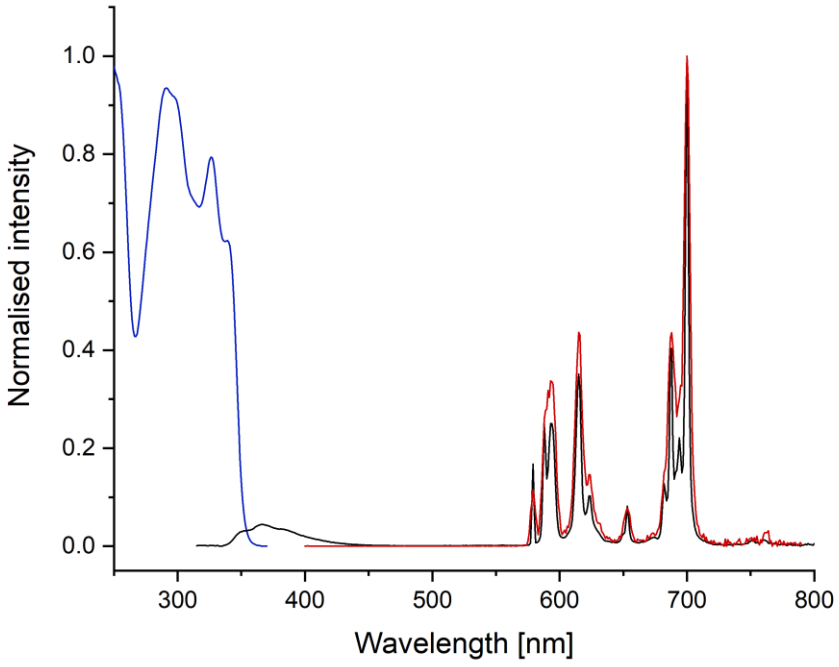

Figure S43 Excitation (blue) and steady-state emission (black) and time-resolved emission (green) spectra of **EuL^{5F}** at 298 K in 0.01 M PIPES-buffered aqueous solution, pH = 6.5, λ_{em} = 615 nm, λ_{ex} = 327 nm, [**EuL^{5F}**] = 10 μM.

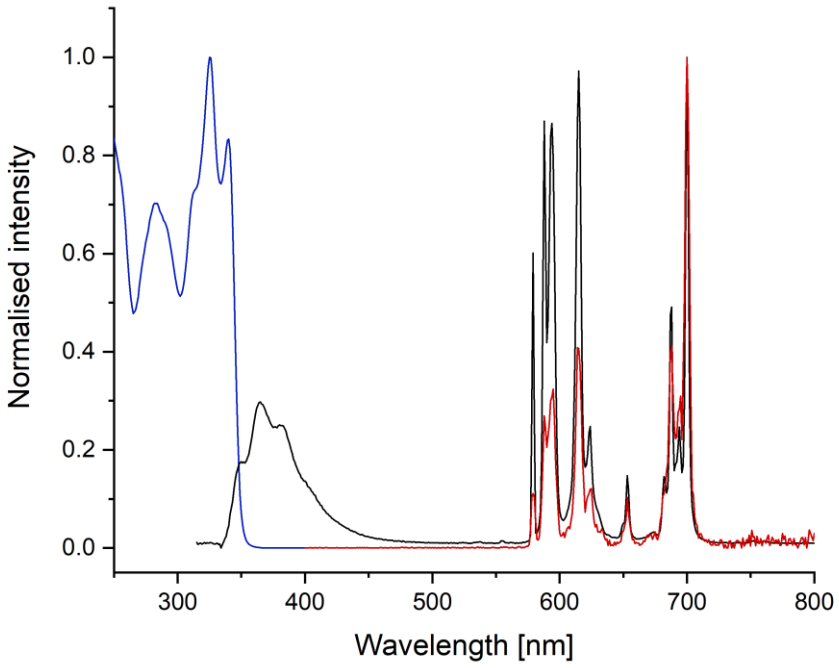

Figure S44 Excitation (blue) and steady-state emission (black) and time-resolved emission (green) spectra of **EuL^{3F}** at 298 K in 0.01 M PIPES-buffered aqueous solution, pH = 6.5, λ_{em} = 615 nm, λ_{ex} = 325 nm, [**EuL^{3F}**] = 10 μM.

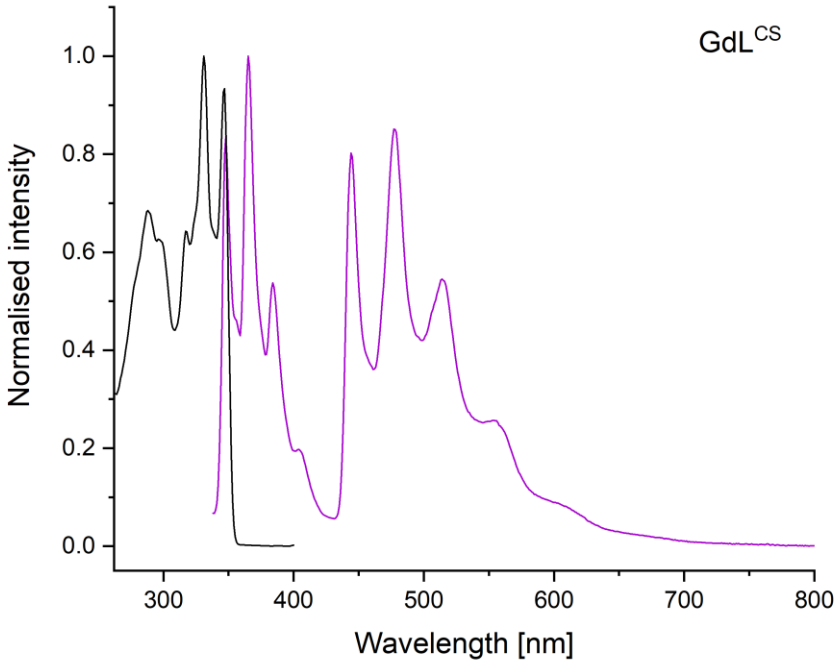

Figure S45 Excitation spectrum of the ligand-centred phosphorescence emissions of **GdL^{H}** (black, λ_{em} = 444 nm), and the steady-state emission spectrum (purple, λ_{ex} = 330 nm) at 77 K with 10% glycerol added to the nominally 10 μM, PIPES buffered (0.01 M, pH = 6.5) aqueous solutions.

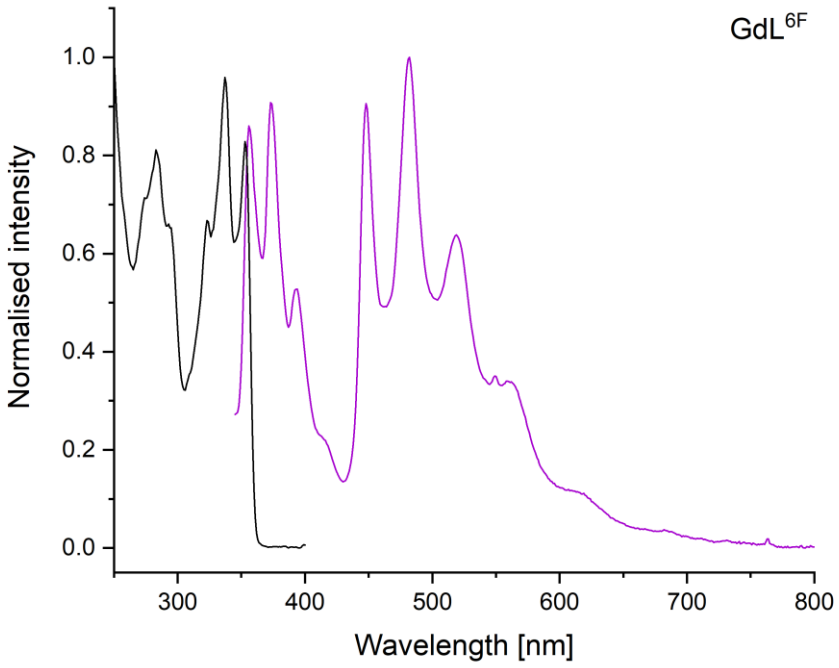

Figure S46 Excitation spectrum of the ligand-centred phosphorescence emissions of **GdL^{6F}** (black, λ_{em} = 448 nm), and the steady-state emission spectrum (purple, λ_{ex} = 335 nm) at 77 K with 10% glycerol added to the nominally 10 µM, PIPES buffered (0.01 M, pH = 6.5) aqueous solutions.

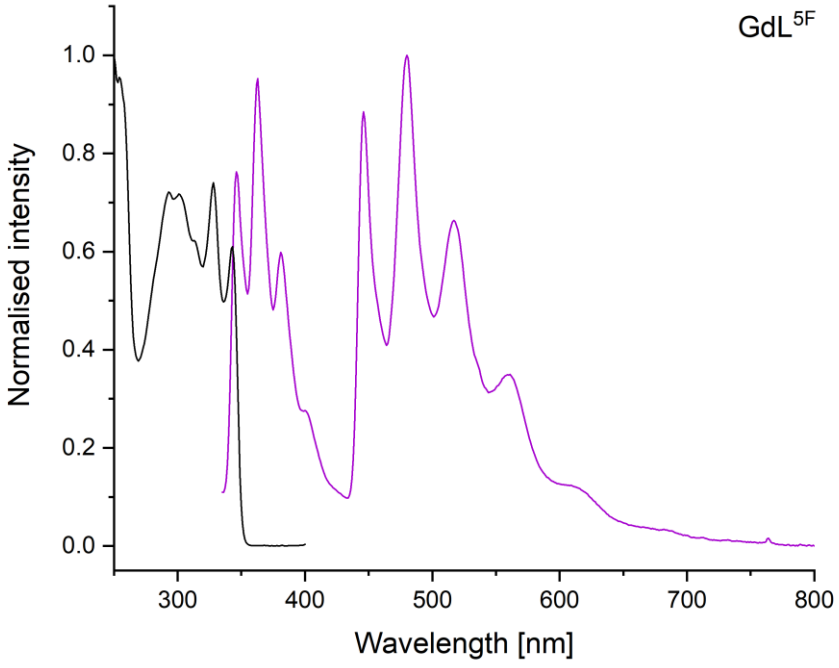

Figure S47 Excitation spectrum of the ligand-centred phosphorescence emissions of **GdL^{5F}** (black, λ_{em} = 446 nm), and the steady-state emission spectrum (purple, λ_{ex} = 327 nm) at 77 K with 10% glycerol added to the nominally 10 µM, PIPES buffered (0.01 M, pH = 6.5) aqueous solutions.

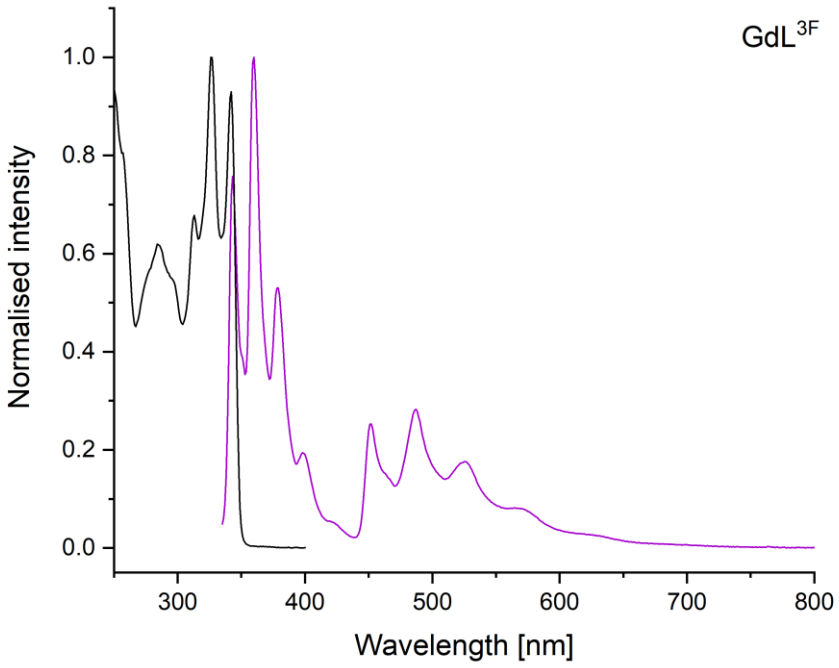

Figure S48 Excitation spectrum of the ligand-centred phosphorescence emissions of **GdL^{3F}** (black, λ_{em} = 452 nm), and the steady-state emission spectrum (purple, λ_{ex} = 325 nm) at 77 K with 10% glycerol added to the nominally 10 µM, PIPES buffered (0.01 M, pH = 6.5) aqueous solutions.

Table S4. Luminescence lifetimes of **TbL** and **EuL** in H_2O and D_2O and calculated *q*-values.

	τ_{H2O} (ms) [a]	τ_{D2O} (ms) [a]	q [b]
TbL^{H}	0.96	1.39	1.31
TbL^{3F}	0.34	0.38	1.38
TbL^{5F}	0.98	1.24	0.77
TbL^{6F}	0.64	0.77	1.05
EuL^{H}	0.62	2.27	0.99
EuL^{3F}	0.62	2.26	0.97
EuL^{5F}	0.60	2.13	1.00
EuL^{6F}	0.61	2.18	0.98

[**LnL**] = 10 µM in 10 mM PIPES buffered H_2O or D_2O at pH (pD) 6.5. *q* values were calculated using the equation $q = 5(1/\tau_{H2O} - 1/\tau_{D2O} - 0.06)$ for Tb, and $q = 1.2(1/\tau_{H2O} - 1/\tau_{D2O} - 0.25 - m{\cdot}0.075)$, where *m* is the number of nearby N-H oscillators.[10]

Table S5. Antenna fluorescence lifetimes fitted with mono- and biexponentials. The lifetime of **EuL^{H}** was too short to measure on the instrumentation available to us.

Compound	λ_{em} [nm]	Monoexp.	χ^2	Biexp.				χ^2
		τ [ns]		τ_1 [ns]	a_1 [%]	τ_2 [ns]	a_2 [%]	
CS	384	1.15(5)	7.201	1.13(4)	99	25.00	1	3.673
CS^{6F}	382	0.41(6)	1.451	0.37(1)	99	1.36(8)	1	1.214
CS^{5F}	387	1.09(2)	1.434	1.22(1)	60	0.67(4)	40	1.176
CS^{3F}	400	2.84(6)	3.670	2.78(4)	99	25.00	1	1.937
GdL^{H}	369	0.34(3)	1.765	0.34(1)	99	25.00	1	1.285
GdL^{6F}	380	0.36(4)	2.688	0.36(2)	99	25.00	1	1.470
GdL^{5F}	368	0.44(8)	1.177	–	–	–	–	–
GdL^{3F}	364	0.60(5)	1.051	–	–	–	–	–
TbL^{H}	369	0.21(4)	1.348	0.23(0)	99	17.33	1	1.294
TbL^{6F}	380	0.28(3)	1.828	0.25(4)	99	2.40(3)	1	1.193
TbL^{5F}	368	0.36(3)	1.179	–	–	–	–	–
TbL^{3F}	364	0.39(2)	1.369	–	–	–	–	–
EuL^{H}	369	-	-	-	-	-	-	-
EuL^{6F}	380	0.28(2)	14.724	0.20(1)	99	2.85(5)	1	1.663
EuL^{5F}	368	0.51(4)	1.831	0.47(6)	99	1.76(5)	1	1.161
EuL^{3F}	364	0.69(7)	3.582	0.93(6)	65	0.41(5)	35	2.391

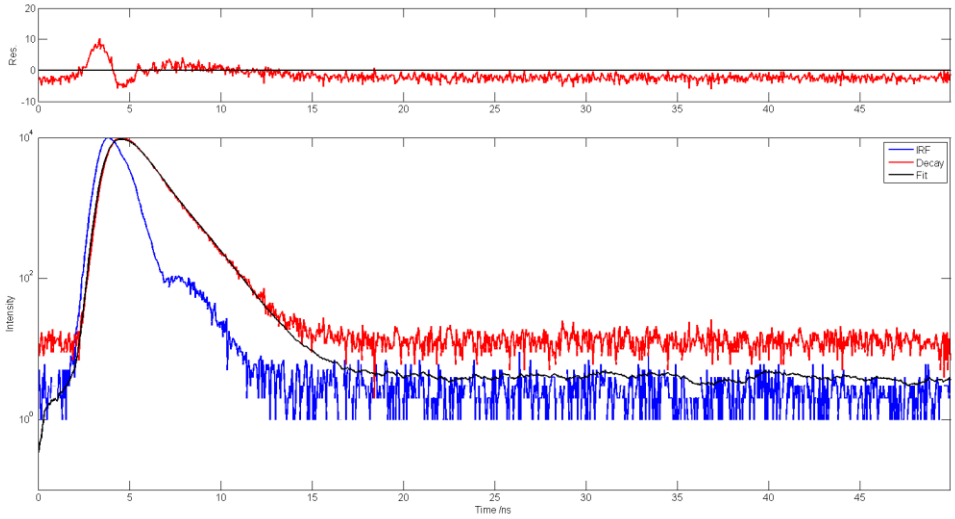

Figure S49 Fluorescence decay and monoexponential reconvolution fit of **CS** in MeCN (bottom) and residuals of the fit (top).

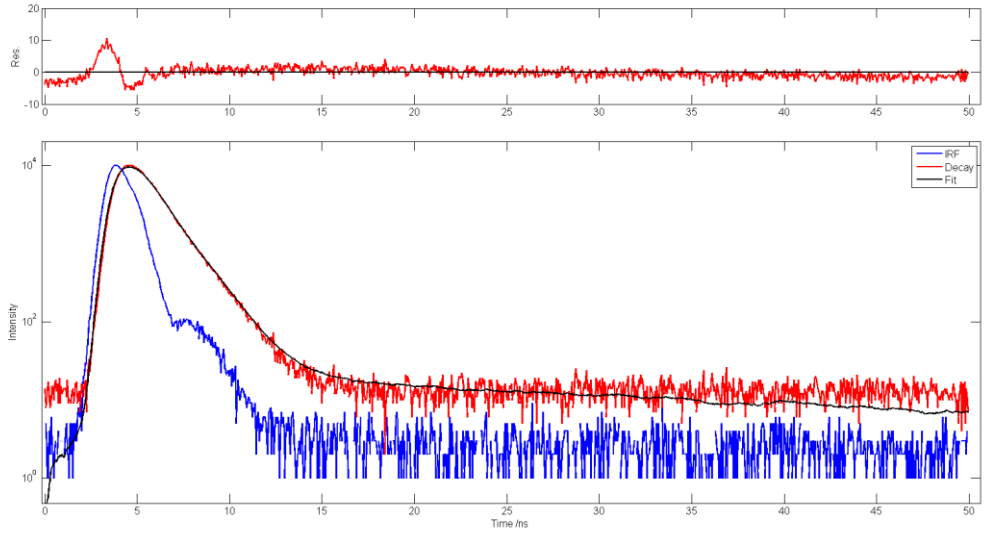

Figure S50 Fluorescence decay and biexponential reconvolution fit of **CS** in MeCN (bottom) and residuals of the fit (top).

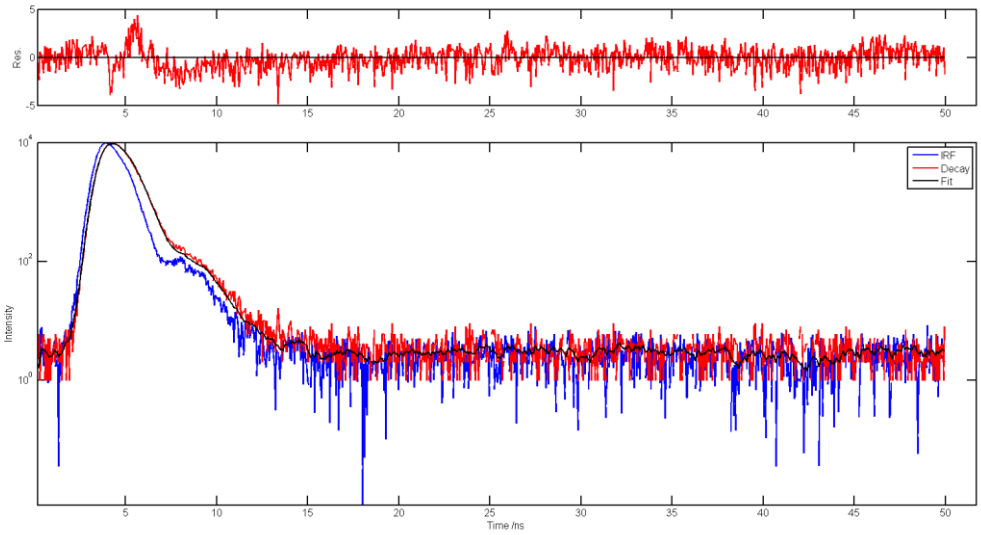

Figure S51 Fluorescence decay and monoexponential reconvolution fit of **CS^{6F}** in MeCN (bottom) and residuals of the fit (top).

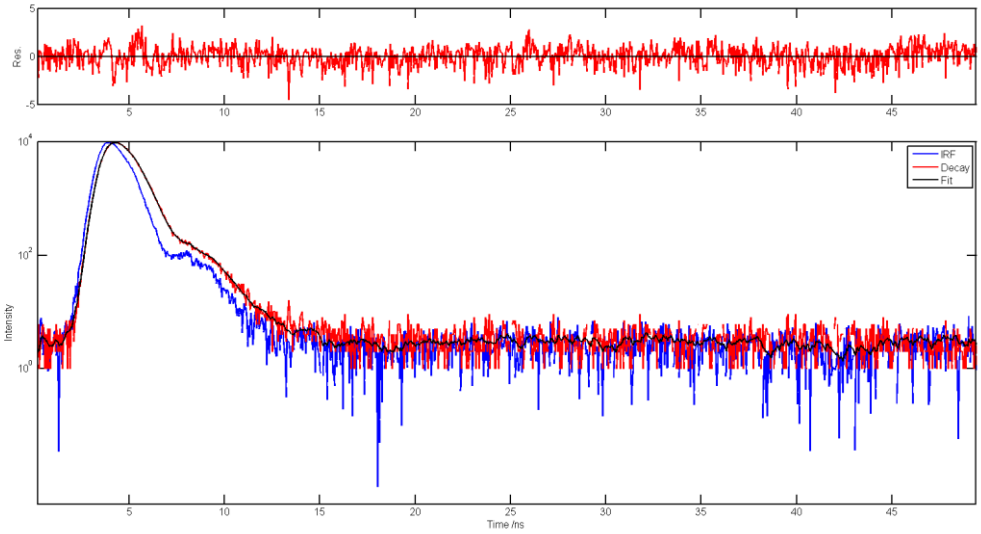

Figure S52 Fluorescence decay and biexponential reconvolution fit of **CS^{6F}** in MeCN (bottom) and residuals of the fit (top).

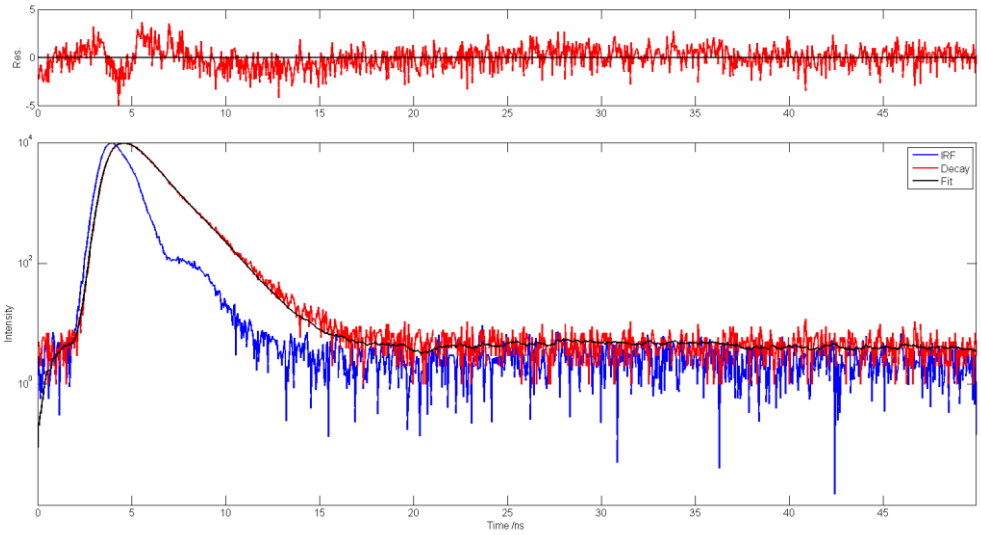

Figure S53 Fluorescence decay and monoexponential reconvolution fit of **CS^{5F}** in MeCN (bottom) and residuals of the fit (top).

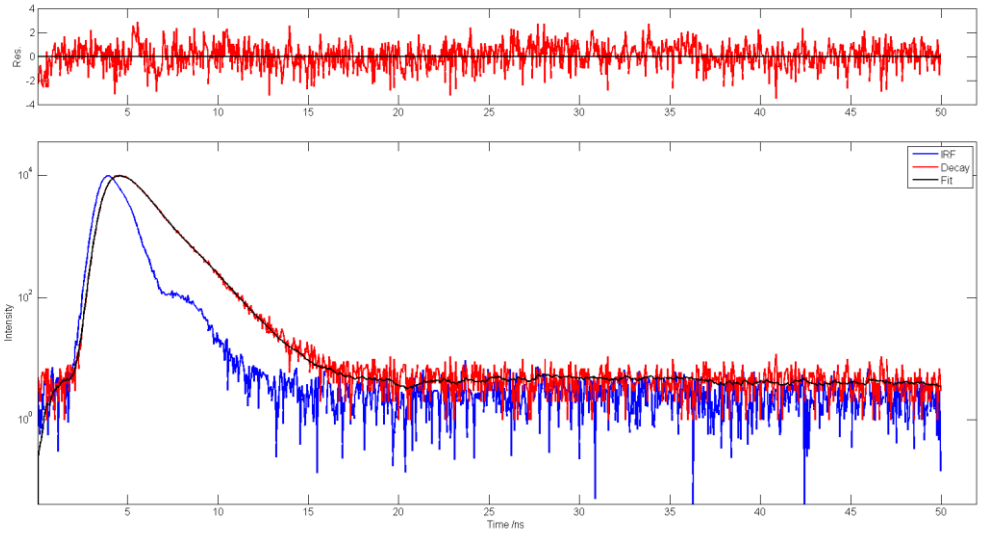

Figure S54 Fluorescence decay and biexponential reconvolution fit of **CS^{5F}** in MeCN (bottom) and residuals of the fit (top).

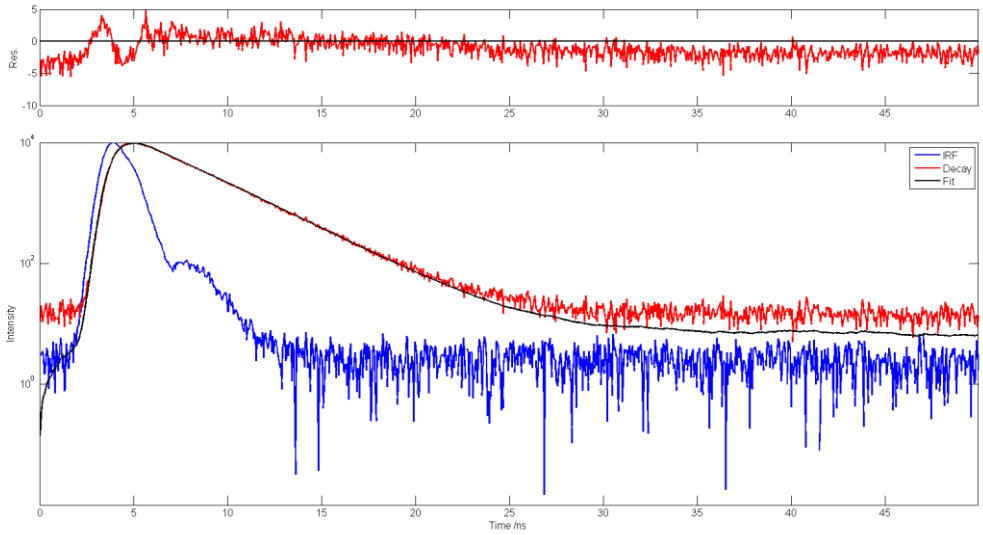

Figure S55 Fluorescence decay and monoexponential reconvolution fit of **CS^{3F}** in MeCN (bottom) and residuals of the fit (top).

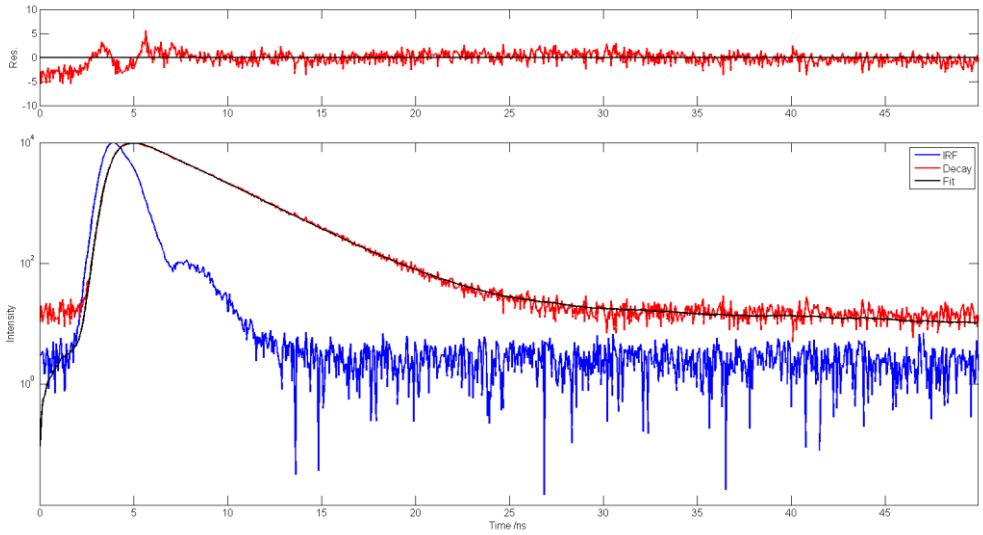

Figure S56 Fluorescence decay and biexponential reconvolution fit of **CS^{3F}** in MeCN (bottom) and residuals of the fit (top).

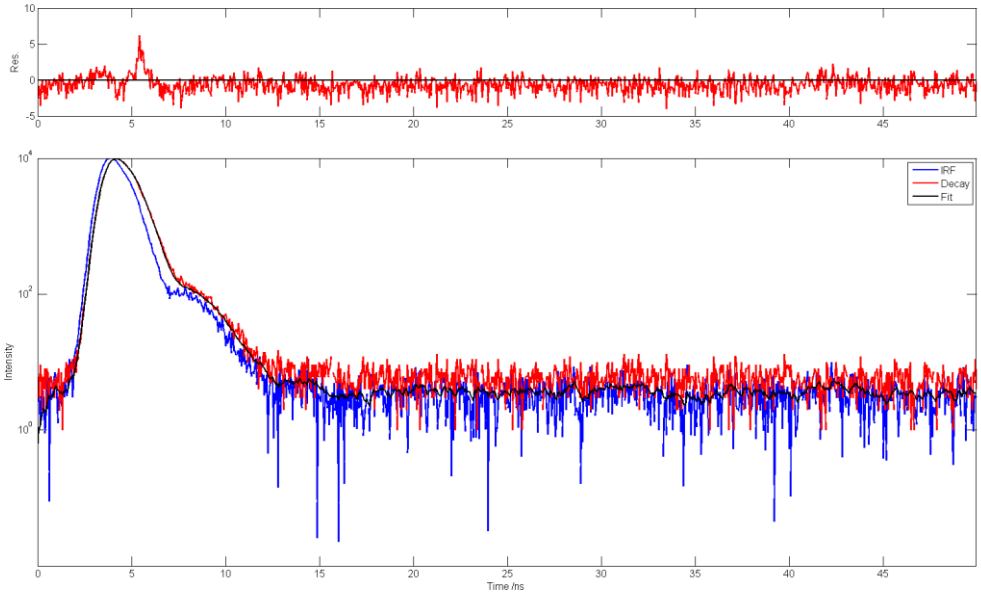

Figure S57 Fluorescence decay and monoexponential reconvolution fit of **GdL^{H}** in PIPES (bottom) and residuals of the fit (top).

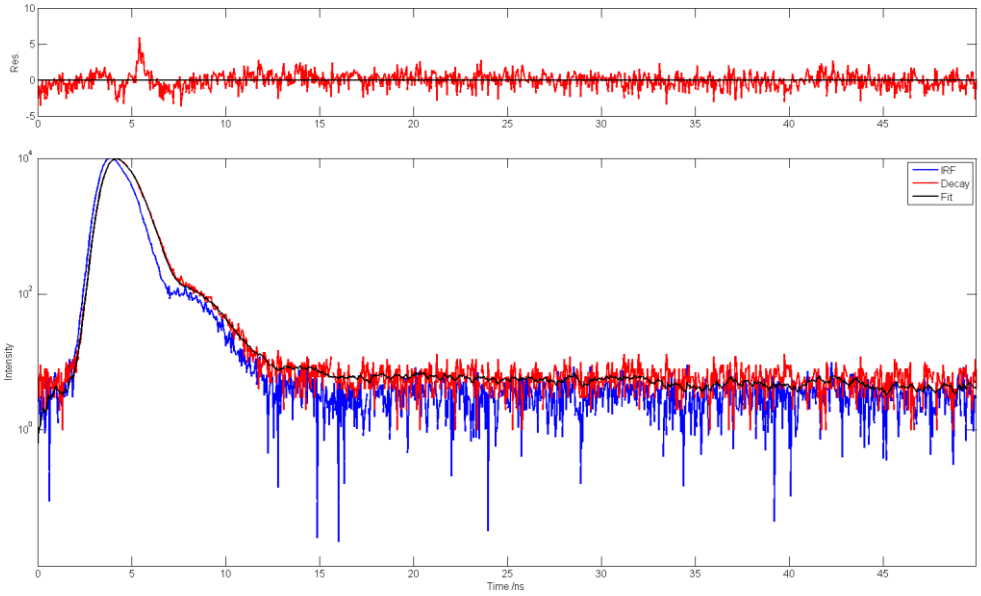

Figure S58 Fluorescence decay and biexponential reconvolution fit of **GdL^{H}** in PIPES (bottom) and residuals of the fit (top).

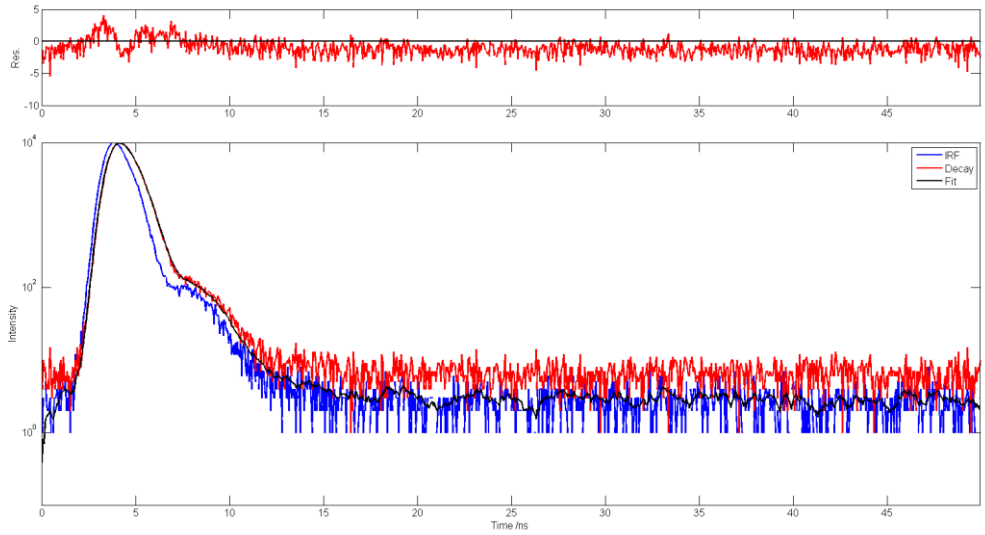

Figure S59 Fluorescence decay and monoexponential reconvolution fit of **GdL^{6F}** in PIPES (bottom) and residuals of the fit (top).

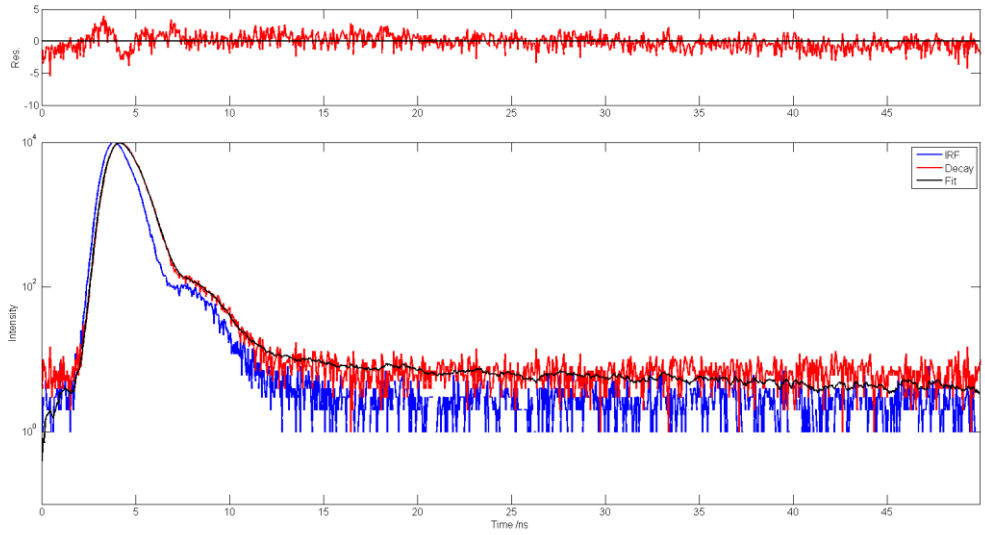

Figure S60 Fluorescence decay and biexponential reconvolution fit of **GdL^{6F}** in PIPES (bottom) and residuals of the fit (top).

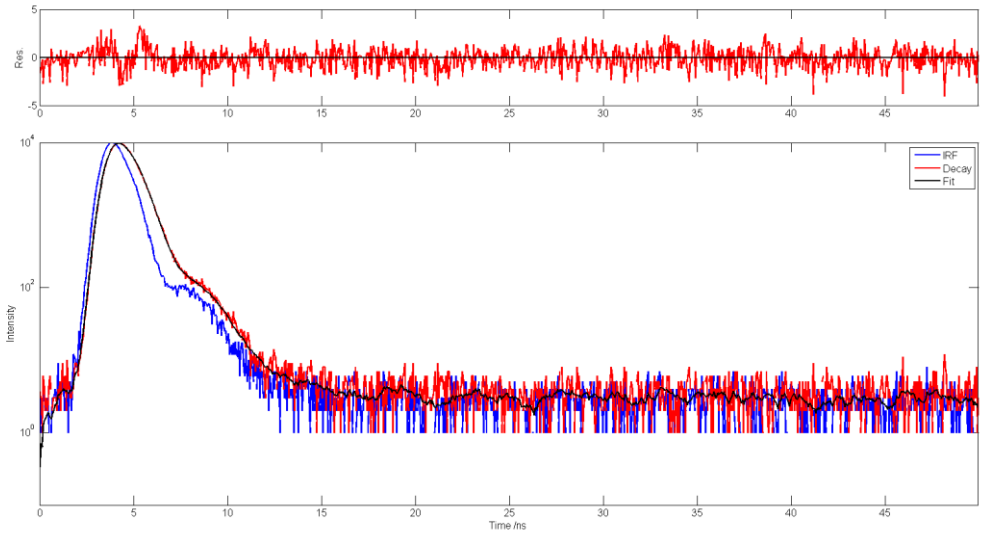

Figure S61 Fluorescence decay and monoexponential reconvolution fit of **GdL^{5F}** in PIPES (bottom) and residuals of the fit (top).

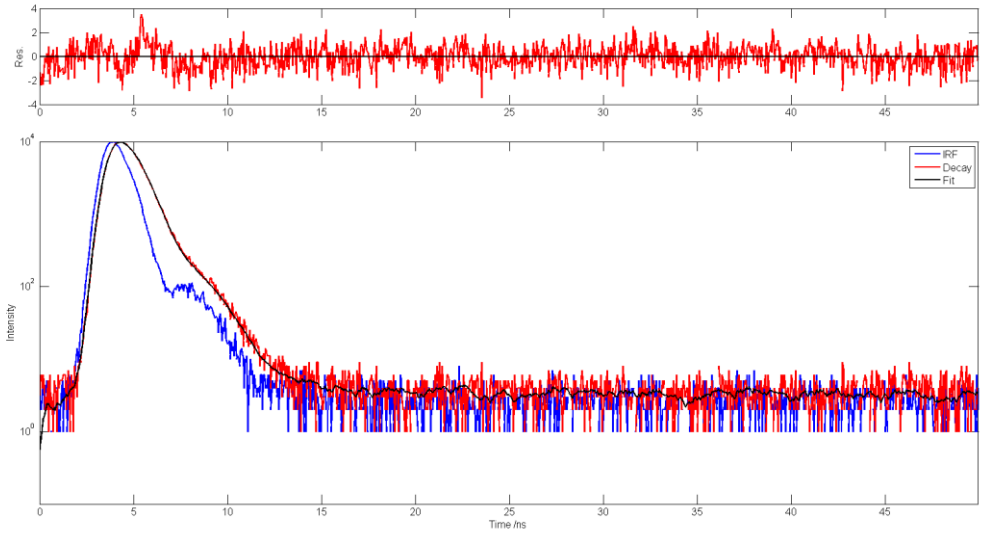

Figure S62 Fluorescence decay and monoexponential reconvolution fit of **GdL^{3F}** in PIPES (bottom) and residuals of the fit (top).

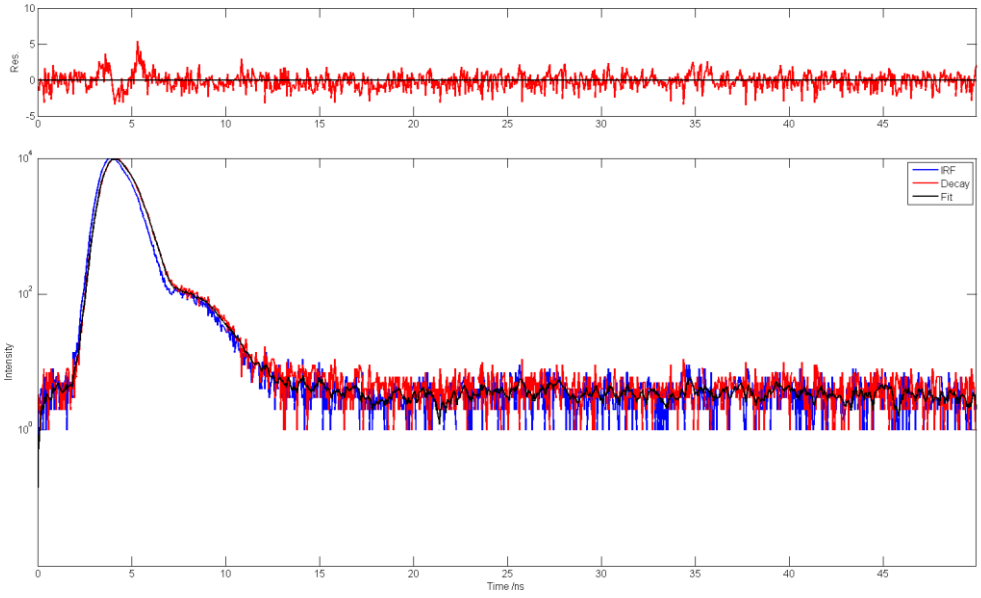

Figure S63 Fluorescence decay and monoexponential reconvolution fit of **TbL^{H}** in PIPES (bottom) and residuals of the fit (top).

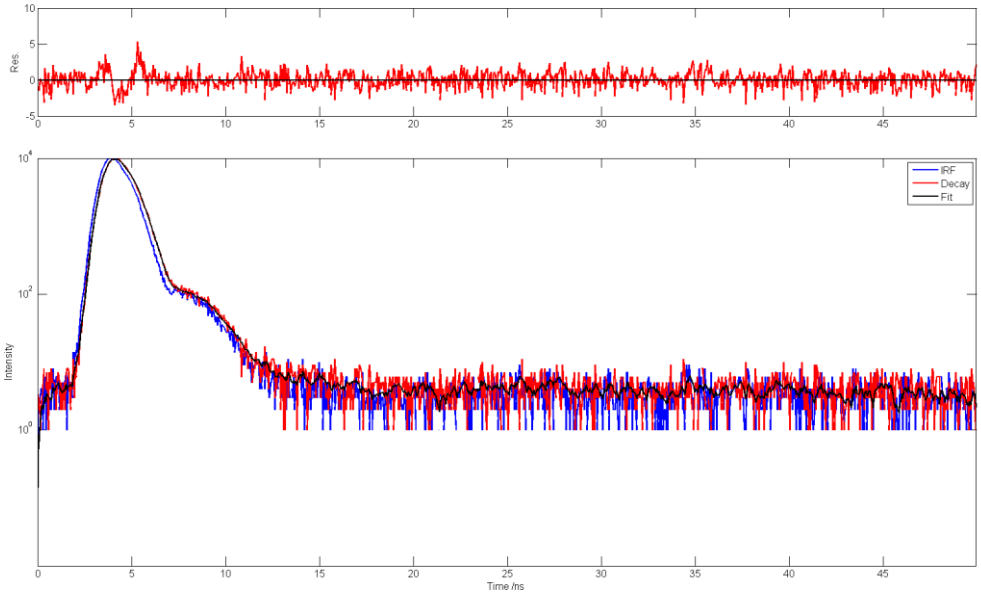

Figure S64 Fluorescence decay and biexponential reconvolution fit of **TbL^{H}** in PIPES (bottom) and residuals of the fit (top).

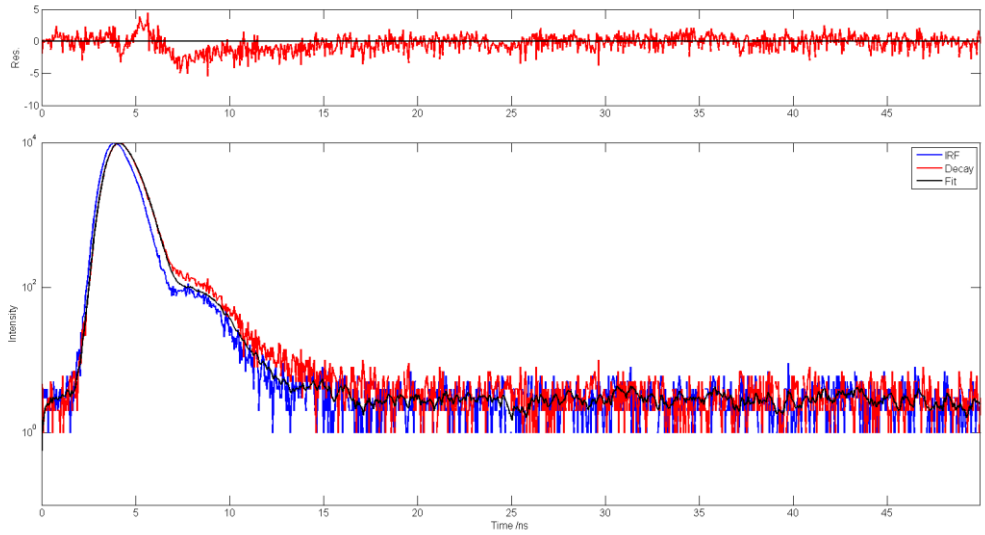

Figure S65 Fluorescence decay and monoexponential reconvolution fit of **TbL^{6F}** in PIPES (bottom) and residuals of the fit (top).

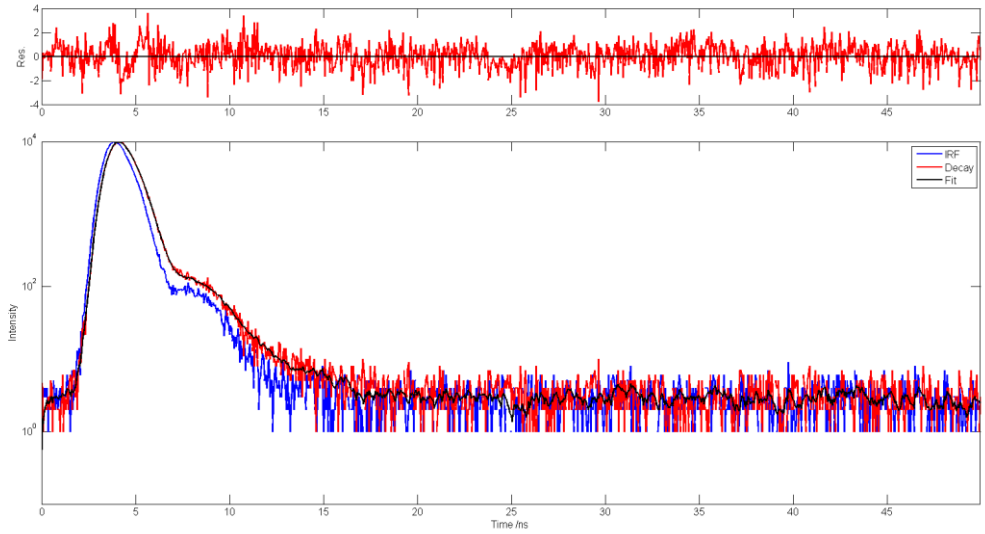

Figure S66 Fluorescence decay and biexponential reconvolution fit of **TbL^{6F}** in PIPES (bottom) and residuals of the fit (top).

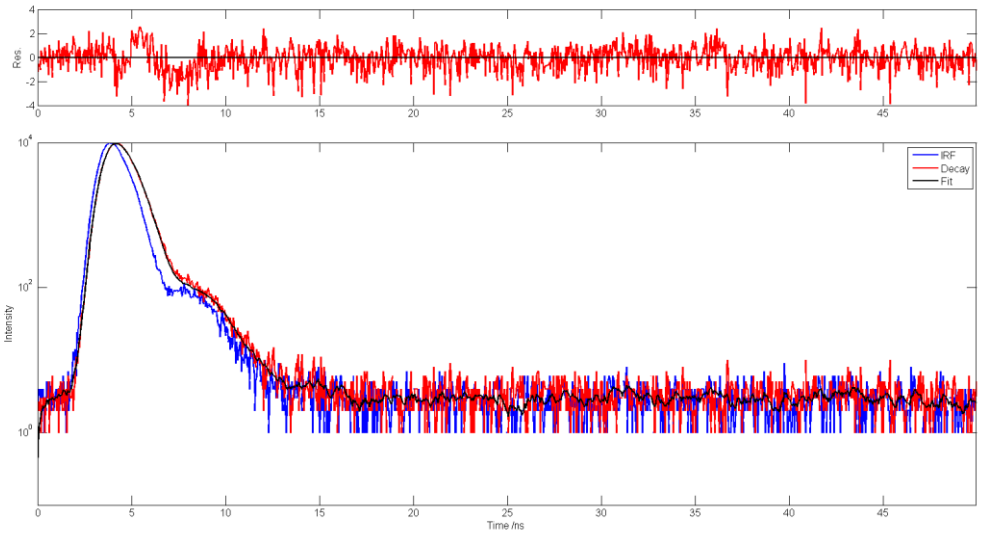

Figure S67 Fluorescence decay and monoexponential reconvolution fit of **TbL^{5F}** in PIPES (bottom) and residuals of the fit (top).

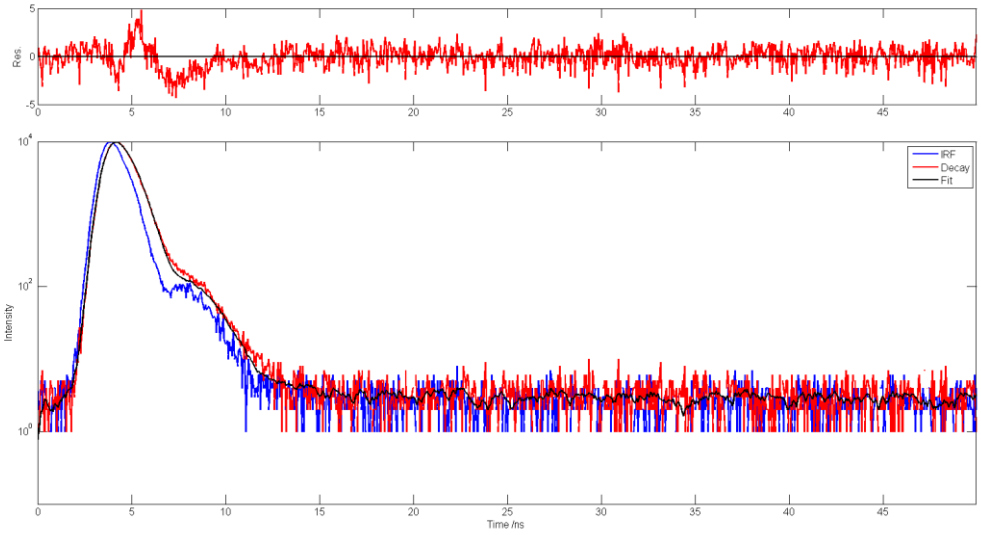

Figure S68 Fluorescence decay and monoexponential reconvolution fit of **TbL^{3F}** in PIPES (bottom) and residuals of the fit (top).

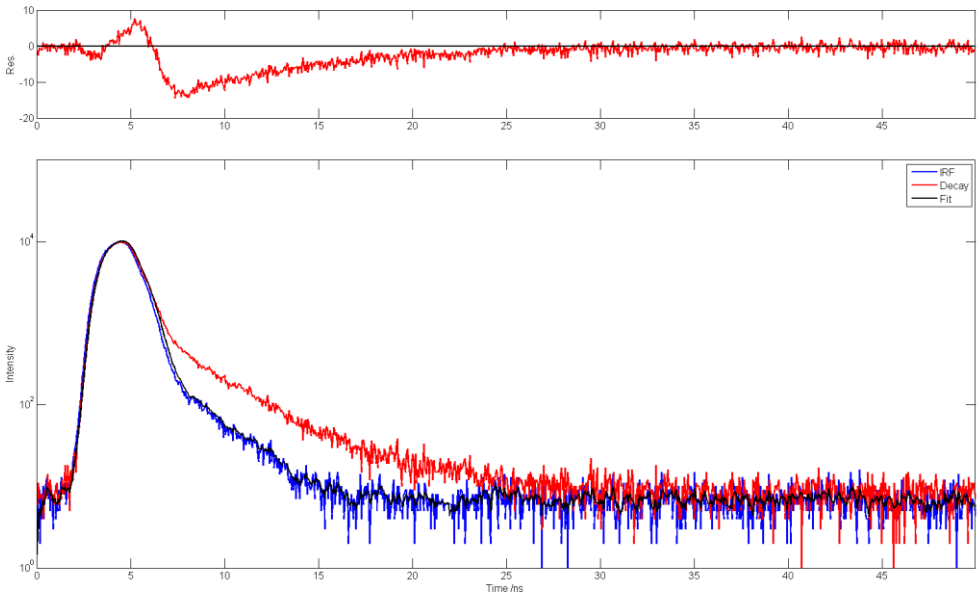

Figure S69 Fluorescence decay and monoexponential reconvolution fit of **EuL^{H}** in PIPES (bottom) and residuals of the fit (top).

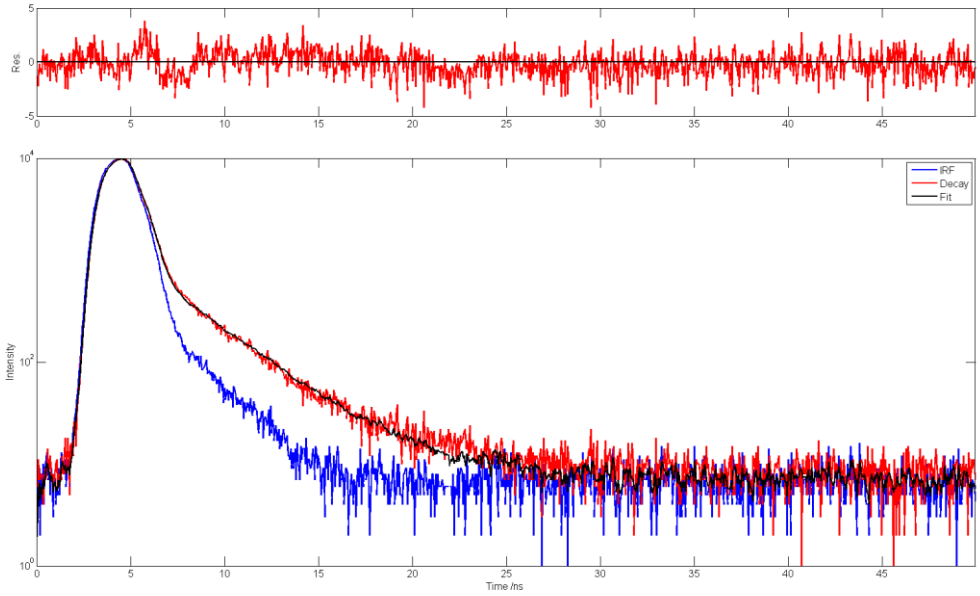

Figure S70 Fluorescence decay and biexponential reconvolution fit of **EuL^{H}** in PIPES (bottom) and residuals of the fit (top).

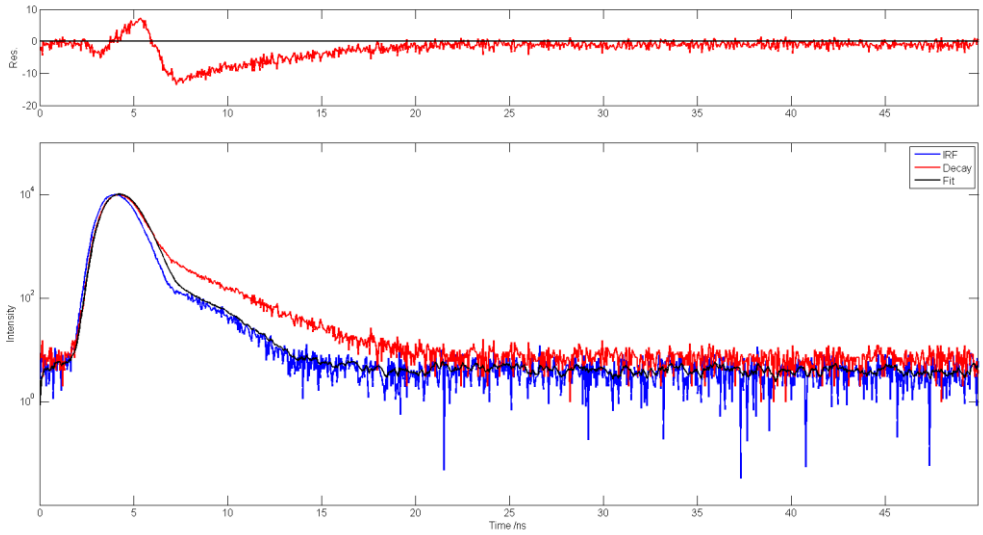

Figure S71 Fluorescence decay and monoexponential reconvolution fit of **EuL^{6F}** in PIPES (bottom) and residuals of the fit (top).

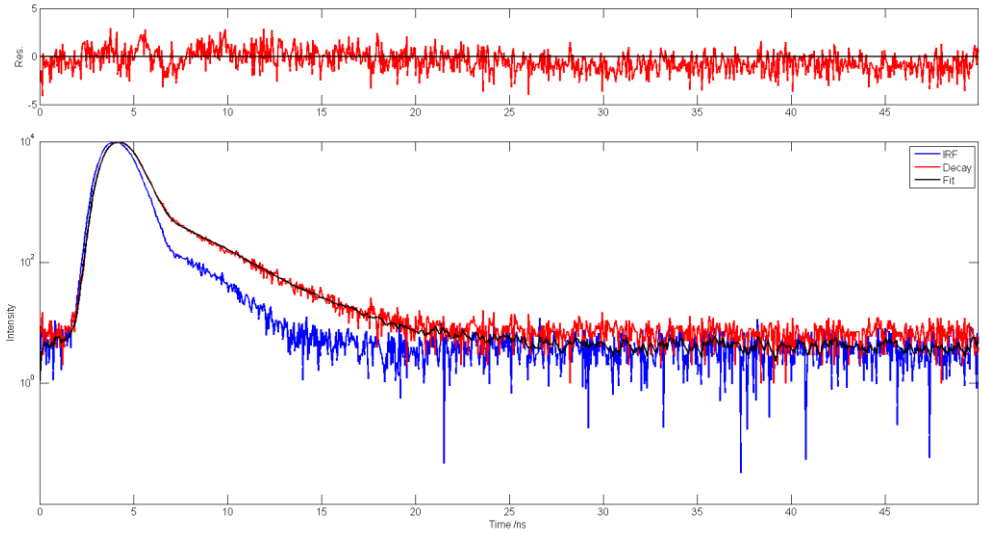

Figure S72 Fluorescence decay and biexponential reconvolution fit of **EuL^{6F}** in PIPES (bottom) and residuals of the fit (top).

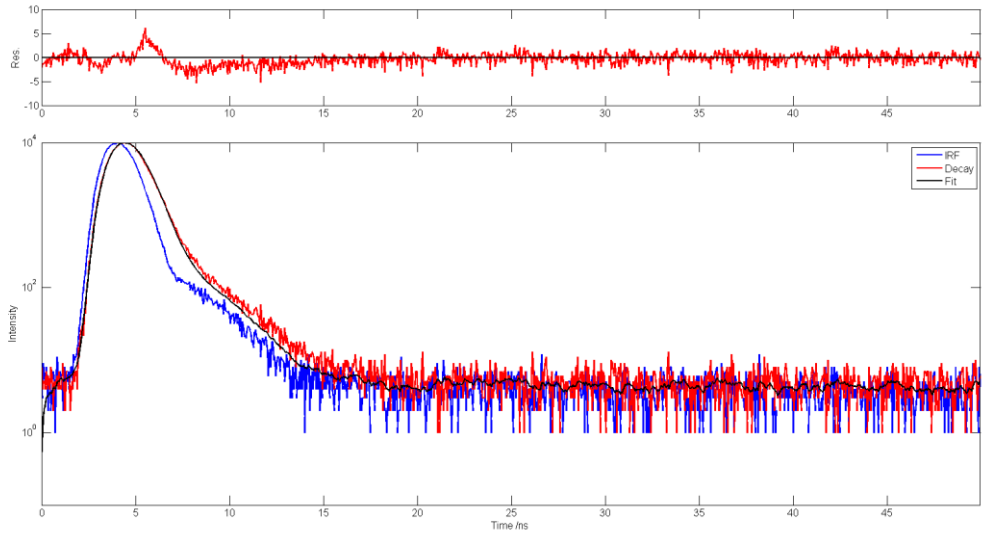

Figure S73 Fluorescence decay and monoexponential reconvolution fit of **EuL^{5F}** in PIPES (bottom) and residuals of the fit (top).

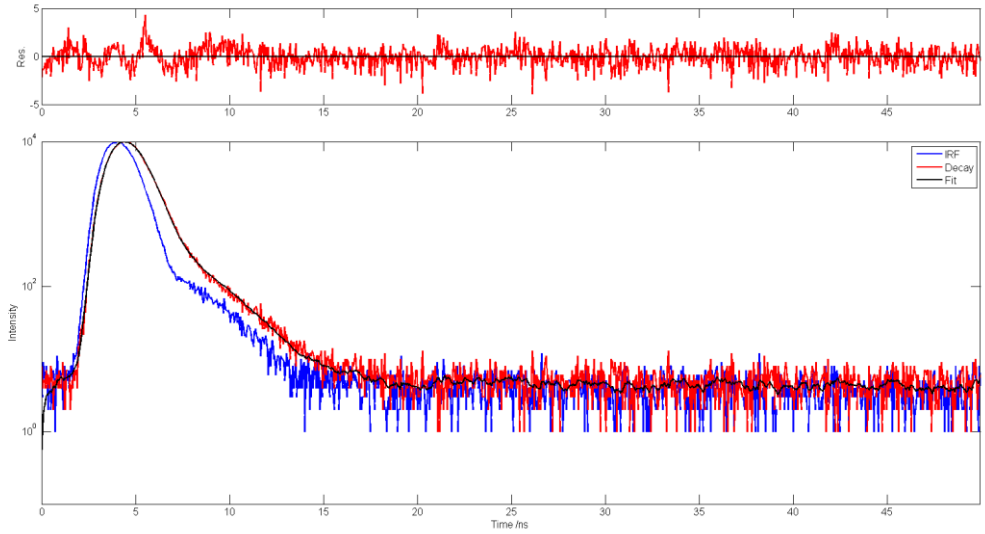

Figure S74 Fluorescence decay and biexponential reconvolution fit of **EuL^{5F}** in PIPES (bottom) and residuals of the fit (top).

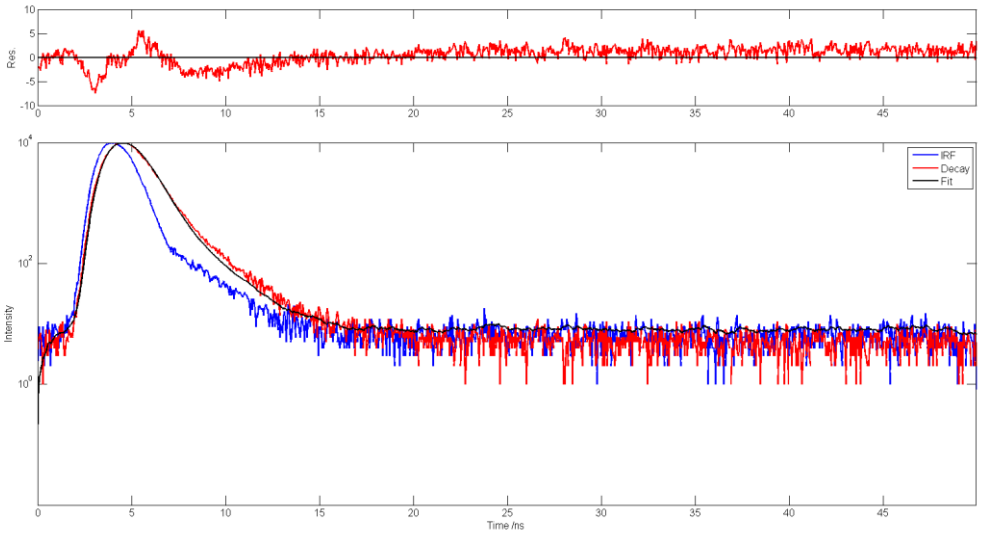

Figure S75 Fluorescence decay and monoexponential reconvolution fit of **EuL^{3F}** in PIPES (bottom) and residuals of the fit (top).

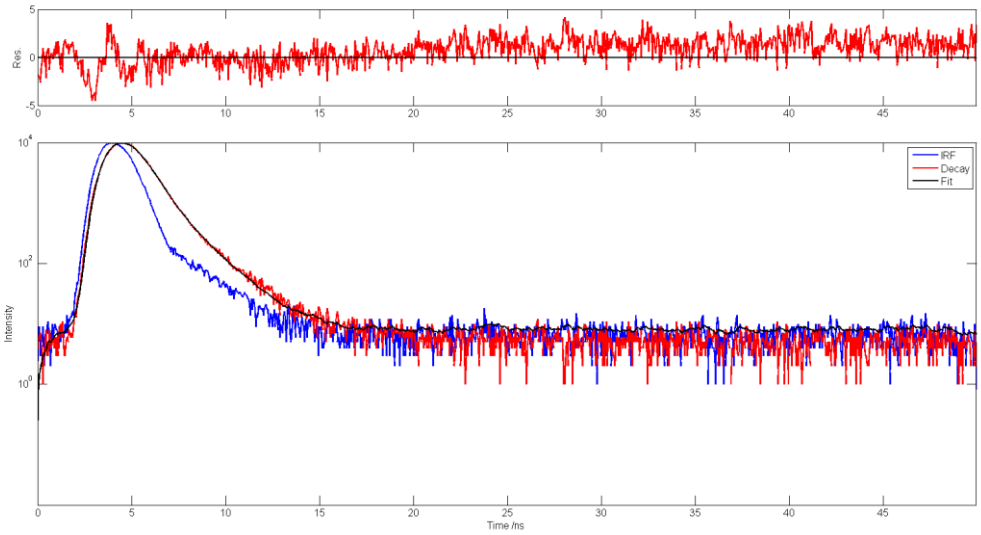

Figure S76 Fluorescence decay and biexponential reconvolution fit of **EuL^{3F}** in PIPES (bottom) and residuals of the fit (top).

^{1}H, ^{13}C, and ^{19}F NMR spectra

5^{3F}

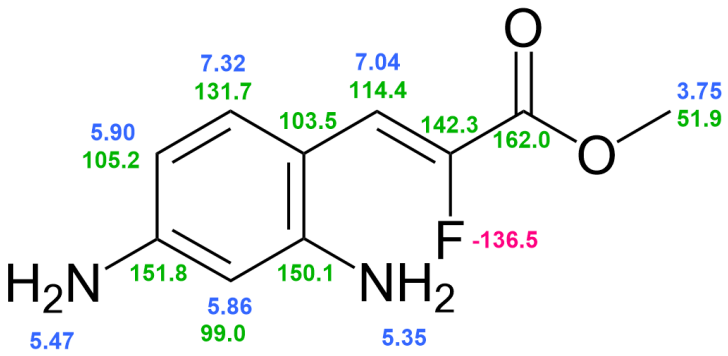

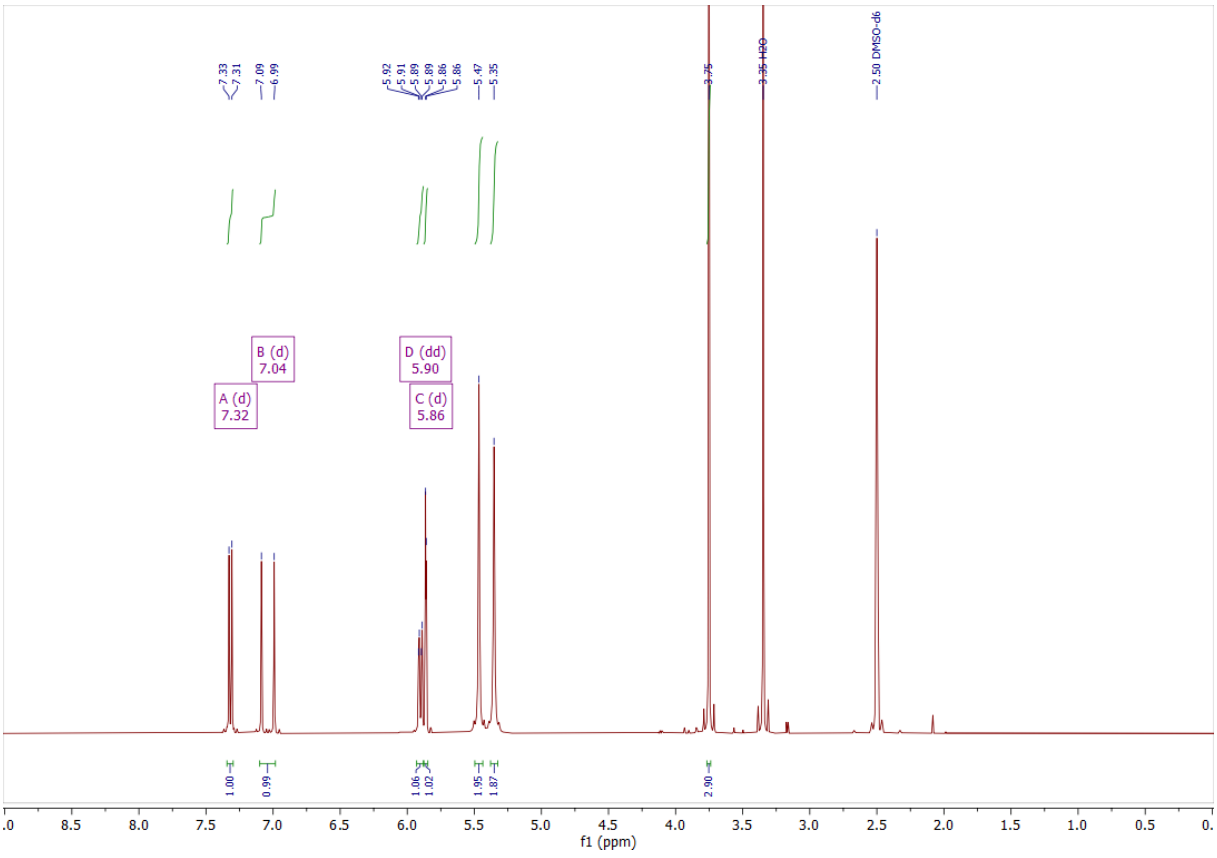

Figure S77 ^{1}H NMR spectrum of **5^{3F}** (400 MHz, DMSO-d_6).

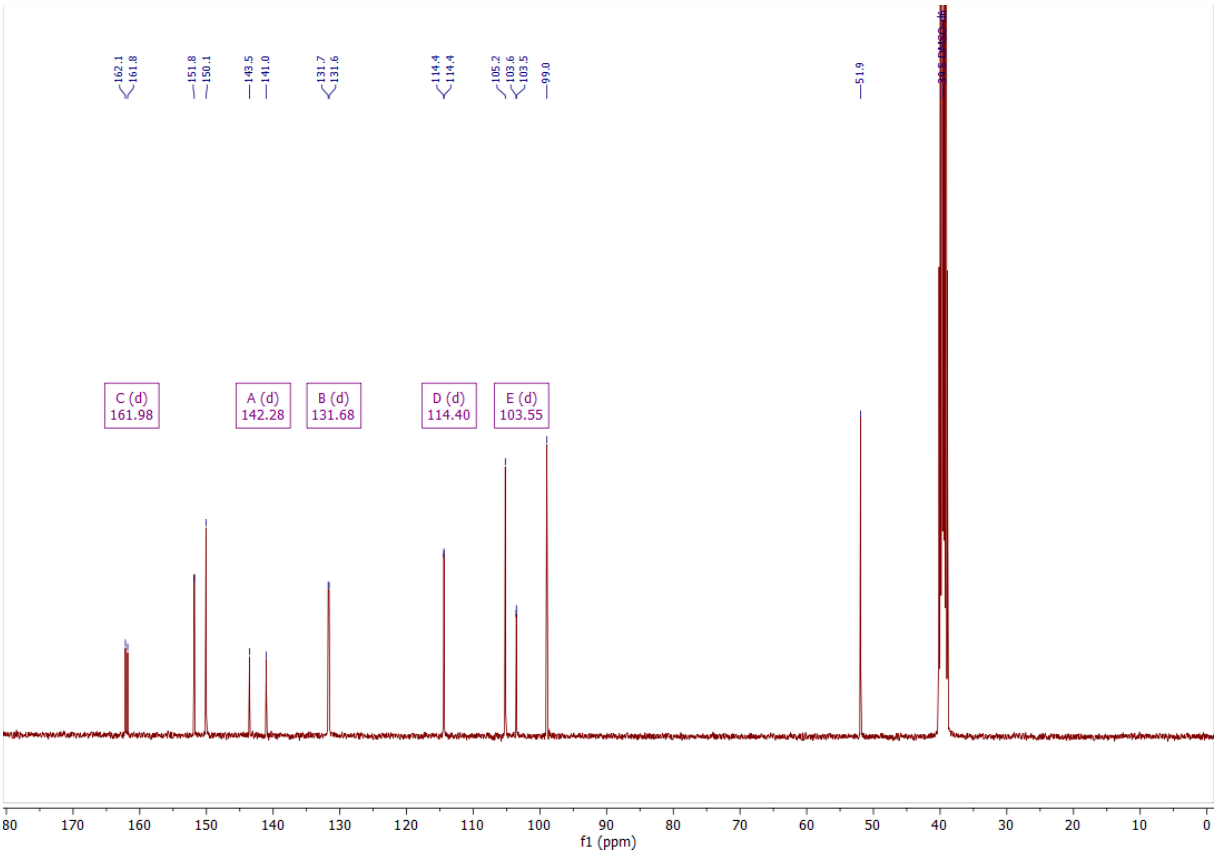

Figure S78 ^{13}C NMR spectrum of **5^{3F}** (101 MHz, DMSO-d_6).

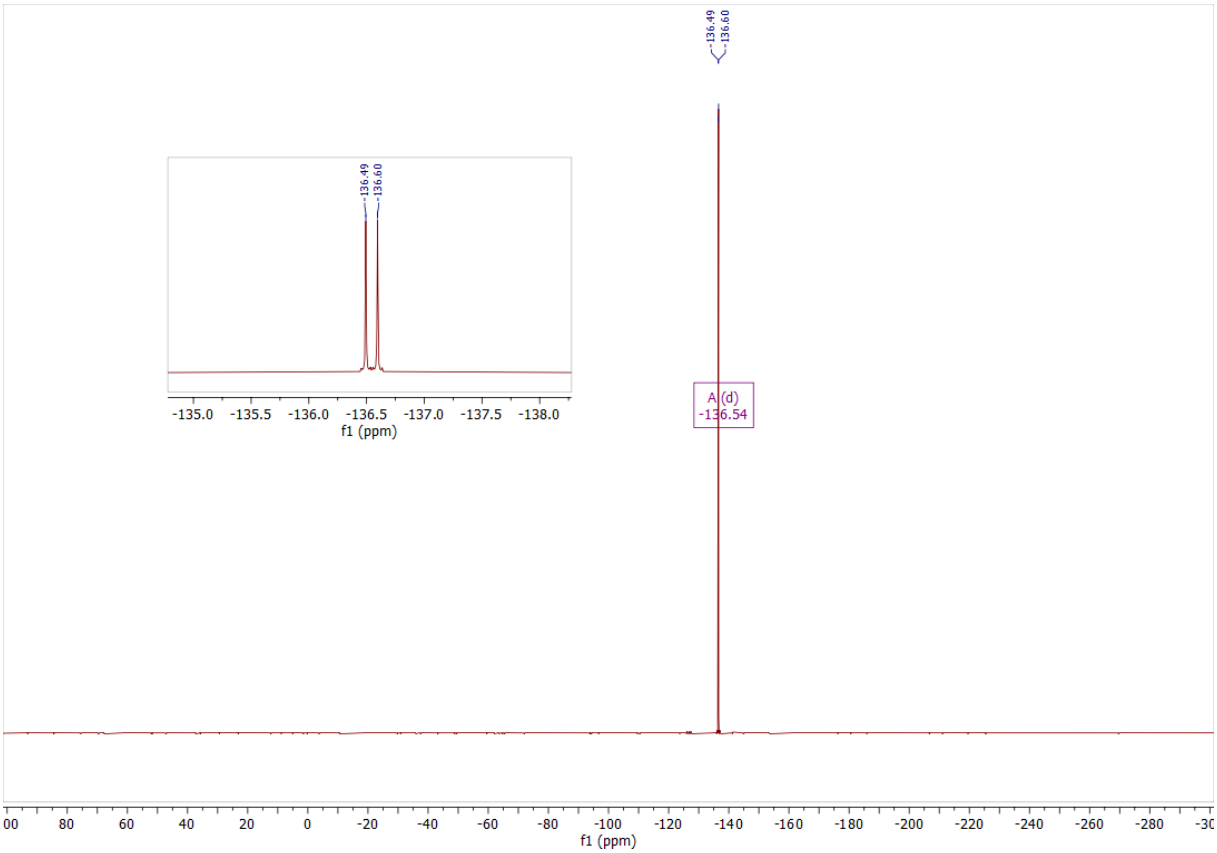

Figure S79 ^{19}F NMR spectrum of **5^{3F}** (376 MHz, DMSO-d_6).

4b

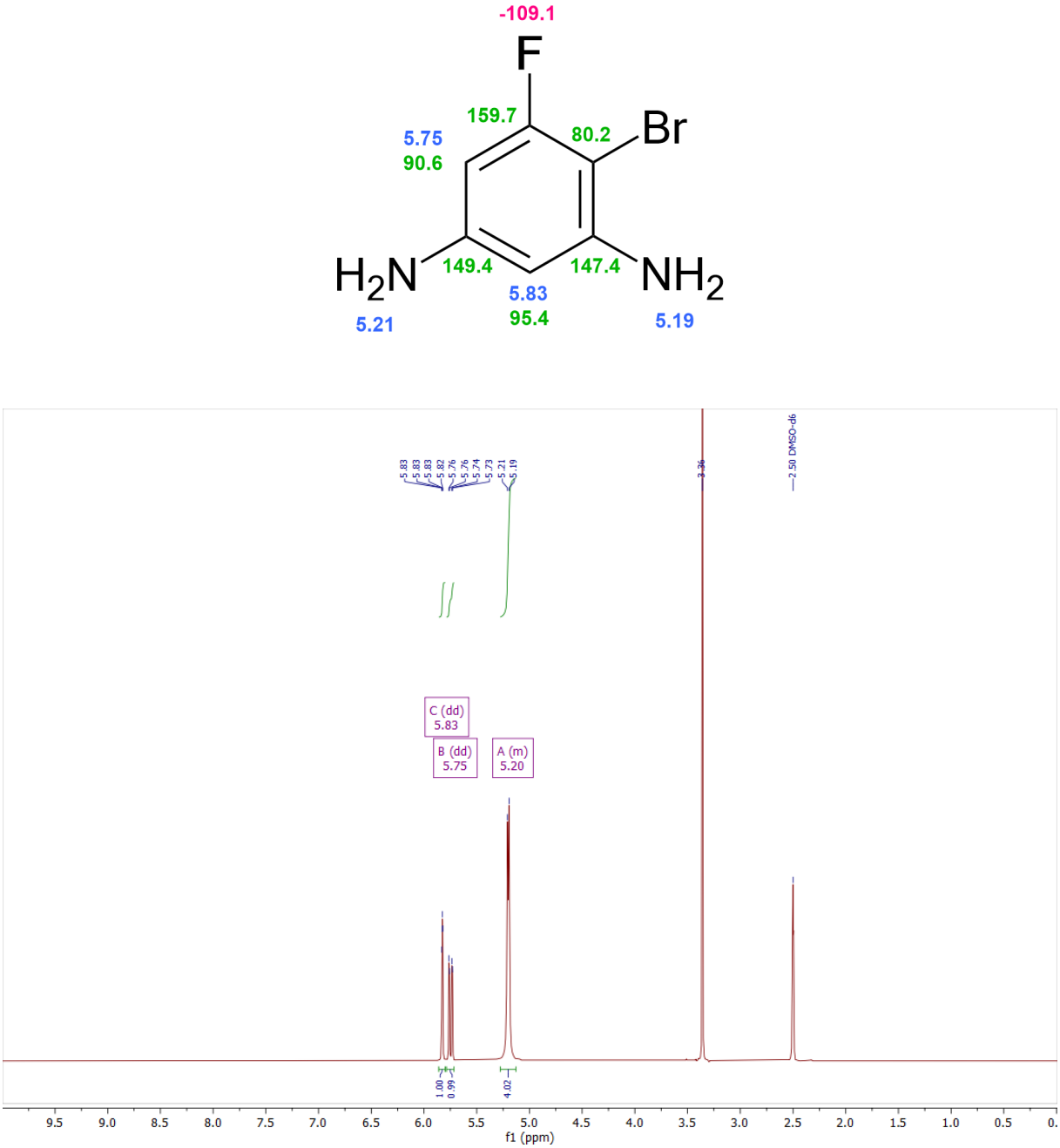

Figure S80 ^{1}H NMR spectrum of **4b** (400 MHz, DMSO-d_6).

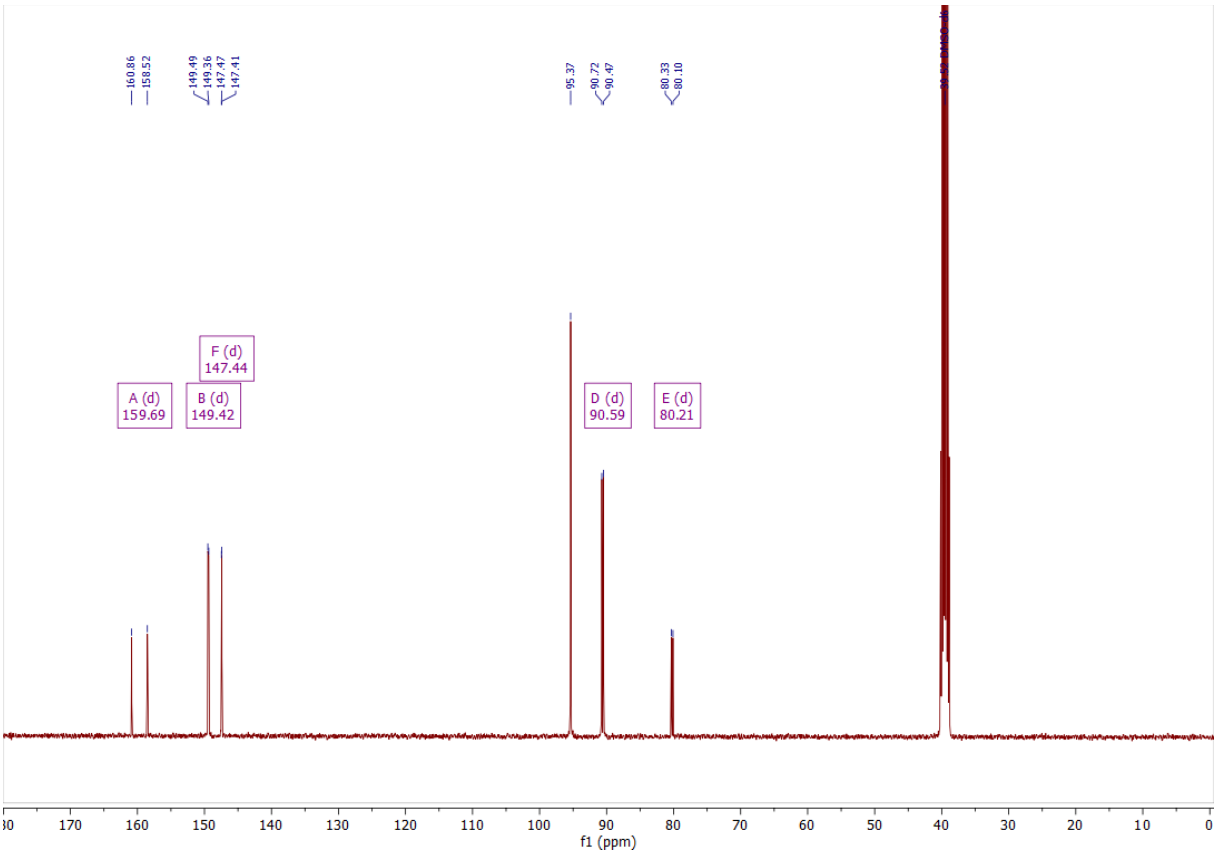

Figure S81 ^{13}C NMR spectrum of **4b** (101 MHz, DMSO-d_6).

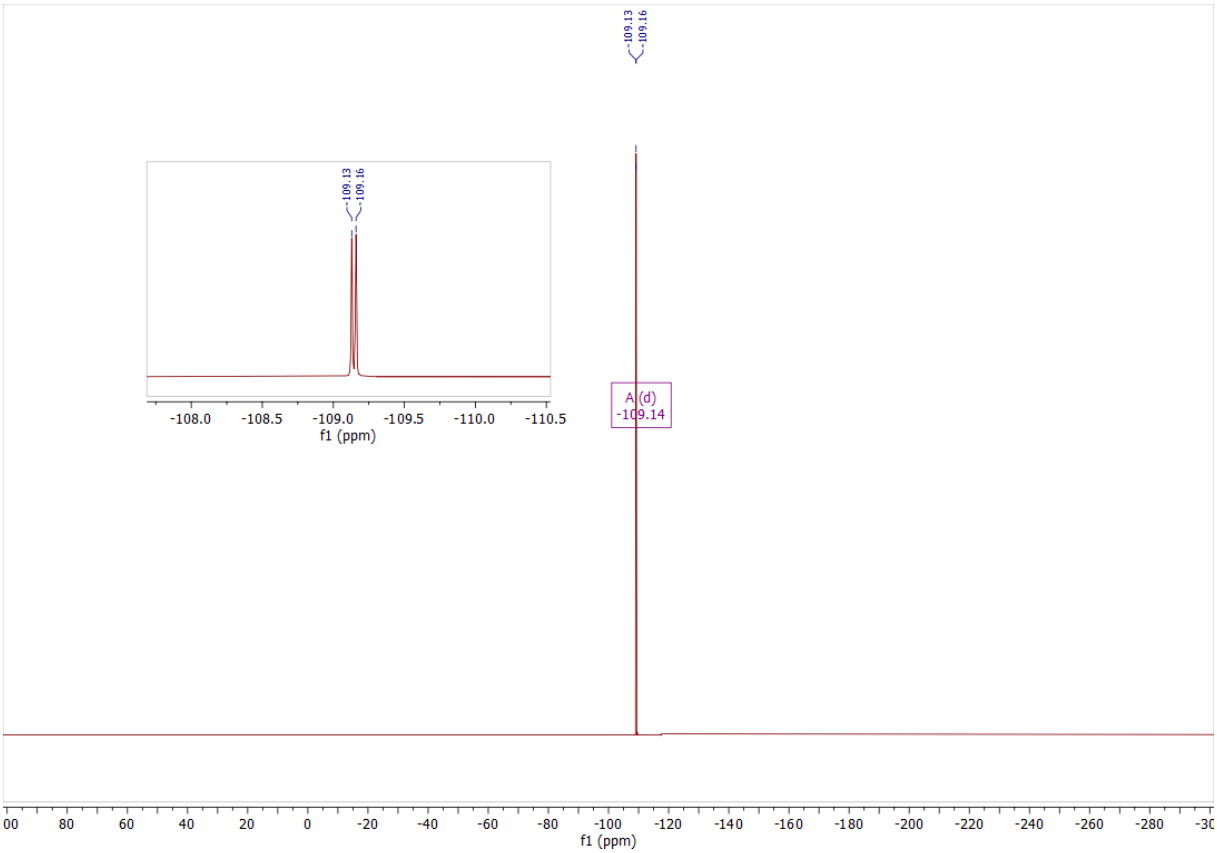

Figure S82 ^{19}F NMR spectrum of **4b** (376 MHz, DMSO-d_6).

4a

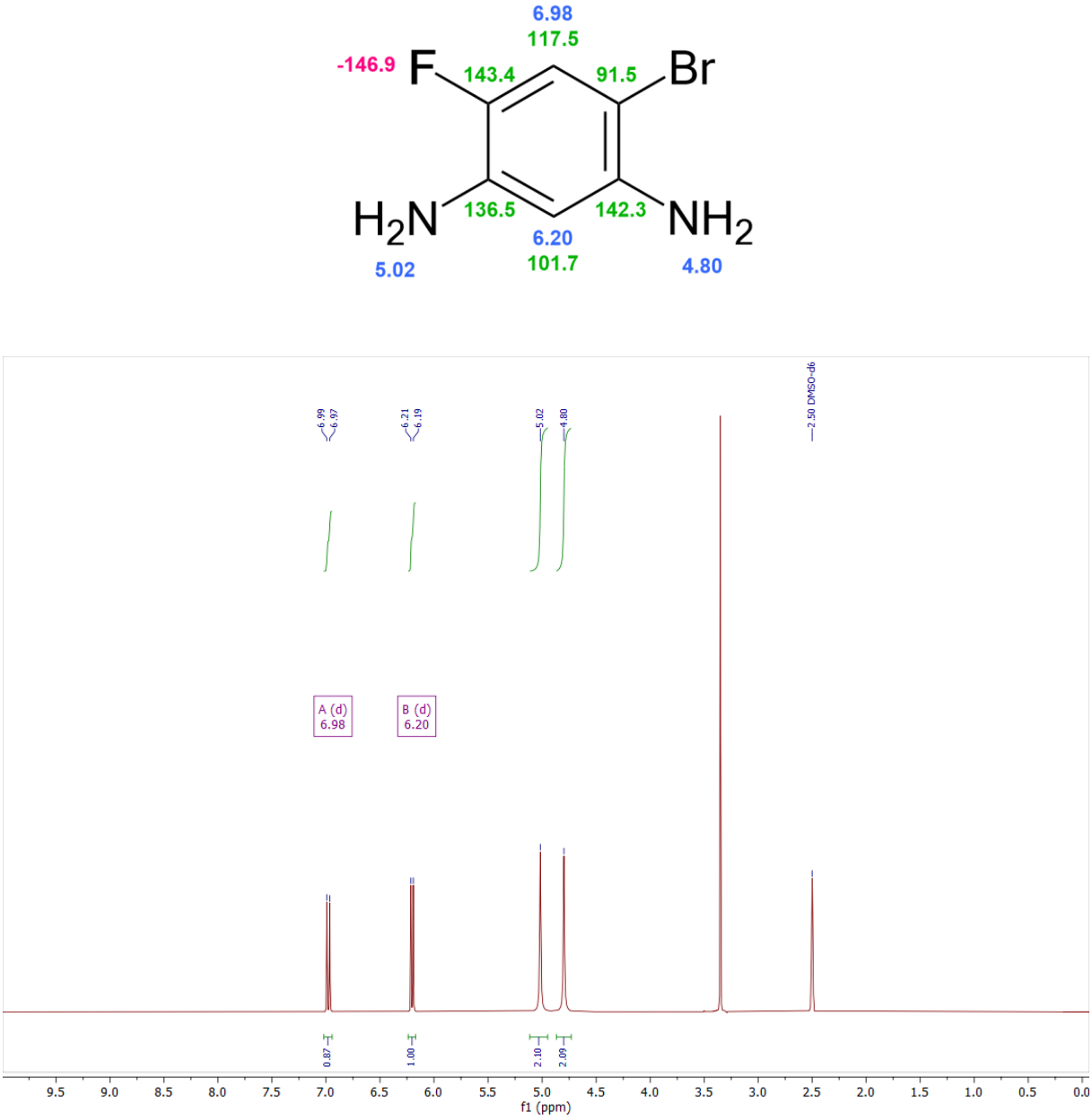

Figure S83 ^{1}H NMR spectrum of **4a** (400 MHz, DMSO-d_6).

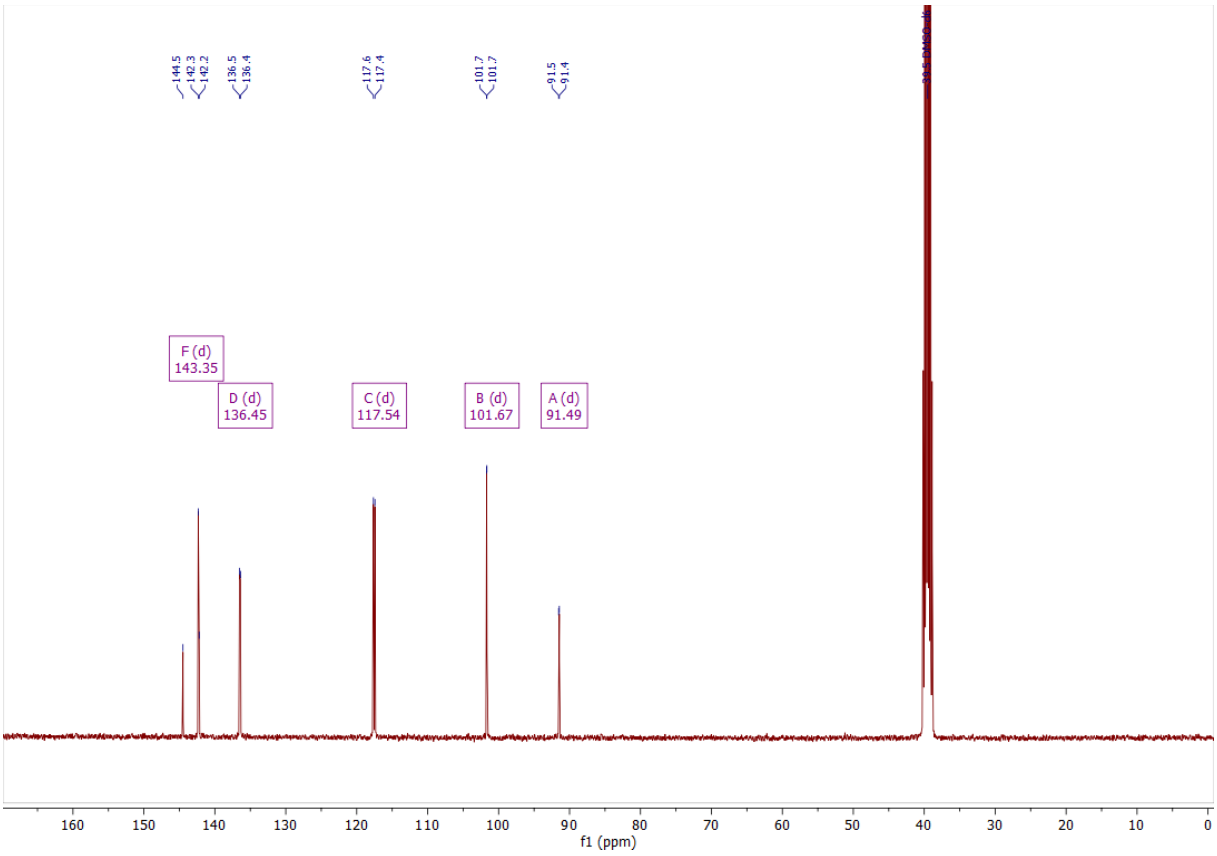

Figure S84 ^{13}C NMR spectrum of **4a** (101 MHz, DMSO-d_6).

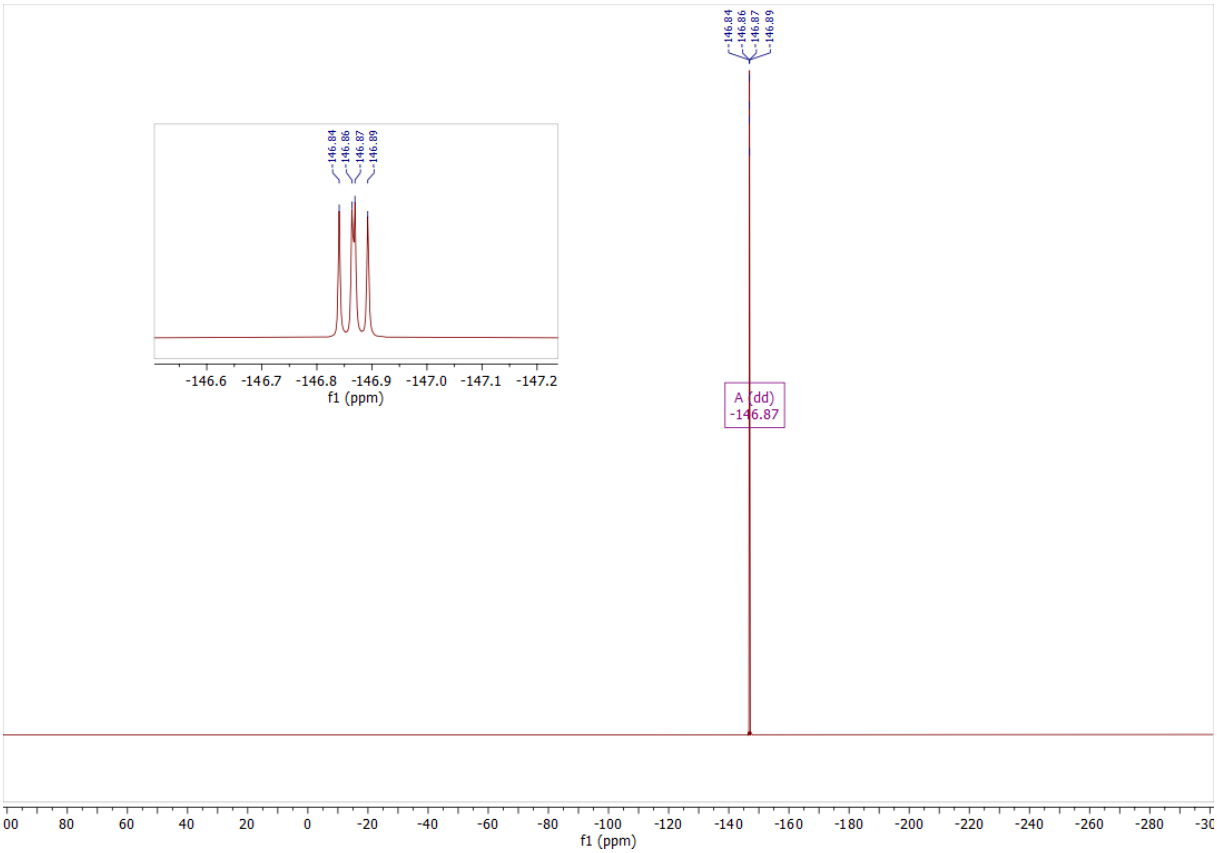

Figure S85 ^{19}F NMR spectrum of **4a** (376 MHz, DMSO-d_6).

5^{5F}

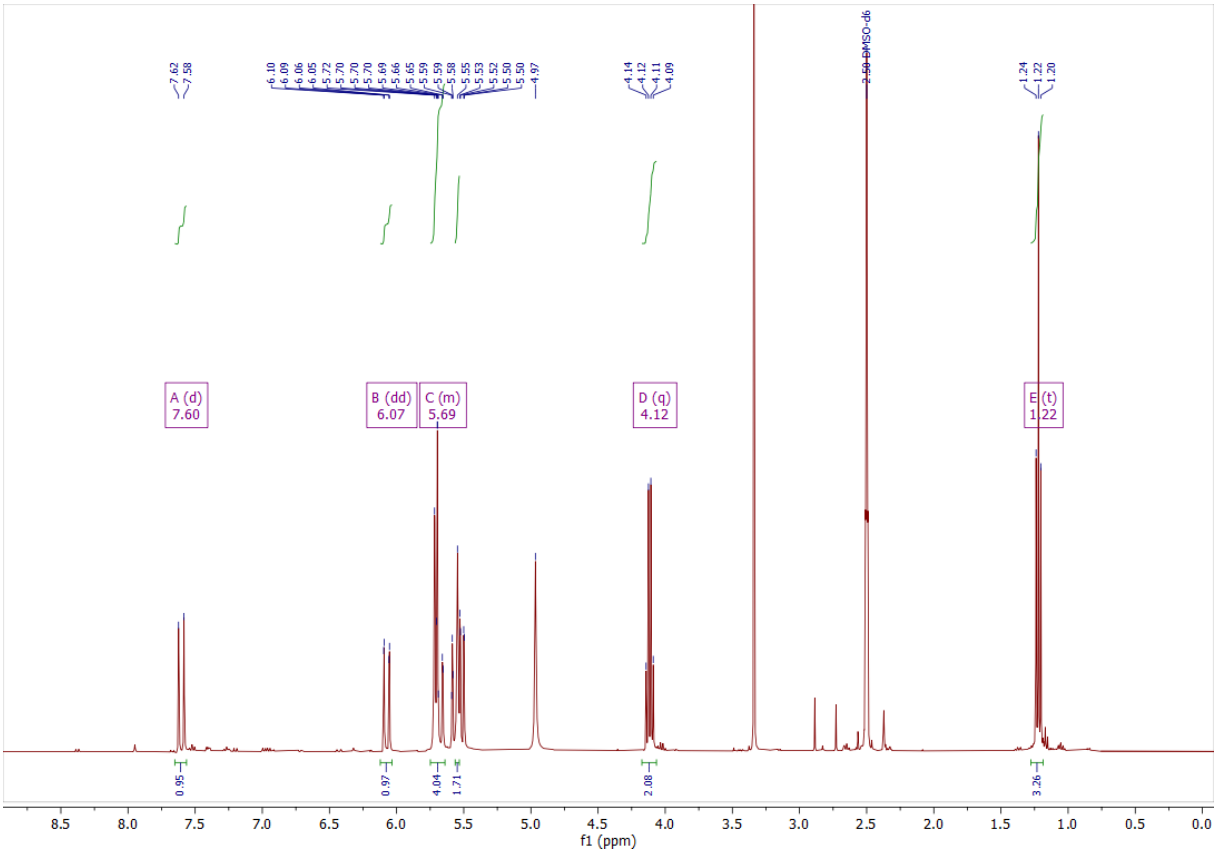

Figure S86 ^{1}H NMR spectrum of **5^{5F}** (400 MHz, DMSO-d_6).

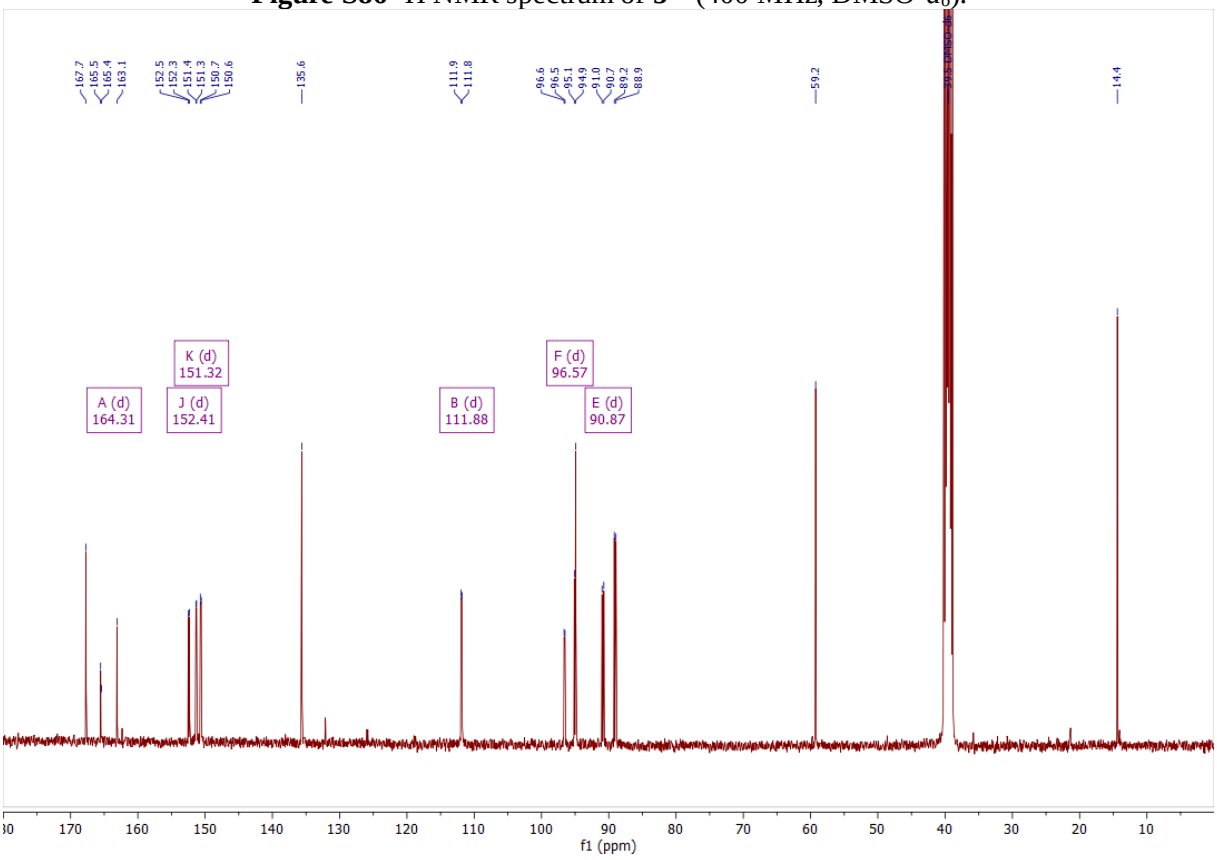

Figure S87 ^{13}C NMR spectrum of **5^{5F}** (101 MHz, DMSO-d_6).

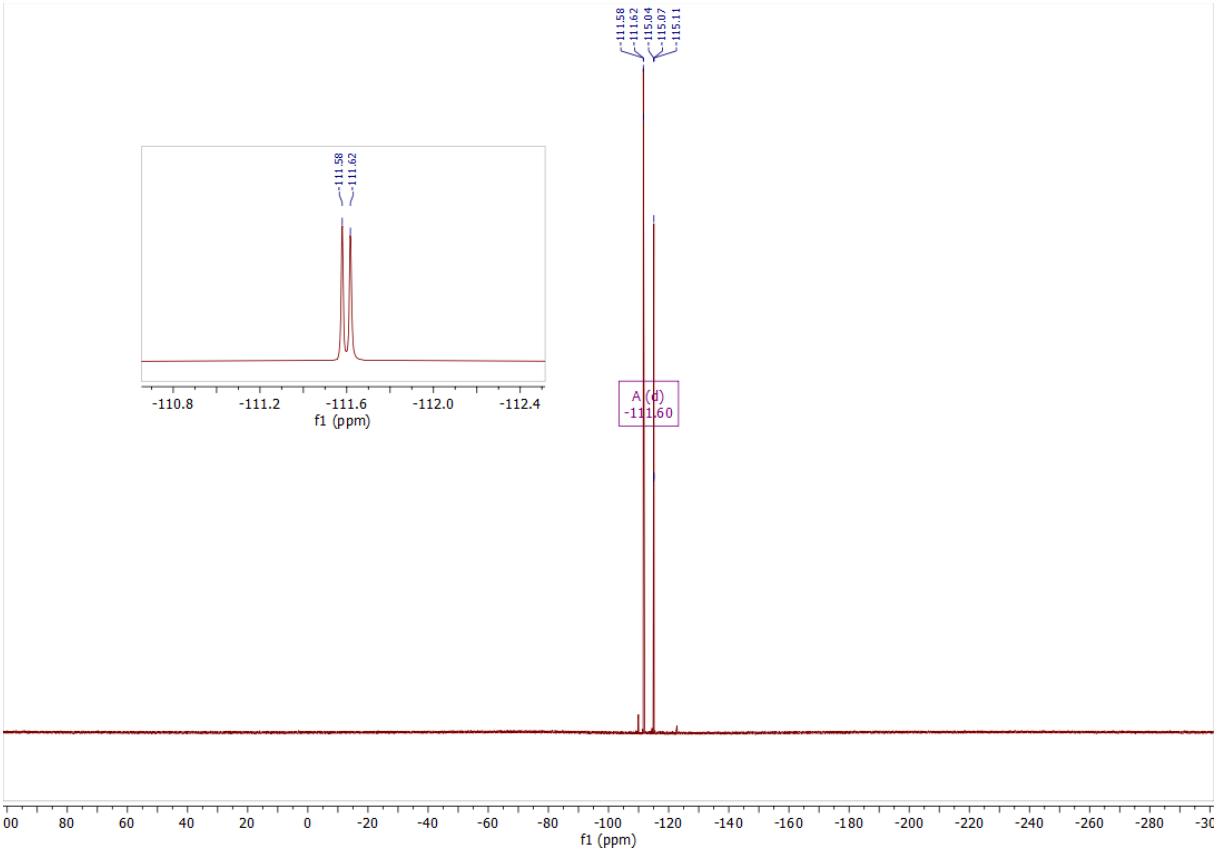

Figure S88 ^{19}F NMR spectrum of **5^{5F}** (376 MHz, DMSO-d_6).

5^{6F}

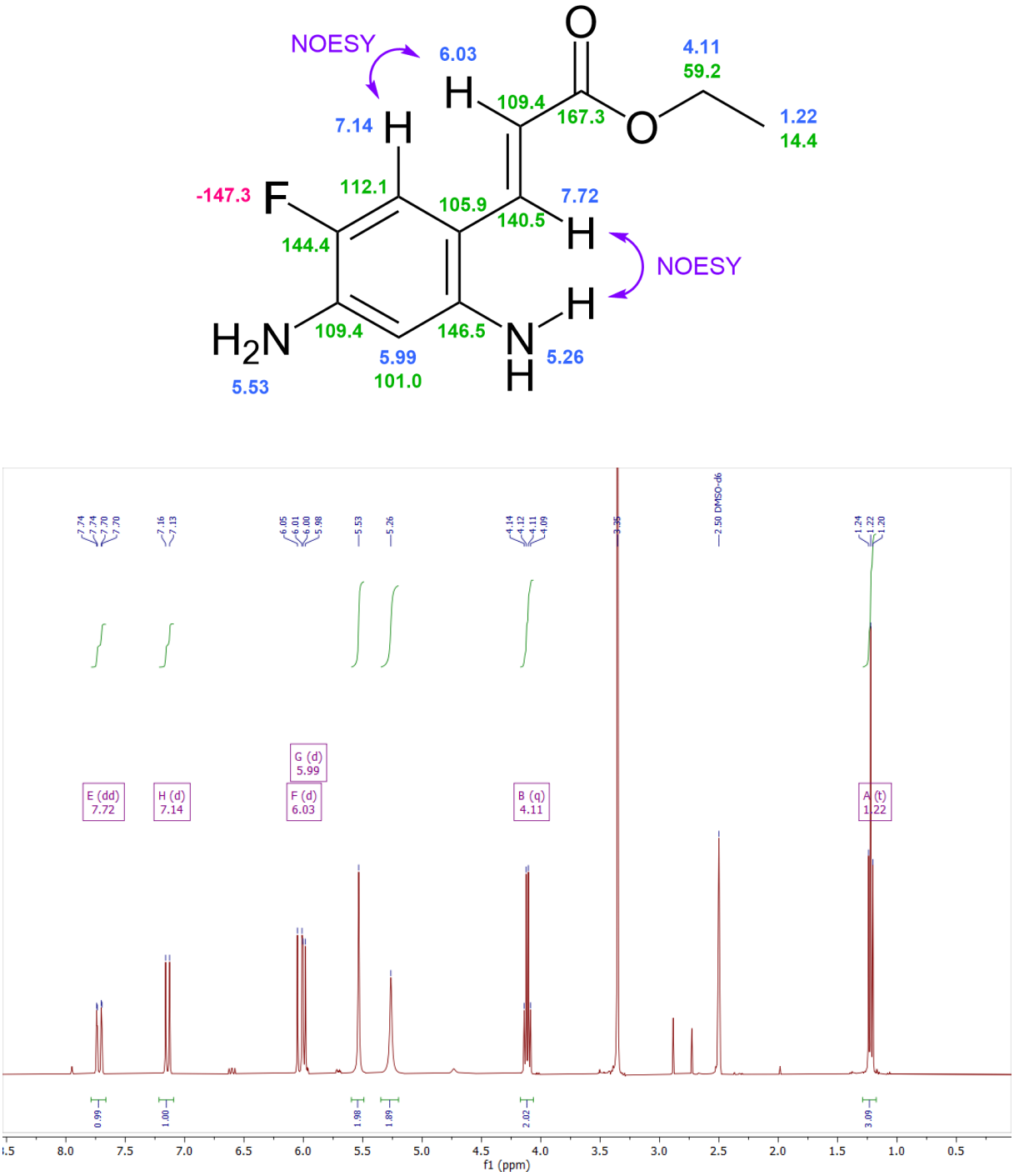

Figure S89 ^{1}H NMR spectrum of **5**^{6F} (400 MHz, DMSO-d_6).

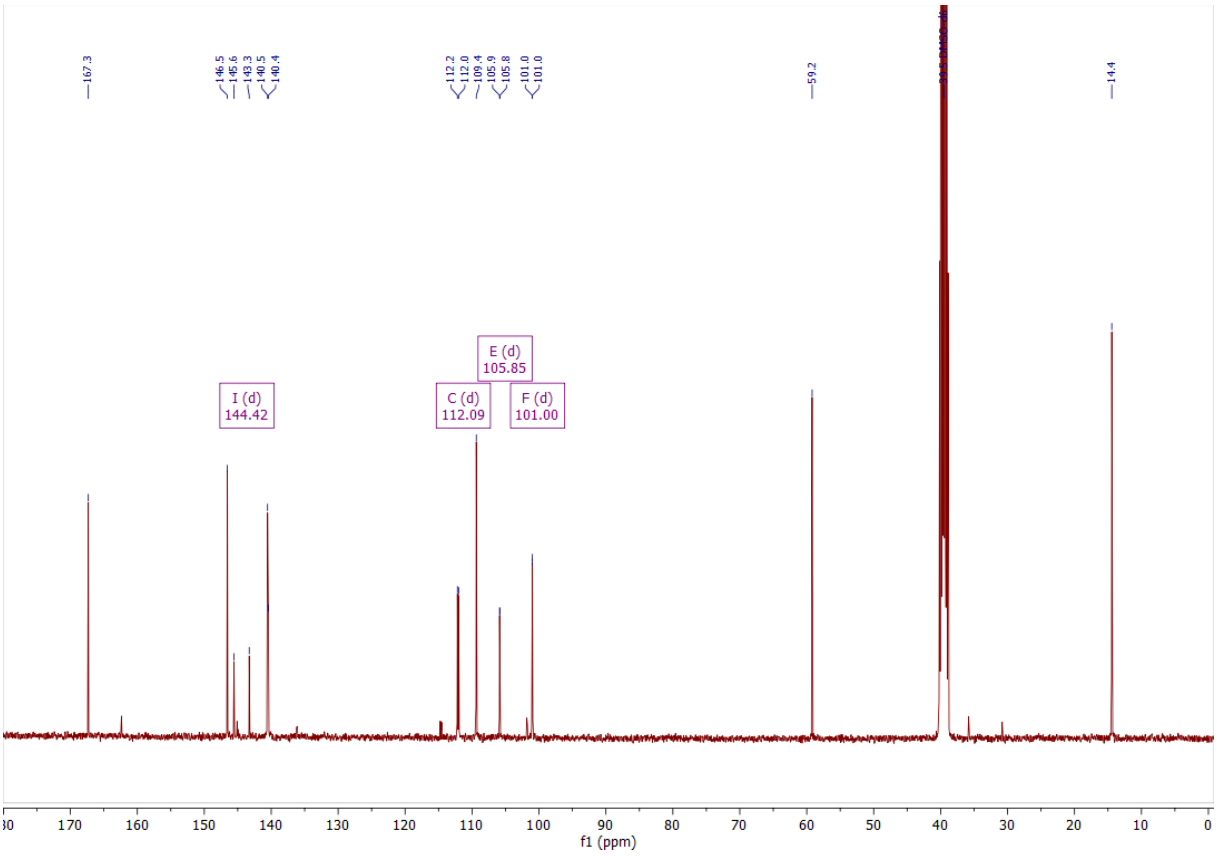

Figure S90 ^{13}C NMR spectrum of **5^{6F}** (101 MHz, DMSO-d_6).

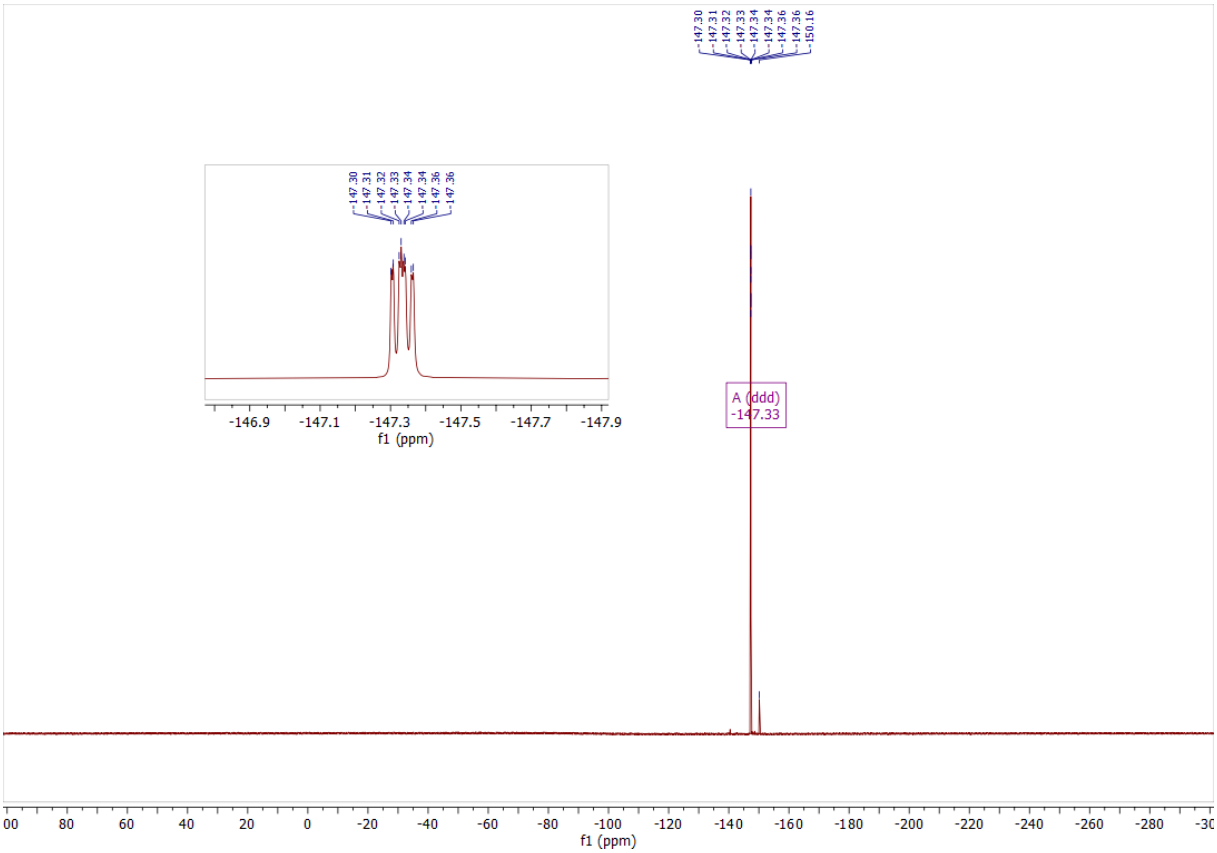

Figure S91 ^{19}F NMR spectrum of **5^{6F}** (376 MHz, DMSO-d_6).

CS^{3F}

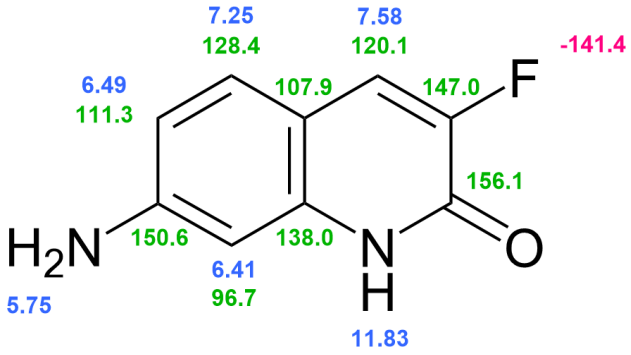

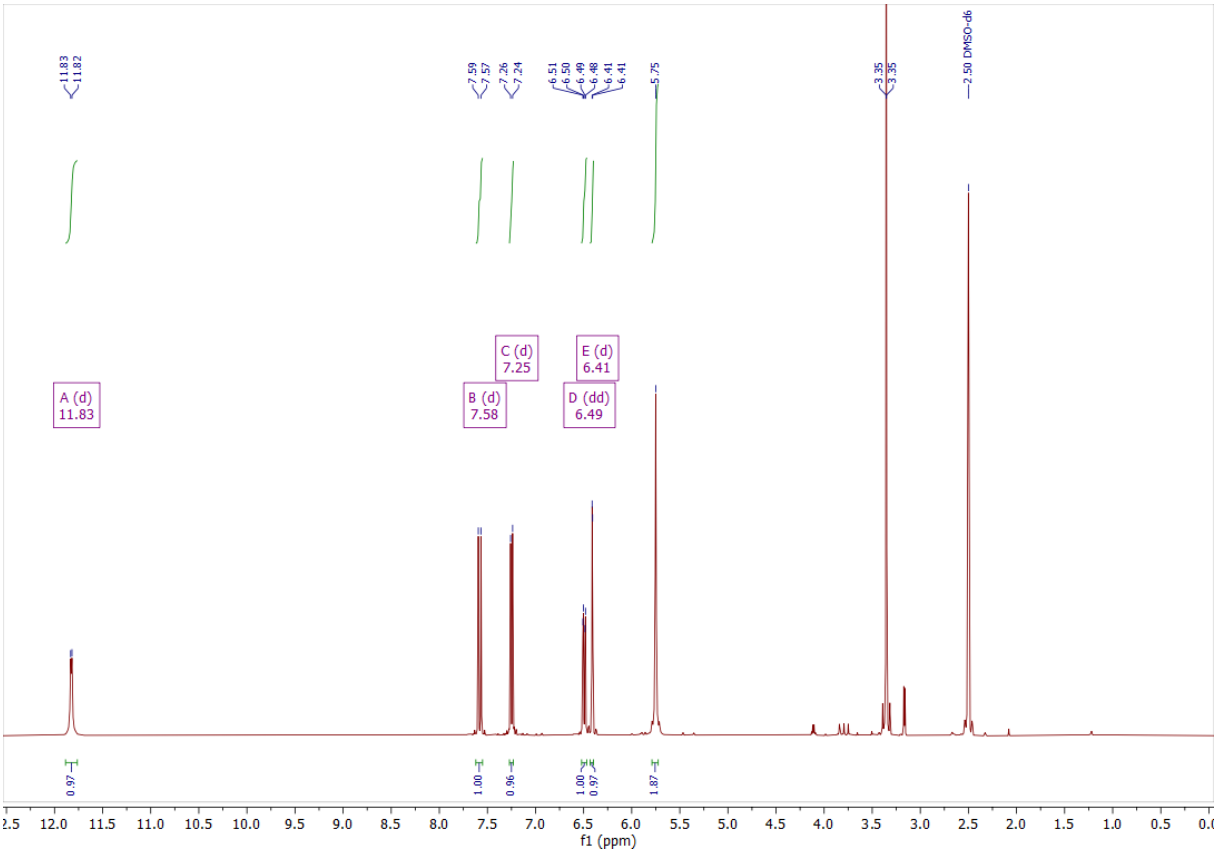

Figure S92 ^{1}H NMR spectrum of **CS^{3F}** (400 MHz, DMSO-d_6).

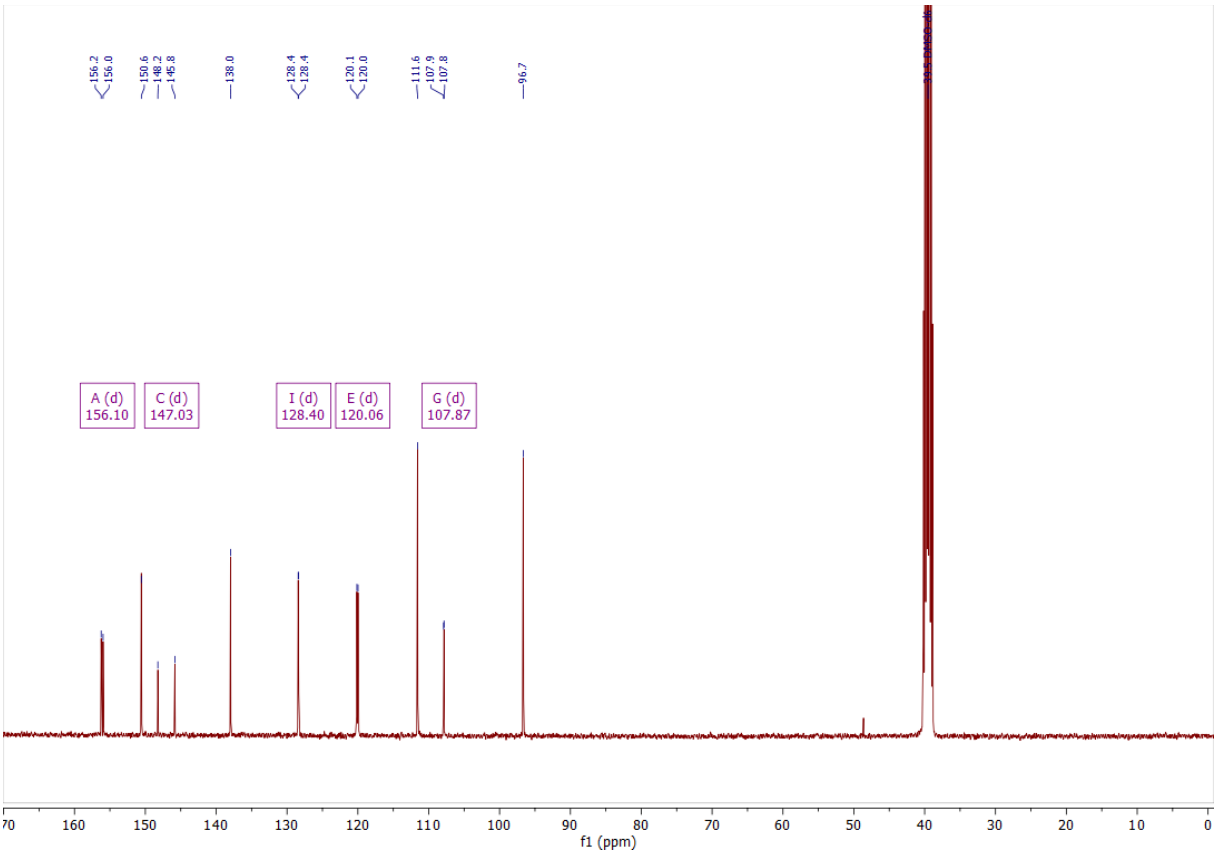

Figure S93 ^{13}C NMR spectrum of **CS^{3F}** (101 MHz, DMSO-d_6).

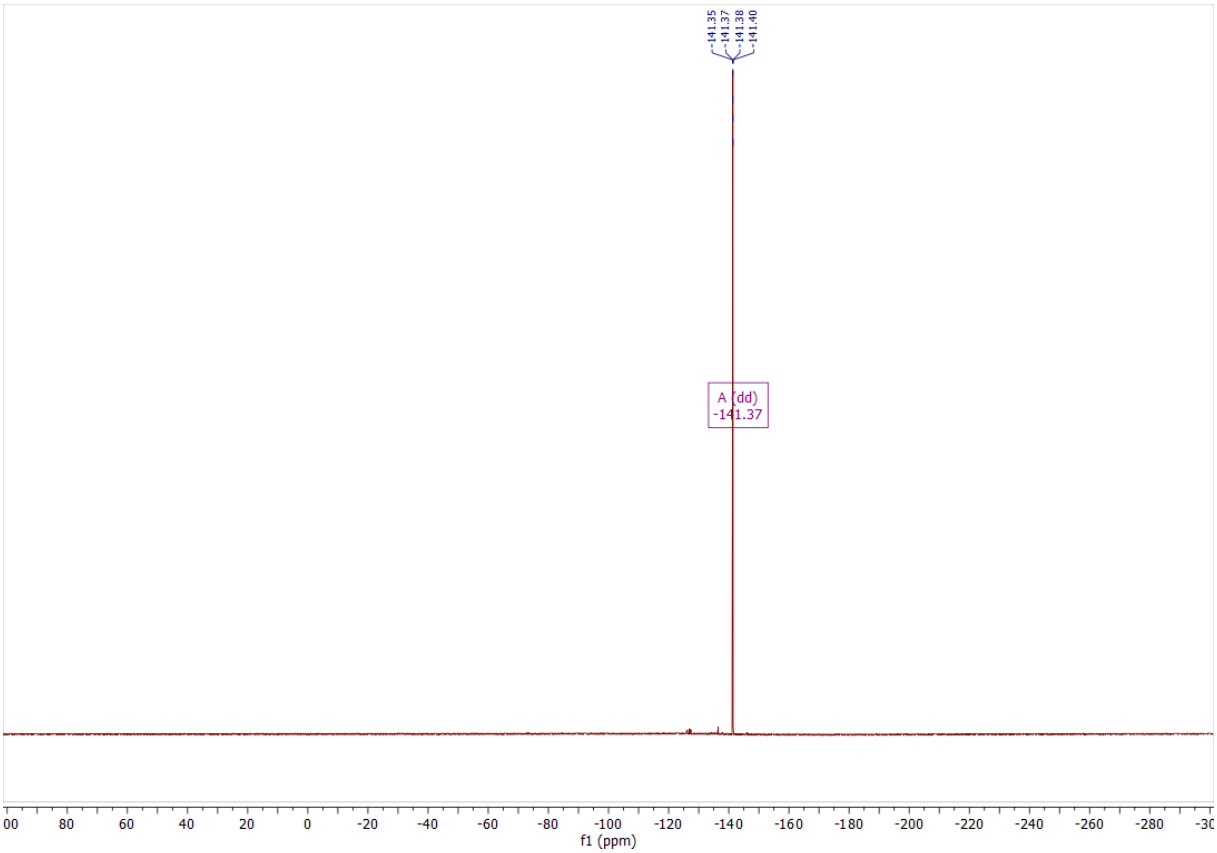

Figure S94 ^{19}F NMR spectrum of **CS^{3F}** (376 MHz, DMSO-d_6).

CS^{5F}

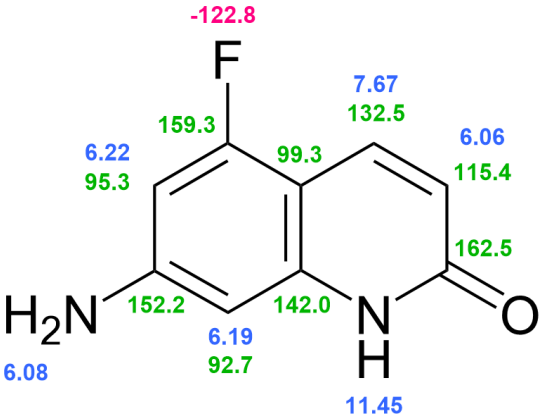

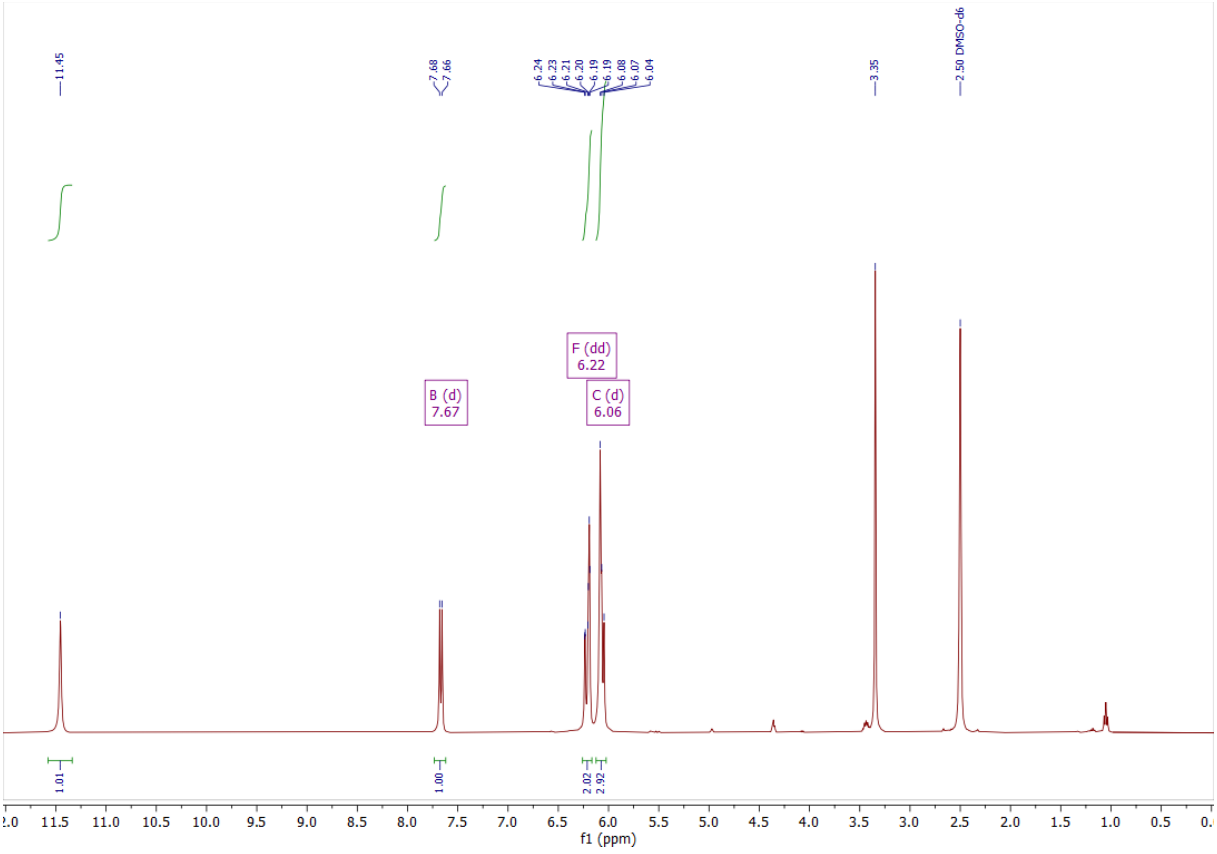

Figure S95 ^{1}H NMR spectrum of **CS^{5F}** (400 MHz, DMSO-d_6).

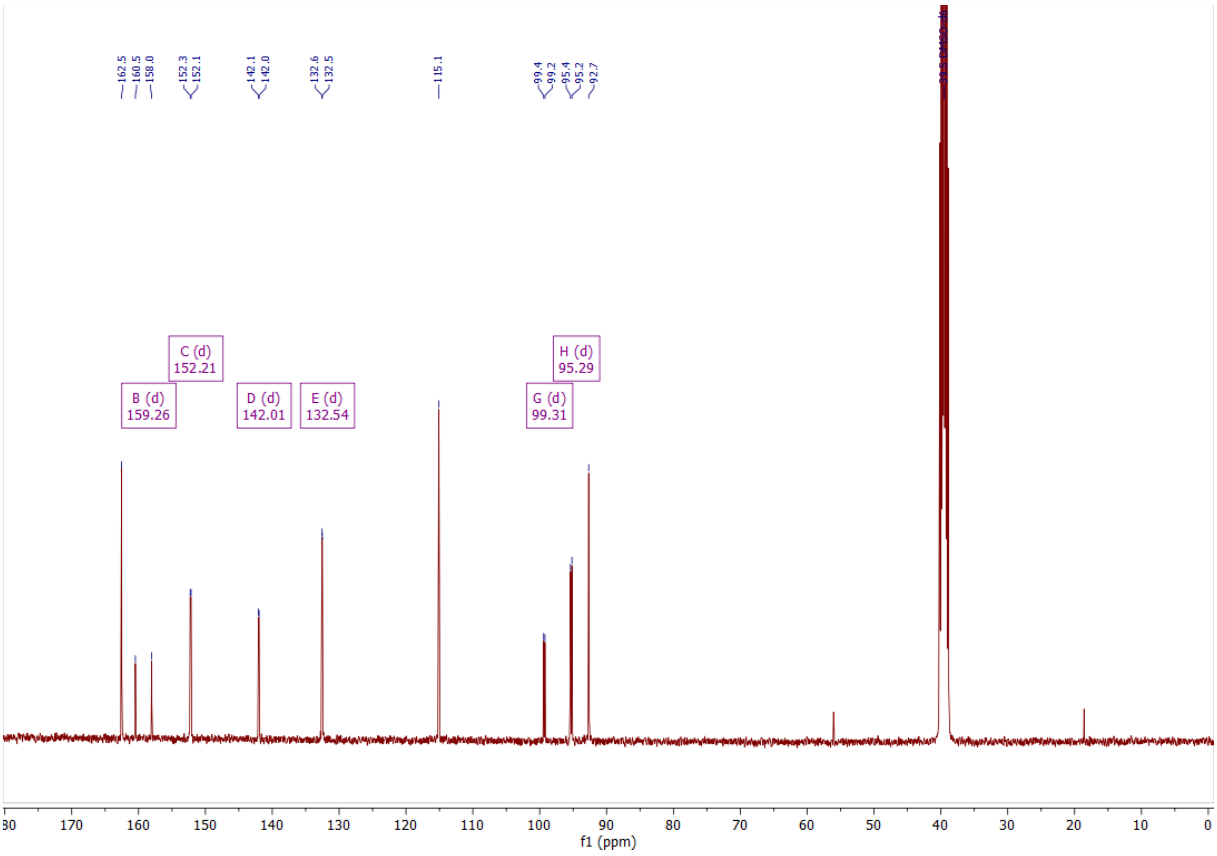

Figure S96 ^{13}C NMR spectrum of **CS^{5F}** (101 MHz, DMSO-d_6).

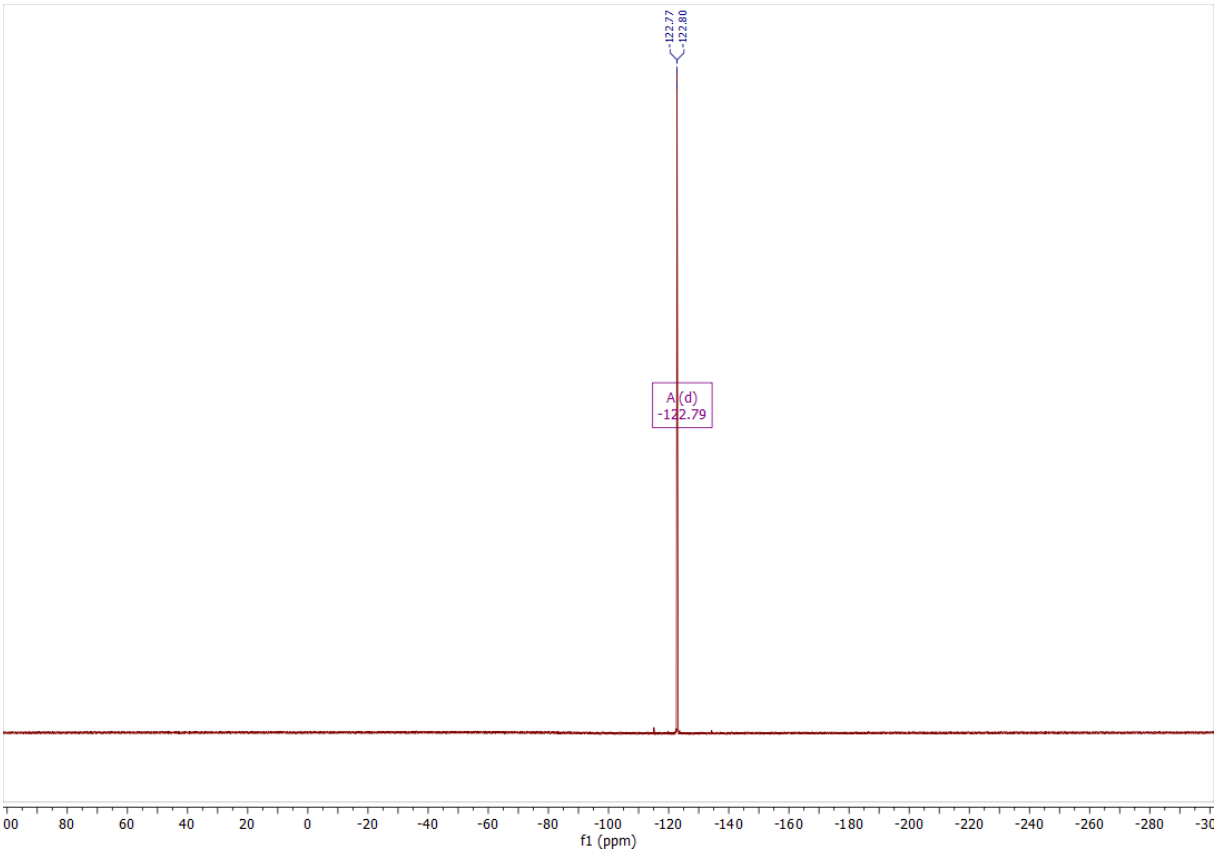

Figure S97 ^{19}F NMR spectrum of **CS^{5F}** (376 MHz, DMSO-d_6).

CS^{6F}

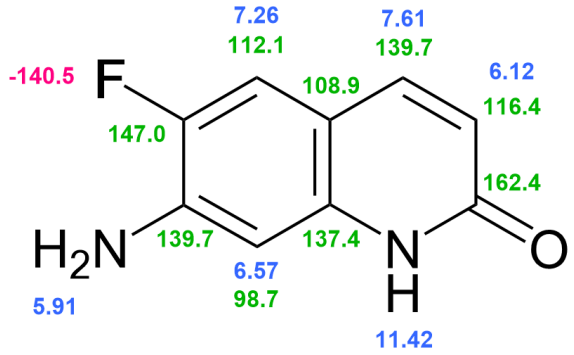

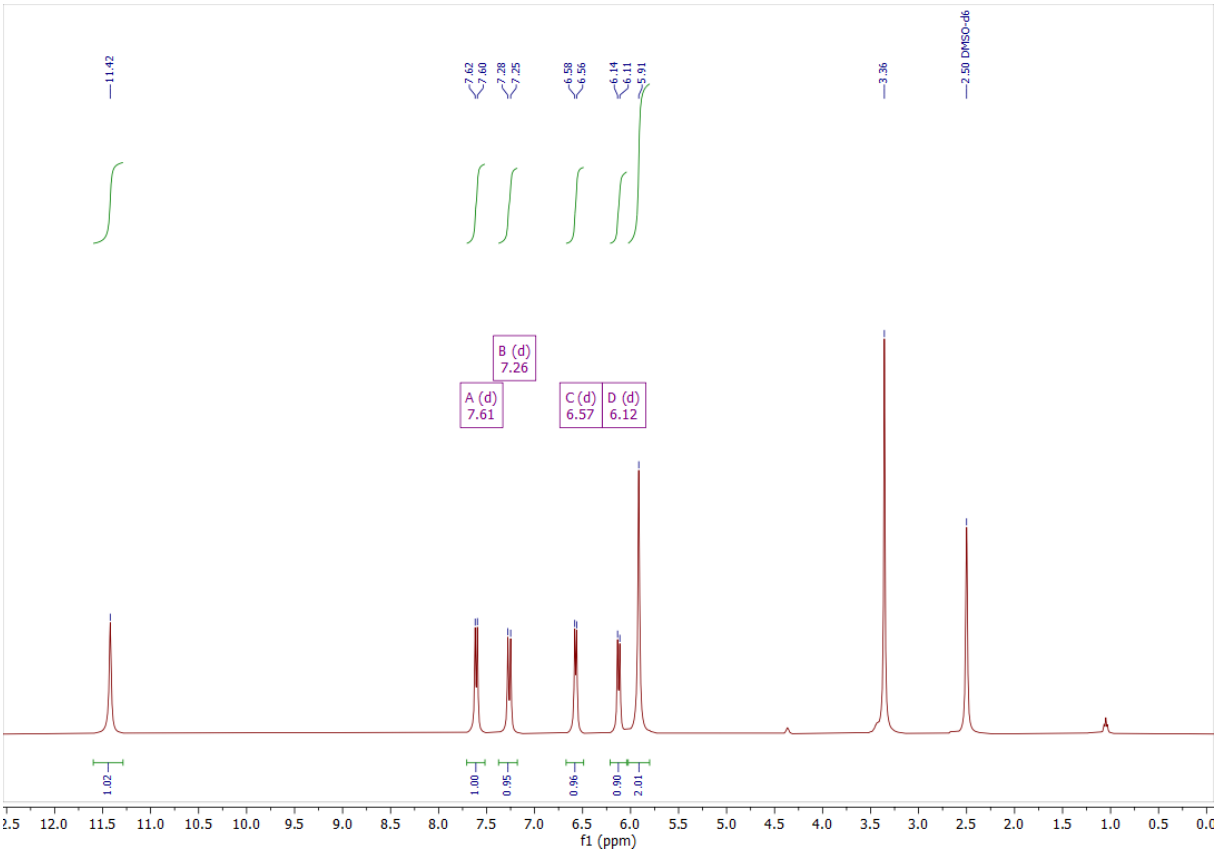

Figure S98 ^{1}H NMR spectrum of **CS^{6F}** (400 MHz, DMSO-d_6).

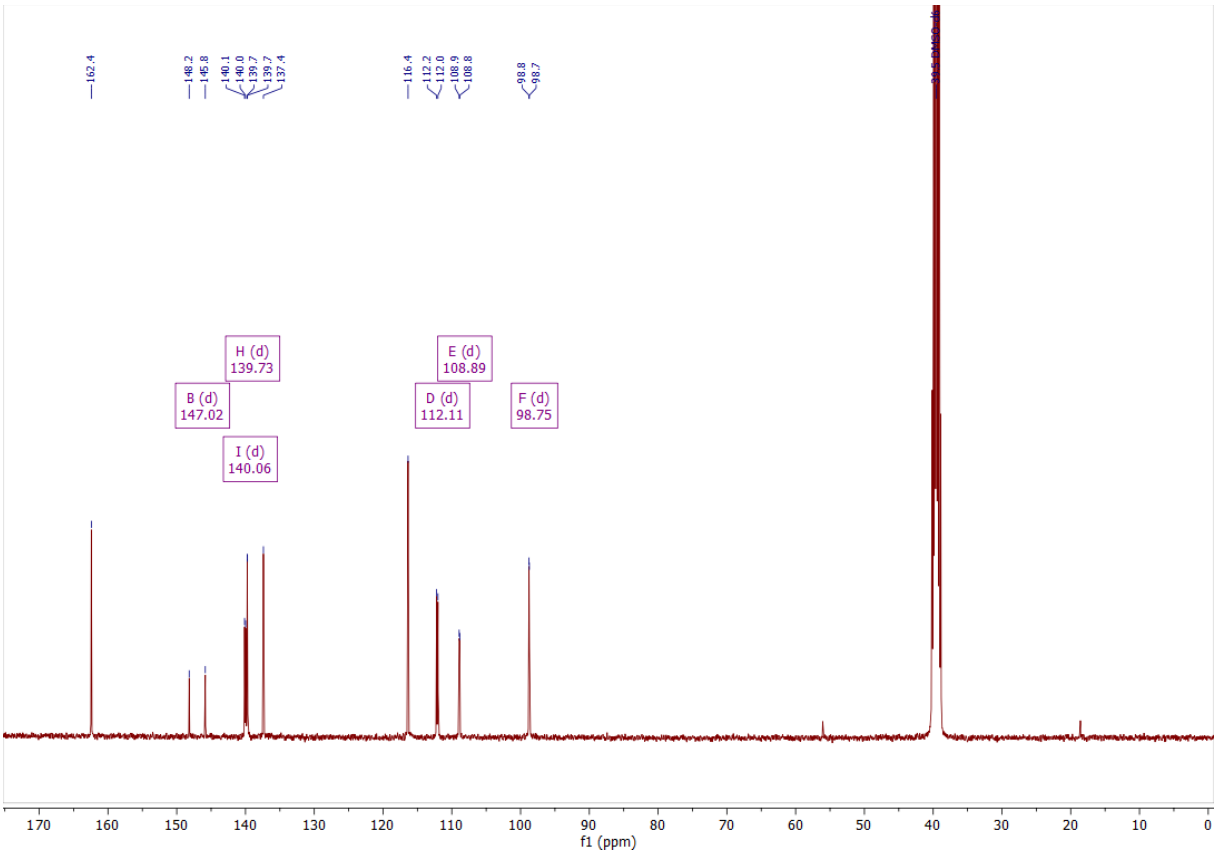

Figure S99 ^{13}C NMR spectrum of **CS^{6F}** (101 MHz, DMSO-d_6).

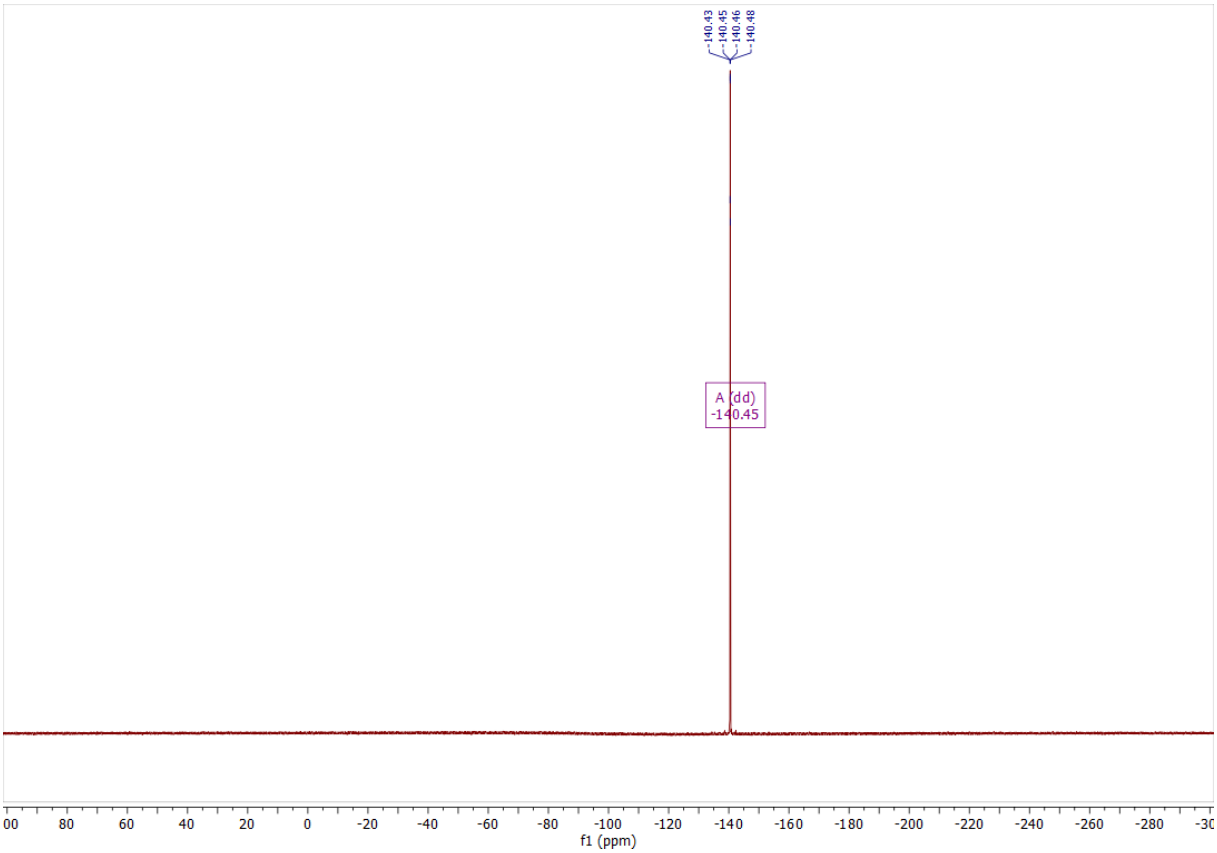

Figure S100 ^{19}F NMR spectrum of **CS^{6F}** (376 MHz, DMSO-d_6).

AcCS

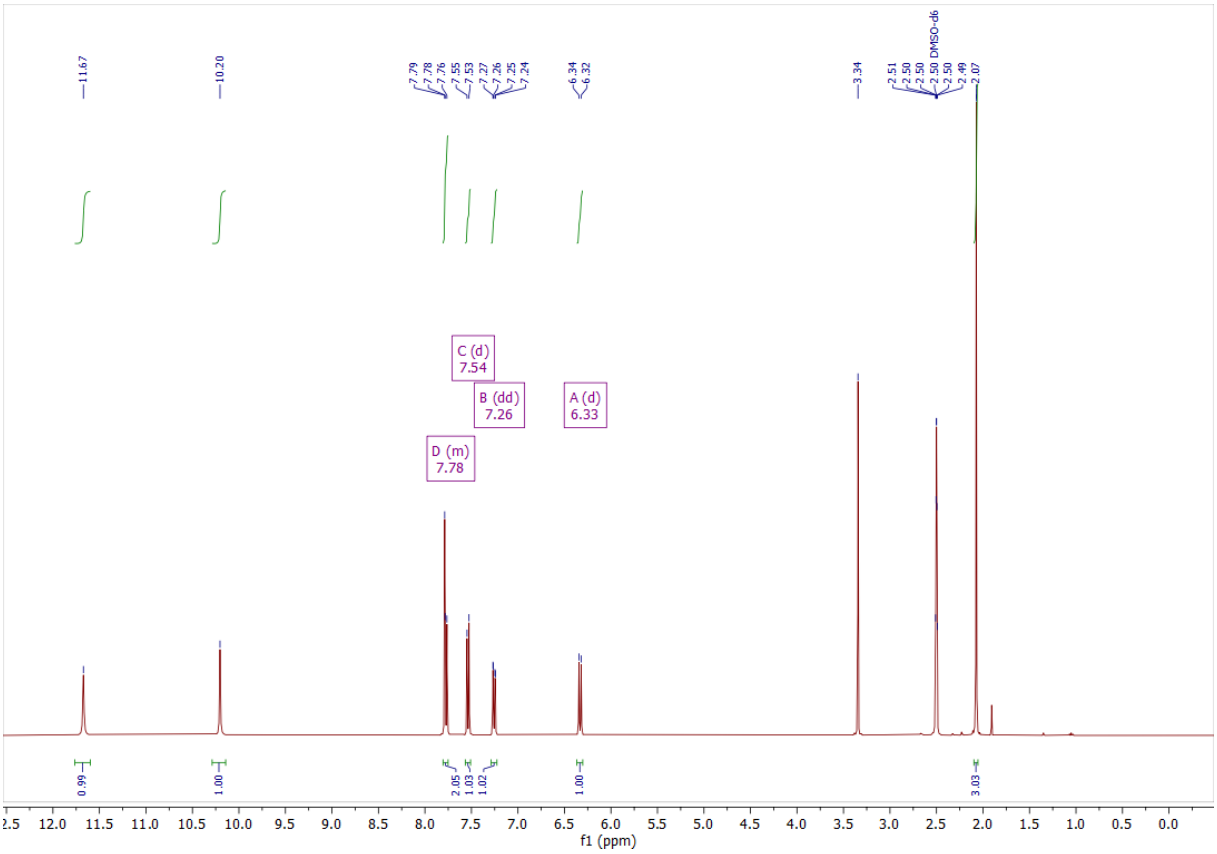

Figure S101 ^{1}H NMR spectrum of **AcCS** (400 MHz, DMSO-d_6).

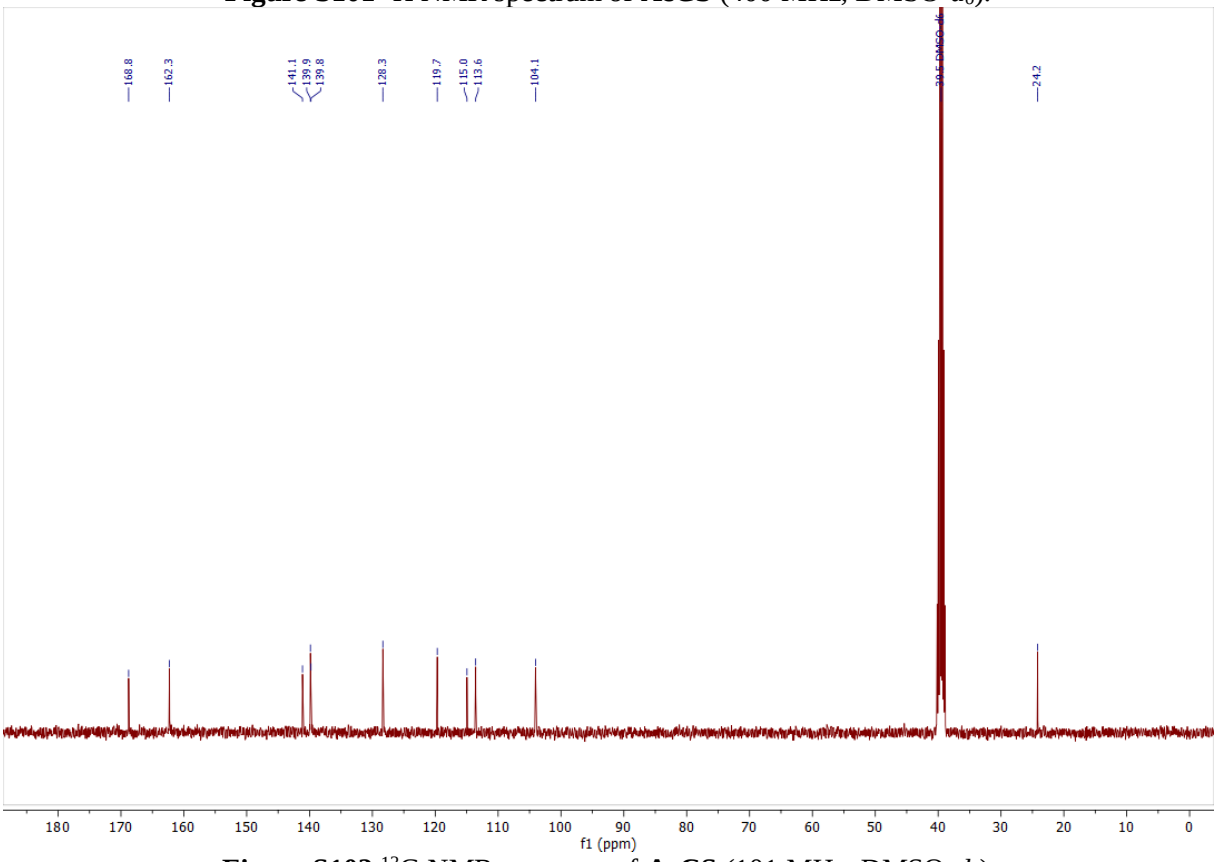

Figure S102 ^{13}C NMR spectrum of **AcCS** (101 MHz, DMSO-d_6).

AcCS^{3F}

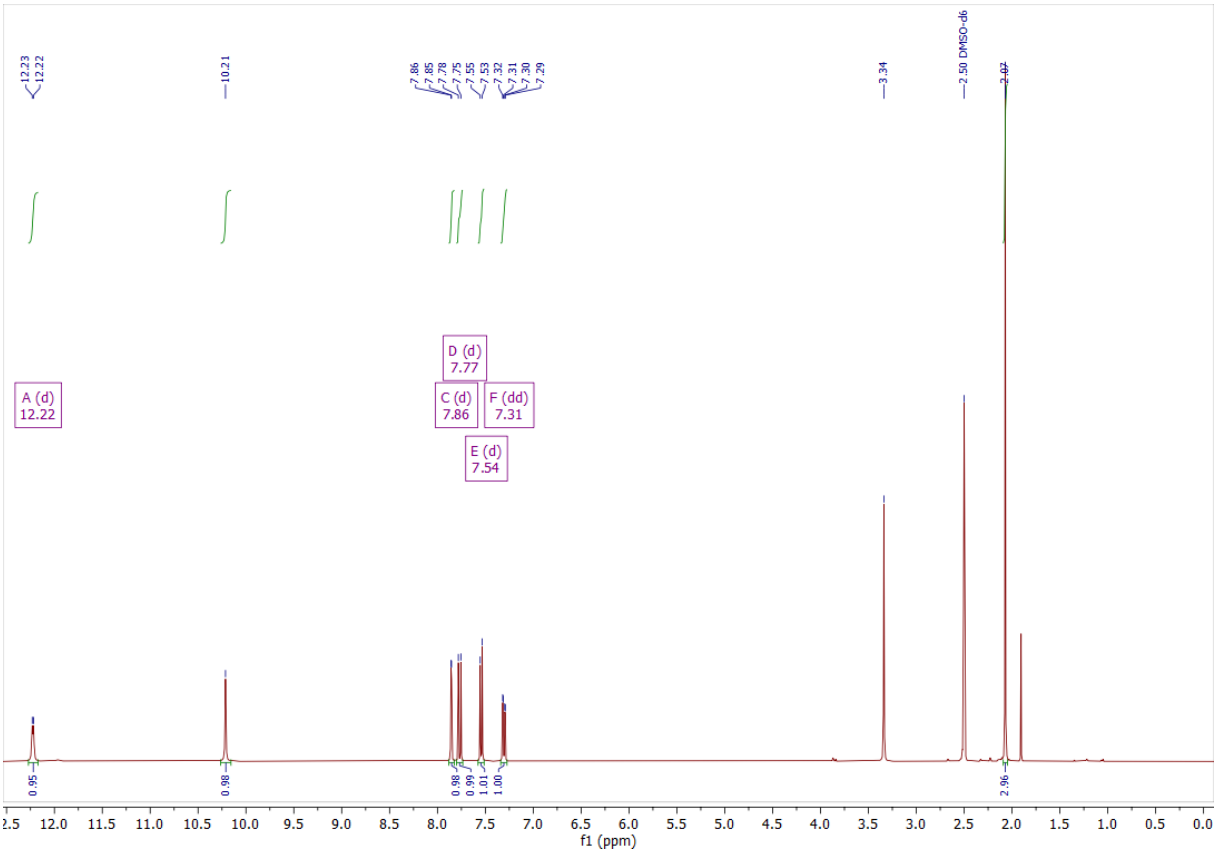

Figure S103 ^{1}H NMR spectrum of **AcCS^{3F}** (400 MHz, DMSO-d_6).

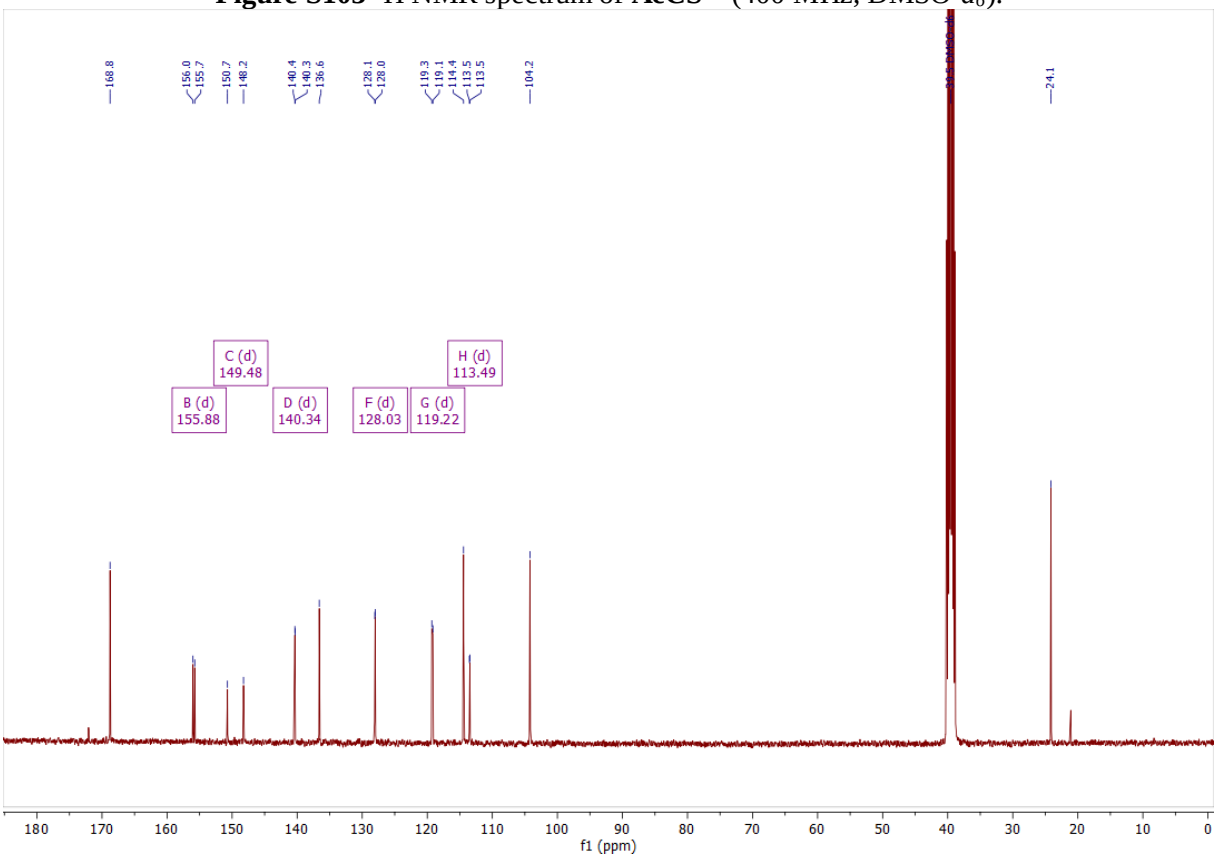

Figure S104 ^{13}C NMR spectrum of **AcCS^{3F}** (101 MHz, DMSO-d_6).

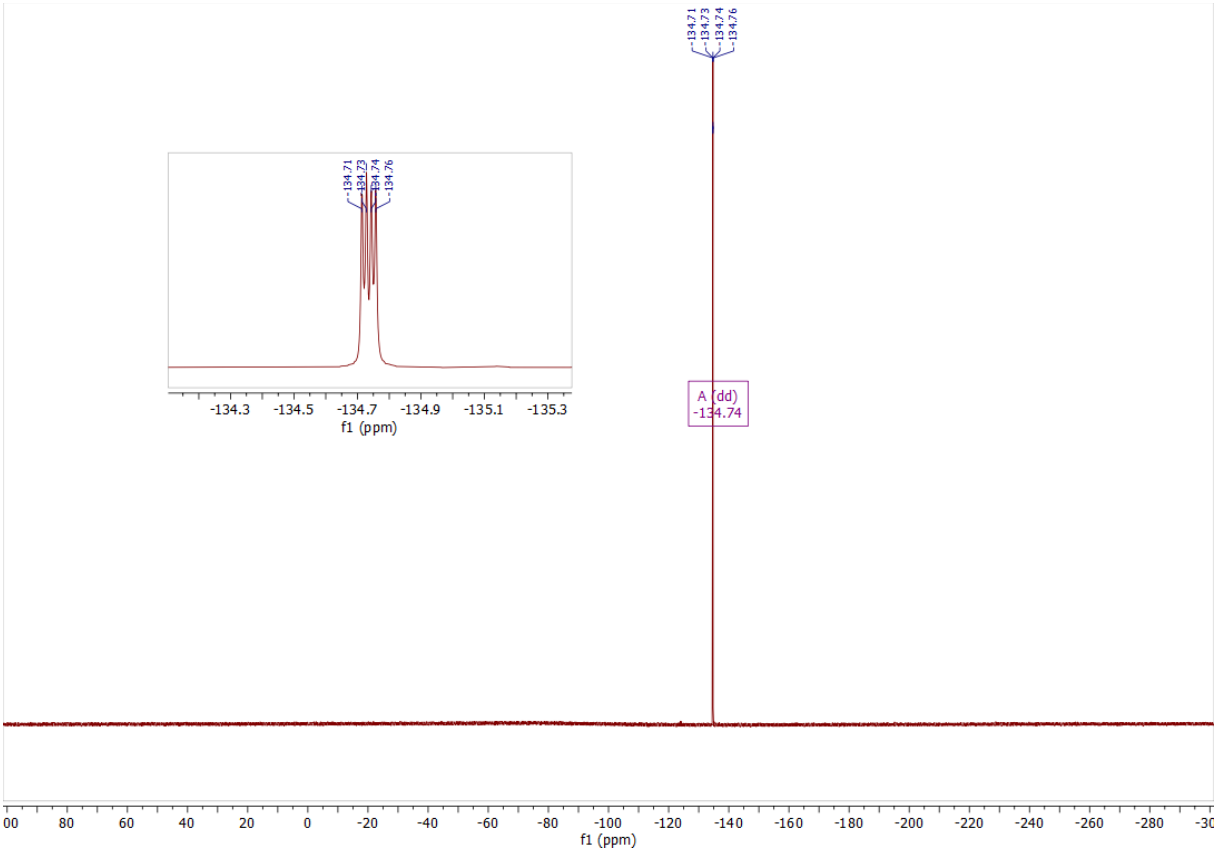

Figure S105 ^{19}F NMR spectrum of **AcCS^{3F}** (376 MHz, DMSO-d_6).

AcCS^{5F}

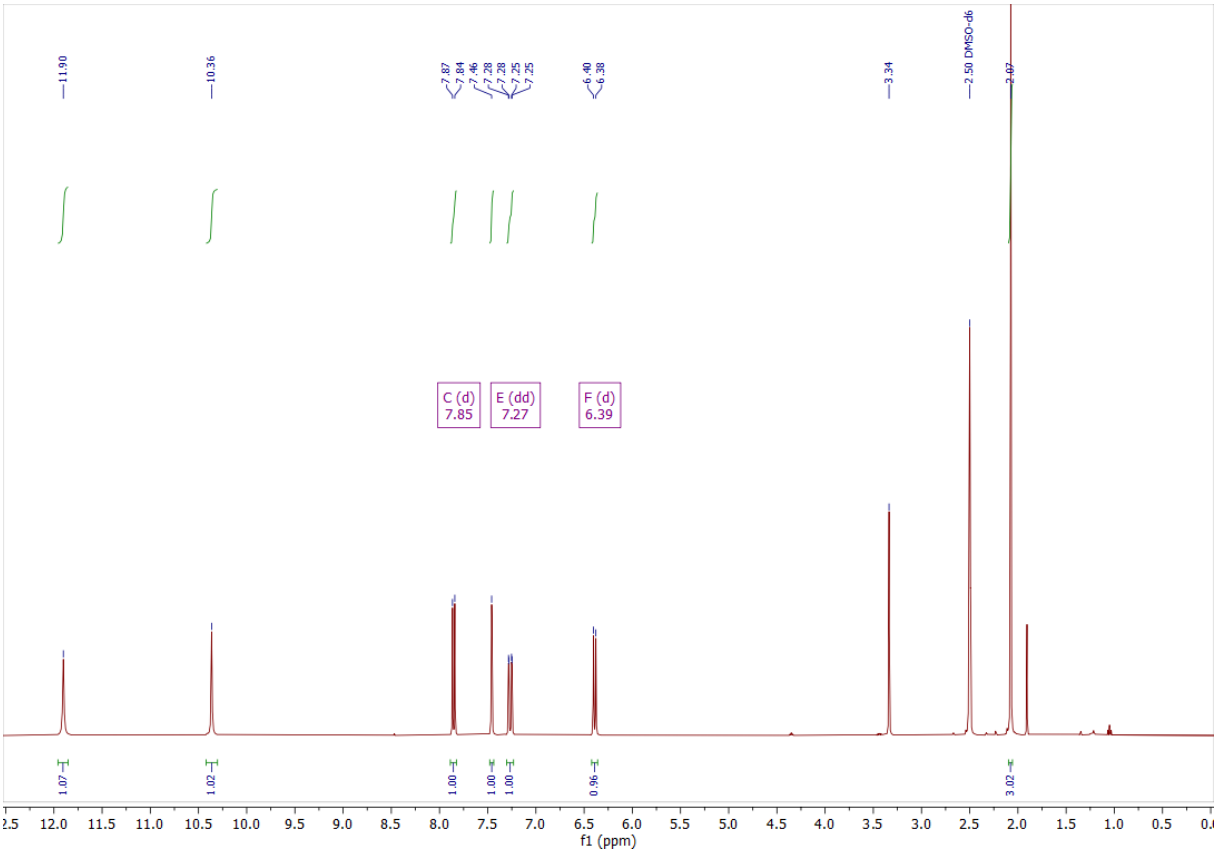

Figure S106 ^{1}H NMR spectrum of **AcCS^{5F}** (400 MHz, DMSO-d_6).

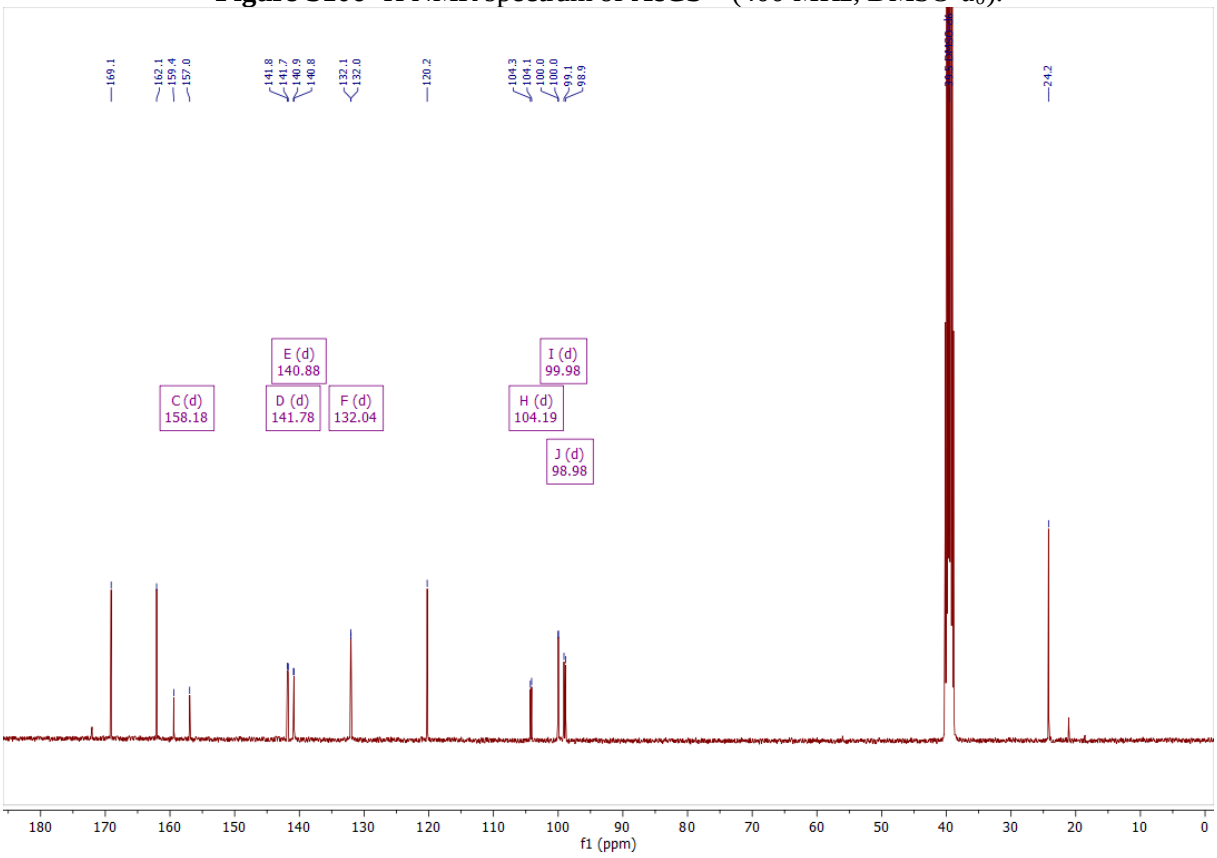

Figure S107 ^{13}C NMR spectrum of **AcCS^{5F}** (101 MHz, DMSO-d_6).

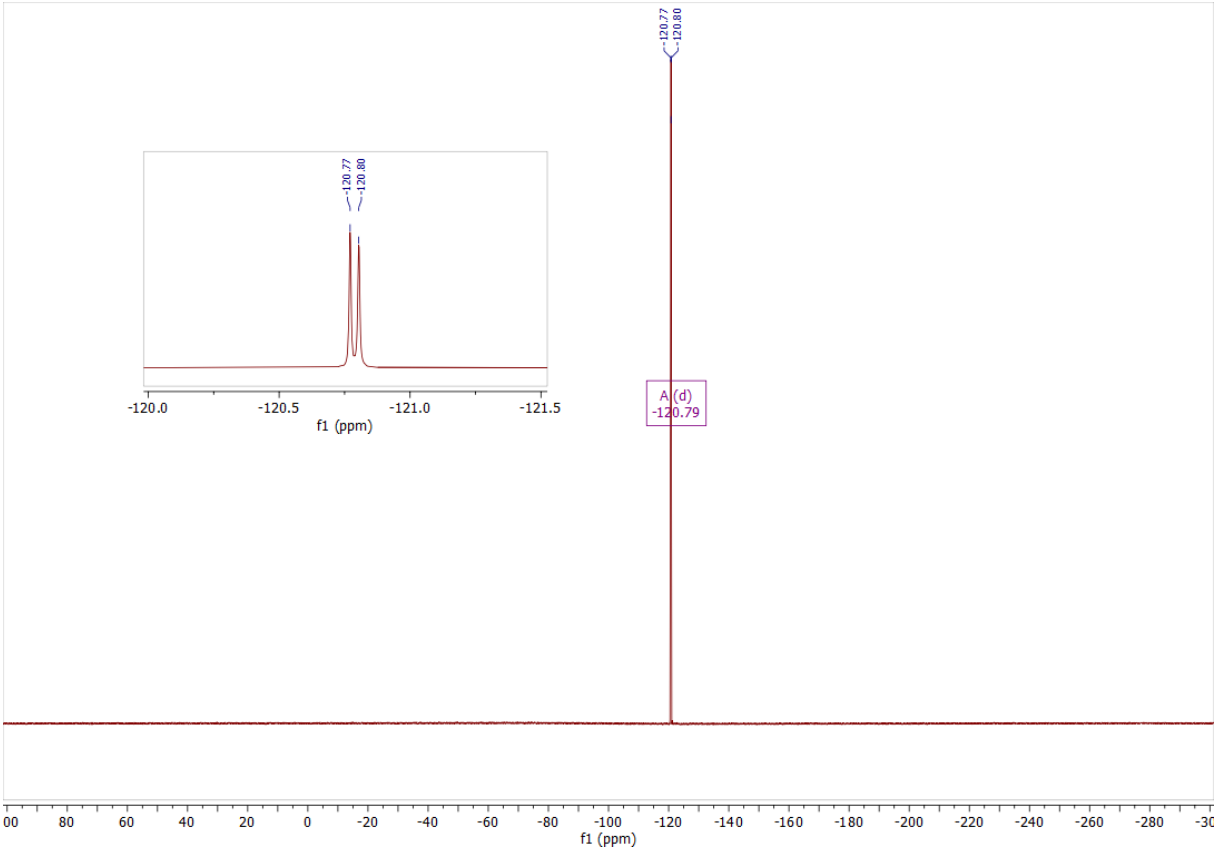

Figure S108 ^{19}F NMR spectrum of **AcCS^{5F}** (376 MHz, DMSO-d_6).

AcCS^{6F}

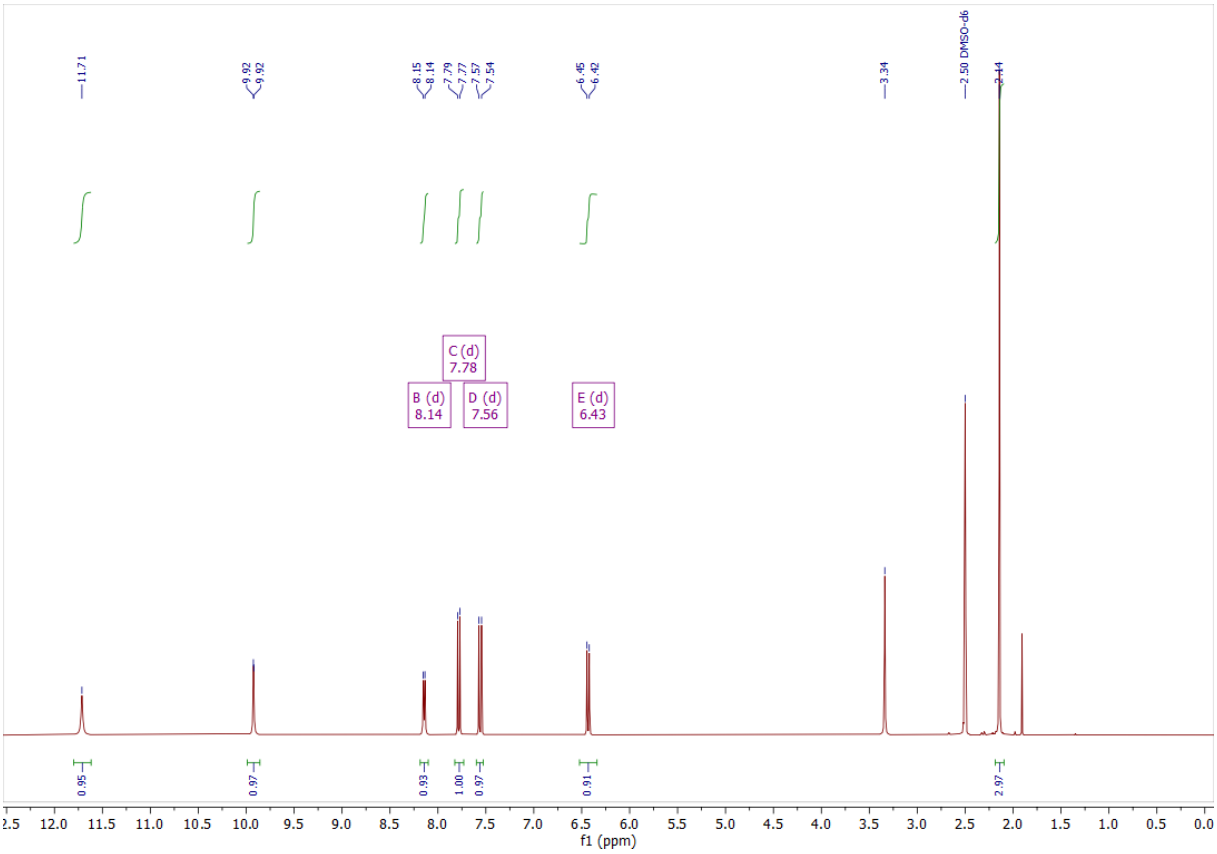

Figure S109 ^{1}H NMR spectrum of **AcCS^{6F}** (400 MHz, DMSO-d_6).

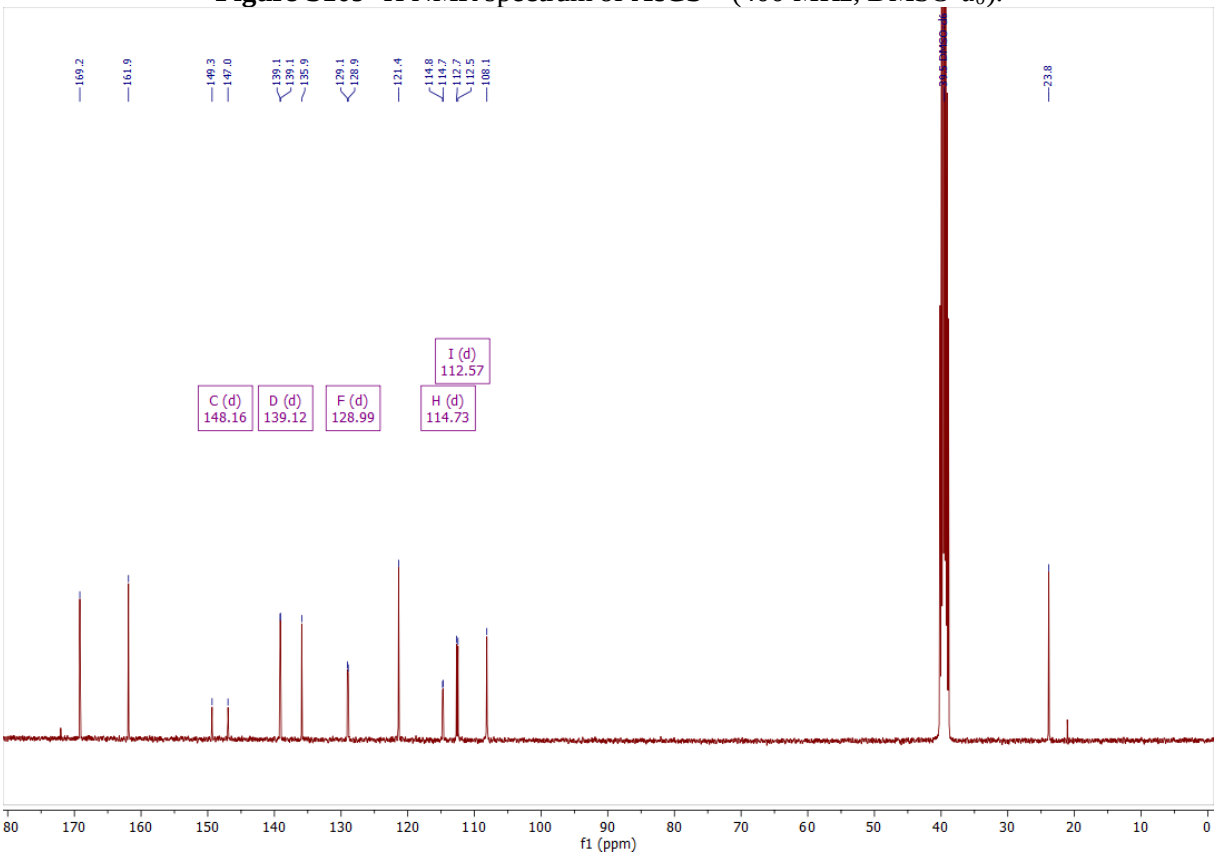

Figure S110 ^{13}C NMR spectrum of **AcCS^{6F}** (101 MHz, DMSO-d_6).

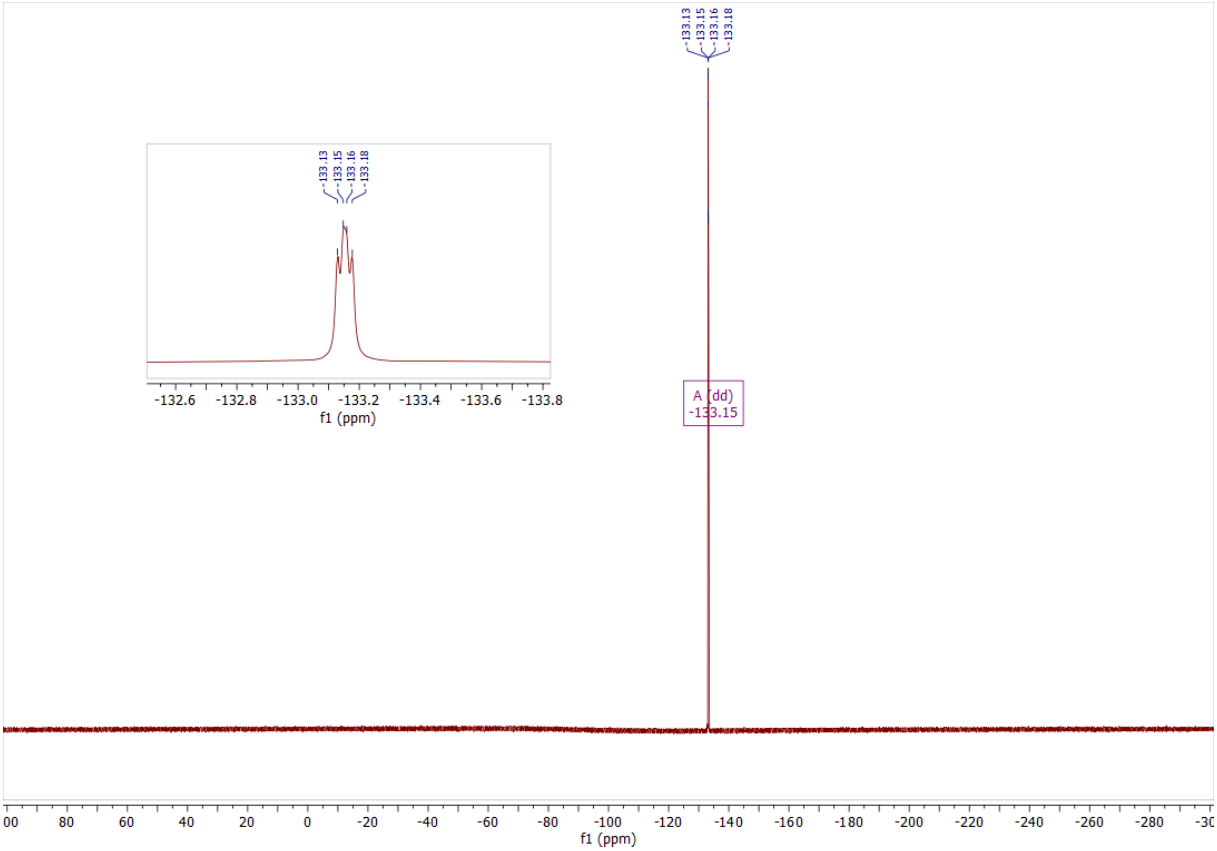

Figure S111 ^{19}F NMR spectrum of **AcCS^{6F}** (376 MHz, DMSO-d_6).

6^{CS}

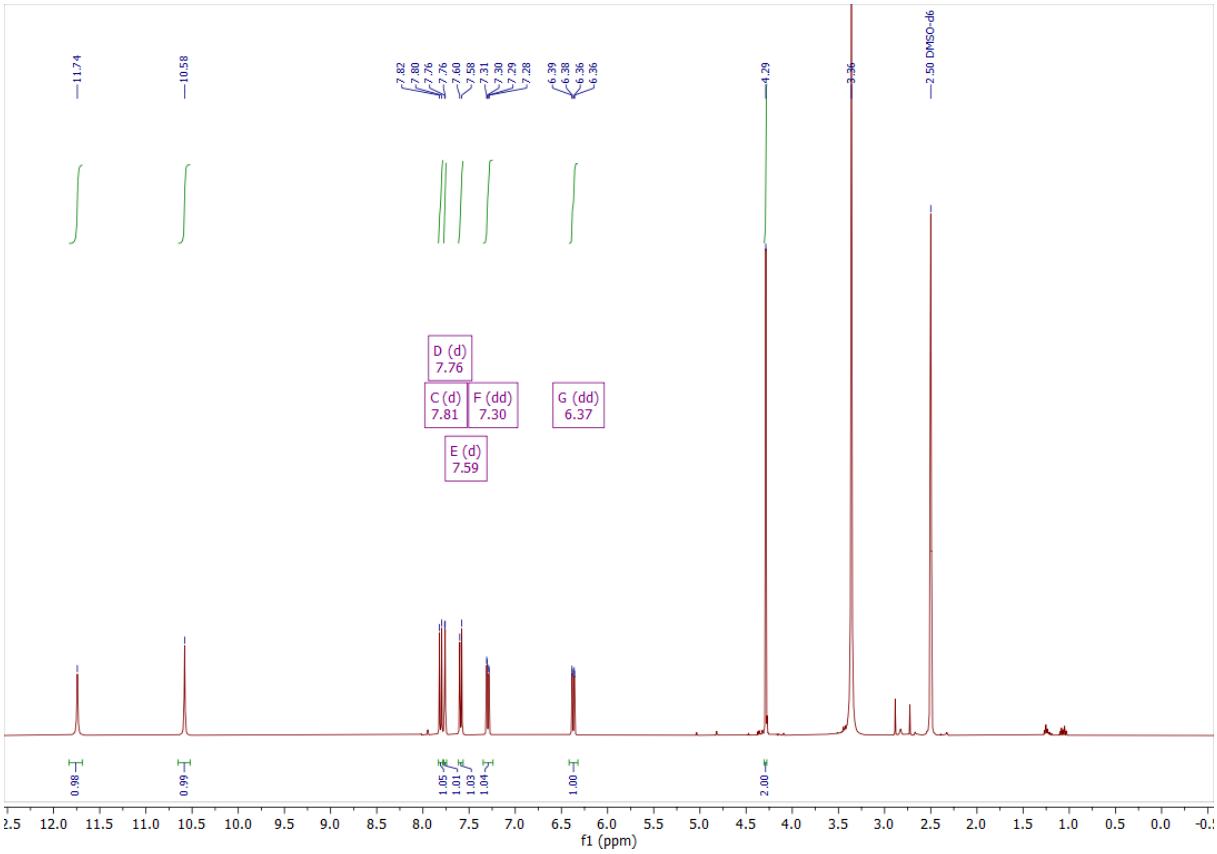

Figure S112 ^{1}H NMR spectrum of **6**^{CS} (400 MHz, DMSO-d_6).

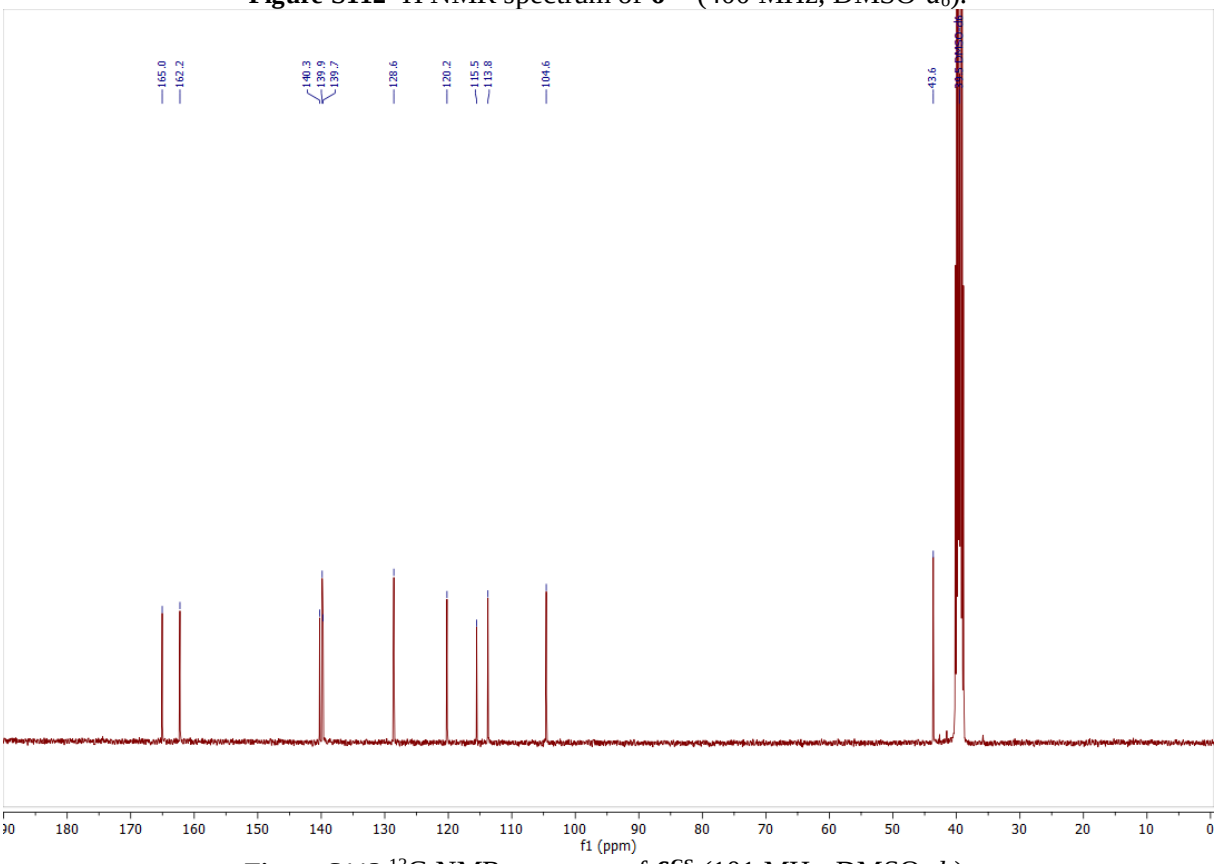

Figure S113 ^{13}C NMR spectrum of **6**^{CS} (101 MHz, DMSO-d_6).

6^{3F}

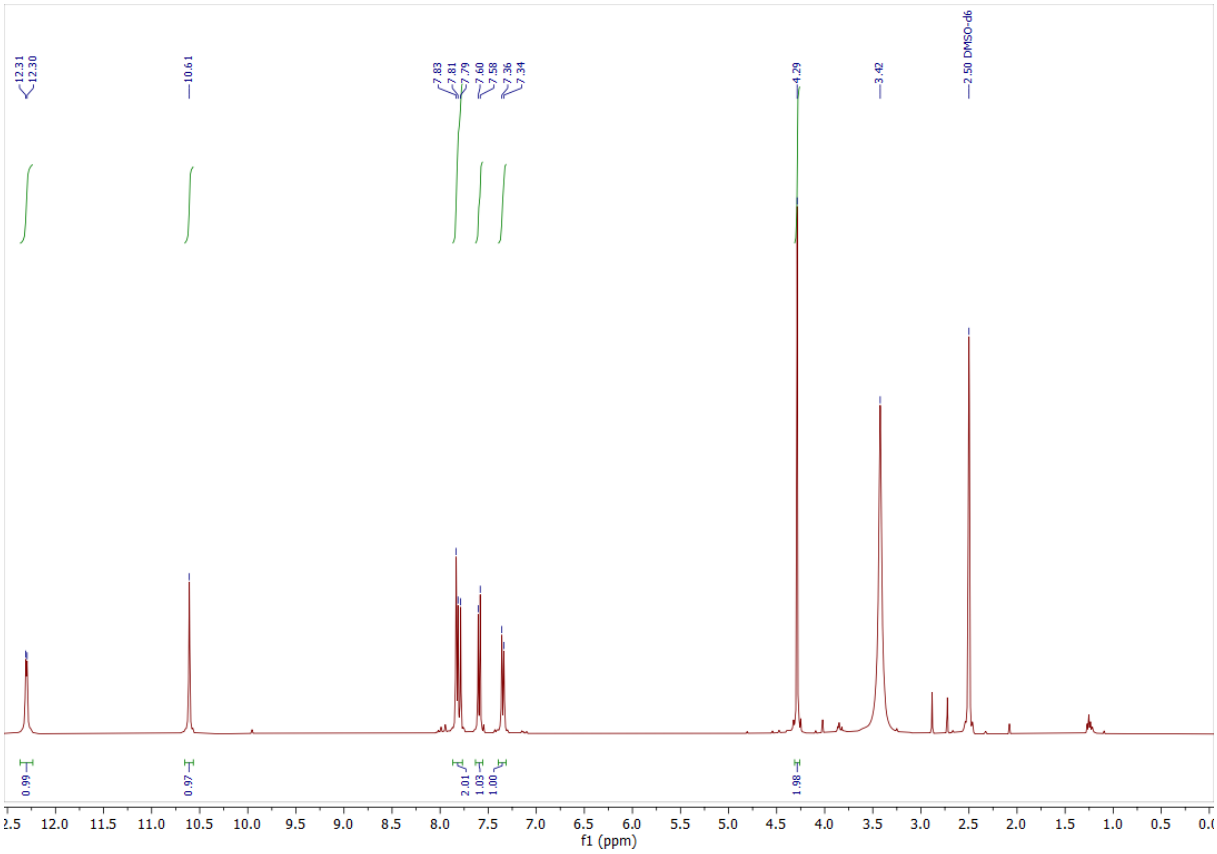

Figure S114 ^{1}H NMR spectrum of **6^{3F}** (400 MHz, DMSO-d_6).

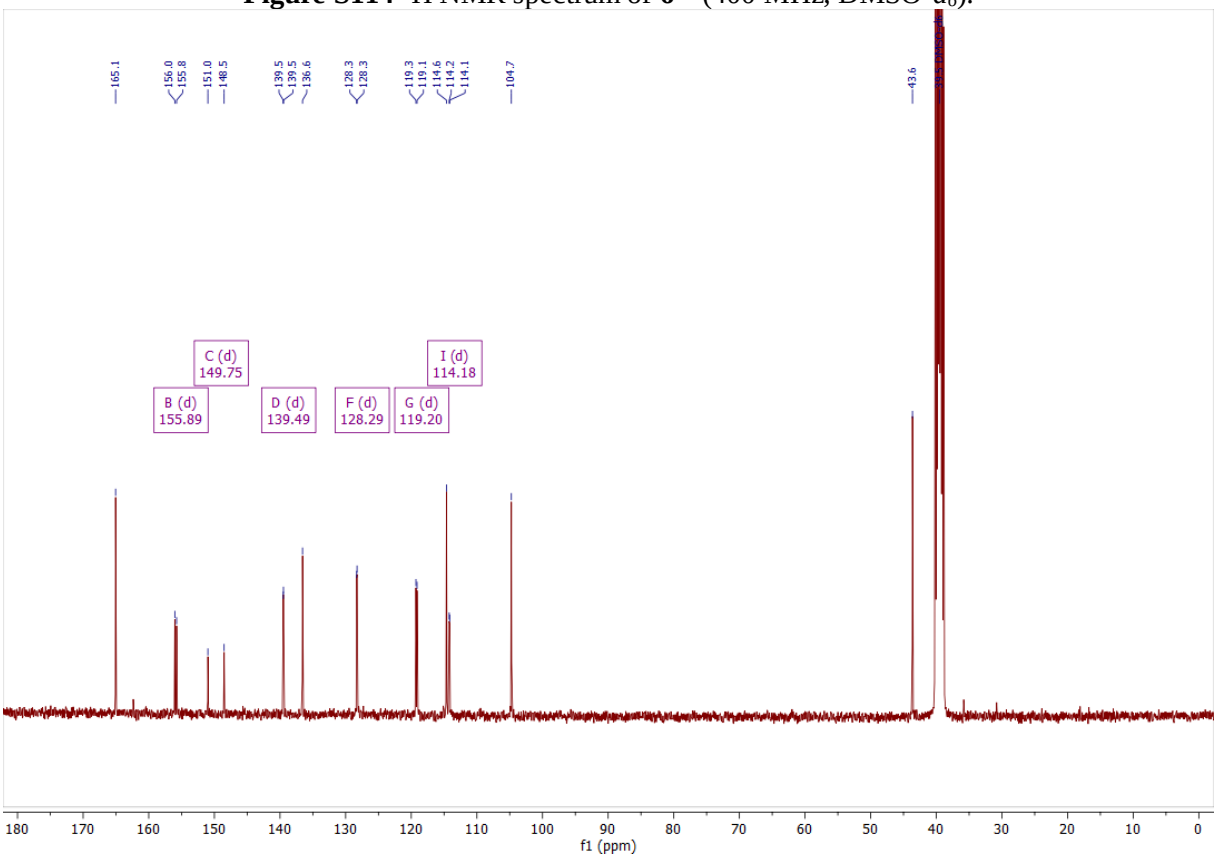

Figure S115 ^{13}C NMR spectrum of **6^{3F}** (101 MHz, DMSO-d_6).

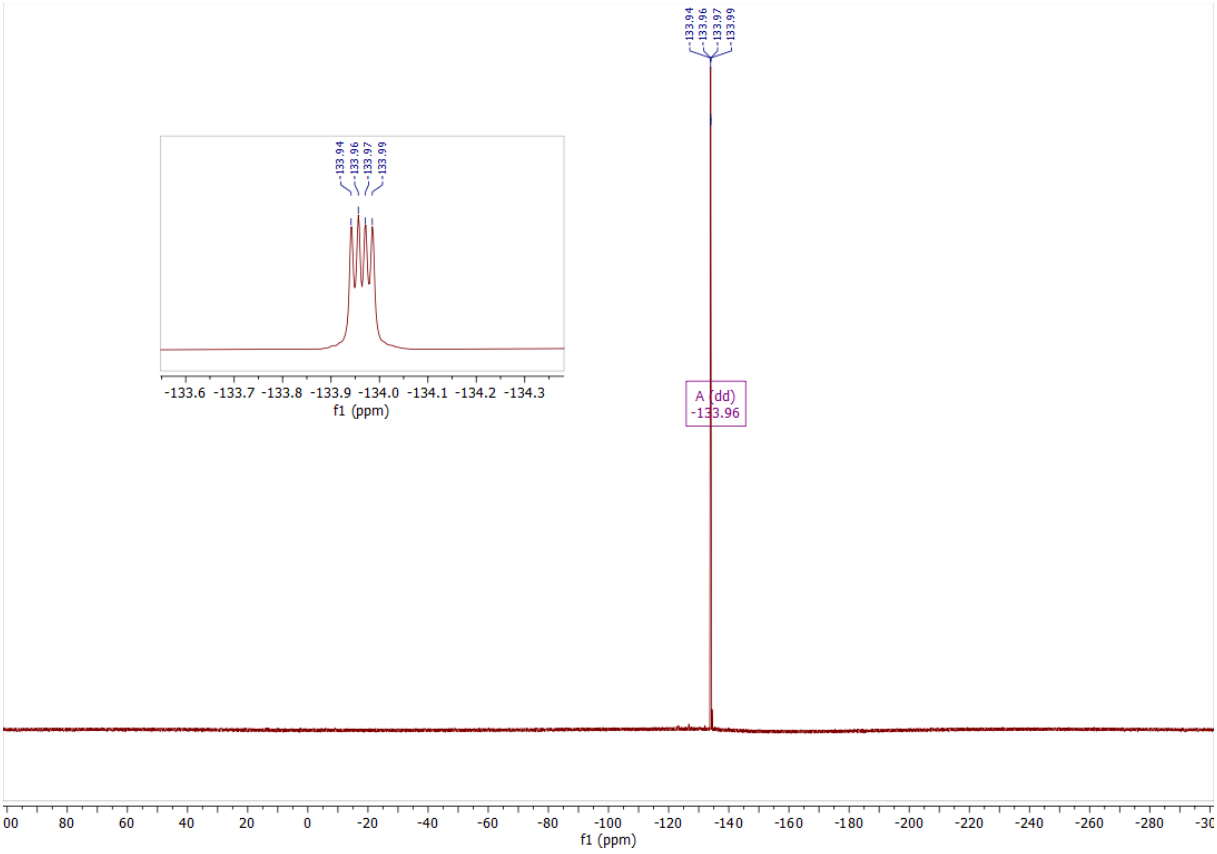

Figure S116 ^{19}F NMR spectrum of **6^{3F}** (376 MHz, DMSO-d_6).

6^{5F}

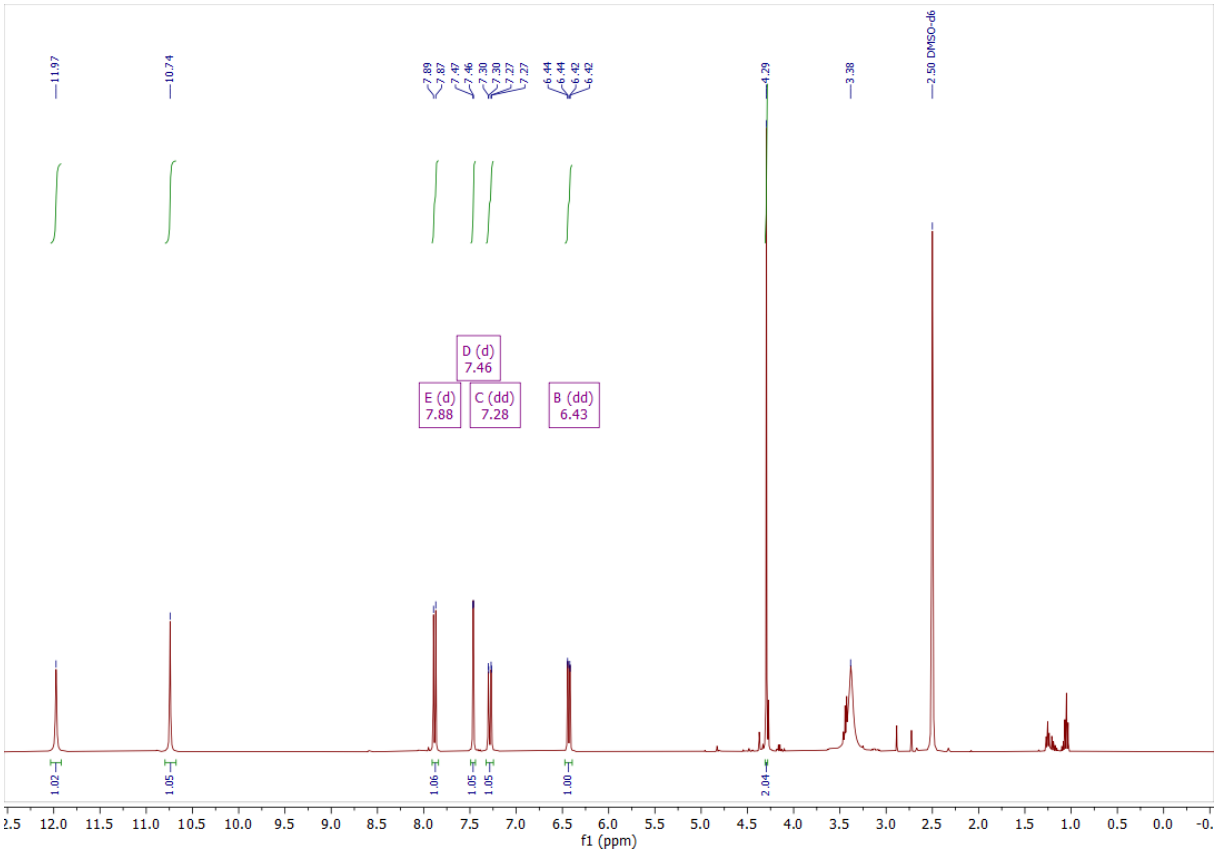

Figure S117 ^{1}H NMR spectrum of **6^{5F}** (400 MHz, DMSO-d_6).

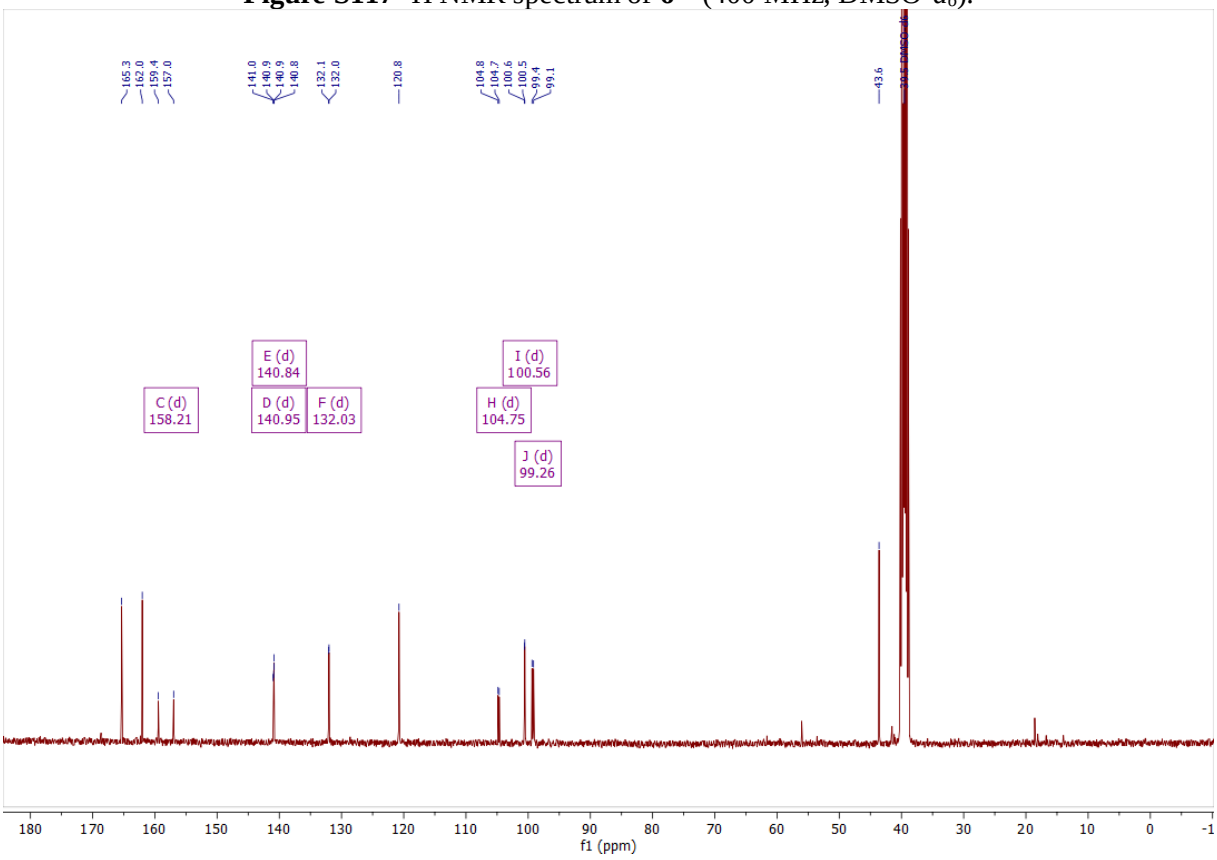

Figure S118 ^{13}C NMR spectrum of **6^{5F}** (101 MHz, DMSO-d_6).

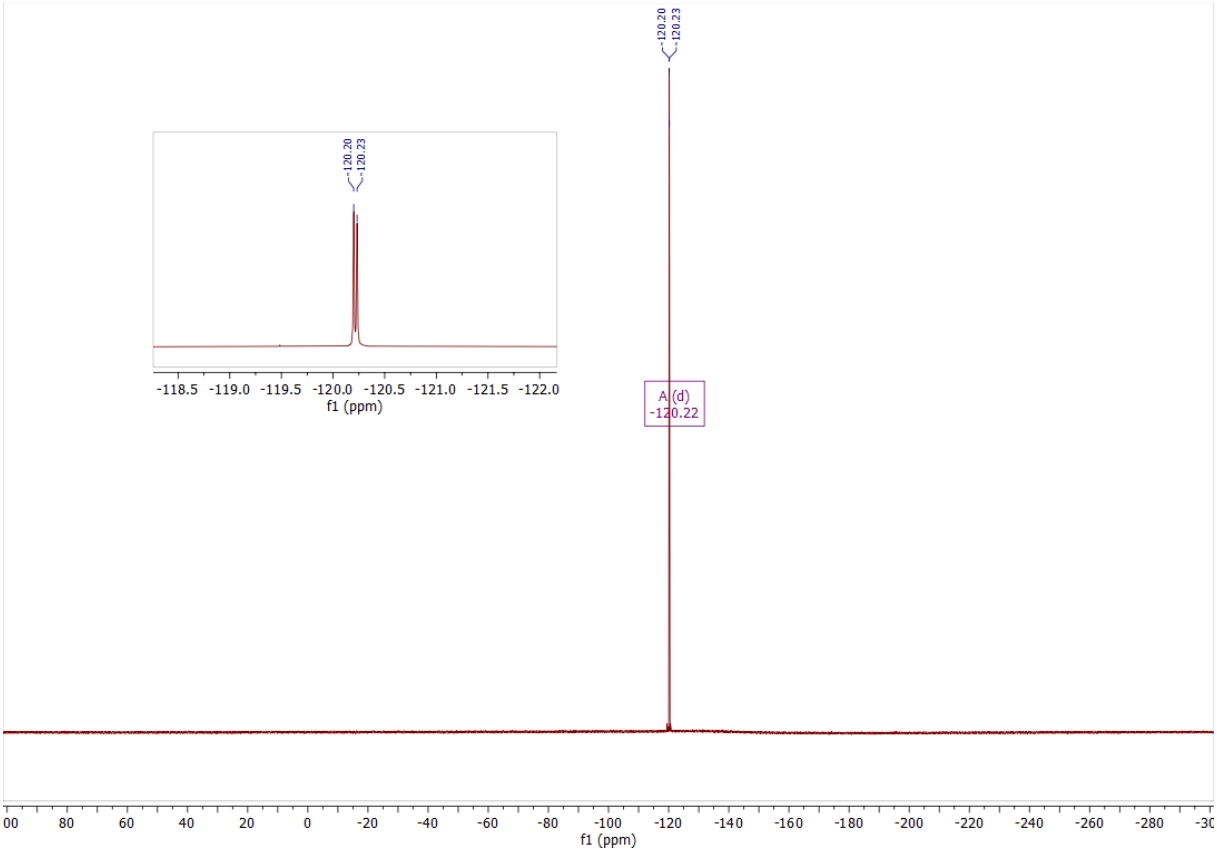

Figure S119 ^{19}F NMR spectrum of **6^{5F}** (376 MHz, DMSO-d_6).

6^{6F}

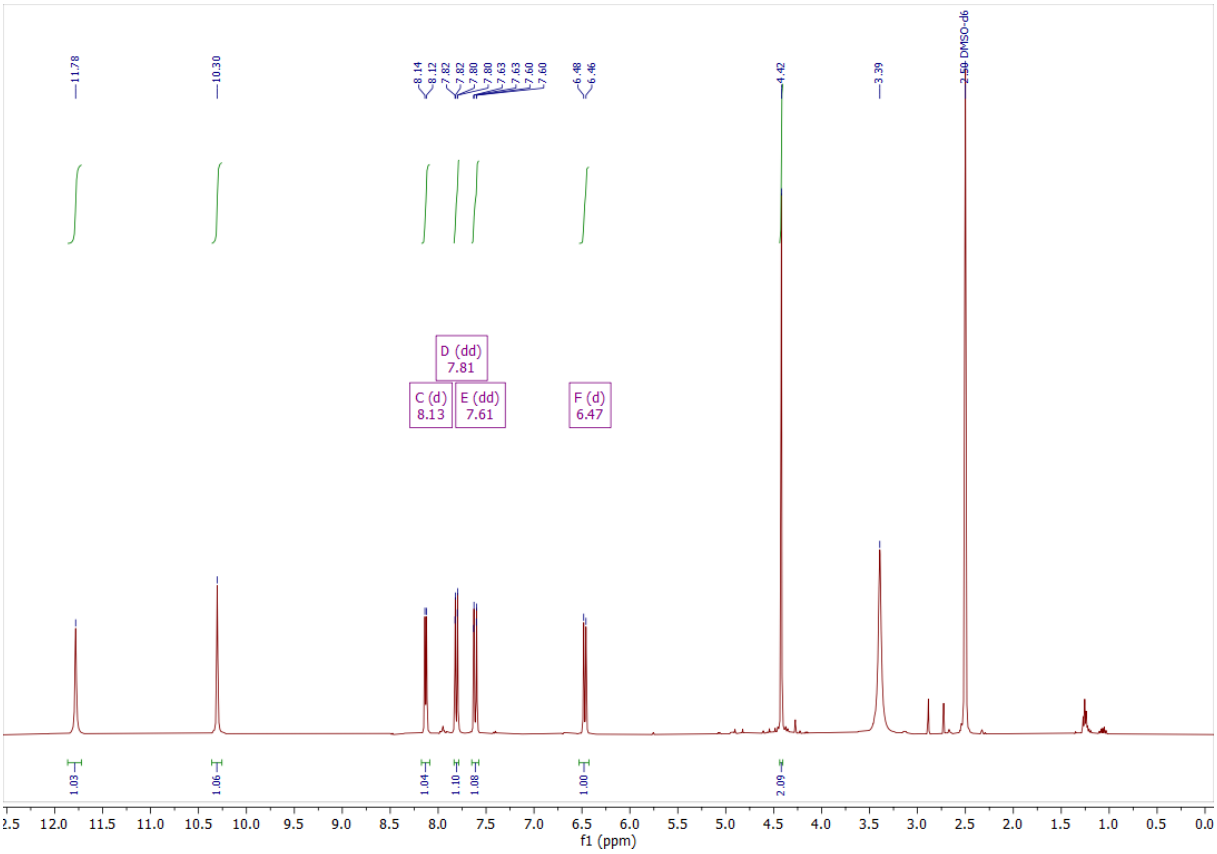

Figure S120 ^{1}H NMR spectrum of **6^{6F}** (400 MHz, DMSO-d_6).

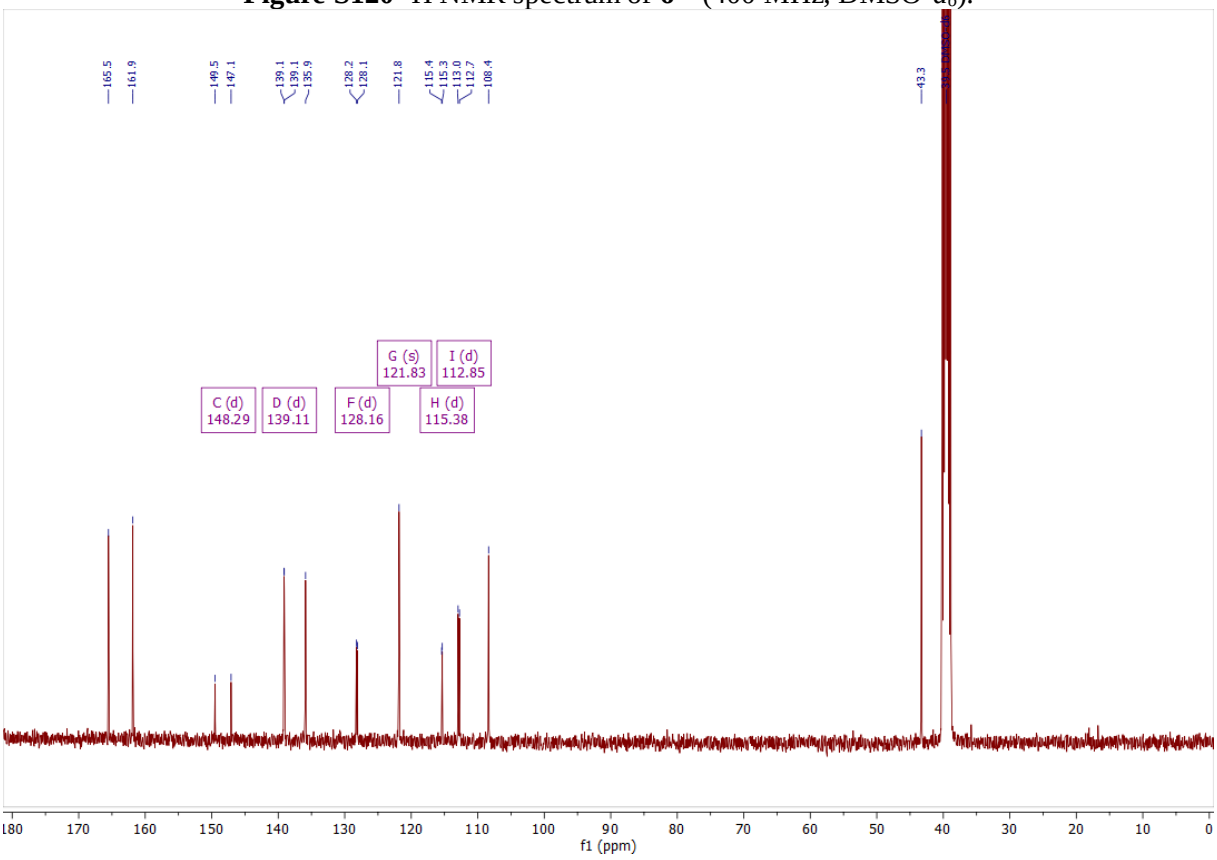

Figure S121 ^{13}C NMR spectrum of **6^{6F}** (101 MHz, DMSO-d_6).

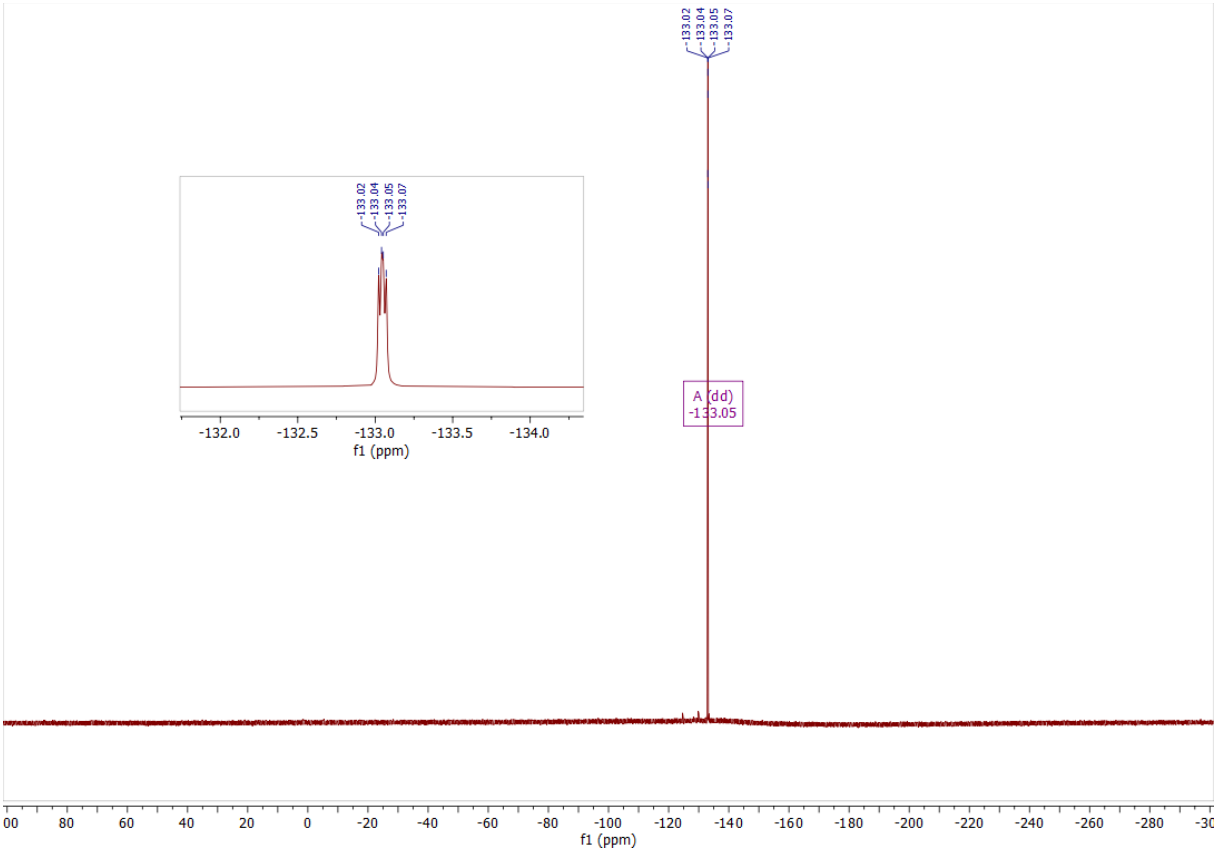

Figure S122 ^{19}F NMR spectrum of **6^{6F}** (376 MHz, DMSO-d_6).

7^{CS}

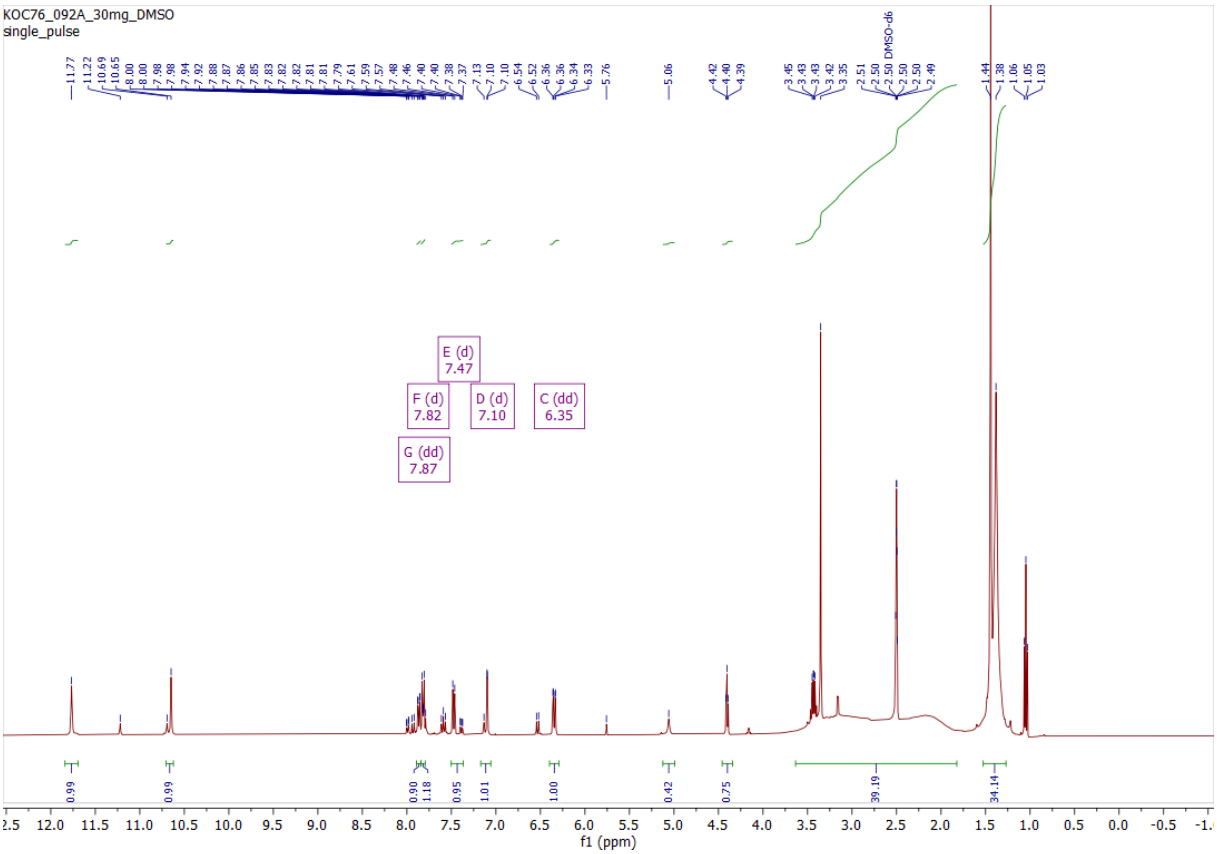

Figure S123 ^{1}H NMR spectrum of **7**^{CS} (400 MHz, DMSO-d_6).

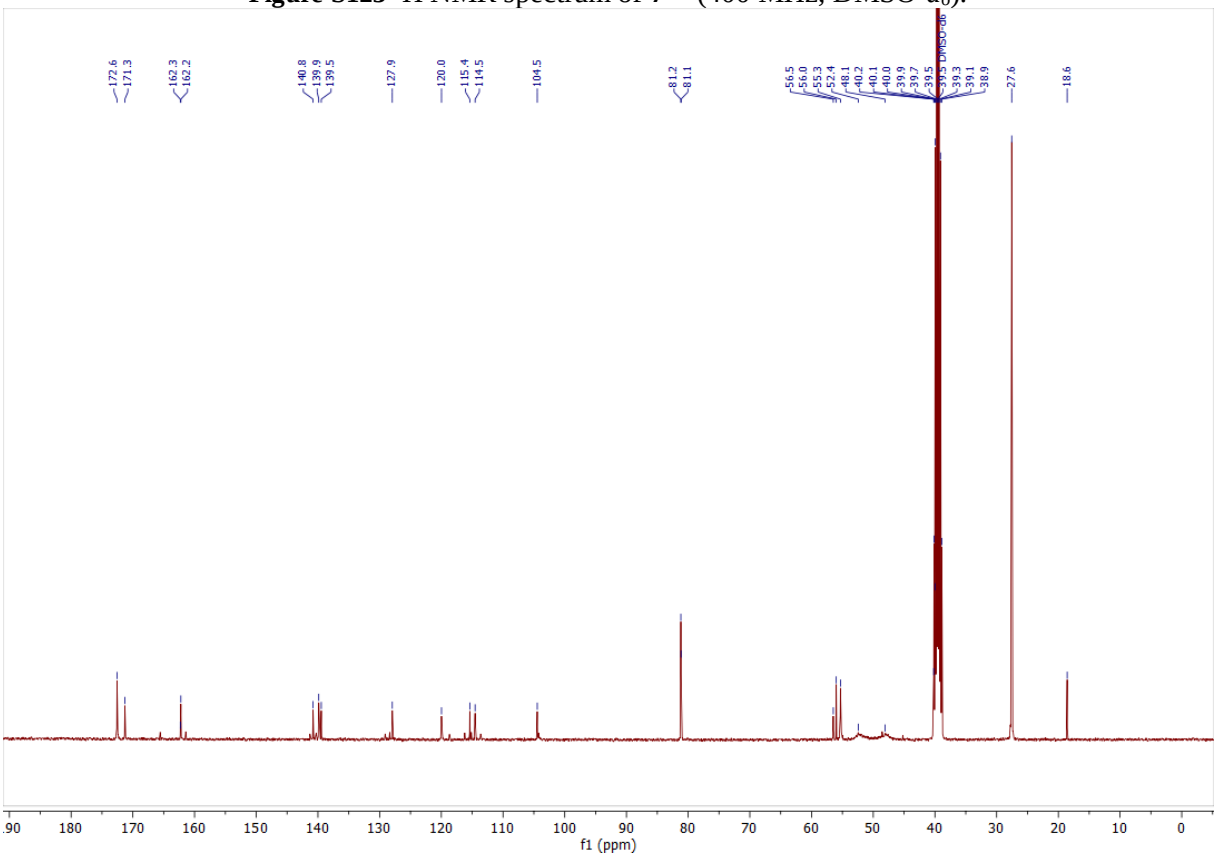

Figure S124 ^{13}C NMR spectrum of **7**^{CS} (101 MHz, DMSO-d_6).

7^{6F}

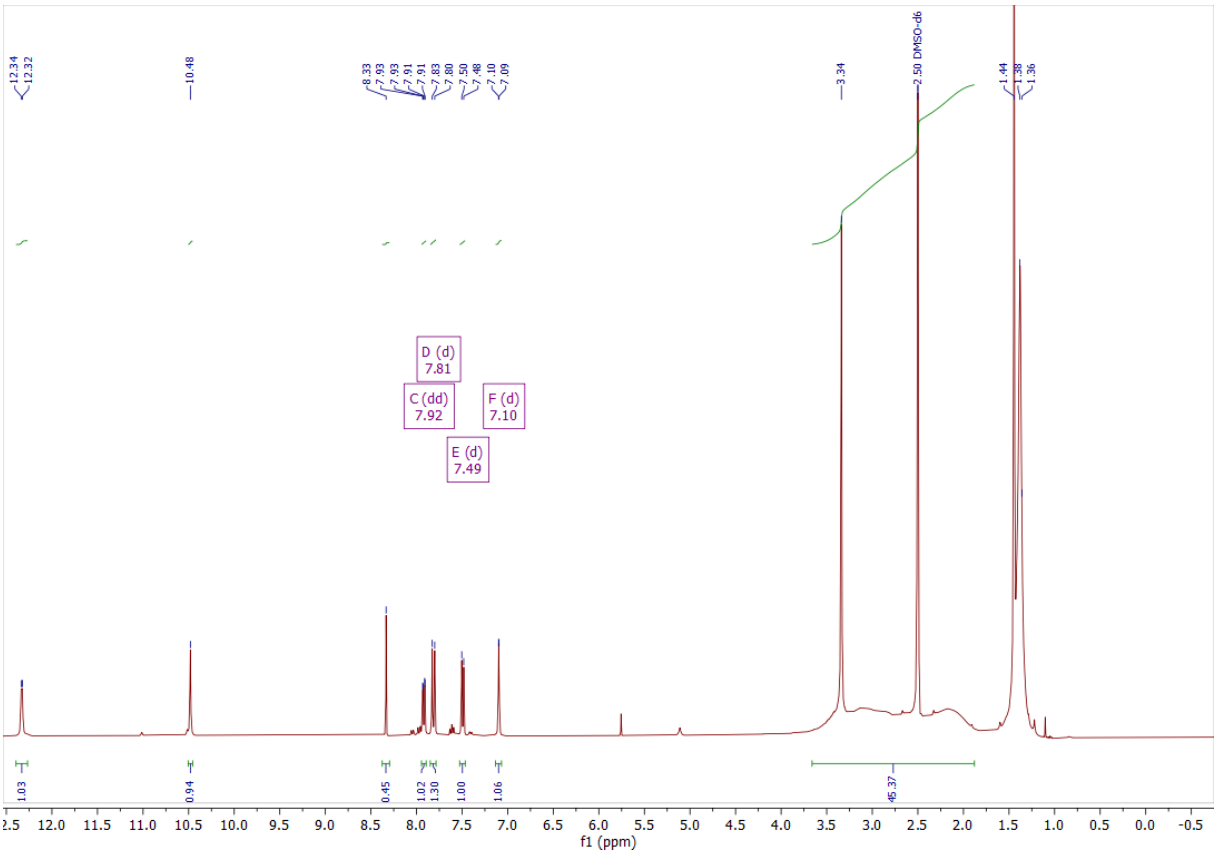

Figure S125 ^{1}H NMR spectrum of **7^{6F}** (400 MHz, DMSO-d_6).

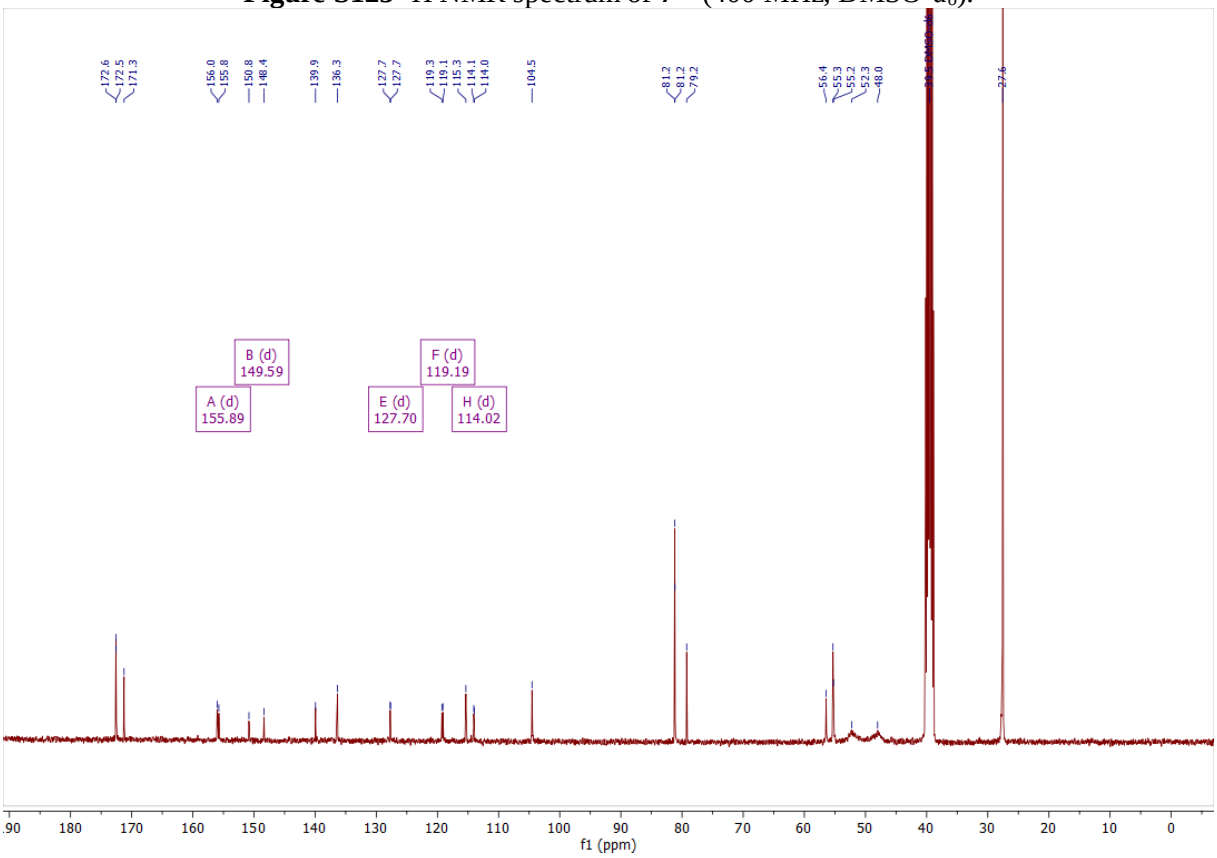

Figure S126 ^{13}C NMR spectrum of **7^{6F}** (101 MHz, DMSO-d_6).

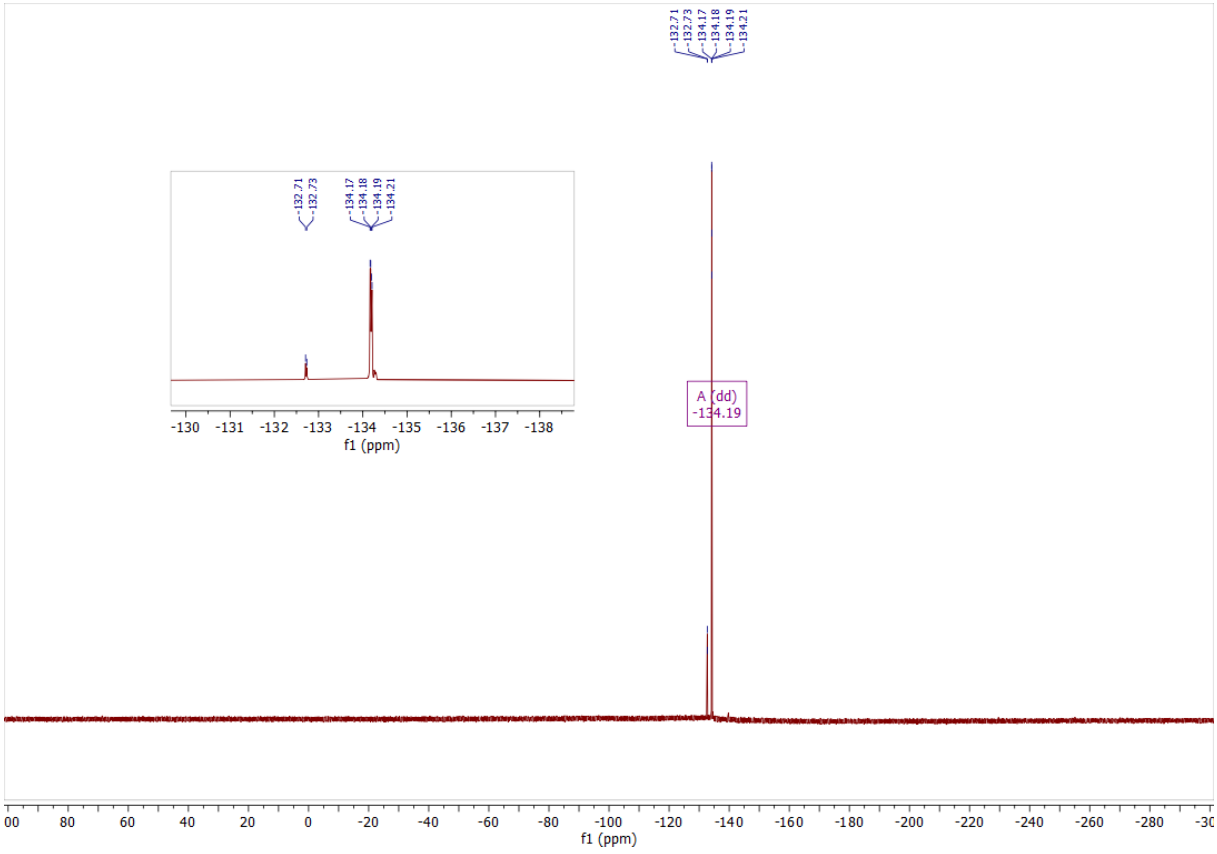

Figure S127 ^{19}F NMR spectrum of **7^{6F}** (376 MHz, DMSO-d_6).

7^{5F}

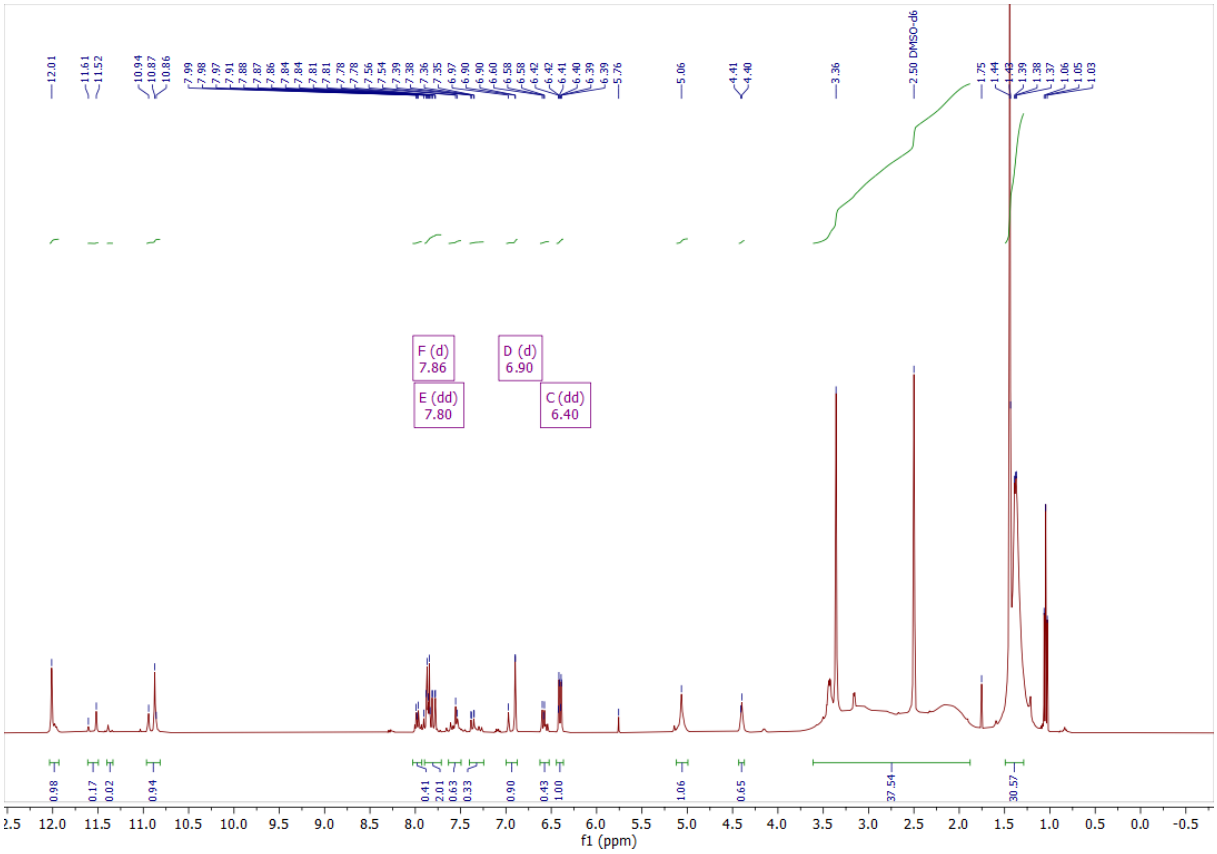

Figure S128 ^{1}H NMR spectrum of **7^{5F}** (400 MHz, DMSO-d_6).

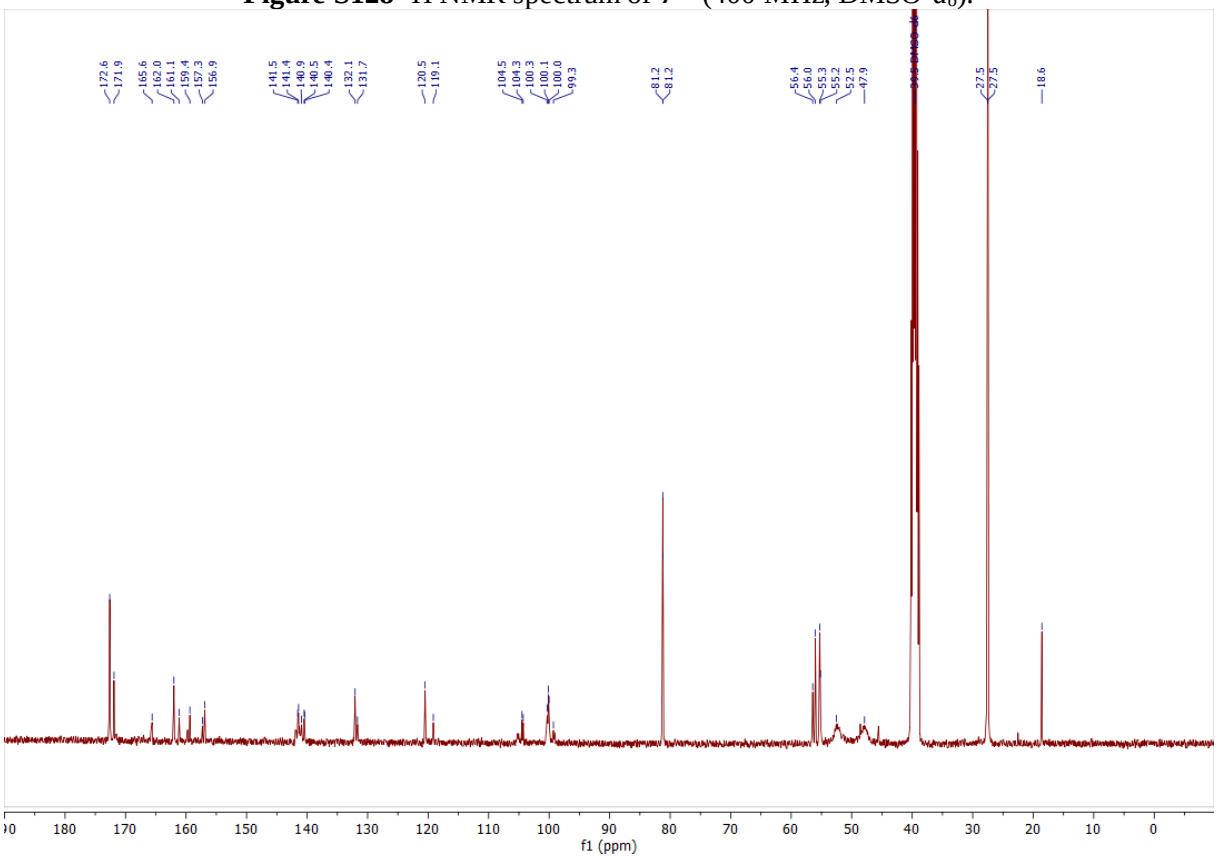

Figure S129 ^{13}C NMR spectrum of **7^{5F}** (101 MHz, DMSO-d_6).

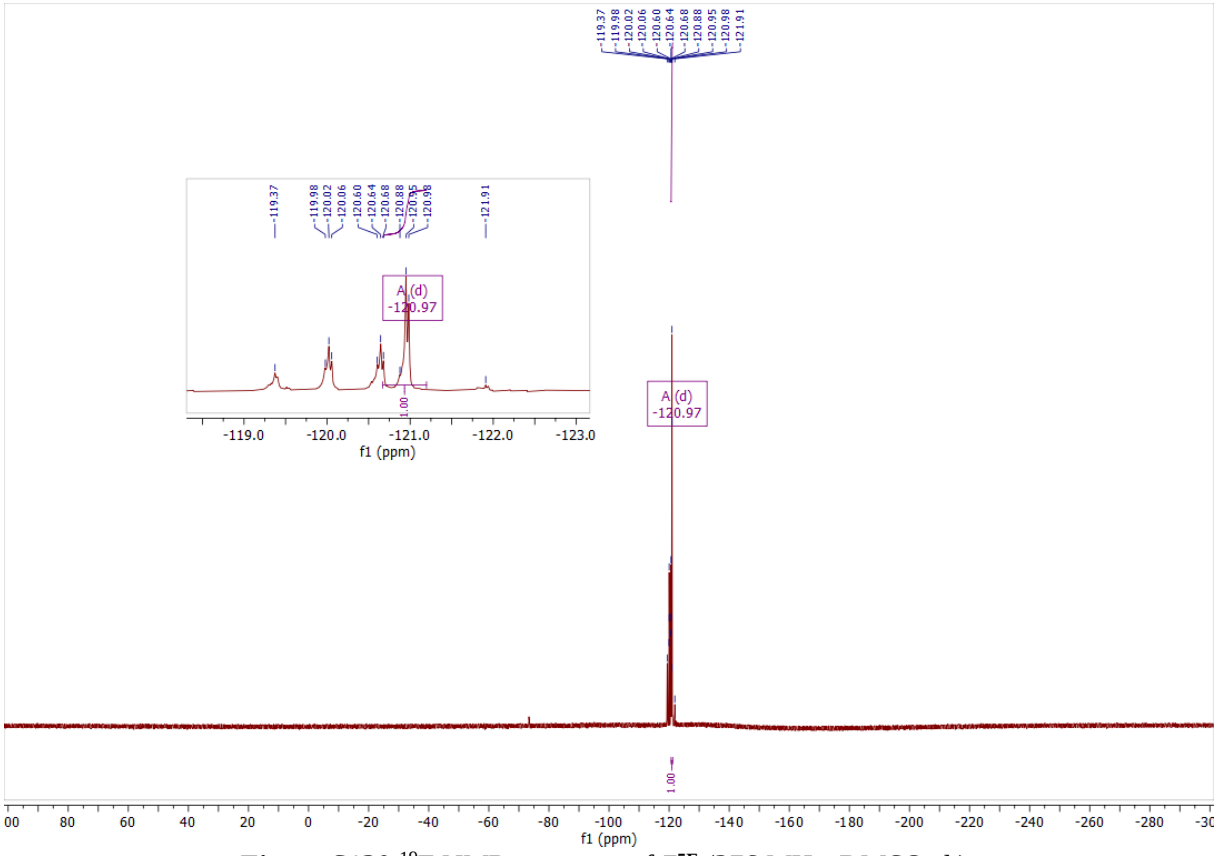

Figure S130 ^{19}F NMR spectrum of **7^{5F}** (376 MHz, DMSO-d_6).

7^{3F}

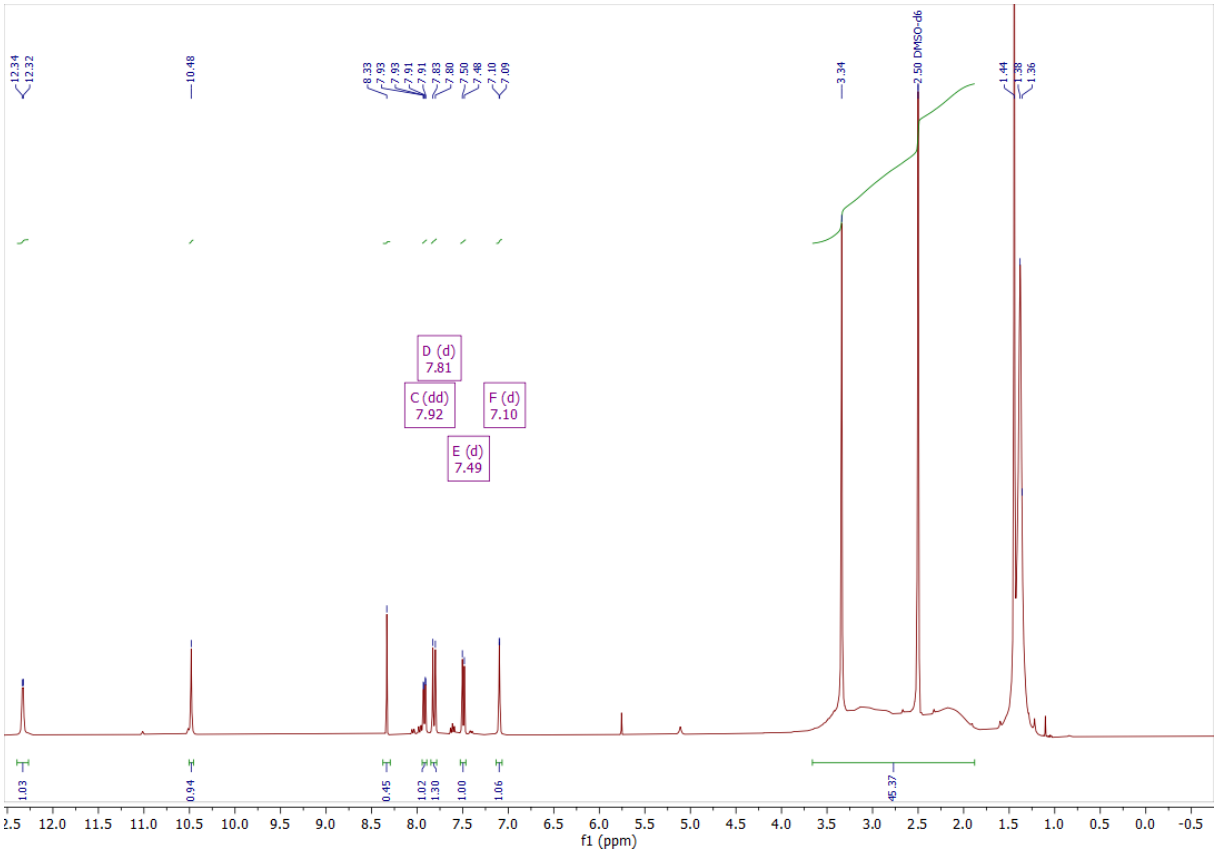

Figure S131 ^{1}H NMR spectrum of **7^{3F}** (400 MHz, DMSO-d_6).

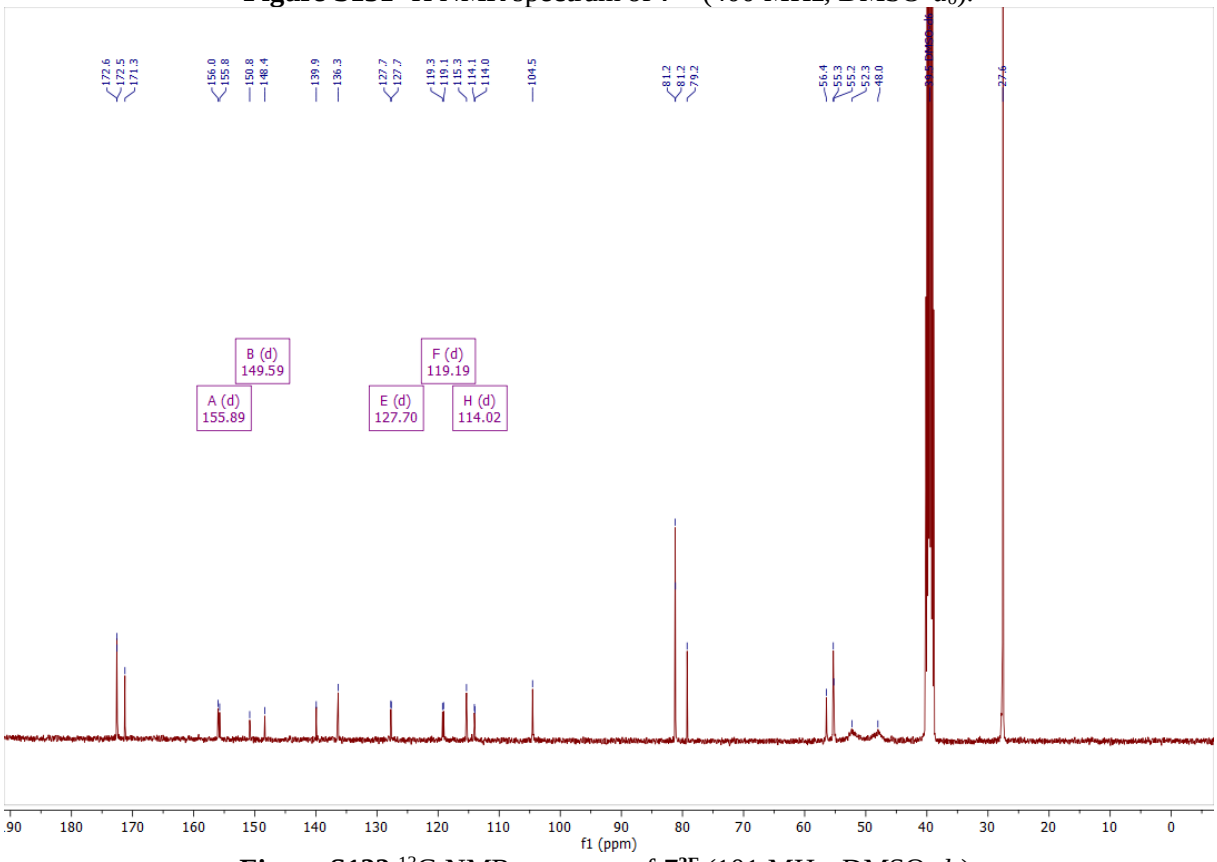

Figure S132 ^{13}C NMR spectrum of **7^{3F}** (101 MHz, DMSO-d_6).

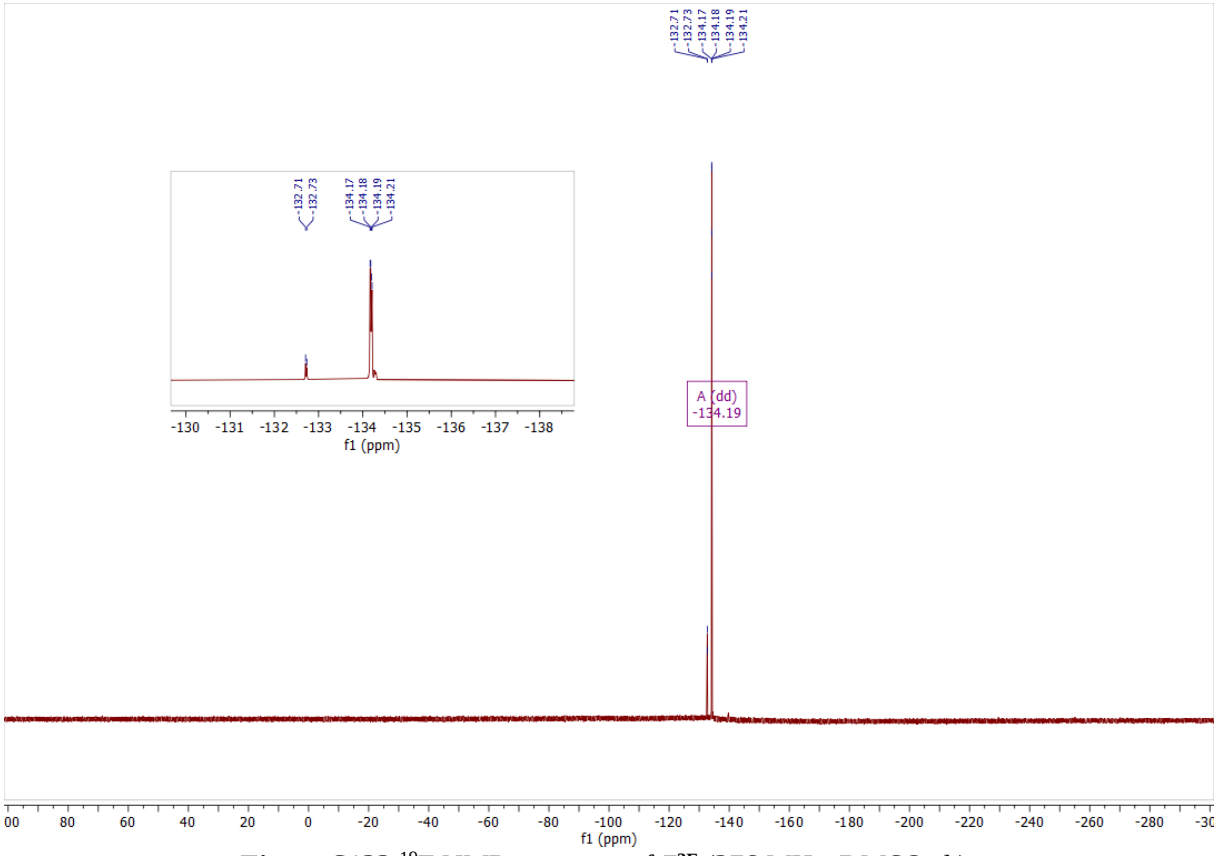

Figure S133 ^{19}F NMR spectrum of **7^{3F}** (376 MHz, DMSO-d_6).

L^{H}

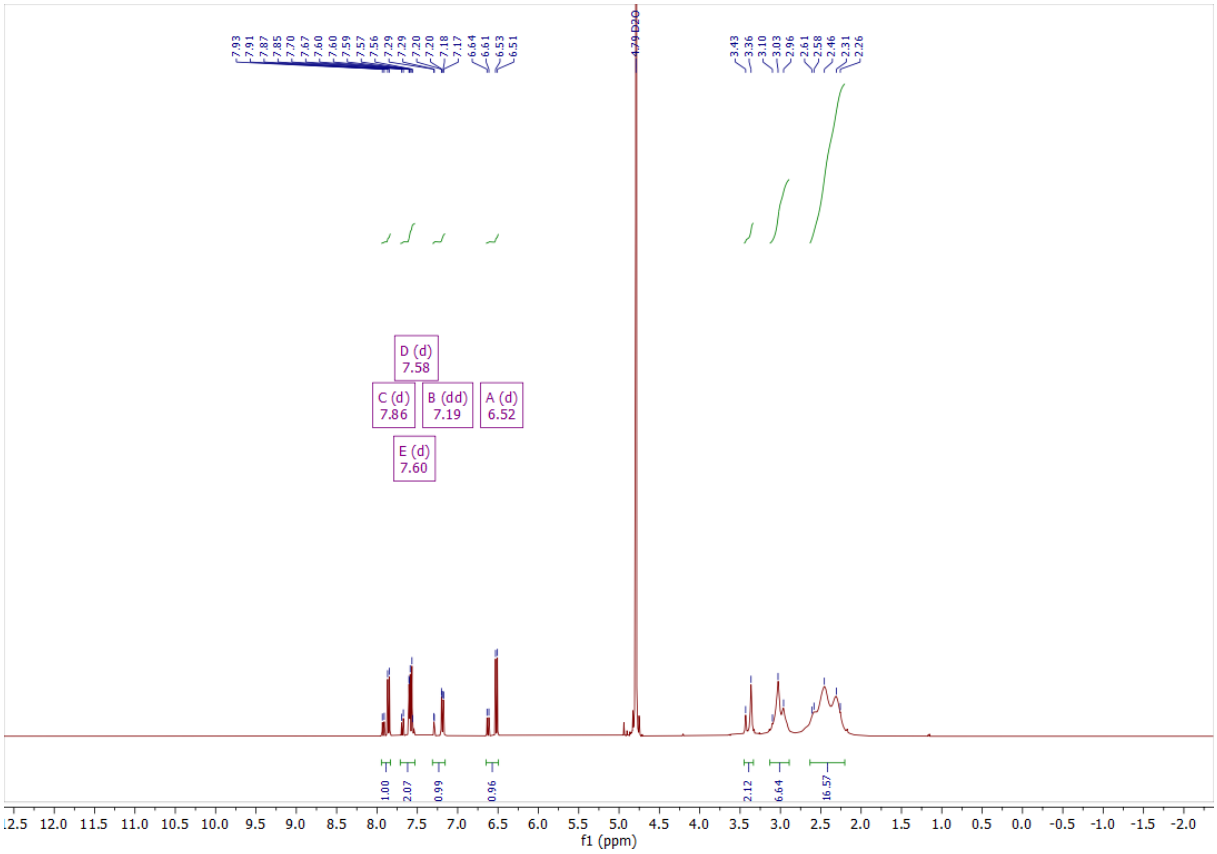

Figure S134 ^{1}H NMR spectrum of **L^{H}** (400 MHz, D_2O).

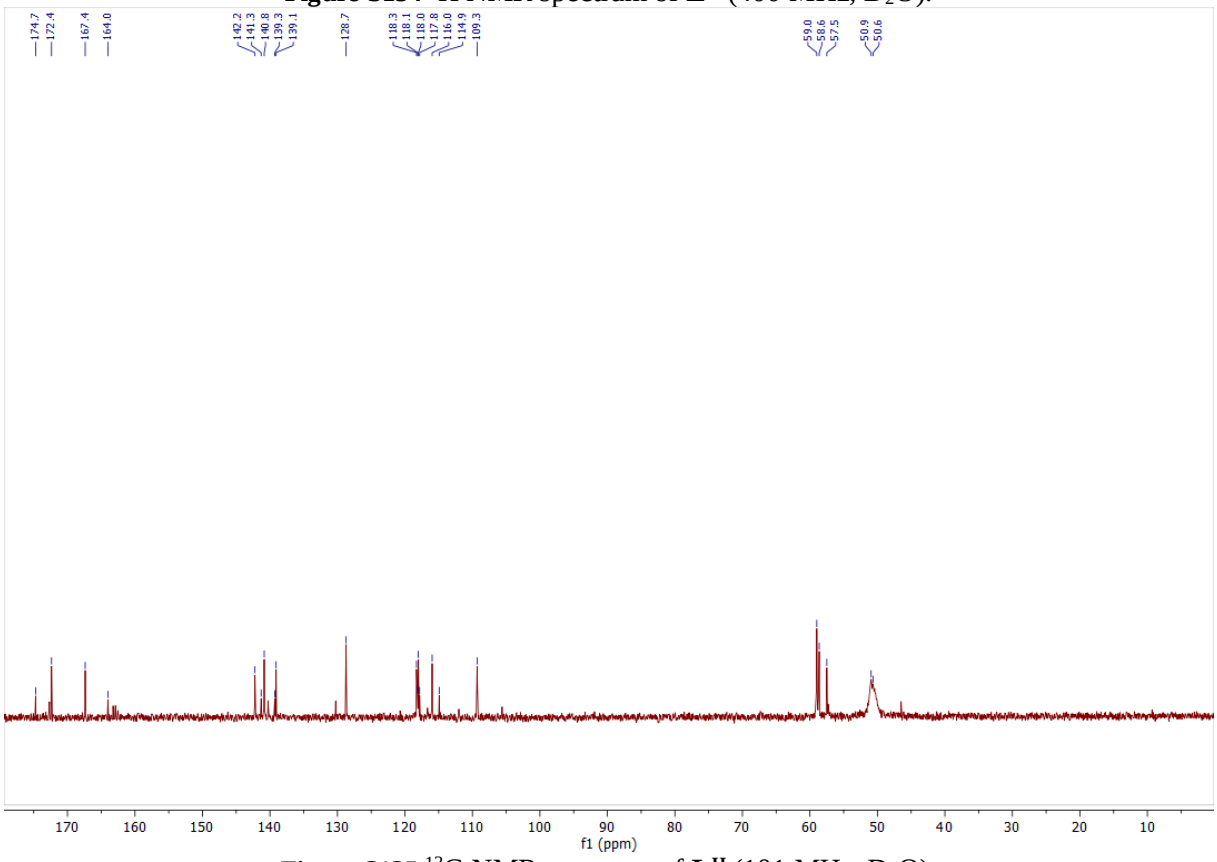

Figure S135 ^{13}C NMR spectrum of **L^{H}** (101 MHz, D_2O).

L^{6F}

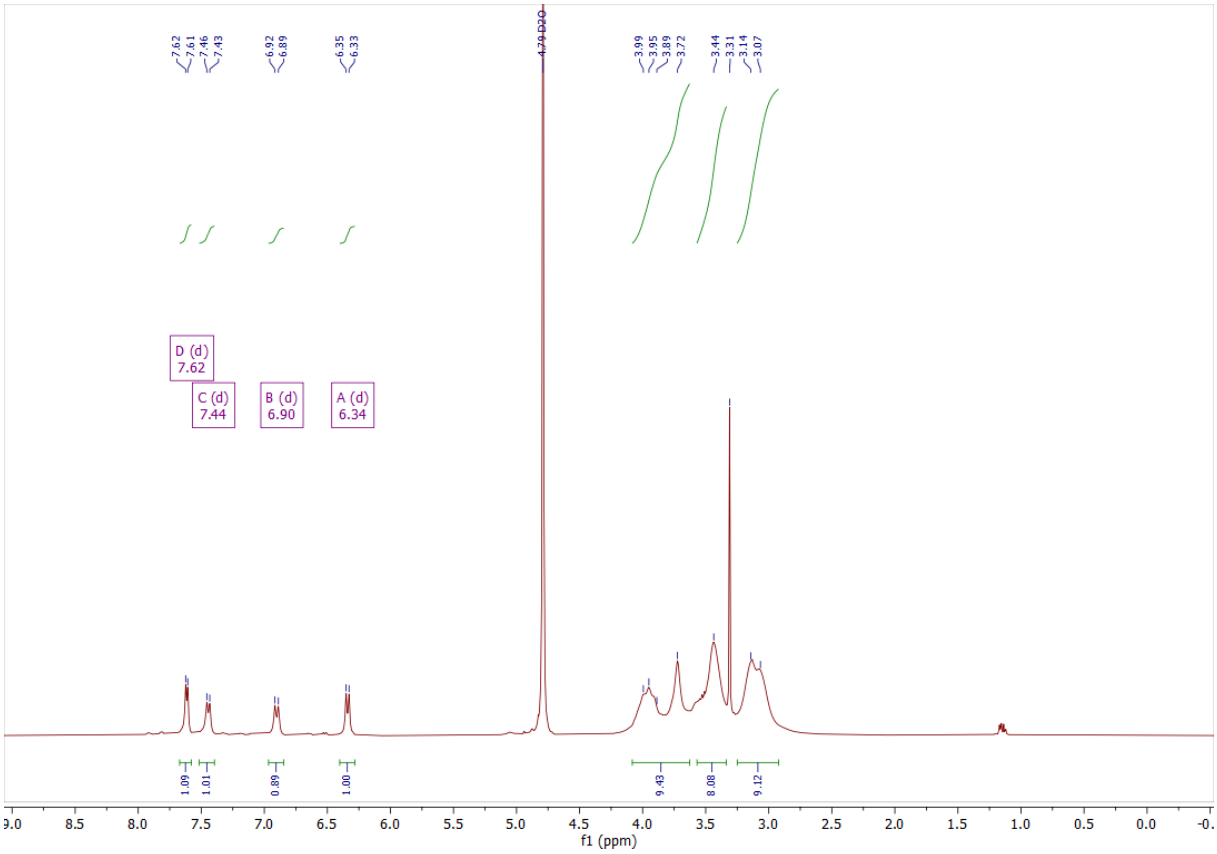

Figure S136 ^{1}H NMR spectrum of **L^{6F}** (400 MHz, D_2O).

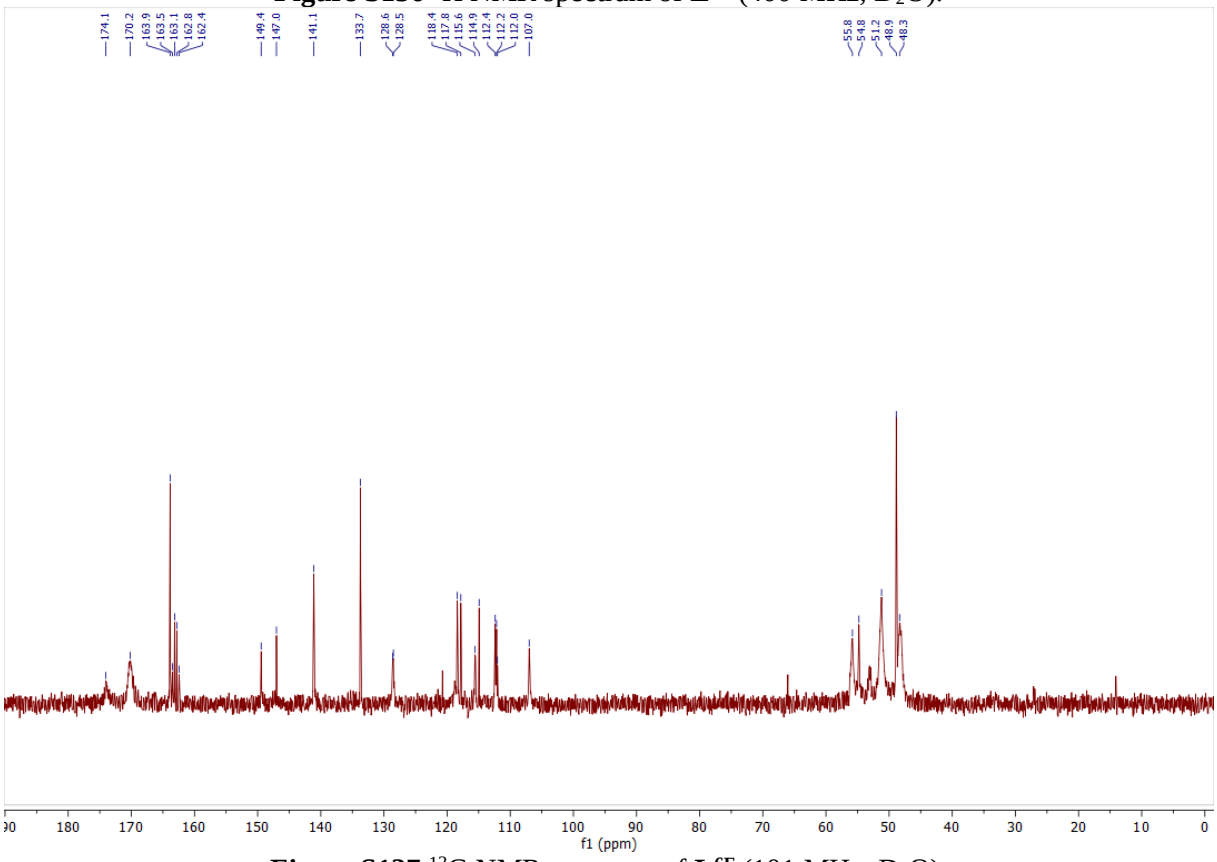

Figure S137 ^{13}C NMR spectrum of **L^{6F}** (101 MHz, D_2O).

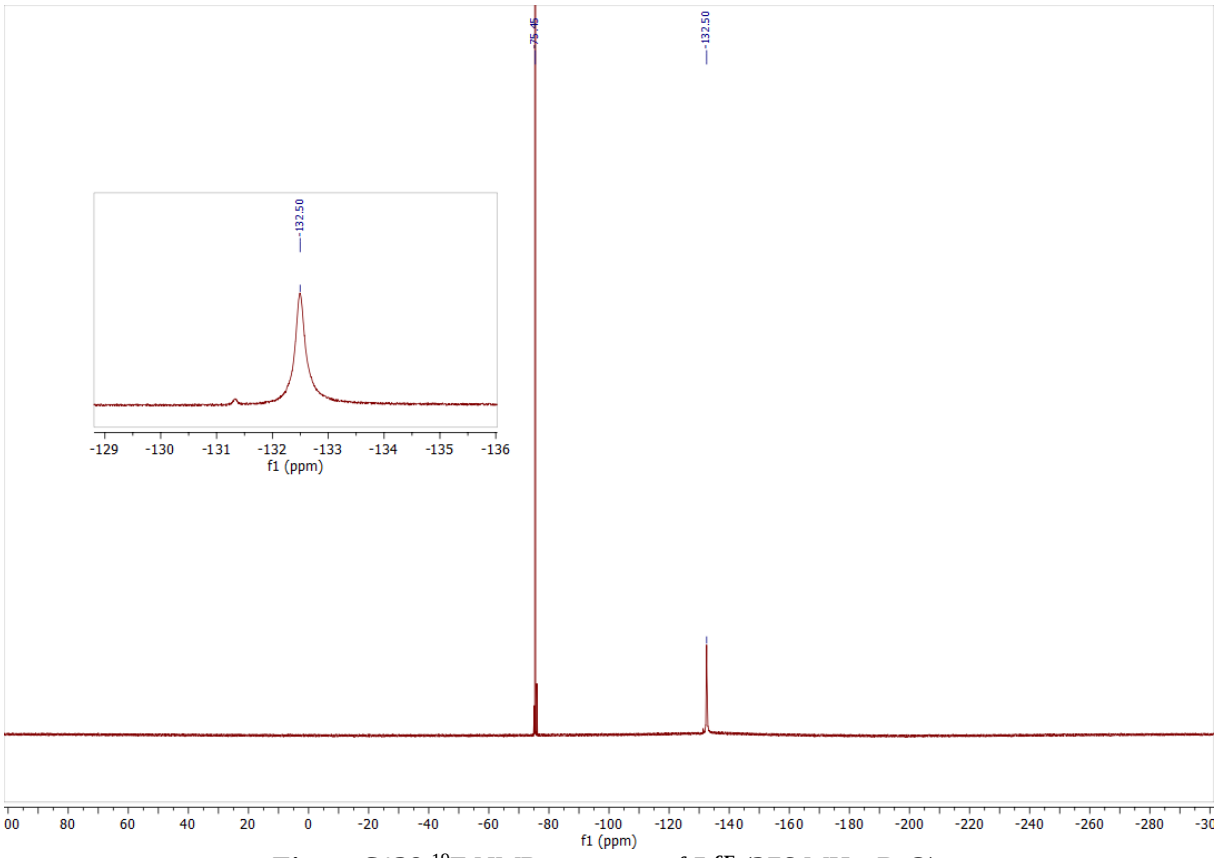

Figure S138 ^{19}F NMR spectrum of **L^{6F}** (376 MHz, D_2O).

L^{5F}

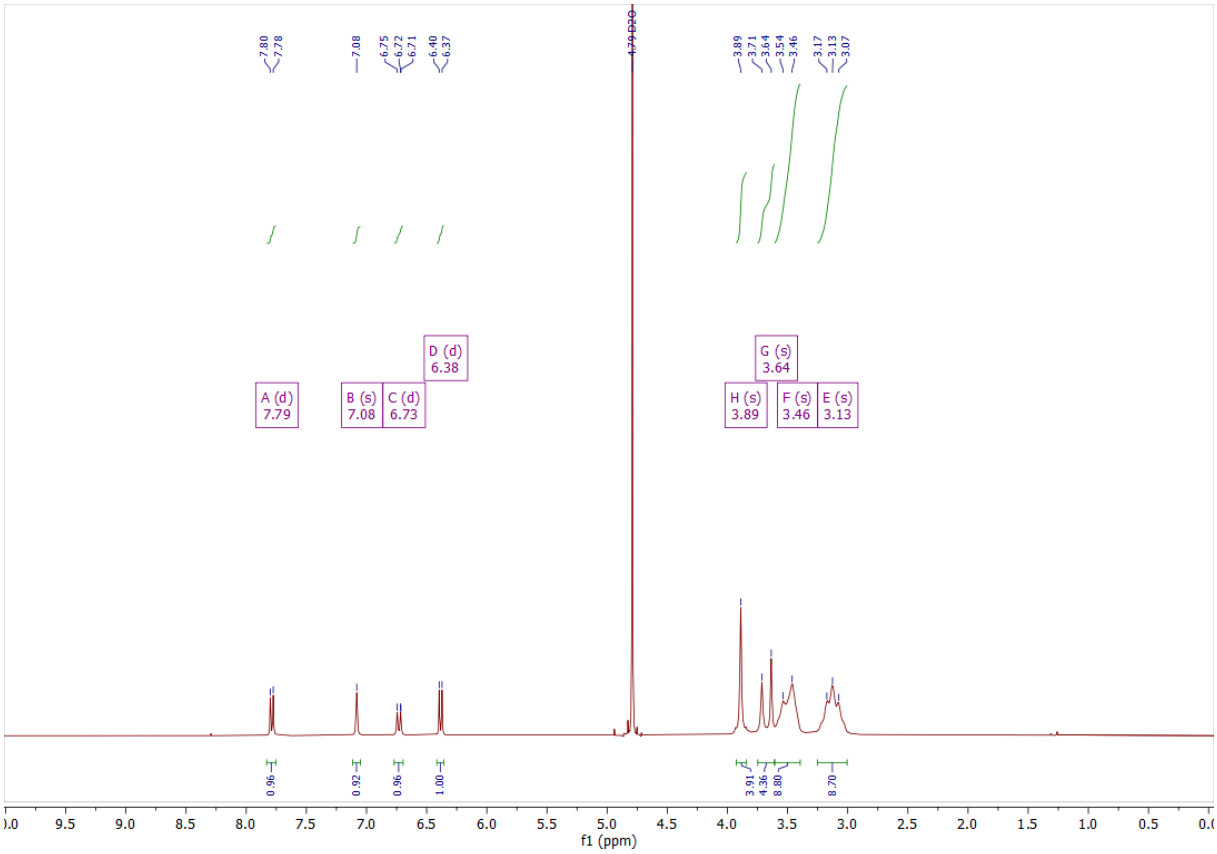

Figure S139 ^{1}H NMR spectrum of **L^{5F}** (400 MHz, D_2O).

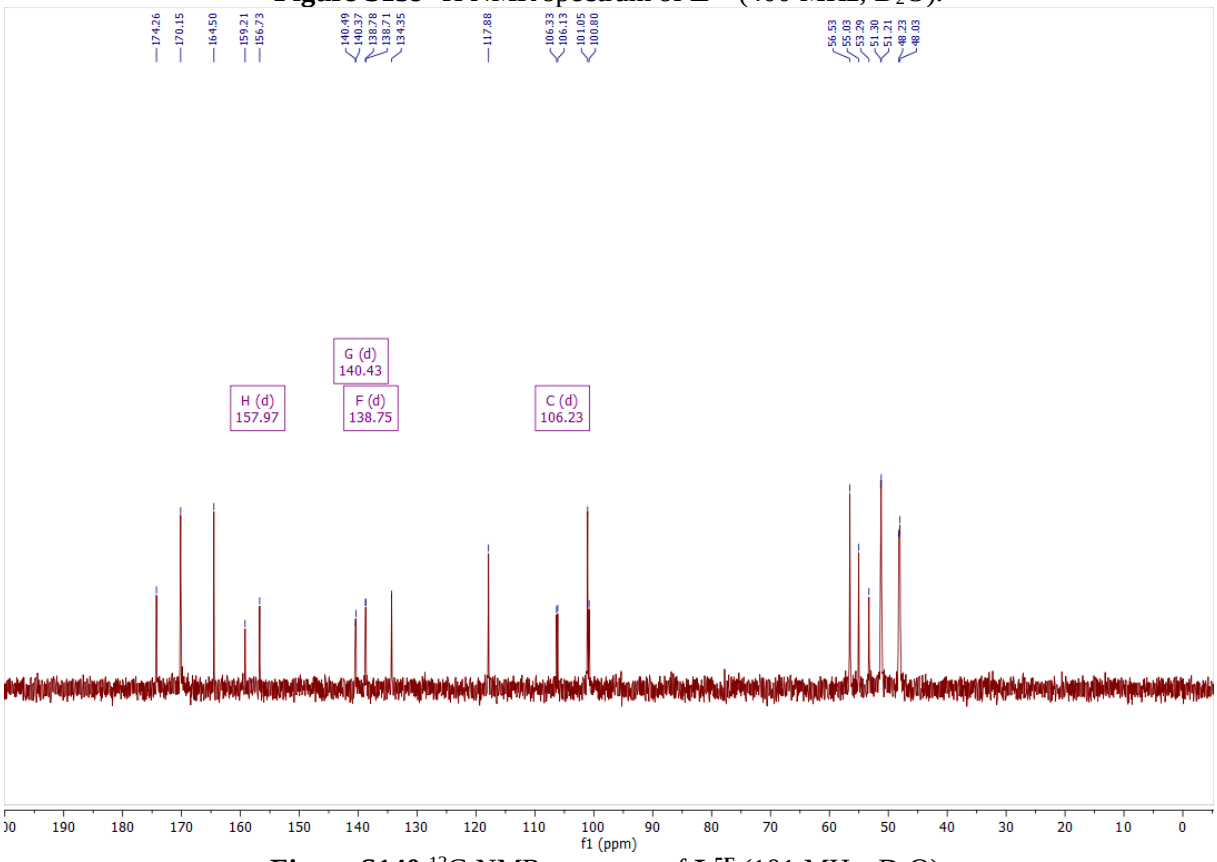

Figure S140 ^{13}C NMR spectrum of **L^{5F}** (101 MHz, D_2O).

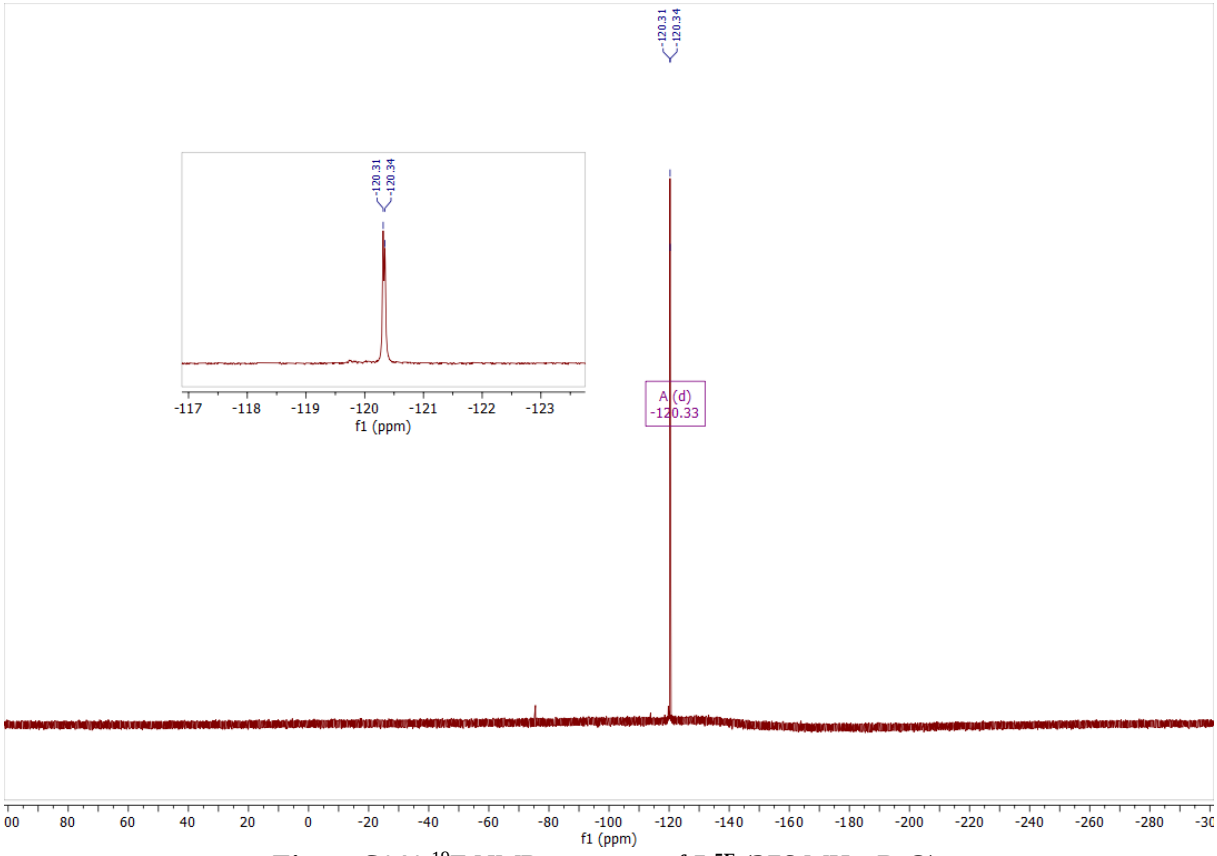

Figure S141 ^{19}F NMR spectrum of **L^{5F}** (376 MHz, D_2O).

L^{3F}

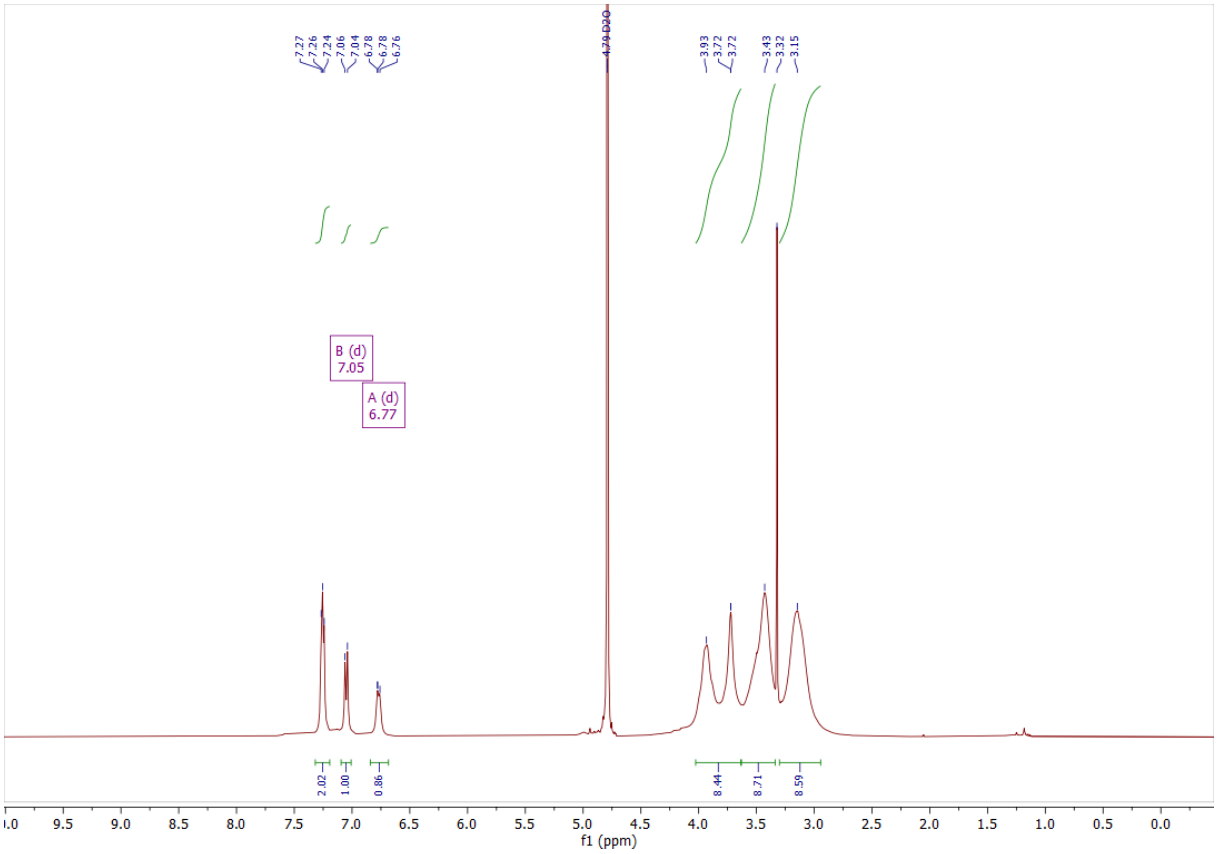

Figure S142 ^{1}H NMR spectrum of **L^{3F}** (400 MHz, D_2O).

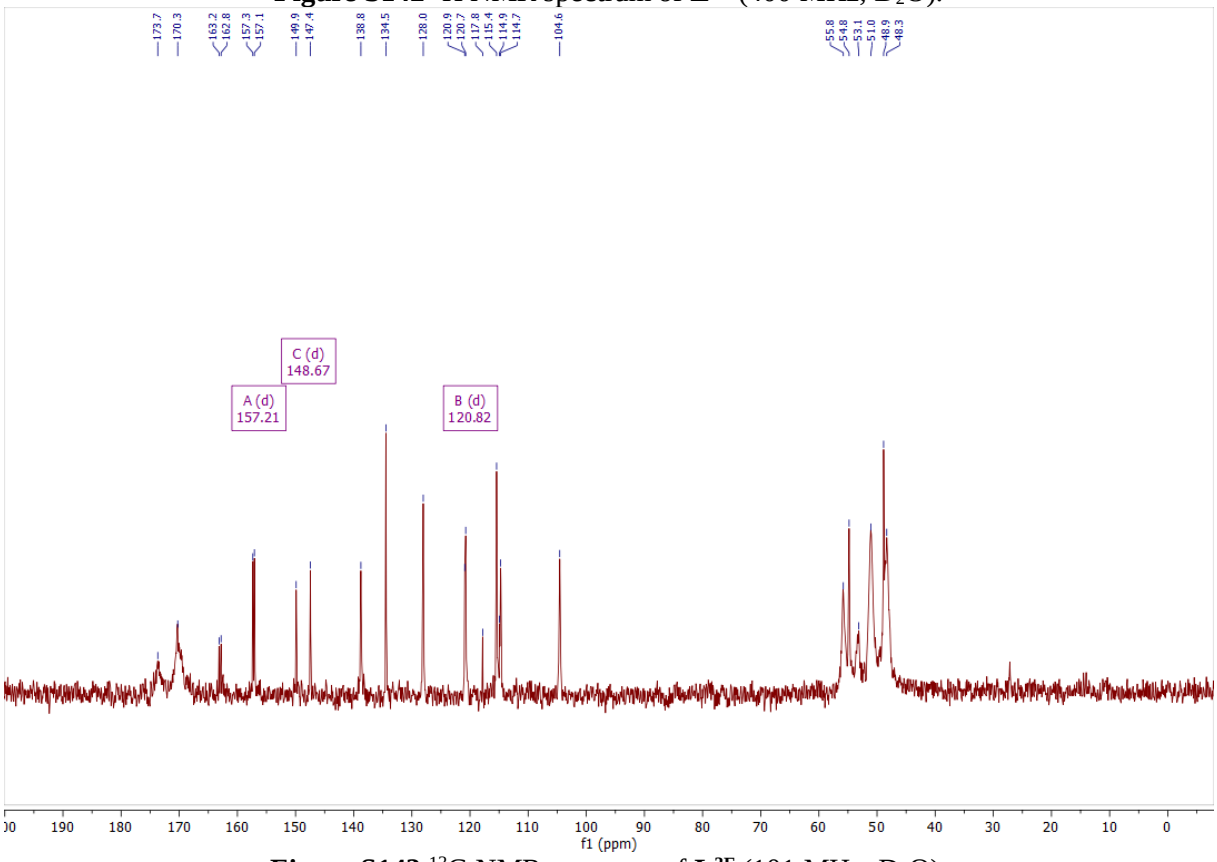

Figure S143 ^{13}C NMR spectrum of **L^{3F}** (101 MHz, D_2O).

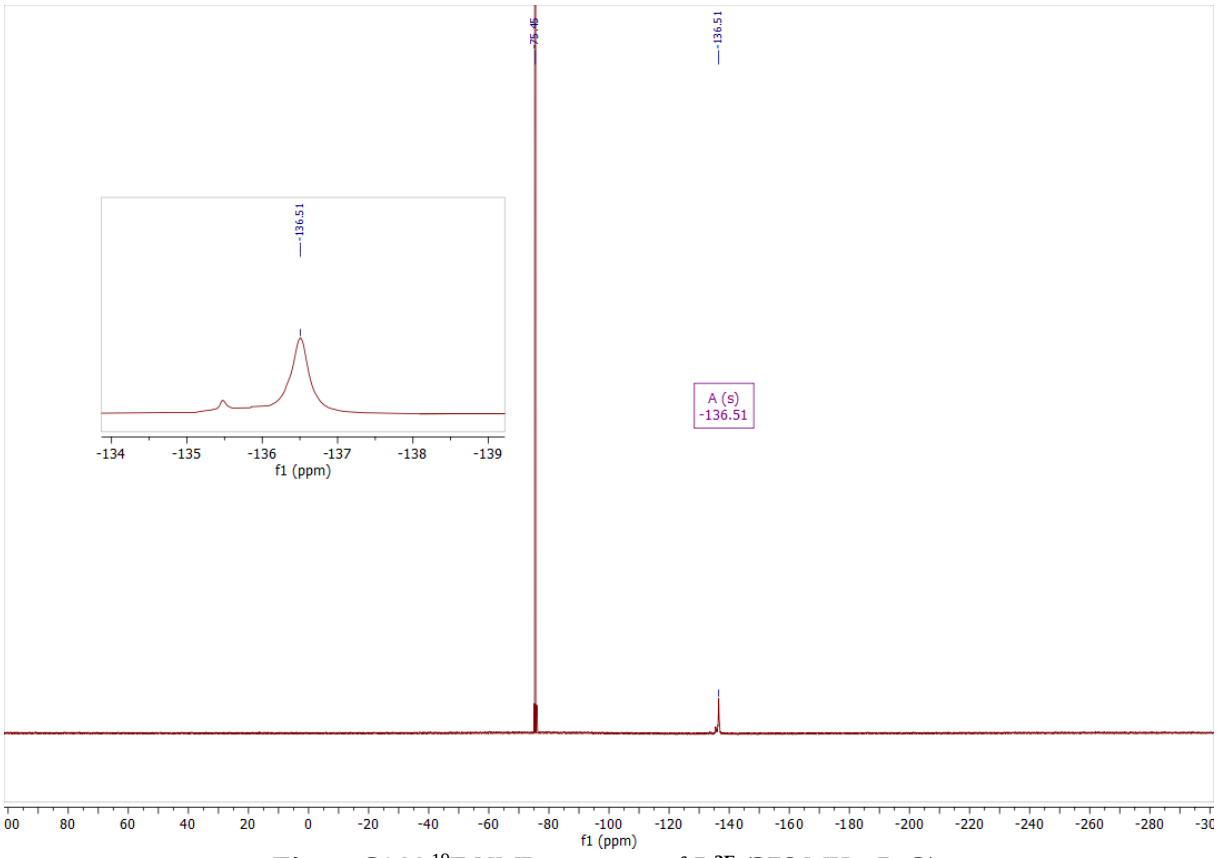

Figure S144 ^{19}F NMR spectrum of $\mathbf{L^{3F}}$ (376 MHz, D_2O).

HPLC-MS traces of Ln(III) complexes

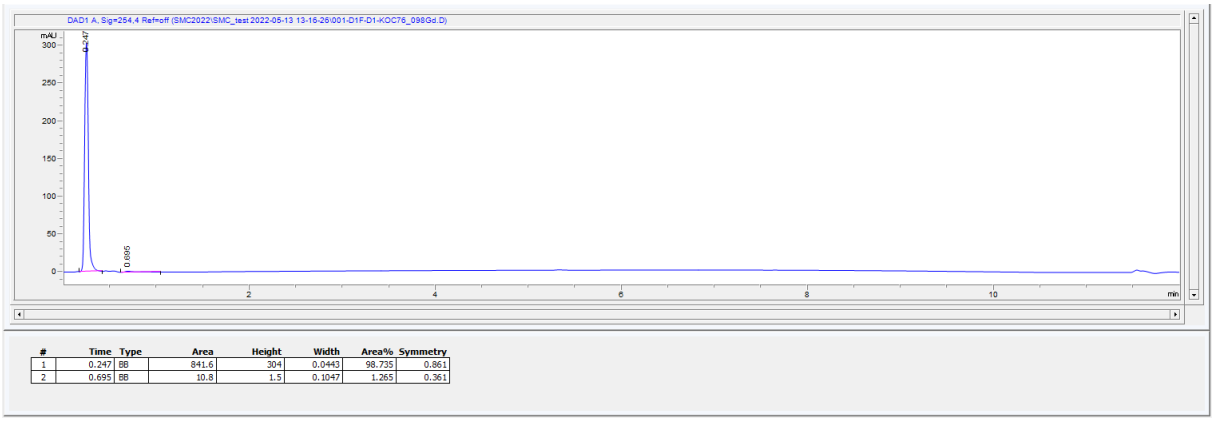

#	Time	Type	Area	Height	Width	Area%	Symmetry
1	0.247	BB	841.6	304	0.0443	98.735	0.861
2	0.695	BB	10.8	1.5	0.1047	1.265	0.361

Figure S145 HPLC-MS trace of **GdL^{H}**.

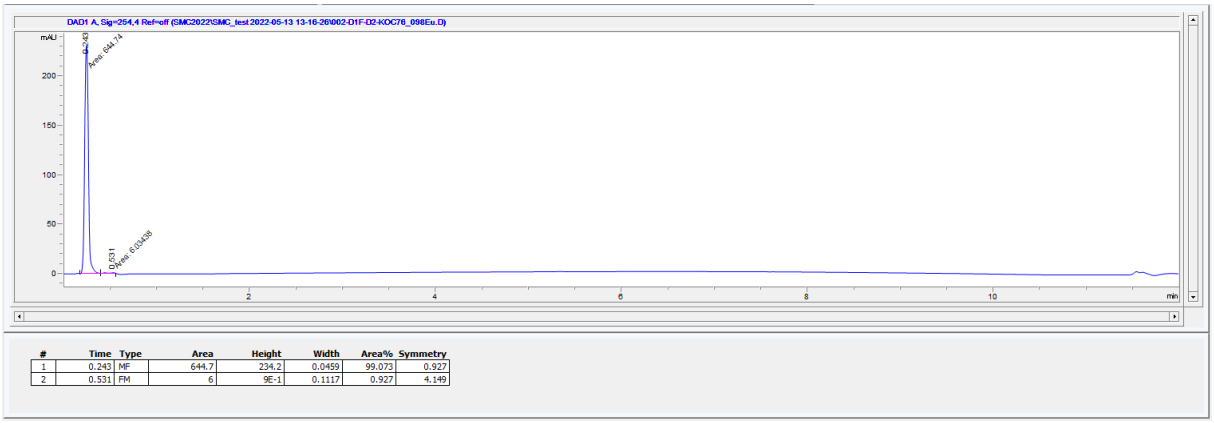

#	Time	Type	Area	Height	Width	Area%	Symmetry
1	0.243	MF	644.7	234.2	0.0459	99.073	0.927
2	0.531	FM	6	9E-1	0.1117	0.927	4.149

Figure S146 HPLC-MS trace of **EuL^{H}**.

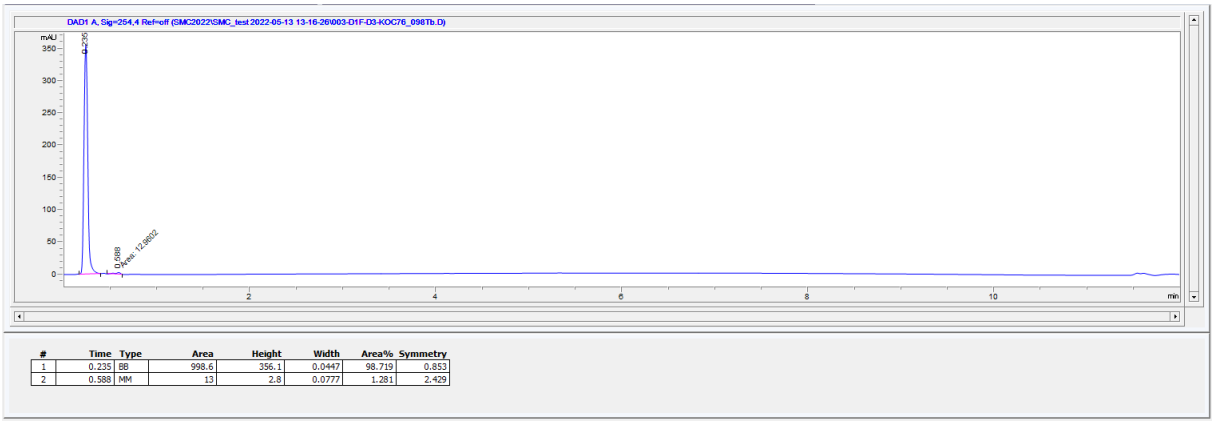

#	Time	Type	Area	Height	Width	Area%	Symmetry
1	0.235	BB	998.6	356.1	0.0447	98.719	0.853
2	0.588	MM	13	2.8	0.0777	1.281	2.429

Figure S147 HPLC-MS trace of **TbL^{H}**.

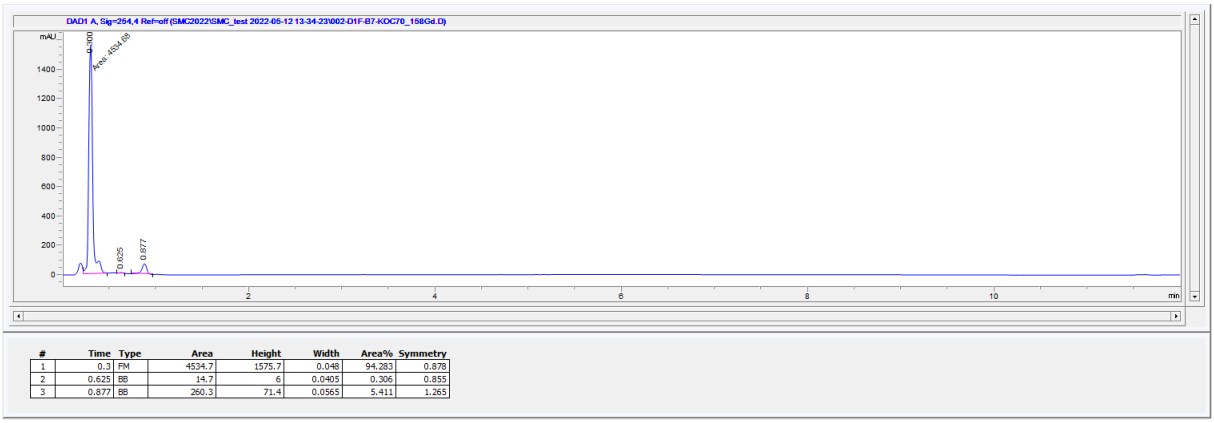

#	Time	Type	Area	Height	Width	Area%	Symmetry
1	0.3	FM	4534.7	1575.7	0.048	94.283	0.878
2	0.625	BB	14.7	6	0.0405	0.306	0.855
3	0.877	BB	260.3	71.4	0.0565	5.411	1.265

Figure S148 HPLC-MS trace of **GdL^{3F}**.

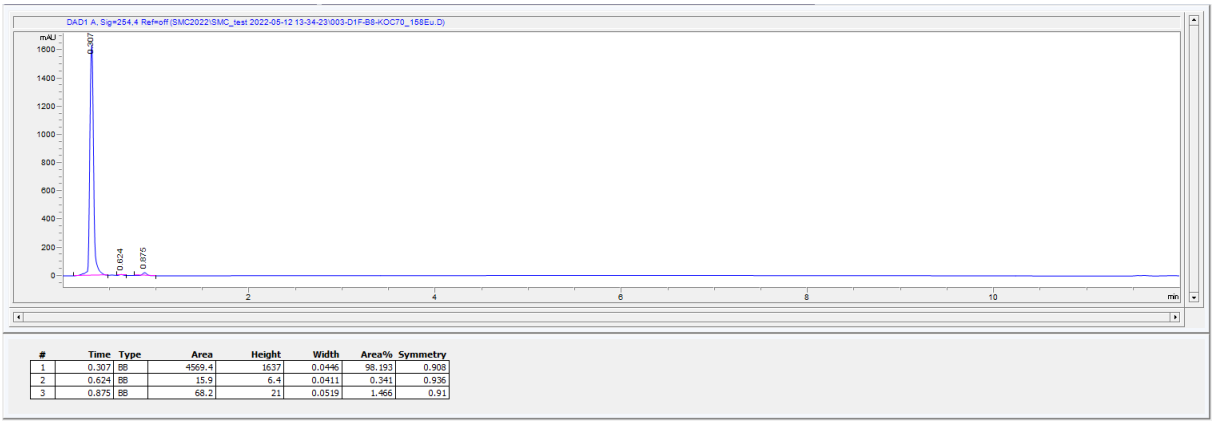

#	Time	Type	Area	Height	Width	Area%	Symmetry
1	0.307	BB	4569.4	1637	0.0446	98.193	0.908
2	0.624	BB	15.9	6.4	0.0411	0.341	0.936
3	0.875	BB	68.2	21	0.0519	1.466	0.91

Figure S149 HPLC-MS trace of **EuL^{3F}**.

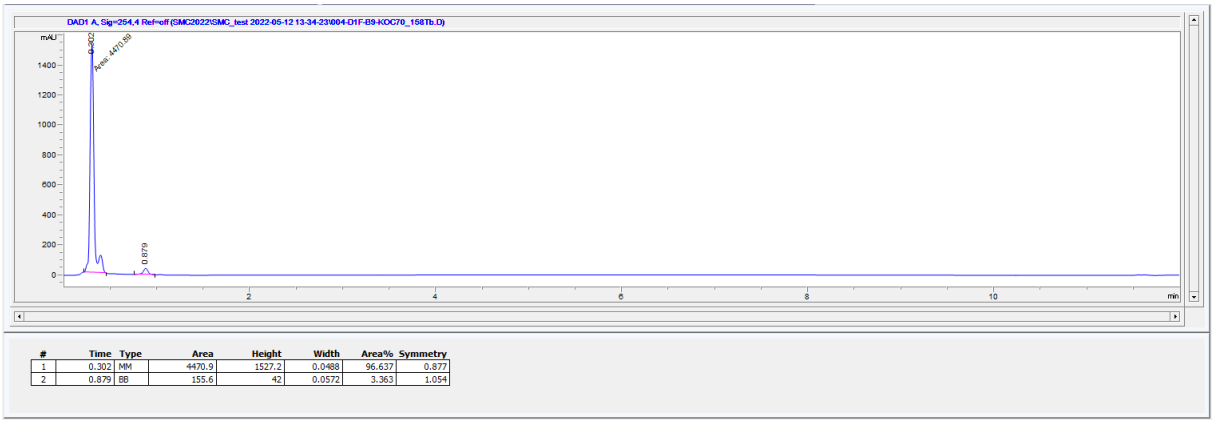

#	Time	Type	Area	Height	Width	Area%	Symmetry
1	0.302	MM	4470.9	1527.2	0.0488	96.637	0.877
2	0.879	BB	155.6	42	0.0572	3.363	1.054

Figure S150 HPLC-MS trace of **TbL^{3F}**.

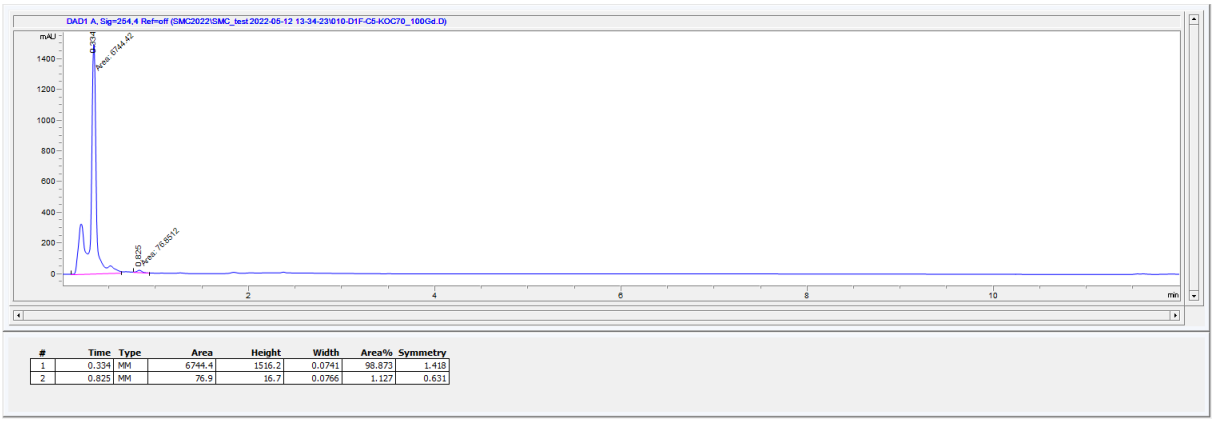

#	Time	Type	Area	Height	Width	Area%	Symmetry
1	0.334	MM	6744.4	1516.2	0.0741	98.873	1.418
2	0.825	MM	76.9	16.7	0.0766	1.127	0.631

Figure S151 HPLC-MS trace of **GdL^{5F}**.

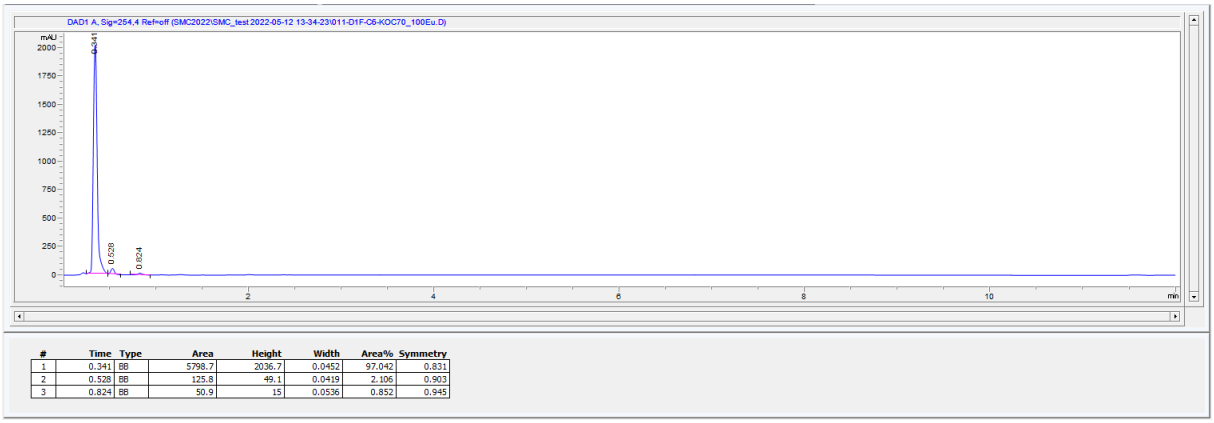

#	Time	Type	Area	Height	Width	Area%	Symmetry
1	0.341	BB	5798.7	2036.7	0.0452	97.042	0.831
2	0.528	BB	125.8	49.1	0.0419	2.106	0.903
3	0.824	BB	50.9	15	0.0536	0.852	0.945

Figure S152 HPLC-MS trace of **TbL^{5F}**.

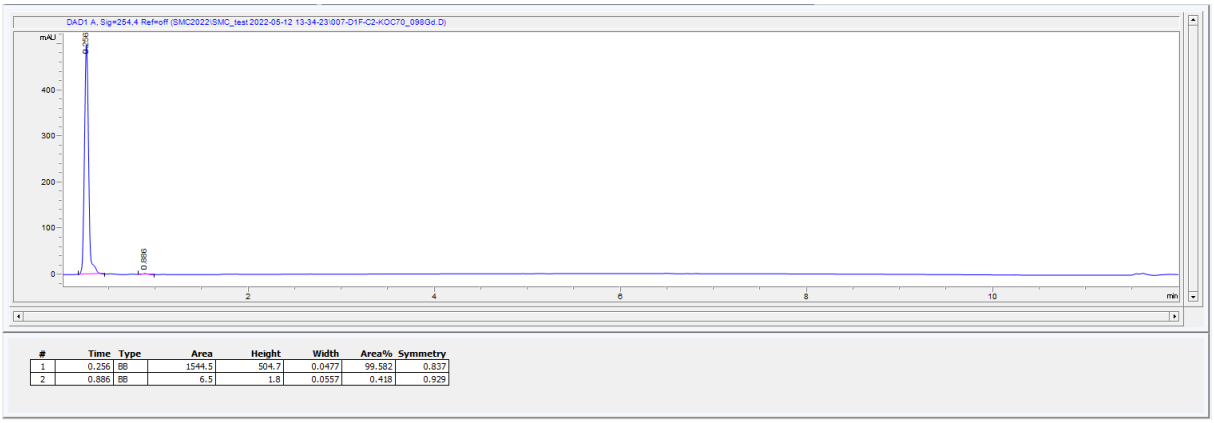

#	Time	Type	Area	Height	Width	Area%	Symmetry
1	0.256	BB	1544.5	504.7	0.0477	99.582	0.837
2	0.886	BB	6.5	1.8	0.0557	0.418	0.929

Figure S153 HPLC-MS trace of **GdL^{6F}**.

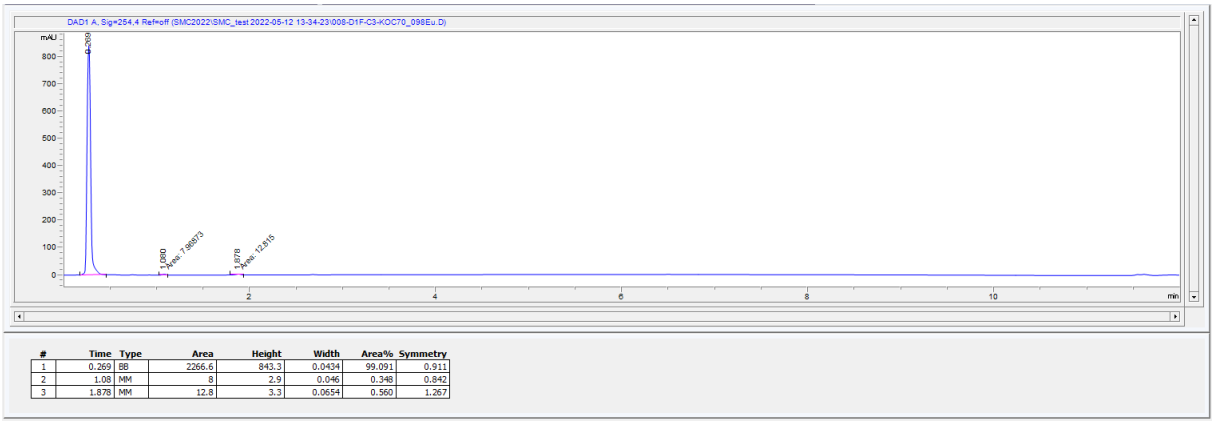

#	Time	Type	Area	Height	Width	Area%	Symmetry
1	0.269	BB	2266.6	843.3	0.0434	99.091	0.911
2	1.08	MM	8	2.9	0.046	0.348	0.842
3	1.878	MM	12.8	3.3	0.0654	0.560	1.267

Figure S154 HPLC-MS trace of **EuL^{6F}**.

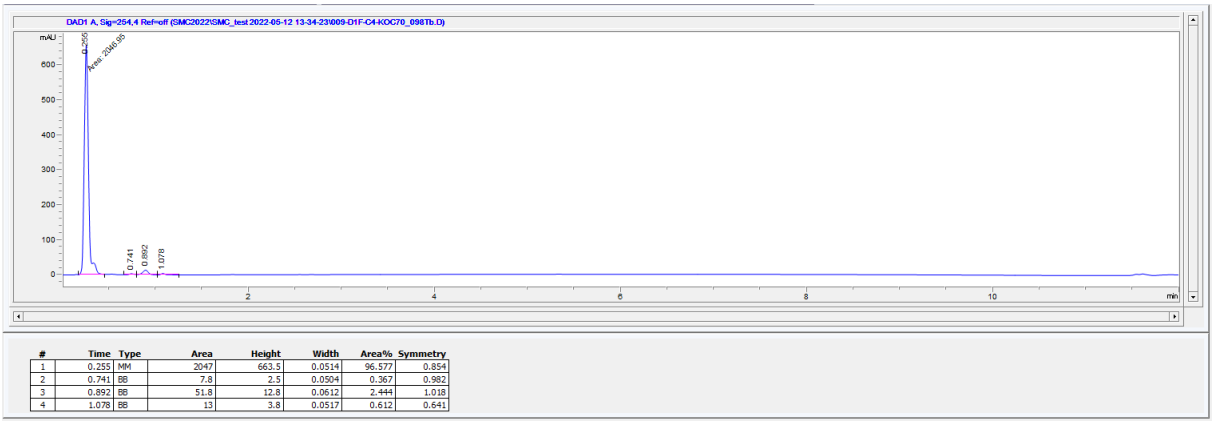

#	Time	Type	Area	Height	Width	Area%	Symmetry
1	0.255	MM	2047	663.5	0.0514	96.577	0.854
2	0.741	BB	7.8	2.5	0.0504	0.367	0.982
3	0.892	BB	51.8	12.8	0.0612	2.444	1.018
4	1.078	BB	13	3.8	0.0517	0.612	0.641

Figure S155 HPLC-MS trace of **TbL^{6F}**.

References

1. Bouazzaoui, O.; Rousée, K.; Mulengi, J. K.; Pannecoucke, X.; Bouillon, J.-P.; Couve-Bonnaire, S., Synthesis of α-Fluorinated Acrylates by a Palladium-Catalyzed Decarboxylative Olefination Reaction. *Eur. J. Org. Chem.* **2018**, 3705-3715.
2. Wang, M.-Z.; Xu, H.; Feng, Q.; Wang, L.-Z.; Wang, S.-H.; Li, Z.-M., Design, Synthesis, and Fungicidal Activity of Novel Analogues of Pyrrolnitrin. *J. Agric. Food Chem.* **2009**, *57*, 7912-7918.
3. Xu, J.; Ali, A.; Zhou, W.; Gao, Y.-D.; Edmondson, S. D.; Mertz, E.; Neelamkavil, S. F.; Liu, W.; Sun, W.; Shen, D.-M.; Harper, B.; Zhu, C.; Bara, T.; Lim, Y.-H.; Yang, M. Macrocyclic compounds as factor XIa inhibitors and their preparation. WO2017074832, 2017.
4. Kovacs, D.; Mathieu, E.; Kiraev, S. R.; Wells, J. A. L.; Demeyere, E.; Sipos, A.; Borbas, K. E., Coordination Environment-Controlled Photoinduced Electron Transfer Quenching in Luminescent Europium Complexes. *J. Am. Chem. Soc.* **2020**, *142*, 13190-13200.
5. Beeby, A.; Faulkner, S.; Williams, J. A. G., pH Dependence of the energy transfer mechanism in a phenanthridine-appended ytterbium complex. *J. Chem. Soc., Dalton Trans.* **2002**, 1918-1922.
6. Suzuki, K.; Kobayashi, A.; Kaneko, S.; Takehira, K.; Yoshihara, T.; Ishida, H.; Shiina, Y.; Oishi, S.; Tobita, S., Reevaluation of absolute luminescence quantum yields of standard solutions using a spectrometer with an integrating sphere and a back-thinned CCD detector. *Phys. Chem. Chem. Phys.* **2009**, *11*, 9850-9860.
7. Odhner, H.; Jacobs, D. T., Refractive Index of Liquid D_2O for Visible Wavelengths. *J. Chem. Eng. Data* **2012**, *57*, 166-168.
8. Saunders, J. E.; Sanders, C.; Chen, H.; Loock, H.-P., Refractive indices of common solvents and solutions at 1550 nm. *Appl. Opt.* **2016**, *55*, 947-953.
9. Supkowski, R. M.; Horrocks, W. D., Jr., On the determination of the number of water molecules, q, coordinated to europium(III) ions in solution from luminescence decay lifetimes. *Inorg. Chim. Acta* **2002,** *340*, 44-48.
10. Beeby, A.; Clarkson, I. M.; Dickins, R. S.; Faulkner, S.; Parker, D.; Royle, L.; de, S. A. S.; Williams, J. A. G.; Woods, M., Non-radiative deactivation of the excited states of europium, terbium and ytterbium complexes by proximate energy-matched OH, NH and CH oscillators: an improved luminescence method for establishing solution hydration states. *J. Chem. Soc., Perkin Trans. 2* **1999**, 493-504.
11. Li, Y.; Liu, X.; Ma, D.; Liu, B.; Jiang, H., Silver-Assisted Difunctionalization of Terminal Alkynes: Highly Regio- and Stereoselective Synthesis of Bromofluoroalkenes. *Adv. Synth. Catal.* **2012**, *354*, 2683-2688.
12. Nair, R. N.; Lee, P. J.; Rheingold, A. L.; Grotjahn, D. B., Single Bifunctional Ruthenium Catalyst for One-Pot Cyclization and Hydration giving Functionalized Indoles and Benzofurans. *Chem. Eur. J.* **2010**, *16*, 7992-7995.
13. Calabri, F. R.; Colotta, V.; Catarzi, D.; Varano, F.; Lenzi, O.; Filacchioni, G.; Costagli, C.; Galli, A., Synthesis and pharmacological studies at the Gly/NMDA, AMPA and Kainate receptors of new oxazolo[4,5-c]quinolin-4-one derivatives bearing different substituents at position-2 and on the fused benzo ring. *Eur. J. Med. Chem.* **2005**, *40*, 897-907.
14. Xue, L.; Deng, D.; Zheng, S.; Tang, M.; Yang, Z.; Pei, H.; Chen, Y.; Yang, T.; Liu, K.; Ye, H.; Chen, L., Design, synthesis and discovery of 2(1H)-quinolone derivatives for the treatment of pulmonary fibrosis through inhibition of TGF-β/smad dependent and independent pathway. *Eur. J. Med. Chem.* **2020**, *197*, 112259.
15. Uchida, H.; Ogawa, S.; Makabe, M.; Maeda, Y. Preparation of heterocyclylidene-N-(heterocyclyl)acetamide derivatives as antagonists of transient receptor potential type I receptor (TRPV1). US20100016285, 2010.
16. Billaud, E. M. F.; Maisonial-Besset, A.; Rbah-Vidal, L.; Vidal, A.; Besse, S.; Béquignat, J.-B.; Decombat, C.; Degoul, F.; Audin, L.; Deloye, J.-B.; Dollé, F.; Kuhnast, B.; Madelmont, J.-C.; Tarrit, S.; Galmier, M.-J.; Borel, M.; Auzeloux, P.; Miot-Noirault, E.; Chezal, J.-M., Synthesis, radiolabeling and preliminary in vivo evaluation of multimodal radiotracers for PET imaging and targeted radionuclide therapy of pigmented melanoma. *Eur. J. Med. Chem.* **2015**, *92*, 818-838.
17. Bertram, H. J.; Boehm, S.; Born, L., A novel reaction of 4-hydroxycoumarins and synthesis of 4-fluorocoumarins. *Synthesis* **1991**, 937.